SPECTRAL ANALYSIS AND MOMENT TENSOR INVERSION OF SEISMIC EVENTS INDUCED IN POLISH COAL MINES: SEARCH FOR NON-SHEARING COMPONENTS

S. J. Gibowicz, J. Niewiadomski, P. Wiejacz

Institute of Geophysics
Polish Academy of Sciences
ul. Ks. Janusza 64
01-452 Warsaw, Poland

G. Sagan, W. Zuberek

Department of Earth Sciences
Silesian University
ul. Bedzinska 60
41-200 Sosnowiec, Poland

Final Report for the U. S. Department of the Air Force
European Office of Aerospace and Development

Special Contract SPC-93-4006

1 January 1993 - 31 December 1993

28 February 1994

REPORT DOCUMENTATION PAGE

Form Approved OMB No. 0704-0188

1. AGENCY USE ONLY (Leave blank)	2. REPORT DATE	3. REPORT TYPE AND DATES COVERED
	28 February 1994	Final Report

4. TITLE AND SUBTITLE

Spectral Analysis and Moment Tensor Inversion of Seismic Events Induced in Polish Coal Mines: Search for Non-Shearing Components

5. FUNDING NUMBERS

F6170893W0207

6. AUTHOR(S)

S.J.Gibowicz, J.Niewiadomski, P.Wiejacz

7. PERFORMING ORGANIZATION NAME(S) AND ADDRESS(ES)

Institute of Geophysics
Polish Academy of Sciences
ul. Ks. Janusza 64
01-452 Warsaw, Poland

8. PERFORMING ORGANIZATION REPORT NUMBER

SPC-93-4006

9. SPONSORING/MONITORING AGENCY NAME(S) AND ADDRESS(ES)

EOARD
PSC 802 BOX 14
FPO 09499-0200

10. SPONSORING/MONITORING AGENCY REPORT NUMBER

SPC-93-4006

11. SUPPLEMENTARY NOTES

12a. DISTRIBUTION/AVAILABILITY STATEMENT

Approved for public release; distribution is unlimited.

12b. DISTRIBUTION CODE

A

13. ABSTRACT (Maximum 200 words)

The investigations conducted under this contract are focused on a research for non-shearing components of the source mechanism of seismic events induced in Polish coal mines. Such seismic events are expected to occur in close vicinity to the mining faces, where favorable conditions for generation of tensile failures or shear failures with tensile components are present. Simultaneous application of spectral analysis of seismic waves and moment tensor inversion was used to study this problem. The ratio of P-wave to S-wave energy radiated from mine tremors is in many cases anomalously large, implying that non-shear failures are often generated by mining excavations. We expected to show that the high P-wave energy tremors are generated by the sources with prominent non-double-couple components, as estimated from the moment tensor solutions.

14. SUBJECT TERMS

15. NUMBER OF PAGES

228

16. PRICE CODE

17. SECURITY CLASSIFICATION OF REPORT	18. SECURITY CLASSIFICATION OF THIS PAGE	19. SECURITY CLASSIFICATION OF ABSTRACT	20. LIMITATION OF ABSTRACT
UNCLASSIFIED	UNCLASSIFIED	UNCLASSIFIED	UL

Table of Contents

List of Illustrations

List of Tables

ABSTRACT

The investigations conducted under this contract are focused on a search for non-shearing components of the source mechanism of seismic events induced in Polish coal mines. Such seismic events are expected to occur in close vicinity to the mining faces, where favourable conditions for generation of tensile failures or shear failures with tensile components are present. Simultaneous application of spectral analysis of seismic waves and moment tensor inversion was used to study this problem. The ratio of *P*-wave to *S*-wave energy radiated from mine tremors is in many cases anomalously large, implying that non-shear failures are often generated by mining excavations. We expected to show that the high *P*-wave energy tremors are generated by the sources with prominent non-double-couple components, as estimated from the moment tensor solutions.

Two coal mines in the Upper Silesian Coal Basin (USCB), located in different tectonic environments, were selected for our study. Wujek coal mine is located in the central part of the USCB, on the southern side of the main antycline structure, which is the area of the highest seismicity in the USCB. The mine has an underground digital seismic network composed of 12 vertical sensors (plus 2 analog channels), favourably covering several longwalls worked out in 1993 in seams 501, 504, and 510. Fifty five seismic events were selected for the experiment. Ziemowit coal mine is situated in the south-eastern part of the USCB in the main syncline structure. Seismicity there is of the middle-level type and is not well understood. The mine has also an underground digital network composed of 16 vertical sensors. There is one active area centrally situated with respect to the network - field 4 in seam 207. Eighty three well recorded seismic events, which occurred in 1993 mostly in seam 207, were selected for our study.

The selected seismic events from Wujek mine have moment magnitude between 1.1 and 2.2 and seismic energy between $1*10^5$ and $2*10^7$ J, and the seismic events from Ziemowit mine are characterized by moment magnitude from 1.4 to 2.4 and seismic energy from $2*10^6$ to $7*10^8$ J. The source radius is similar at both mines, ranging from 40 to 100 m. The stress drop at Ziemowit mine is about five times higher than that at Wujek mine, ranging from 0.2 to 5.7 MPa. Similarly, the apparent stress at Ziemowit mine is about ten times higher than that at Wujek mine and ranges between 0.05 and 4.8 MPa. The ratio of S-wave to P-wave energy is at both mines in a similar range of values from about 0.1 to 18. The scaling relations at both mines imply that the self-similarity rule is probably valid there, though the relations are based on a very narrow range of seismic moment values.

The general moment tensor solutions were decomposed into an isotropic part, a compensated linear vector dipole and a double couple. The double-couple component in most cases forms 60-80 % of the solution, whereas the compensated linear vector dipole and the isotropic components correspond to 10-20 % of the solution. The double-couple component in the restrained deviatoric moment tensor solutions is in most cases the dominant part of the source mechanism. The relationships between the ratio of *P*- to *S*-wave energy and the indicators of a double couple component, a compensated linear vector dipole, and an isotropic part in the general solution are not entirely clear. Although there is a positive correlation between the energy ratio and the double-couple indicator, and negative correlations between the ratio and the compensated linear vector dipole and volumetric change indicators, the correlation coefficients in all three cases are small.

I. INTRODUCTION

Recent results from earthquake focal mechanism studies indicate growing evidence that alternative mechanisms other than shear failure are possible. The most prominent cases of what appear to be anomalous focal mechanisms are reported from studies of seismicity induced by mining. The results from studies mostly based on first-motion polarity and radiation patterns were reviewed by Gibowicz (1990a,b).

Spectral analysis has become a standard technique used in studies of small earthquakes. Early attempts to apply the spectral theory of a seismic source to seismic events induced by mining (Smith *et al.*, 1974; Spottiswoode and McGarr, 1975; Gibowicz *et al.*, 1977; Hinzen, 1982; Gibowicz, 1984) have shown that the simple source models in the form of a circular dislocation (Brune, 1970, 1971; Madariaga, 1976) or a rectangular fault (Savage, 1972) can be successfully used for the interpretation of seismic spectra and the determination of source parameters of mine tremors. A recent study of the source parameters of seismic events at the Heinrich Robert coal mine in the Ruhr basin, Germany, provides some evidence for non-double-couple events (Gibowicz *et al.*, 1990). It has been found that the ratio of *S*- to *P*-wave energy ranges from 1.5 to 30 for selected tremors occurring in a cluster. The high *P*-wave energy and low apparent stress events are thought to be the most likely candidates for non-double-couple events. A similar result was also found from a study of the source parameters of seismic events induced by the excavation of a shaft in granite at the Underground Research Laboratory in Manitoba, Canada (Gibowicz *et al.*, 1991). The observed high P-wave energy events were most probably the events with non-double-couple focal mechanisms, implying that tensile failures, or at least shear failures with tensile components, were generated by the excavation of the shaft.

A more general approach to this problem is based on the moment tensor inversion. Moment tensors describe completely, in a first order approximation, the equivalent forces of general seismic point sources; the double-couple source being just one of them. In many applications a point source approximation may be quite satisfactory, provided that the source dimensions are small in comparison to the observed wavelenghts of seismic waves. A moment tensor can be decomposed into an isotropic part, a compensated linear vector dipole and a double couple. Such a decomposition seems to be the most interesting one for source studies of seismic events induced by mining. The isotropic component of the source mechanism corresponds to a volumetric change, the compensated linear vector dipole corresponds to a sort of uniaxial compression, and the double couple corresponds of course to a shear failure.

Although moment tensor inversions on a teleseismic scale have been routinely performed for several years, the application of this technique to local seismic events is a relatively recent innovation (e.g., Saikia and Herrmann, 1985, 1986; Oncescu, 1986; De Natale *et al.*, 1987; O'Connell and Johnson, 1988; Ebel and Bonjer, 1990; Koch, 1991a,b). A few works only have been published so far that are related to the use of moment tensor inversion in studies of seismic events induced by mining (Sato and Fujii, 1989; Fujii and Sato, 1990; Wiejacz, 1991, 1992; Feignier and Young, 1992; McGarr, 1992). These were reviewed by Gibowicz (1993).

The investigations conducted under this contract are focused on a search for non-shearing components of the source mechanism of seismic events induced in Polish coal mines. We propose to use an innovative approach to study source mechanism by simultaneous application of spectral analysis of seismic waves and moment tensor inversion. We expect to show that the high P-wave energy tremors are generated by the sources with prominent non-double-couple components, as estimated from the moment tensor solutions. Such seismic events are expected to occur in close vicinity to the active mine faces, where favourable conditions for the generation of tensile failures or shear failures with tensile components are obviously present. If this is the case, then a comparatively simple calculation of *P*-wave and *S*-wave energies

would provide an indication of the mode of failure in the source of seismic events induced by mining.

Two coal mines in the Upper Silesian Coal Basin (USCB), located in different tectonic environments, were selected for our study. Wujek coal mine is located in the central part of the USCB, on the southern side of the main antycline structure, which is the area of the highest seismicity in the USCB. Several longwalls worked out in 1993 in this mine were favourably covered by an underground seismic network, and fifty five seismic events were selected for our experiment. Ziemowit coal mine is situated in the south-eastern part of the USCB in the main syncline structure. Seismicity there is of the middle-level type and is not well understood. In 1993 there was one active area centrally situated with respect to the operating seismic network, and eighty three well recorded seismic events were selected for our study. The analyses were performed on the digital seismic data which were available from each mine.

This report is divided into six sections including this introduction. In Section II geological and tectonic structures of the USCB and Wujek and Ziemowit mines are briefly described. The underground seismic networks in these mines and the data used for the analyses are introduced in Section III. Source parameters of selected seismic events, calculated from spectral analysis of *P* and *S* waves, and their various relations are presented in Section IV. The results of moment tensor inversions and relations between spectral and moment tensor source parameters are described in Section V. Finally, the main conclusions from the presented studies are summarized in Section VI.

II. GEOLOGICAL STRUCTURE AND TECTONICS

2.1 Upper Silesian Coal Basin

The Upper Silesian Coal Basin (USCB), situated in the central part of southern Poland, is one of the biggest coal basins in the world. The coal production reached the maximum value of almost 200 million ton in 1979, and the production has been continued for over two hundred years. The Basin is of typical multilayer structure with the coal seam thickness of up to 24 m. The maximum depth of mining operations reaches at present 1200 m. A small fraction (about 10 %) of the USCB is situated in the northern-central part of the Czech Republic and is known as the Ostrava-Karvina Coal Basin.

The USCB is a part of the Paleozoic platform of Central Europe, situated in the foreland and partly in the basement of the folded Carpathian Arc and the Fore-Carpathian Depression. The Basin was developed and finally formed during the evolution of the Variscian geosynclinal system (Devonian-Permian), occupying special position in the contact of three important structural elements of the Variscian orogene (e.g., Bukowy, 1984): the Silesian-Moravian Folded Zone extending from Brno in Slovakia to Upper Silesia in Poland and surrounding the Bohemian Massif from the east, the Cracow Folded Zone running along the north-eastern boundary of the Basin with the general NW-SE direction, and the Upper Silesian Block forming rigid structure situated at the base of the USCB. In relation to the other regional geological units, the USCB is a syncline filled with the molasse deposits, developed along the border between the former geosynclines of two branches of the orogene: the Silesian-Moravian and Cracow Variscidians.

Two main factors affected the present shape of tectonic structure of the USCB: the nature of the basement of the Variscian deposits and its discontinuities, and the shape and position of the Upper Silesian

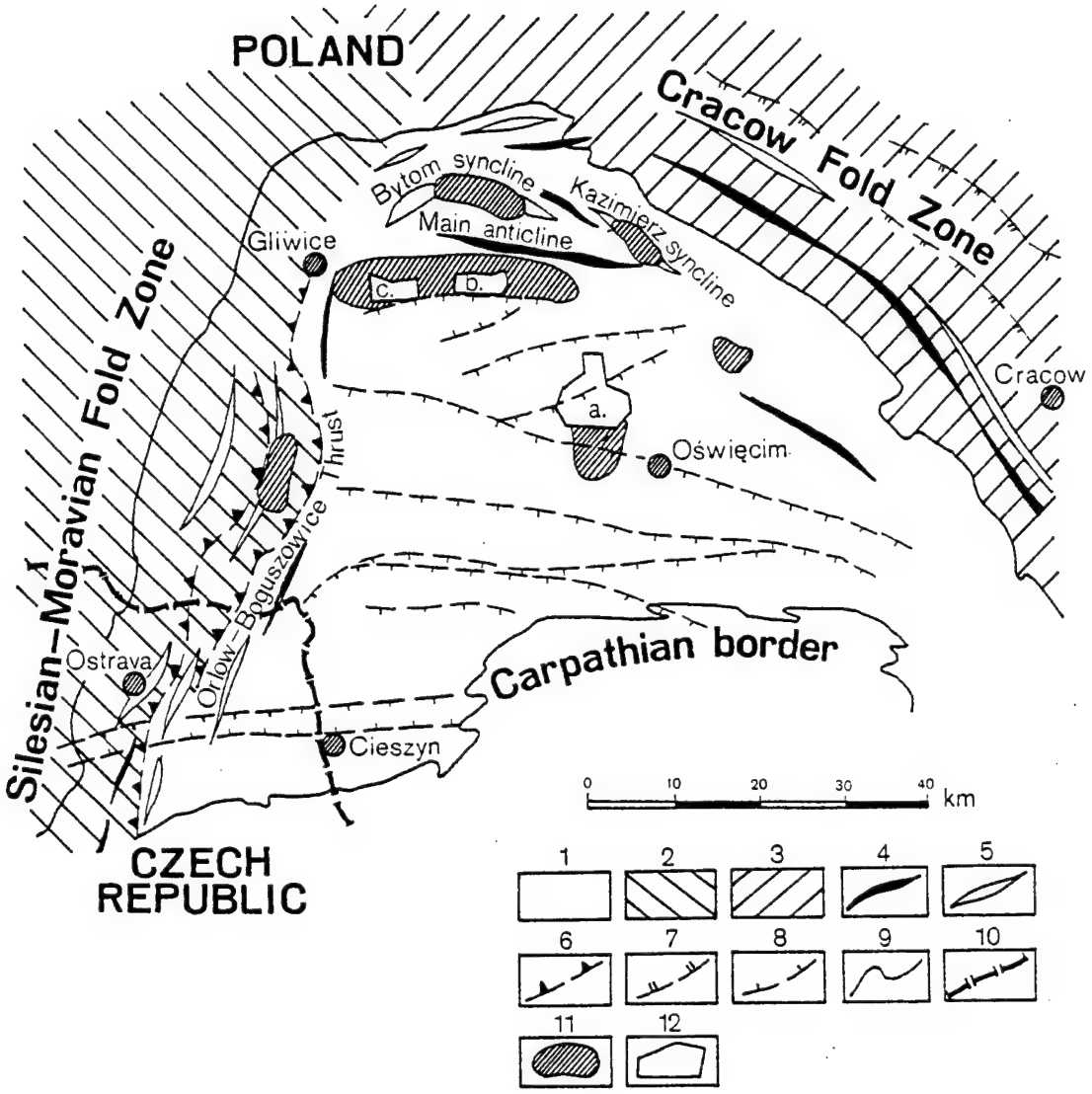

Fig. 1. Tectonic zones of the Upper Silesian Coal Basin (USCB): (1) zone of disjunctive tectonics, (2) zone of fold tectonics, (3) zone of fold-block tectonics, (4) anticlines, (5) synclines, (6) thrusts, (7) main faults, (8) main Alpine faults or reactivated faults, (9) border of the USCB, (10) state border, (11) seismic areas, (12) investigated mines: (a) Ziemowit, (b) Wujek.

Block between two folded zones. Thus three main zones with different types of tectonic structure can be distinguished (Fig. 1): folded tectonics zone - a narrow belt in the western part of the Basin, parallel to the Silesian-Moravian Fold Zone, with the structure created in a compressive stress field with compression direction decreasing from the west to the Orlow-Boguszowice thrust; folded-block tectonics zone - specific and typical for the Cracow branch of orogene in the north-eastern part of the Basin with the general NW-SE direction of folded structures; and disjunctive tectonics zone - the central part of the USCB, where the main strike direction of geological structures is west-east, reflecting the block construction of the basement.

In relation to the units formed during the Alpine orogeny, the USCB is a part of the Paleozoic platform of Central Europe in a close neighbourhood of the Alpine folded structures. According to Kotas (1985), the USCB position is in the basement of the Fore-Carpathian Depression, although only its eastern part is covered by a huge Cenozoic cap-rock. The southern part of the Basin is situated under the allochtone of the outer Carpathian thrusts. The small north-eastern part of the Basin is covered by a Mesozoic cap-rock of the Silesian-Cracow Monocline.

The USCB area was situated on the edge of two main units of the Paleozoic platform during the Alpine sedimentary cycle: the central syncline developed along the Teisseyre-Tornquiste zone from Trias to the Laramian inversion and the Fore-Carpathian Depression developed after the Laramian inversion. As a result of large stratigraphic gap, there are no described fault structures in the Stephan-Miocene time interval (Upper Carboniferous-Tertiary), excluding the small part of the USCB covered by Triassic deposits. According to Herbich (1981), the Triassic fault pattern is similar to the Carboniferous pattern. The simplified stratigraphic structure of USCB deposits is presented in Fig. 2.

Four strike directions of faults are recognized in the USCB: two main directions N-S and E-W, and two supplementary directions NE-SW and NW-SE. It is believed that the E-W faults have been reactivated at least once during the Alpine orogeny (Kotas *et al.*, 1983; Kotas,

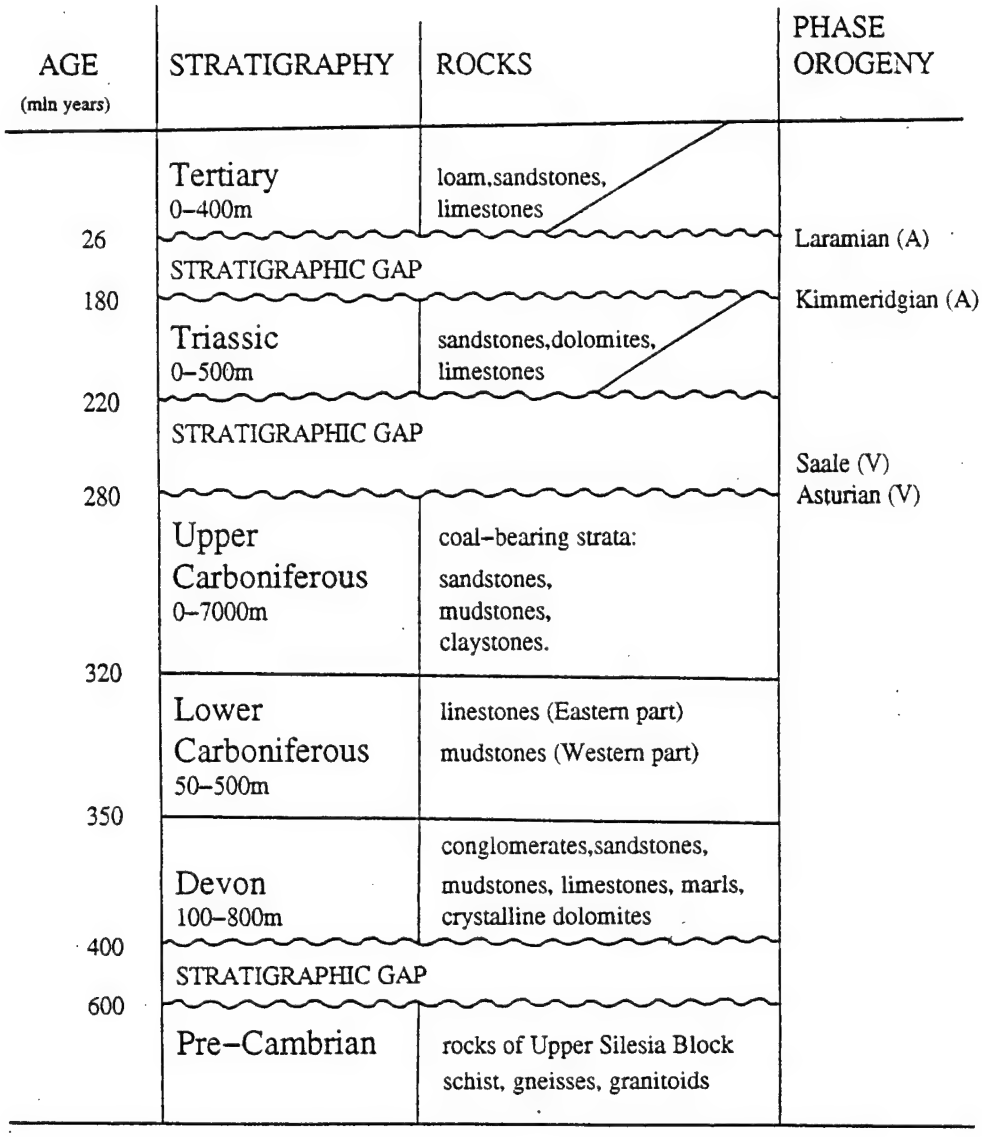

Fig. 2. Simplified stratigraphic structure of the Upper Silesian Coal Basin.

1985). The reactivation of the Variscian structures is an expression of submission to the Carpathian trends, and it happened most probably during the Kimmeridgian phases of the Alpine orogeny. During the Laramian phase an uplifting of the USCB area occurred and its morphological differentiation along the earlier founded tectonic direction, extending latitudinally. Moreover, the sinistral movement assumed along the peri-Penninian collision zone should cause derivative sinistral movements along the parallel of latitude fault systems in the foreland, also in the USCB area (Herbich, 1981).

2.2 Wujek coal mine

Wujek coal mine is situated in the central part of the Upper Silesian Coal Basin, on the southern side of the Main Anticline structure (Fig. 1). The mine was founded in 1899 and its mining area is 7.98 km^2. The coal output is about 8 thousand ton per day. Roof caving is the most often used mining technique, but about 30 % of excavations are filled up by sand. The depth of mining ranges from 560 to 740 m.

The Wujek mine area contains Quaternary and Carboniferous rocks. The Quaternary deposits occur in the whole area, and they overly Carbonifeorus rocks. There are Holocene fluvial deposits and fluvial-glacial and glacial deposits of Pleistocene. The Holocene deposits are muds and sands sedimented in the small rivers and stream valleys as well as the erosion clays on the hill sides. The Pleistocene deposits are mainly boulder clays or carboniferous rocks and glacial boulders. The thickness od Quaternary deposits ranges from zero on the highest hills to about 60 m.

The Carboniferous rocks are divided stratigraphically into four groups. ORZESZE BEDS form the highest part of the Carboniferous profile, but only their lower part is present in the mine area. The upper part was removed by erosion during the Mesozoic and Cenozoic periods. The Orzesze beds consist of clay and mudstones with small sandstone inserts. Numerous coal seams are present, but only a few of them reach thickness of 1 m. The most important seams for mining are coal seams 350, 352, 353, 354, 360, 364/1, 364/2. They are however

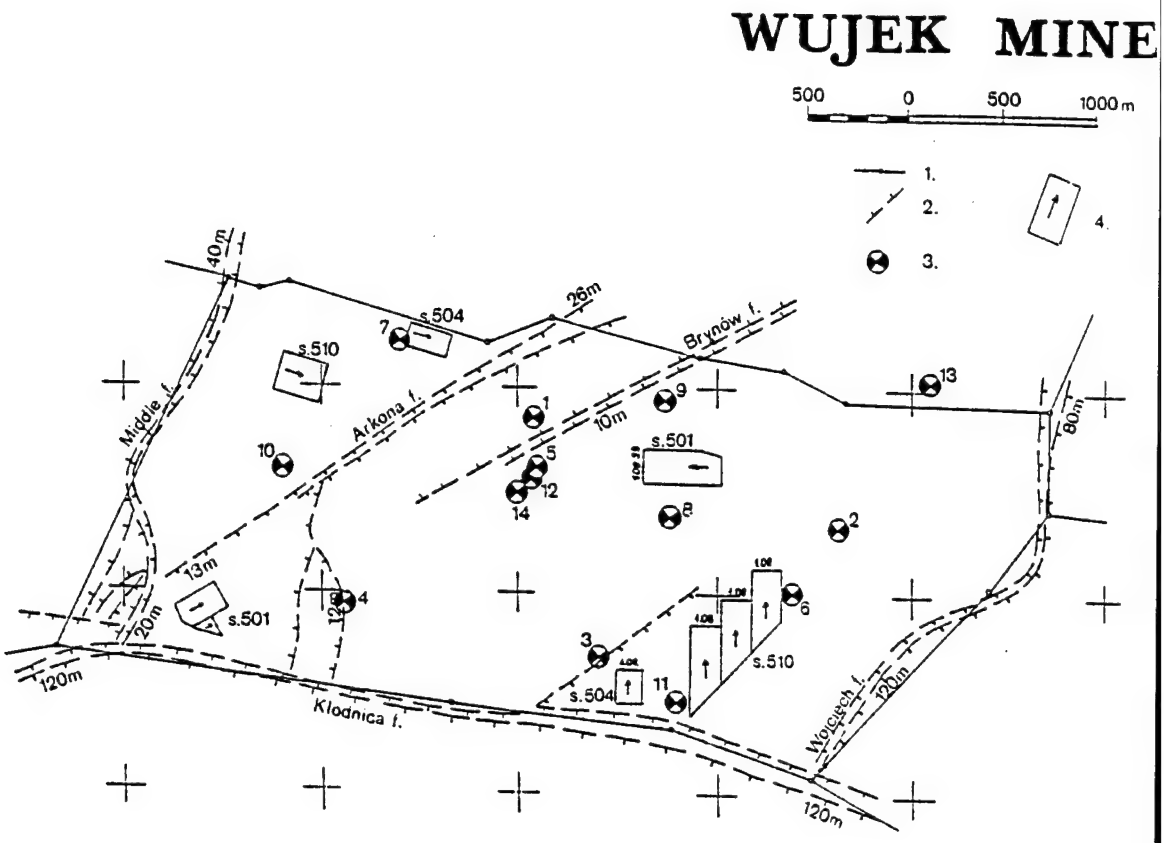

Fig. 3. Map of the Wujek coal mine: (1) mine boundary, (2) major faults, (3) seismic stations, (4) longwall excavations in 1992 and 1993.

worked out at Wujek mine. RUDA BEDS consist of claystones with a small number of sandstone beds, althought in the lower part the sandstones become the main rock of these beds. The thickness of coal seams is greater then in the Orzesze beds. In the upper part of Ruda beds the most important coal seams are 402, 403/2, 405, and 407. The lower sandstone part has only one coal seam of the thickness accepted by mining, coal seam 416 with thickness up to 5.5m. The total thickness of the lower sandstone part of Ruda beds ranges from 250 to 270 m, and the thickness of the whole Ruda beds range from 410 to 500 m. The Ruda beds stratigraphically belong to Namurian C. SADDLE BEDS are the most important in the Carboniferous profile in the Wujek mine area. The petrographic structure is similar to that in the lower part of Ruda beds. These beds contain the thickest coal seams in the area. Five coal seams with a maximum thickness up to 9 m are numbered as seams 501 (with thickness up to 9 m), 504 (with thickness 2.5-3 m), 506, 507 (with thickness up to 1.5 m),and 510 (with thickness up to 6.5 m). These seams are excavated at present at Wujek coal mine. The Saddle beds stratigraphically belong to Namurian B. POREBA BEDS are situated at depths below 600-800 m. They form the highest part of Namurian A, and consist mainly of claystones. Nine coal seams are present in the mine area with thickness ranging from 0.3 to 1.2 m The thickest are seams 615, 618, 620, and 621. But they are not yet excavated.

Wujek coal mine is situated on the southern side of the Main Anticline, dipping gently to the south and cut by the Klodnica fault. The strike direction of Carboniferous beds is E-W and the dip angle is 4-6^{o} to the south. The mine area is bounded by the following faults (Fig. 3):

(1) Middle (Środkowy) fault is a natural western boundary of the mine area. Dip of the fault ranges from 40 to 65^{o} to the west. The strike direction is N-S (NNE-SSW) and the maximum throw of the fault reaches 40 m.

(2) Arkona fault is bounding the western part of the mine area, and its strike direction is NE-SW (partly NNE-SSW). The throw of the fault ranges from zero in the Saddle beds in the south-western part to 30 m in its central part belonging to the Ruda beds. The dip angle of the fault is 80-83^{o} to the south-east.

(3) Brynow fault is situated in the northern part of the mine area and has the NE-SW strike direction. Its maximum throw is 10 m in

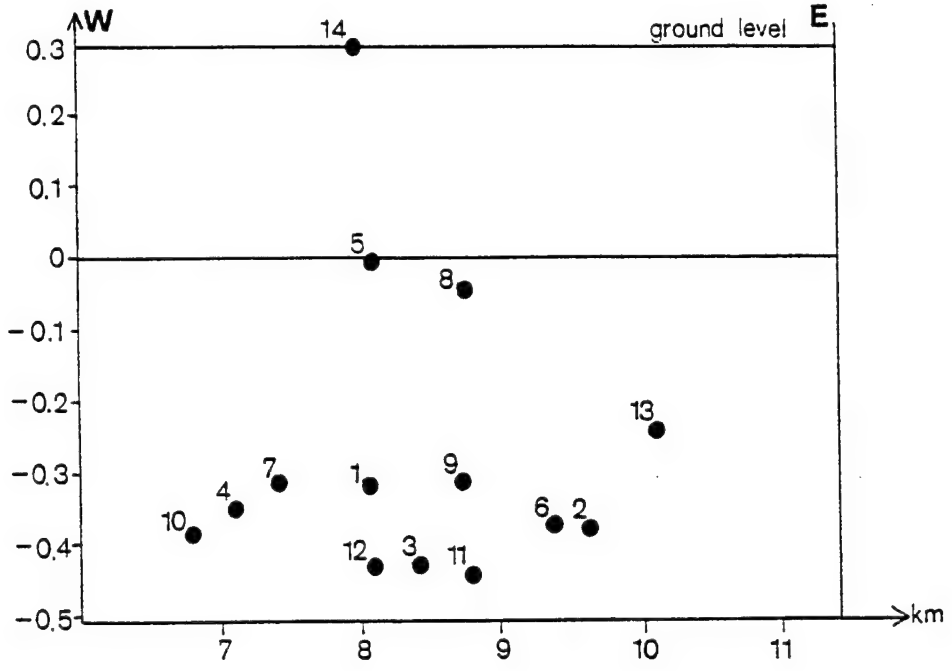

Fig. 4. Vertical distribution of seismic stations at Wujek mine. Ground and sea levels are marked.

the mine area, but in the north, off the mine boundary, it increases to 30 m. The dip angle of the fault is above 80^{o}.

(4) Wojciech fault forms the eastern boundary of the mine area and its strike direction is NE-SW. The throw of this fault ranges from 80 m in the north to 120 m in its southern part. The dip angel ranges from 45 to 75^{o}; the smallest angels are observed in the northern part.

(5) Klodnica fault is one of the most important fault dislocations affecting tectonics of the Upper Silesian Coal Basin. Its strike direction is E-W. In the Wujek mine area the throw of the main fault is from 130 to 220 m, and the fault forms a natural southern boundary of the mine. The fault cuts the Carboniferous and Tertiary deposits situated on its southern side. The fault is of Miocene age, or at least strongly renewed during the Alpine orogeny.

(6) There are many minor faults in the area, with throws up to 10 m. The largest of them are situated in close vicinity of the main faults. Smaller faults (with throws up to 3 m) are considered in particular coal seams as local fractures.

The region of the Main Anticline, where Wujek mine is situated, is the area of the highest seismicity in the Upper Silesian Coal Basin. The strongest seismic events are characterized by seismic energy in excess of 10^{8}J. The catalogue, for example, of the strongest tremors between 1984 and 1992 contains 2 events with energy exceeding 10^{8}J, 22 events with energy over 10^{7}J, and 89 events with energy over 10^{6}J. The strongest events in the mine are connected with the described fault zones. The tremors cause occasionally rockburts in the mining excavations, and 16 serious rockburts occurred between 1984 and 1992 in coal seams 416, 501, 507, and 510. Seismicity at Wujek mine is monitored by an underground seismic network composed of 14 seismometers. Their horizontal distribution is shown in Fig. 3 and their vertical distribution is presented in Fig. 4.

2.3 Ziemowit coal mine

Ziemowit coal mine is situated in the south-eastern part of the Upper Silesian Coal Basin, in the Main Syncline structure (Fig. 1). It was founded in 1952 as a one of the biggest Polish coal mines with an area of 61.1 km^{2}. It has the biggest coal output in Poland (about

27 thousand ton per day). The coal is mined entirely with roof caving. technique. The present depth of mining ranges from 260 to 620 m.

The Ziemowit mine area consists of rocks from the following stratigraphic stages:Quaternary, Tertiary, Triassic,and Carboniferous.

The Quaternary rocks are fine and middle grain sands with clay, partly with lenses of a gray boulder clay. The deposits show considerable differentation, both in the horizontal and vertical directions in the entire area. The thickness of deposits ranges from 0.5 m in the southern and north-eastern part of the mine area to about 50 m in the northern part. The deposits were mainly formed during the Cracow glaciation in the Lower Pleistocene, and they are of a fluvio-glacial origin. The Holocene deposits in the river valleys (sands and muds) are the youngest geological deposits in the described area.

The Tertiary deposits are situated on the rough surface of the Carboniferous and Triassic deposits, except the northern and central part of the mining area. Their thickness reaches a maximum value of 210 m. Generally, the thickness of Tertiary strata increases from the central to peripheral parts of the mine, but reduction of thickness is also observed to the south and east from the mine boundary. The Tertiary deposits are represented by marine deposits of the Miocene age (gray and gray-green marl clays with claystones in the lower part and thin inserts of fine grain and mud grain sandstones). In some boreholes gypsum-bearing beds were detected, represented by clays with pure crystalline gypsum inserts. The lower part of Tertiary deposits consists of 0-30 m thick beds of sand-bearing clays and claystones, and in the eastern part clay-bearing sands and sandstones and conglomerates with parts of Triassic and Carboniferous rocks are present.

The Triassic rocks are observed in the southern part of the mine area. In the central and northern area the Triassic deposits consist of separated, local parts. The rocks of the Lower (gray marl) and Middle (Gogolin limestones) Triassic are present in the area. The thickness of Triassic strata ranges from 0 to 130 m in the southern part,and from 0 to 80 m in the northern and central parts of the mine.

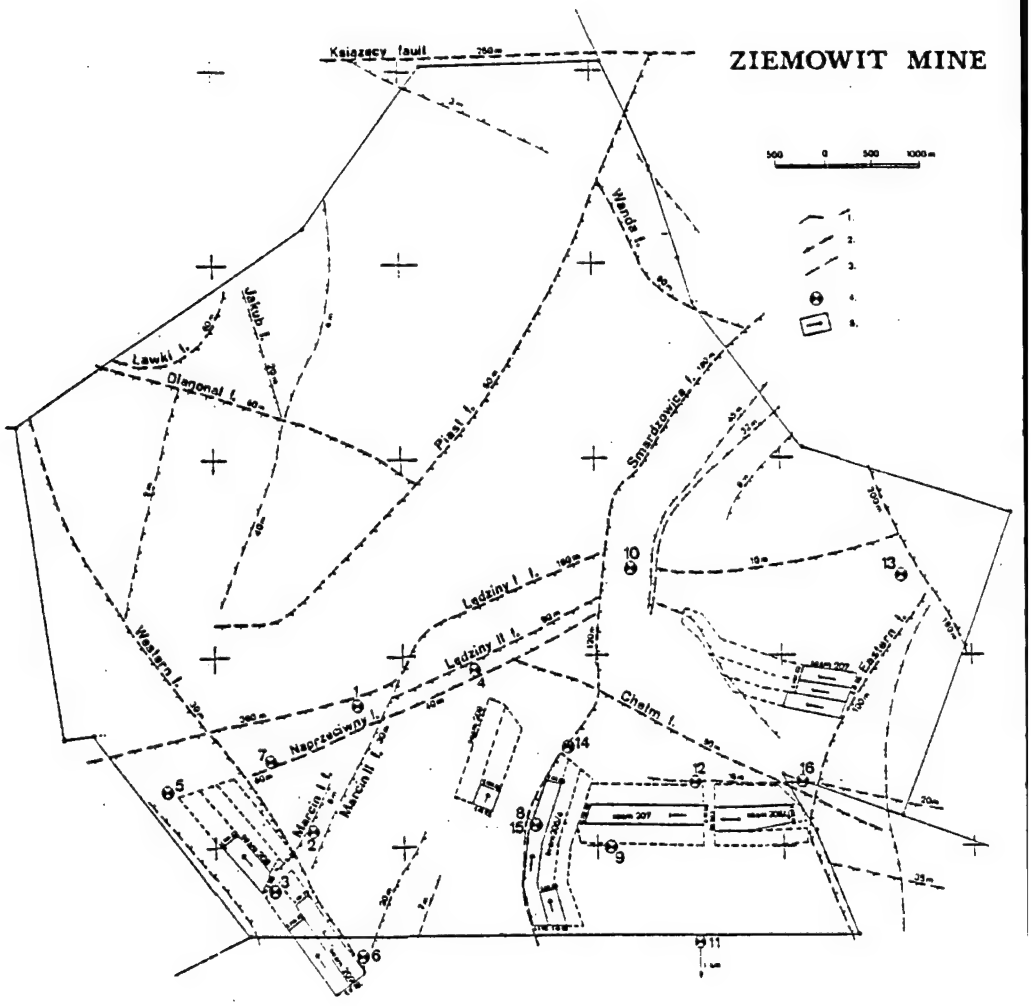

Fig.5. Map of the Ziemowit coal mine: (1) mine boundary, (2) major faults, (3) minor faults, (4) seismic stations, (5) longwall excavations in 1992 and 1993.

The Carboniferous strata up to a depth of 1000 m is represented by Libiaz, Laziska, and Orzesze beds. The Libiaz beds contain fine grain sandstones with claystones and coal, and they form the upper part of the Carboniferous deposits in the area. The Laziska beds have thickness from 540 m in the south-east to 260 m in the north-east. They consist of thick sandstones and conglomerates with parts of quartz, igneous rocks and claystones, and 24 coal seams (numbered from 202-216). The thickest are coal seams 207 and 209. The Laziska coal seams are present only in the southern part of themine. The Orzesze beds are mined out only in their upper part, to the north from the Ledziny fault, where seam 308 is excavated. The total thickness of the Orzesze beds reaches 620 m in the north- eastern part and 700 m in the south-western part..of the mine. The Orzesze beds consist of arenaceous shales and mudstones with smaller amount of sandstones than in the Laziska beds. The thickness of coal seams ranges from 0.7 to 3.6 m.

The Ziemowit mine is situated in the central part of the Main Syncline, and the general dip of strata is 3-4^{o} to SE. This is an area of typical fault tectonics, with numerous major faults forming a local horst structure called the Ledziny horst (Fig.5). The horst is bounded by the Ledziny and Smardzowice fault with throws from 10 to 30 m. Two generations of faulting can be considered in the area: faults younger than Tertiary; called Ledziny, Diagonal, Western, Northern, and Chelm; and faults elder than Tertiary; named Jakub, Marcin, Smardzowice, Imielin, and Eastern. The angular discordance is observed between the deposits of Carboniferous, Triassic, and Tertiary. The Triassic deposits are characterized by a small dip of 3^{o} to NW and they overlay an erosion surface of Carboniferous rocks. The Tertiary (Miocen) deposits are horizontal and overlay the submiocen erosion surface formed during the Alpine orogeny in the Lower Tertiary.

The Ziemowit mine is located in the south-eastern part of the Upper Silesian Coal Basin, where rather low seismicity induced by mining is observed. The mine is characterized by a middle level of seismic activity. Piast and Czeczott coal mines, situated to the south are also characterized by a low level of seismicity and they form the southern part of the seismic zone. The seismic area in the Ziemowit

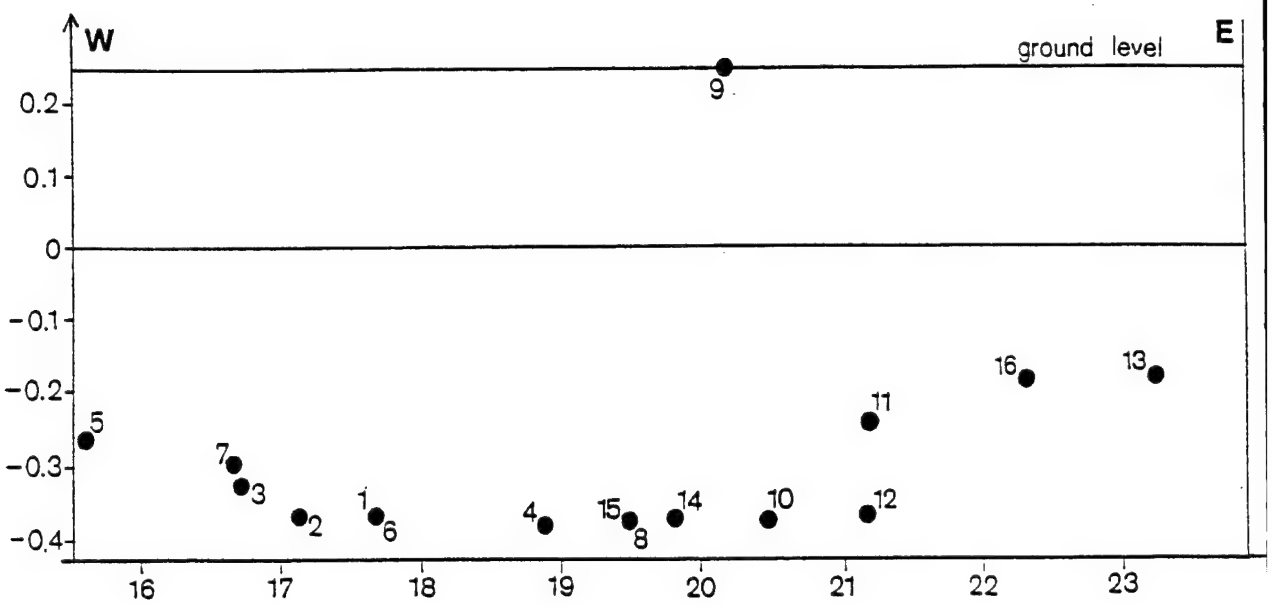

Fig. 6. Vertical distribution of seismic stations at Ziemowit mine. Ground and sea levels are marked.

mine itself is limited to its southern part between the Ledziny fault in the north and the Eastern fault in the east (Fig. 5). Seismicity at Ziemowit coal mine is not well understood. The mine is relatively new, and although seismicity there is observed to be increasing, it was not expected when rockmass properties in the mine were considered. So far, no rockburts have occurred. The underground seismic network at Ziemowit coal mine is composed of 15 digital seismometers. Their horizontal and vertical distributions are shown in Figs. 5 and 6, respectively.

III. SEISMIC NETWORKS AND DATA

3.1 Wujek coal mine

Wujek coal mine has a local seismic network composed of fourteen vertical component sensors. Twelve of these sensors are connected to a digital station and have been used in this study. The other two sensors, numbered 6 and 14 (Figs. 3 and 4), are recorded in analogue form and have not been used. The limit number of twelve sensors is due to the automatic seismic station PCM-G which has only 12 channels.

The digital network is working under a system called PCM-G and the registration is done under system Aramis. The system Aramis allows for 16 channels, 12 of which are used to record the seismic data from the 12 channels of PCM-G. Of the remaining 4 channels, 2 are connected to geophones and 2 are idle. The digital network may be thought as consisting of 12 vertical seismometers SPI-70, transmission line (with maximum resistance of 700 Ohm at 6 km distance), 10 bit a/d converter, and recording and analyzing devices.

The characteristics of the digital network are as follows:

- SPI-70 seismometers of 1.5 s free period, Polish production, are used. The seismometers are powered by 10 Volt D.C.; a full 10 Volt output is their maximum amplitude, 0 Volt output corresponds to their minimum amplitude, while in absence of seismic signal they give an output of about 5 Volts.
- The seismic signals are digitized at the central station; a 10-bit converter is used. The sampling frequency is 250 Hz and the system dynamics is 60 dB. Ground velocity is recorded and the frequency response is flat between 0.6 and 25 Hz.
- The system works in a triggering mode and an automatic detection of signals is in use, based on any single channel. The system therefore is not very effective and often noise turns the recording system on. The length of the seismic signals depends on their size, typically it is of the order of three seconds and the end of the signal is cut off.

The signals from different seismometers were calibrated according to the amplitude-frequency characteristics for the appropriate seismic channels. The characteristics were taken from an internal report of June 1993 entitled "Characteristics of transmission lines and amplifications of channels of seismic equipment working at Wujek coal mine".

The digital seismic data are written to files on a hard disk of an IBM PC-486 computer. Since the automatic detection is based on a single channel, the files written down are mostly noise. Therefore, they are subject to manual selection. Noise files are removed from the hard disk at this step, as well as signal files of seismic events from mines other than Wujek. The remaining files are stored as long as there is free space on the hard disk. Then they are copied to 5.25 inch floppies and deleted from the hard disk. For the purpose of our study, the files were copied to 5.25 or 3.5 inch floppies on a monthly basis.

3.2 Ziemowit coal mine

Ziemowit coal mine has a local seismic network composed of twenty two seismometers. Fifteen of these seismometers are connected to a digital recording system and have been used in this study (Figs. 5 and 6). The other seven stations are analogue and therefore they have not been used. The seismic stations are divided into two subnetworks of eight stations each (one station is common to both subnetworks), oriented for recording seismic events in two different regions of the mine (Eastern and Western). Each of the subnetworks may work independently. Strong seismic events are recorded by the both subnetworks, while small events activate only one of the subnetworks.

The digital network is working under a system called LKZ (Lokalny Koncentrator Zapisow - Local Recording Concentrator). The seismic channel of LKZ consists of SPI-70 seismometer of 1.5 s free period (Polish production), transmission line, a/d converter, and recording and analyzing device. The characteristics of the digital LKZ network are as follows:

- SPI-70 seismometers are powered by 10 Volt D.C.; a full 10 Volt output is their maximum amplitude, 0 Volt output corresponds to their minimum amplitude, while in absence of seismic signal they give an output of about 5 Volts.
- The seismic signals are digitized at the central seismic station; a 12-bit converter is used, so 0 Volt output is written down as zero probes and maximum 10 Volt output is written down as 4096 probes. The sampling frequency is 200 Hz and the system dynamics is 68 dB. Ground velocity is recorded and the frequency response is flat between 0.6 and 65 Hz.
- The system works in a triggering mode and an automatic detection of signals is in use. Noise level must be exceeded on at least two channels simultaneously. The detection algorithm runs independently on the two subnetworks, and it often happens that a seismic event is actually recorded only by the subnetwork closer to its source. The seismic signal is recorded for ten seconds, regardless of the size of the seismic event.

The signals from different seismometers were calibrated according to the frequency response for the appropriate seismic channels. The characteristics were taken from an internal report of April 1992, entitled "Amplitude-frequency characteristics of the seismic equipment working at Ziemowit coal mine". It is a general practice of the mine to produce such a report every three years or if any changes to the seismic equipment are made.

The digital seismic data are written to files on a hard disk of an IBM PC-486 computer. Since the automatic detection is based on two channels, there is a considerable amount of files containing just noise. The data is stored for at least three months and then it is deleted. For the purpose of our study, the files were copied to 3.5 inch floppies on a monthly basis.

3.3 Data

At the start of our project, we have selected two mines for this study: Halemba (marked by c in Fig. 1) and Ziemowit. Our choice was based on the quality of the seismic data, taking into account the

TABLE 1. ORIGIN TIME AND LOCATION OF SELECTED SEISMIC EVENTS AT WUJEK COAL MINE.

Event number	Date			Local time		Hypocenter coordinates		
	y	m	d	h	m	X (m)	Y (m)	Z (m)
201	93	02	01	13	35	19040	-9340	-440
202	93	02	02	06	16	19110	-9310	-440
203	93	02	02	23	17	18400	-7360	-380
204	93	02	03	05	40	19090	-9310	-440
205	93	02	08	16	14	19050	-9260	-440
206	93	02	10	13	40	19090	-9310	-440
207	93	02	11	13	05	19080	-9370	-440
208	93	02	11	18	11	19050	-9340	-440
209	93	02	16	05	44	19070	-9270	-440
211	93	02	16	21	46	18530	-7300	-380
214	93	02	18	19	34	19270	-9060	-440
215	93	02	19	21	57	18570	-8660	-380
216	93	02	20	06	36	19020	-9370	-440
217	93	02	22	09	10	19310	-9070	-440
220	93	02	24	18	46	19270	-8990	-440
221	93	02	24	19	11	19140	-9320	-440
302	93	03	02	10	25	19030	-9300	-440
303	93	03	16	04	59	19040	-9280	-440
304	93	03	16	12	08	19070	-9360	-440
305	93	03	17	04	37	18650	-8800	-380
306	93	03	17	05	40	19040	-9360	-440
307	93	03	18	03	06	19010	-9360	-440
308	93	03	20	05	16	19260	-9030	-440
309	93	03	23	19	14	19050	-9310	-440
310	93	03	26	04	55	19030	-9350	-440
311	93	03	26	19	53	19050	-9370	-440
312	93	03	27	00	04	19210	-9030	-440
313	93	03	30	05	36	19210	-9170	-440
314	93	03	30	05	39	19030	-9320	-440
315	93	03	31	18	36	18990	-9360	-440
316	93	03	31	22	48	19230	-8980	-440
401	93	04	13	13	10	19100	-9330	-440

Event number	Date			Local time		Hypocenter coordinates		
	y	m	d	h	m	X (m)	Y (m)	Z (m)
402	93	04	17	04	30	19050	-6800	-380
403	93	04	21	13	35	19010	-9350	-440
405	93	04	26	20	41	19260	-8980	-440
407	93	04	28	08	05	19010	-9350	-440
516	93	05	25	19	39	19030	-9330	-440
518	93	05	31	14	54	18970	-9250	-440
519	93	05	11	12	57	18980	-9310	-440
601	93	06	01	10	58	19240	-8970	-440
602	93	06	01	11	08	19200	-8980	-440
603	93	06	02	06	40	19180	-9140	-440
604	93	06	03	12	07	19270	-9090	-440
606	93	06	08	12	19	19210	-6880	-380
607	93	06	14	16	47	19310	-6810	-380
608	93	06	15	03	48	18980	-9280	-440
609	93	06	23	03	50	19160	-6910	-440
610	93	06	24	20	20	17650	-7380	-400
611	93	06	25	00	53	19400	-8500	-400
612	93	06	25	07	42	18550	-6850	-300
613	93	06	25	11	51	18880	-7300	-380
614	93	06	28	20	24	19370	-6850	-380
615	93	06	28	22	43	19300	-6880	-380
616	93	06	29	23	56	19170	-6910	-380
617	93	06	30	05	05	18000	-6300	-280

number and distribution of seismometers, frequency range, sampling frequency, and dynamic range of the seismic system. At Halemba mine we have run into problems. The frequency response curves of the seismic system there have not been updated and the seismic channels were not properly calibrated. The Halemba staff was not too collaborative and we could not obtain new frequency response curves. In such a situation we were forced to select another mine in the same area as Halemba and our choice was Wujek coal mine (Fig. 1). In comparison to Halemba, the seismic system at Wujek has fewer seismometers (12 versus 14) and lower dynamic range (60 dB versus 68), but the area of the mine is rather small. We have ended collecting the seismic data on July 31, 1993, and the time span for our data is from 1 January to 31 July 1993.

The seismic system at Wujek mine writes the digital data to files on a hard disk of an IBM PC-486 computer. Since the automatic detection is based on a single channel, the files contain mostly noise and they are subject to manual selection at the mine. Noise files are deleted, as well as signal files of seismic events from mines other than Wujek. Most of the remaining data were signals of small events picked up by one or two seismometers closest to the source. Another group of events, which had been deleted, are those associated with blasting. A further few events had to be deleted because their signals overlapped with seismic signals of earlier events, or events from other mines.

This selection procedure has left us with a total number of 129 seismic events. The high-quality records of 55 events out of these 129 events were selected for this study. These events are listed in Table 1. The horizontal source locations, in a local "Sucha Gora" coordinate system, were taken from the catalogue of the mine. The vertical axis X is directed toward the south, the horizontal axis Y is directed toward the west, and the vertical axis Z is directed downward with the beginning at the sea level. The local elevation of the area is about 300 m above the sea level and this value must be added to the listed values of the coordinate Z to obtain the depth below the earth's surface. The vertical locations were assumed at the mining level. In the period of the study, mining was taking place at three levels, at

TABLE 2. ORIGIN TIME AND LOCATION OF SELECTED SEISMIC EVENTS AT ZIEMOWIT COAL MINE.

Event number	Date	Local time	Hypocenter coordinates		
	y m d	h m	X (m)	Y (m)	Z (m)
1	93 01 04	15 46	33720	-20330	-230
2	93 01 06	21 08	33660	-20320	-220
3	93 01 07	22 45	33720	-20310	-250
4	93 01 09	10 49	33770	-20360	-340
5	93 01 11	08 31	33770	-20350	-340
6	93 01 14	13 32	33680	-20260	-220
7	93 01 19	06 47	34830	-17400	-400
8	93 01 19	14 36	33760	-20270	-430
9	93 01 20	12 10	33780	-20300	-350
10	93 01 26	09 10	33720	-20240	-230
11	93 01 26	09 37	32600	-22250	-300
12	93 01 27	14 37	33780	-20270	-360
13	93 01 28	17 53	33760	-20270	-350
14	93 01 28	21 23	33770	-20240	-260
15	93 02 03	16 33	32530	-22160	-250
16	93 02 03	20 49	33770	-20170	-220
17	93 02 08	17 04	33760	-20200	-250
18	93 02 09	10 45	33780	-20230	-250
19	93 02 09	23 00	33710	-20180	-310
20	93 02 11	10 09	33740	-20190	-250
21	93 02 12	09 10	33720	-20140	-280
23	93 02 15	09 45	33730	-20190	-250
24	93 02 15	23 48	33700	-20200	-260
25	93 02 16	20 13	33680	-20190	-250
26	93 02 17	09 53	33750	-20160	-260
28	93 02 18	12 35	33740	-20160	-320
29	93 02 19	15 41	33720	-20200	-260
30	93 02 19	22 08	33700	-20110	-200
31	93 02 19	23 50	32470	-22250	-250
32	93 02 22	09 39	33590	-21050	-410
33	93 02 23	05 20	33750	-20180	-270
34	93 02 24	14 33	33700	-21760	-200
35	93 02 24	16 22	33580	-21020	-250
36	93 02 26	12 16	33740	-20150	-240
37	93 02 26	13 13	32440	-22200	-250
38	93 03 01	21 39	33710	-20100	-210
39	93 03 02	22 42	33550	-20960	-250
40	93 03 03	17 02	33740	-20120	-350
41	93 03 03	21 39	34490	-19430	-200
42	93 03 09	22 47	33700	-20050	-290
43	93 03 10	21 22	33630	-19980	-240
44	93 03 11	12 53	33700	-20110	-230
45	93 03 12	22 01	33790	-21800	-210
46	93 03 16	14 49	33690	-20080	-210
47	93 03 16	23 38	32490	-22170	-250
48	93 03 17	15 30	33730	-20080	-260
49	93 03 18	20 23	33700	-20090	-260

Event number	Date			Local time		Hypocenter coordinates		
	y	m	d	h	m	X (m)	Y (m)	Z (m)
50	93	03	19	20	52	33710	-20100	-250
51	93	03	22	16	27	33700	-20100	-250
52	93	03	23	13	12	33750	-20070	-260
53	93	03	24	11	09	33700	-20070	-210
54	93	03	24	11	54	33680	-21420	-200
55	93	03	25	01	39	32480	-22140	-250
56	93	03	25	21	30	33730	-20020	-270
57	93	03	26	19	07	33740	-20010	-280
58	93	03	28	22	40	33570	-18490	-400
59	93	03	29	23	03	33680	-20070	-240
60	93	03	30	15	55	33700	-20060	-250
61	93	04	02	00	42	33730	-20080	-260
62	93	04	02	12	26	33730	-21830	-200
63	93	04	05	14	36	33690	-20060	-260
65	93	04	06	23	49	33850	-21810	-200
67	93	04	13	10	04	33720	-21860	-200
68	93	04	14	12	32	33670	-19970	-250
69	93	04	15	00	04	33710	-21850	-200
70	93	04	15	17	21	33700	-20050	-240
71	93	04	15	18	18	33690	-21860	-200
72	93	04	16	08	50	34480	-16360	-400
73	93	04	16	10	34	33690	-20030	-230
74	93	04	16	11	03	33720	-21850	-210
75	93	04	16	22	43	33710	-21820	-200
76	93	04	19	18	11	33760	-21870	-200
77	93	04	22	18	12	33710	-21860	-200
78	93	04	24	13	54	33760	-21860	-200
79	93	04	27	22	20	33720	-21910	-200
80	93	04	28	14	24	33720	-21960	-200
81	93	04	30	00	39	33730	-21950	-350
82	93	05	05	00	33	33720	-21900	-200
83	93	05	05	05	18	33540	-18490	-400
84	93	05	05	06	48	34400	-17130	-400
85	93	06	04	11	49	34470	-17110	-400
86	93	06	21	15	07	32300	-22170	-250
87	93	06	28	13	35	32630	-18510	-400

seams 501, 504 and 510, at the vertical coordinates -380, -400 and -440 meters, respectively. These values are practically constant. In the area of the mine the may differ by approximately 10 meters each way. For the few events not associated with mining levels, the vertical location is based on the observed damage.

The seismic system at Ziemowit mine writes the digital data to files on a hard disk of an IBM PC-486 computer. Since the system is composed of two subnetworks of 8 seismometers, each working independently, two data files should be written for each seismic event. In practice, however, only stronger events are recorded in this way. This is because of the way the automatic detectors have been set. Generally, there was more seismic activity in the area of the second, eastern, subnetwork of seismometers than in the area of the first, western, subnetwork (Fig. 6). The automatic detection is based on two channels, separately for each subnetwork, and it happens that some data files contain just noise. Other data files contained small events, recorded only by a few channels. All such files have not been accepted for our database. Some other files also had to be taken out. These include strong events from other nearby mines and events triggered by blasting.

After the selection, there were 87 events left, 37 of which have been recorded by the both subnetworks, 46 by the second subnetwork, and only 4 by the first subnetwork. The seismograms of 83 seismic events out of these 87 events were accepted for our study. They are listed in Table 2. The source locations, horizontal as well as vertical, in a local "Sucha Gora" coordinate system, were taken from the catalogue of the mine.

IV. SOURCE PARAMETERS

4.1 Spectral analysis

The selected 55 events at Wujek coal mine were recorded at distances from about 100 to 3800 m, and the selected 83 events at Ziemowit mine were recorded at distances from about 450 to 6350 m from the hypocenters. The spectral analysis was carried out using interactive computer graphics allowing the choice and rapid change of signal windows on various ground velocity traces. Windows containing *P* and *S* pulses with a variable length were selected in each case. The time series was tapered using a cosine taper affecting a tenth of the window. The ground velocity spectra were then calculated by an FFT routine and corrected for instrumental response. The FFT routine was applied to a moving time window containing from 2^7 to 2^9 data points. If the time series was longer than a single window, then the spectrum for the whole frequency range was calculated by averaging the values obtained from particular windows. In a contrary case, the time series was supplemented by zeros and a special correction for the effect of the added zeros was applied. The correction was adopted from the test carried out on sinusoids. After single integration in the frequency domain, the displacement spectra were obtained. At Wujek mine, the instrumental response is flat for frequencies above 0.6 Hz and below 25 Hz, and the Nyquist frequency is 125 Hz. A spectral bandwidth from 4 to 20 Hz was accepted for further interpretation of the spectra. The observed corner frequencies are well within this interval. The effects of the bandwidth limitation on the estimates of source parameters can be significant when the corner frequencies are not in the middle of the selected frequency band (Di Bona and Rovelli, 1988). At Ziemowit mine, the instrumental response is flat for frequencies above 0.6 Hz and below 65 Hz, and the Nyquist frequency is 100 Hz. A spectral bandwidth from 2 to 40 Hz was accepted for further interpretation; the observed corner frequencies are again well within this interval.

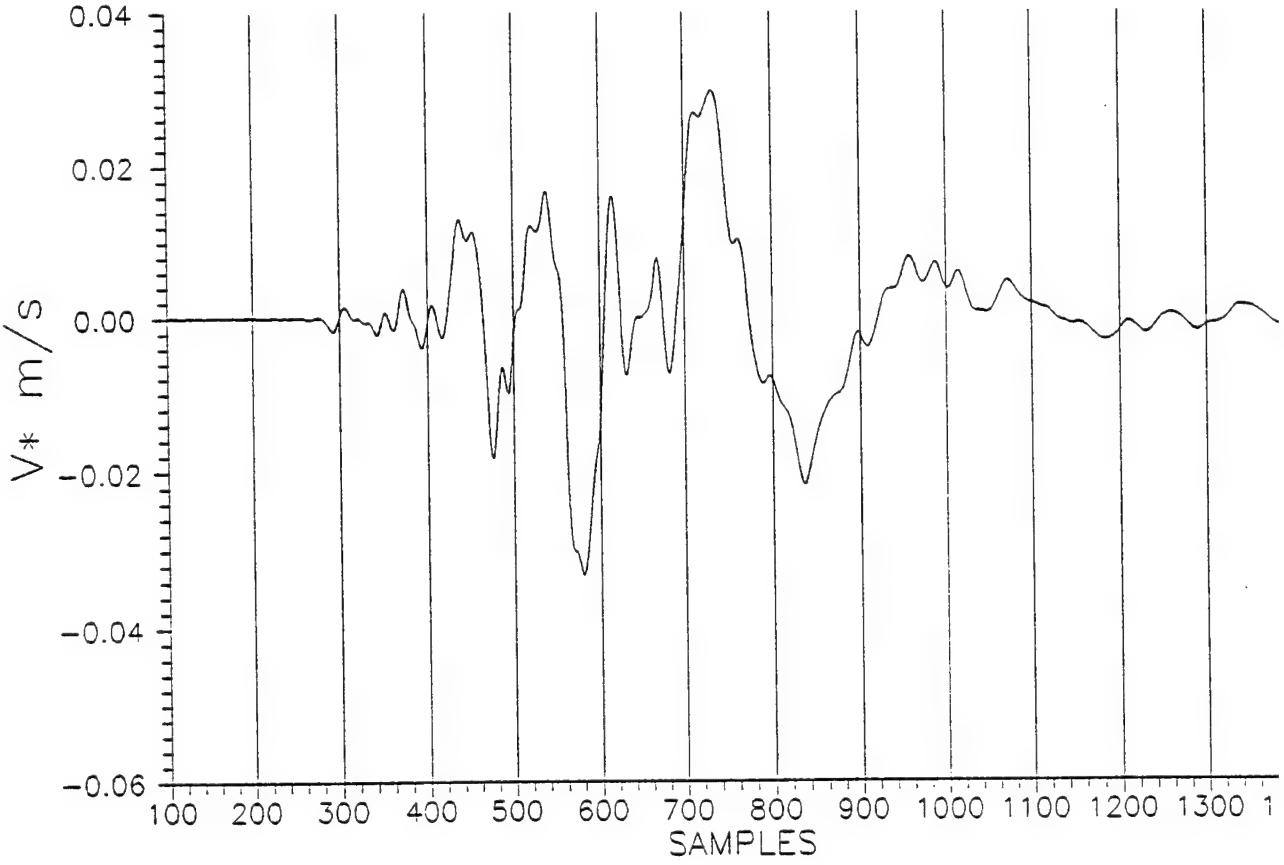

Fig.7. Example of a typical seismogram recorded at Wujek mine from the seismic event of 17 April 1993 (event 402), with moment magnitude M = 2.0, at a distance of 2064 m (channel 10).

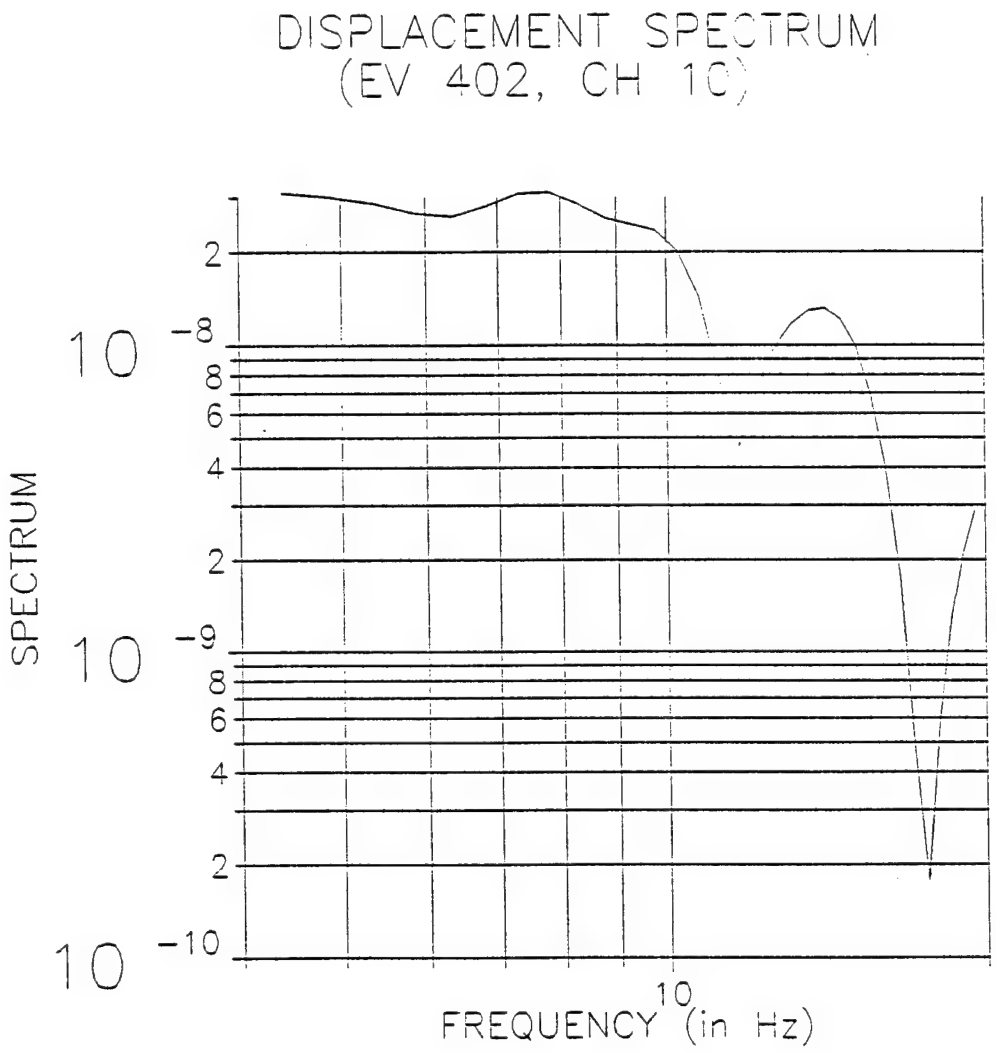

Fig.8. Example of a *P*-wave displacement spectrum from the seismic event of 17 April 1993 (event 402) recorded at Wujek mine at a distance of 2064 m (channel 10). The window for the analysis is taken between samples 271 and 422 (Fig.7).

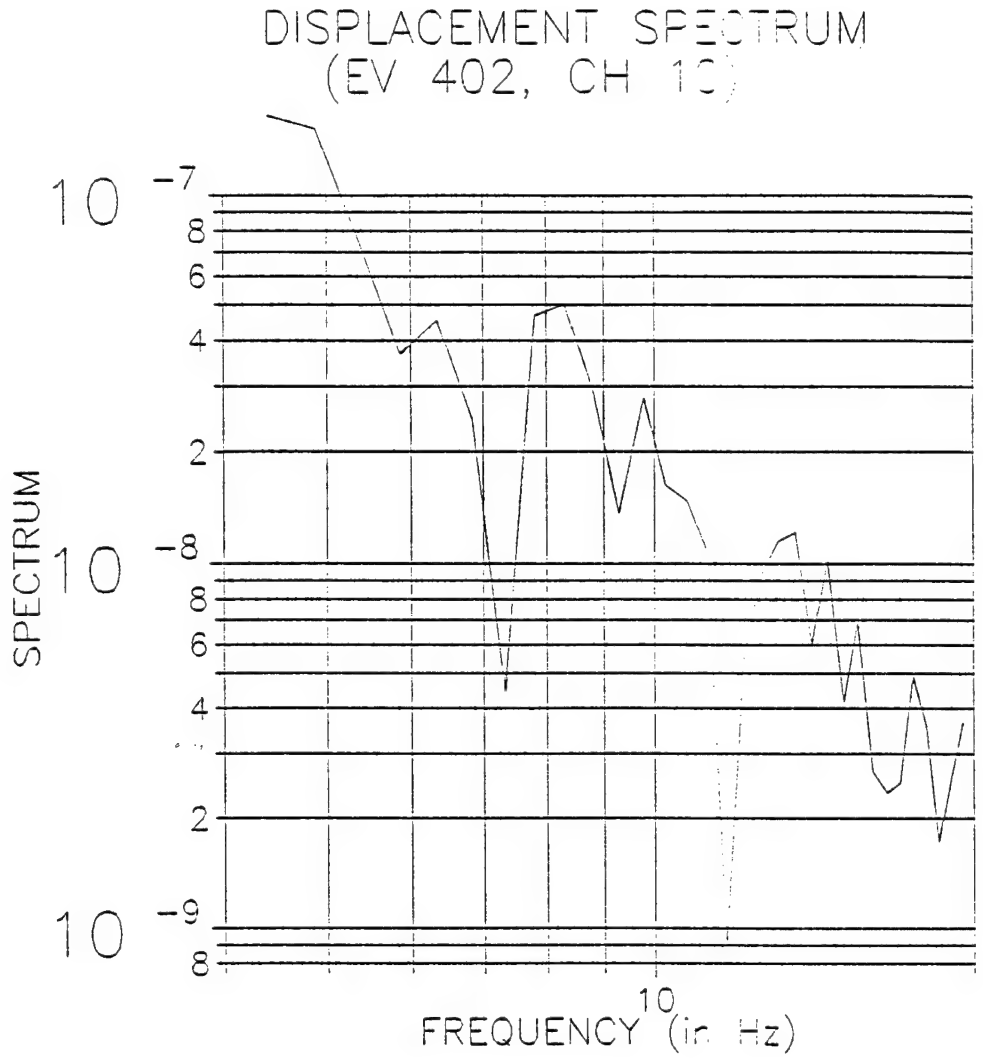

Fig. 9. Example of a *S*-wave displacement spectrum from the seismic event of 17 April 1993 (event 402) recorded at Wujek mine at a distance of 2064 m (channel 10). The window for the analysis is taken between samples 420 and 808 (Fig. 7).

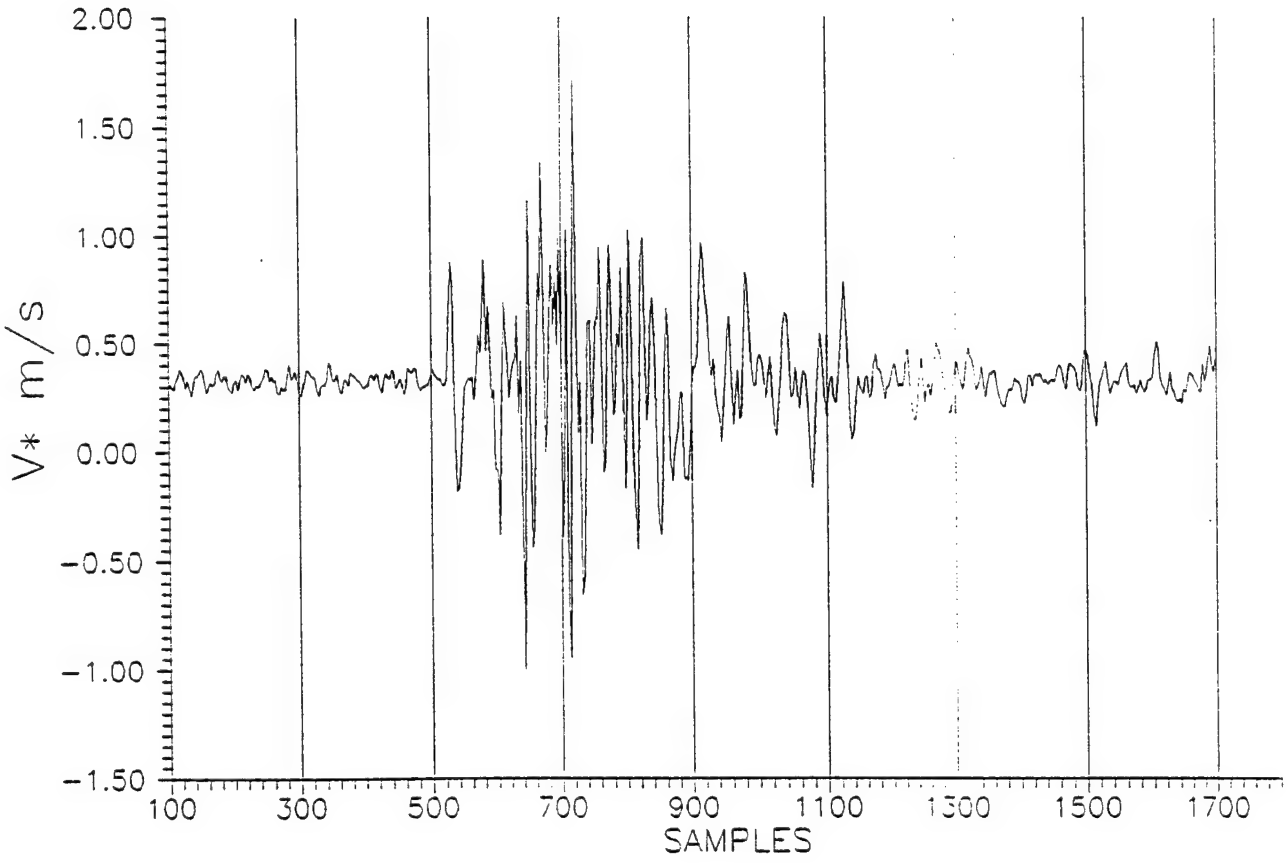

Fig. 10. Example of a typical seismogram recorded at Ziemowit mine from the seismic event of 12 February 1993 (event 21), with moment magnitude M = 1.9, at a distance of 2935 m (channel 4).

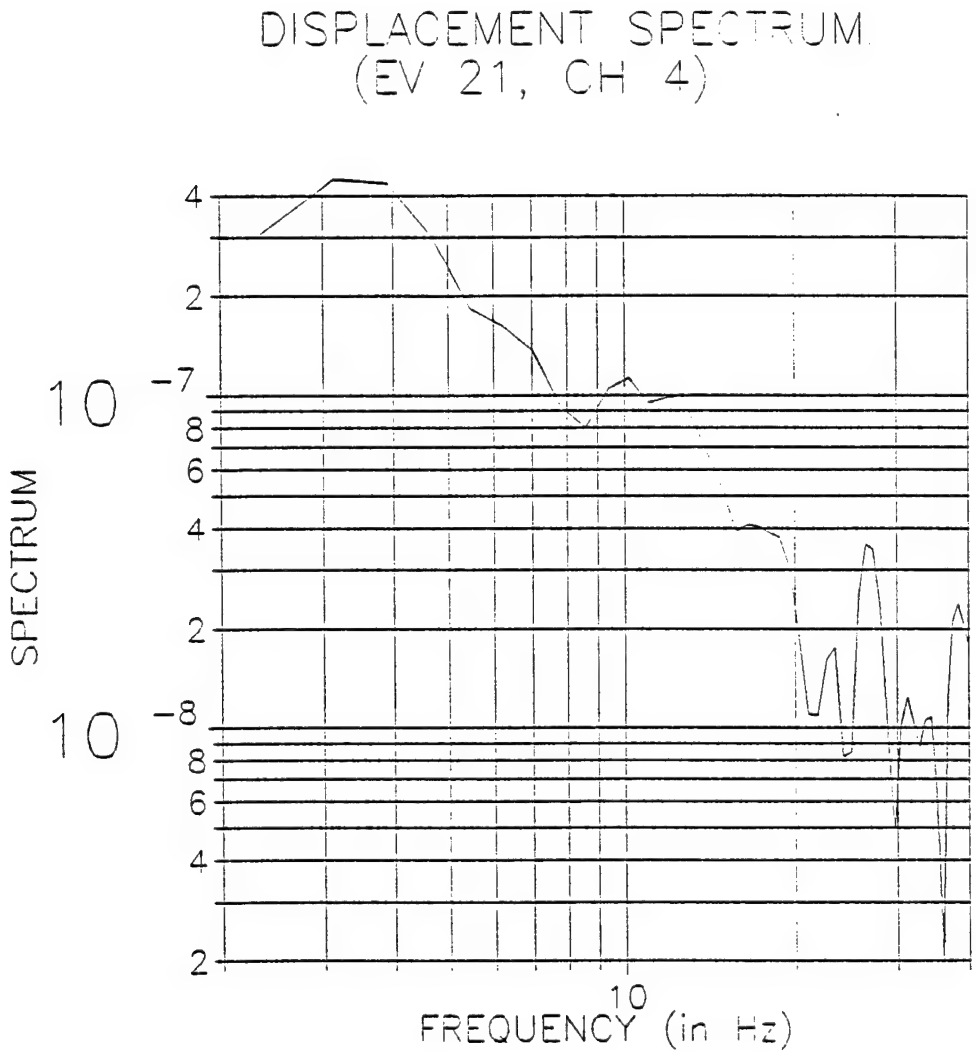

Fig. 11. Example of a *P*-wave displacement spectrum from the seism: event of 12 February 1993 (event 21) recorded at Ziemowi mine at a distance of 2935 m (channel 4). The window for t analysis is taken between samples 520 and 653 (Fig. 10).

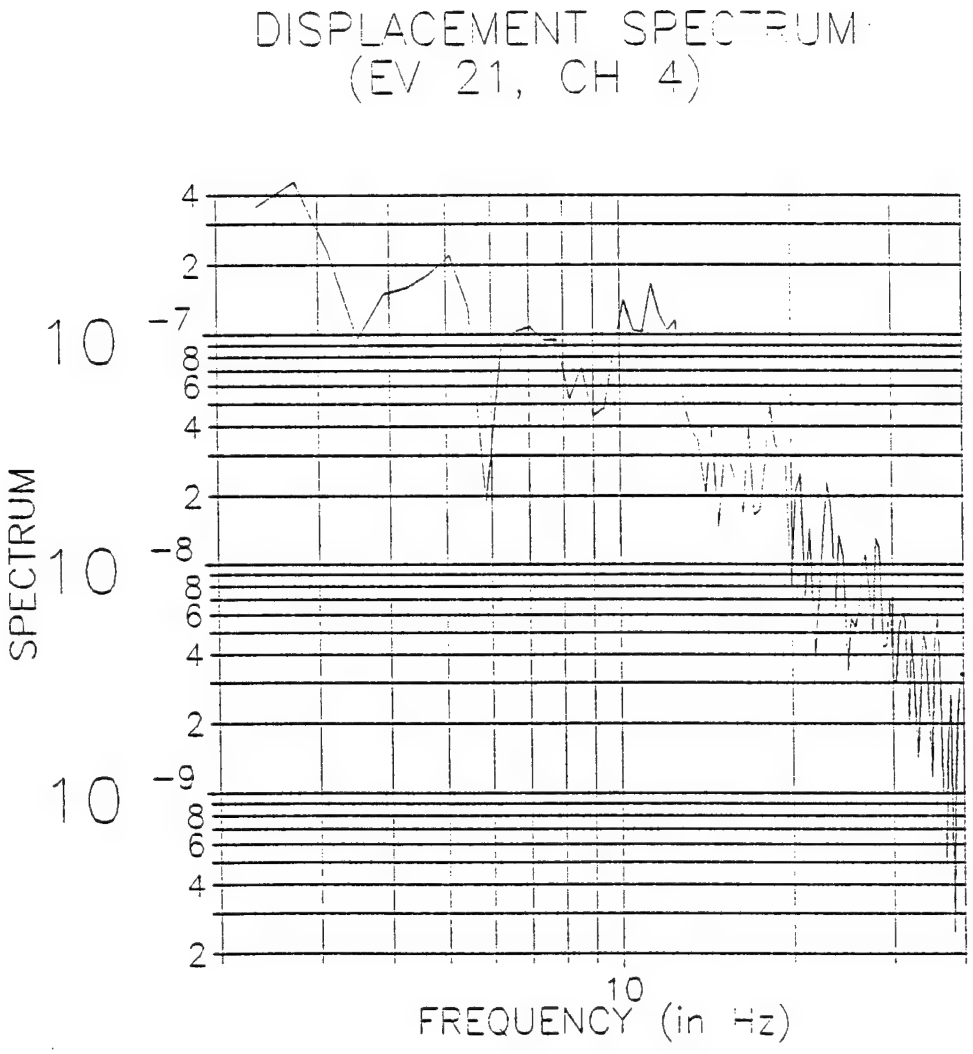

Fig. 12. Example of a *S*-wave displacement spectrum from the seismic event of 12 February 1993 (event 21) recorded at Ziemowice mine at a distance of 2935 m (channel 4). The window for the analysis is taken between samples 656 and 974 (Fig. 10).

The observed spectra must be corrected for attenuation and scattering effects along the travel path of seismic waves. Such corrections are of the utmost importance for the proper retrieval of source parameters of small earthquakes, even if they are recorded at close distances (e.g., Rovelli *et al.*, 1991). The uncorrected spectra are often characterized by the decay coefficient distinctly higher than the most often observed value of 2. In contrast, the corrected spectra of mine tremors are well described by a f^{-2} fall-off (e.g., Gibowicz, 1990a). To correct for attenuation, the displacement spectra were multiplied by the exponential term $\exp(\omega R / cQ_c)$, where R is the hypocentral distance, c is either P- or S-wave velocity, Q_c is the quality factor of either P or S waves, and $\omega = 2\pi f$, in which f is the frequency. The P-wave velocity of 3.8 km/s and the S-wave velocity of 2.2 km/s, reprezenting the average values in the USCB area, were accepted for the calculations. Unfortunetely, no *in situ* attenuation properties of the USCB rock mass are recognized as yet. An assumption that $Q_p = (9/4)Q_s$ (e. g., Burdick, 1978), therefore, was accepted and an approximate value of the quality factor for S waves equal to 200 was chosen for the attenuation correction (e. g., Gibowicz *et al.*, 1977). The attenuation corrections here are not significant. The uncorrected spectra are characterized by a decay coefficient only slightly higher than the most often observed value of 2, and the corrected spectra are well described by a f^{-2} fall-off. The spectral noise level was considerably lower than the signal level in all cases and at all frequencies. An example of a typical seismogram recorded at Wujek mine is shown in Fig. 7, and examples of corrected spectra of P and S waves are shown in Figs. 8 and 9. Similarly, a typical seismogram recorded at Ziemowit mine is presented in Fig. 10 and the corresponding spectra are shown in Figs. 11 and 12.

Various methods are used for the accurate and objective interpretation of seismic spectra to provide reliable estimates of source parameters. The simplest and most often used spectral model is that described by the low-frequency spectral level Ω_o and the corner frequency f_o, above which the spectrum is assumed to fall off as a second power of frequency (Brune, 1970, 1971). For many spectra, however, the corner frequency f_o cannot be determined reliably from the intersection of two asymptotes (e.g., Brune *et al.*, 1979; Snoke *et*

al., 1983). For this reason, the approach proposed by Snoke (1987) can be used, replacing f_o as a spectral observable by a parameter which can be determined reliably, providing a more robust procedure than that conventionally used. The integral J of the square of the ground velocity is such an observable, which is a direct measure of the energy flux of *P* or *S* waves as well. The energy flux, in turn, is a measure of the energy radiated in the *P* or *S* waves, which can be calculated from the relation derived by Boatwright and Fletcher (1984). The simplest calculation of the energy flux is done in the frequency domain, following the method described by Snoke (1987). Such an approach was also used in the previous studies (Gibowicz *et al.*, 1990, 1991).

Thus, two independent parameters Ω_o and J_c were calculated directly from the spectra; Ω_o is the value of the low-frequency level of the spectrum, and J_c is the integral of the square of ground velocity of either *P* or *S* waves. The spectral plateau Ω_o was estimated by inspection on a graphic screen within an interactive computer procedure, into which the calculation of J_c was implemented, following the method described by Snoke (1987), assuming a constant level of the spectrum for $f < f_1$ and an f^{-2} decay for $f > f_2$, where f_1 and f_2 are the limits of the spectral bandwidth. From the low-frequency level Ω_o and the energy flux J_c, the corner frequency f_c was calculated (Snoke, 1987). Thus our input data for the calculation of source parameters are Ω_o, J_c, and f_c, from *P* and *S* waves recorded by several seismometers at Wujek and Ziemowit coal mines.

4.2 Relations between various source parameters

The values of full-displacement vector Ω_o are needed for proper estimates of seismic moment. To account for this, our values Ω_o, obtained from single-component records, were divided by direction cosines which were calculated assuming a straight-line ray geometry between the sources and the sensors. The values of the radiation coefficient, calculated from the double-couple solutions of the moment tensor inversion (described in Section V) for each sensor and for both *P* and *S* waves, were used for the computation of seismic moment. The accepted values of seismic moment M_o, averaged from the values from *P*

TABLE 3. SEISMIC MOMENT AND SOURCE RADIUS

OF SEISMIC EVENTS AT WUJEK COAL MINE

Event number	Seismic moment M_o x 10^{10} (N·m)	Moment magnitude M	P-wave corner frequency f_p (Hz)	S-wave corner frequency f_s (Hz)	Source radius r_o (Hz)
201	5.35	1.12	9.8	8.4	64
202	13.6	1.39	10.3	6.8	68
203	60.0	1.82	11.6	6.9	64
204	4.40	1.07	16.1	13.1	40
205	7.80	1.23	8.7	7.5	71
206	15.5	1.43	8.5	7.5	72
207	6.50	1.18	10.4	6.8	68
208	10.1	1.31	9.7	10.8	58
209	9.15	1.28	8.0	8.8	70
211	41.0	1.71	11.3	7.0	64
214	4.60	1.08	7.9	9.5	69
215	33.0	1.65	7.7	6.9	80
216	8.30	1.25	9.9	8.8	62
217	18.5	1.48	11.5	7.8	60
220	12.4	1.37	10.3	9.4	59
221	16.5	1.45	8.7	7.8	70
302	19.0	1.49	8.8	7.0	73
303	9.05	1.27	9.2	7.2	70
304	9.20	1.28	9.5	6.3	74
305	45.5	1.74	11.3	7.5	62
306	34.0	1.66	7.7	7.2	78
307	14.5	1.41	12.8	9.0	53
308	8.45	1.25	8.7	6.5	76
309	6.95	1.20	9.8	8.2	64
310	13.5	1.39	7.6	5.9	85
311	31.3	1.63	7.9	6.6	80
312	9.30	1.28	8.8	5.6	81
313	226.	2.21	6.0	5.6	100
314	5.25	1.12	11.0	9.2	57
315	6.30	1.17	10.5	7.7	64
316	15.0	1.42	8.5	7.6	72

Event number	Seismic moment M_o x 10^{10} (N·m)	Moment magnitude M	P-wave corner frequency f_p (Hz)	S-wave corner frequency f_s (Hz)	Source radius r_o (Hz)
401	25.0	1.57	6.6	5.1	100
402	121.	2.03	8.6	5.4	84
403	12.5	1.37	9.0	6.1	77
405	13.6	1.39	7.0	6.2	87
407	14.8	1.42	8.3	5.7	83
516	46.5	1.75	7.9	6.1	82
518	10.5	1.32	9.3	6.2	75
519	7.70	1.23	8.3	5.7	83
601	10.0	1.30	8.1	6.3	80
602	13.0	1.38	9.1	6.3	75
603	11.6	1.35	9.9	7.6	66
604	190.	2.16	7.3	4.8	97
606	54.0	1.79	7.2	5.9	88
607	67.5	1.86	9.2	7.4	69
608	32.5	1.64	11.6	6.4	67
609	144.	2.08	6.6	5.8	95
610	42.3	1.72	9.0	6.5	75
611	14.6	1.41	11.5	7.7	61
612	22.5	1.54	11.5	7.1	63
613	17.0	1.46	7.8	6.9	79
614	135.	2.06	6.1	5.4	98
615	21.0	1.52	9.3	6.7	72
616	18.0	1.47	8.3	5.8	82
617	173.	2.13	7.3	4.9	96

TABLE 4. SEISMIC ENERGY AND STRESS-RELEASE ESTIMATE

FOR SEISMIC EVENTS AT WUJEK COAL MINE

Event number	P-wave energy Ep $\times 10^5$ (J)	S-wave energy Es $\times 10^5$ (J)	Total seismic energy E $\times 10^5$ (J)	Stress drop $\Delta\delta$ (MPa)	Apparent stress δa (MPa)
201	0.47	0.58	1.10	0.089	0.027
202	3.60	16.0	20.0	0.190	0.190
203	110.	56.0	170.	1.001	0.368
204	1.90	8.40	10.0	0.301	0.295
205	3.70	1.60	5.30	0.095	0.088
206	1.80	8.00	9.80	0.182	0.082
207	2.70	1.40	4.10	0.090	0.082
208	1.10	2.50	3.60	0.228	0.046
209	1.70	3.20	4.90	0.117	0.070
211	44.0	8.20	52.0	0.684	0.165
214	0.30	2.70	3.00	0.061	0.085
215	1.40	0.41	1.80	0.282	0.007
216	1.00	6.10	7.10	0.152	0.111
217	0.32	5.60	6.00	0.375	0.042
220	0.98	15.0	16.0	0.264	0.168
221	0.88	7.00	7.80	0.210	0.061
302	0.54	1.30	1.90	0.214	0.013
303	3.50	2.50	5.90	0.115	0.085
304	1.60	1.20	2.80	0.099	0.040
305		77.0	77.0	0.835	0.220
306	2.40	1.60	3.90	0.313	0.015
307		18.0	18.0	0.426	0.161
308	2.00	1.20	3.20	0.084	0.049
309		1.10	1.10	0.116	0.021
310	1.60	0.33	2.00	0.096	0.019
311	1.70	0.30	1.90	0.268	0.008
312	1.60	0.79	2.40	0.077	0.033
313	6.40	9.40	16.0	0.989	0.009
314	2.70	0.53	3.20	0.124	0.079
315	1.30	0.93	2.20	0.105	0.045

Event number	P-wave energy Ep x 10^5 (J)	S-wave energy Es x 10^5 (J)	Total seismic energy E x 10^5 (J)	Stress drop $\Delta\delta$ (MPa)	Apparent stress δa (MPa)
316	0.40	3.30	3.70	0.176	0.032
401	0.76	1.50	2.30	0.109	0.012
402	3.50	16.0	19.0	0.897	0.020
403	3.30	1.20	4.50	0.120	0.047
405	6.10	3.30	9.30	0.091	0.088
407	4.60	1.40	6.00	0.113	0.053
516	6.50	14.0	20.0	0.370	0.006
518	2.90	0.42	3.30	0.109	0.041
519	2.30	0.39	2.70	0.059	0.046
601	1.20	0.65	1.80	0.085	0.023
602		1.40	1.40	0.135	0.014
603	6.40	0.37	6.80	0.177	0.076
604		15.0	15.0	0.911	0.010
606	1.20	3.00	4.30	0.347	0.010
607	4.00	5.70	9.70	0.899	0.019
608	5.20	5.10	10.0	0.473	0.040
609		8.90	8.90	0.737	0.008
610	3.30	0.46	3.80	0.439	0.012
611	3.60	1.80	5.30	0.282	0.047
612	0.15	1.80	1.90	0.394	0.011
613	2.60	0.90	3.50	0.151	0.027
614	120.	63.0	190.	0.627	0.183
615	3.50	0.32	3.90	0.246	0.024
616	2.10	2.00	4.10	0.143	0.030
617	1.80	14.0	16.0	0.858	0.012

TABLE 5. SEISMIC MOMENT AND SOURCE RADIUS

OF SEISMIC EVENTS AT ZIEMOWIT COAL MINE

Event number	Seismic moment M_o x 10^{11} (N·m)	Moment magnitude M	P-wave corner frequency f_p (Hz)	S-wave corner frequency f_s (Hz)	Source radius r_o (Hz)
1	9.88	1.97	11.2	5.3	75
2	22.0	2.20	13.7	6.4	62
3	7.92	1.90	10.0	7.1	68
4	2.20	1.53	20.3	9.0	43
5	1.55	1.43	15.0	9.6	48
6	19.5	2.16	9.3	4.9	85
7	8.50	1.92	10.6	6.2	70
8	1.57	1.43	15.8	9.1	48
9	2.35	1.55	10.2	8.5	62
10	10.8	1.99	8.9	6.3	76
11	12.6	2.04	16.5	9.4	46
12	1.20	1.36	14.3	7.6	55
13	1.30	1.38	15.8	8.9	48
14	5.60	1.80	11.3	7.4	62
15	6.50	1.85	14.1	7.8	55
16	10.6	1.99	13.4	6.1	65
17	38.0	2.36	8.3	5.4	86
18	3.90	1.70	20.5	7.5	48
19	4.20	1.72	15.1	6.0	62
20	5.70	1.81	13.5	8.2	54
21	6.75	1.86	13.9	7.7	55
23	7.25	1.88	12.7	5.7	68
24	1.83	1.48	14.7	10.0	47
25	4.90	1.76	15.7	10.1	46
26	9.75	1.96	12.9	6.6	62
28	2.88	1.61	14.1	7.5	56
29	3.70	1.68	12.3	6.4	65
30	4.50	1.74	15.4	5.5	64
31	7.45	1.88	12.0	8.2	58

Event number	Seismic moment M_o x 10^{11} (N·m)	Moment magnitude M	P-wave corner frequency f_p (Hz)	S-wave corner frequency f_s (Hz)	Source radius r_o (Hz)
32	4.45	1.74	12.5	6.0	67
33	6.20	1.83	11.4	7.4	62
34	2.40	1.56	16.8	12.0	41
35	3.05	1.63	12.2	7.3	61
36	4.73	1.75	12.8	7.2	60
37	16.0	2.11	14.1	7.0	58
38	2.92	1.61	11.6	6.6	66
39	6.70	1.85	8.4	6.1	80
40	16.0	2.11	10.1	7.1	68
41	3.20	1.64	10.6	6.1	71
42	8.65	1.93	8.3	5.3	86
43	11.5	2.01	10.3	4.8	82
44	8.76	1.93	8.8	6.4	76
45	20.5	2.18	12.1	7.8	59
46	3.30	1.65	11.7	6.8	64
47	15.5	2.10	7.6	10.9	67
48	23.5	2.22	9.5	5.0	83
49	7.65	1.89	11.4	5.9	70
50	12.4	2.03	11.2	8.6	58
51	28.0	2.27	9.6	4.8	85
52	6.50	1.85	10.4	5.4	77
53	4.95	1.77	8.9	4.0	100
54	1.80	1.47	11.4	6.3	68
55	11.1	2.00	7.7	4.8	94
56	6.98	1.87	10.5	4.2	89
57	1.90	1.49	11.9	4.9	76
58	27.0	2.26	7.6	4.2	100
59	19.0	2.16	9.2	4.3	93
60	4.50	1.74	12.7	4.7	77
61	9.15	1.94	12.3	8.7	55
62	10.0	1.97	11.8	7.7	60
63	13.0	2.05	10.4	5.4	76
65	18.0	2.14	8.3	6.7	77
67	23.0	2.21	12.5	6.0	66

Event number	Seismic moment M_o x 10^{11} (N·m)	Moment magnitude M	P-wave corner frequency f_p (Hz)	S-wave corner frequency f_s (Hz)	Source radius r_o (Hz)
68	6.20	1.83	15.4	10.0	46
69	14.0	2.07	7.7	6.8	80
70	3.04	1.63	13.2	7.7	56
71	14.1	2.07	8.3	6.1	80
72	4.25	1.72	12.1	9.0	55
73	2.55	1.57	13.4	9.4	51
74	42.3	2.39	6.3	5.6	96
75	3.80	1.69	9.3	10.6	60
76	13.5	2.06	9.3	6.1	75
77	9.10	1.94	9.4	4.1	93
78	9.80	1.96	7.7	6.8	79
79	3.20	1.64	9.8	7.6	66
80	7.80	1.90	10.1	8.8	61
81	23.0	2.21	9.4	6.6	72
82	5.20	1.78	8.4	6.1	80
83	16.0	2.11	6.6	5.1	100
84	3.50	1.67	17.6	13.1	38
85	5.65	1.80	12.6	6.3	65
86	5.10	1.77	10.6	7.9	62
87	3.10	1.63	18.1	8.7	46

TABLE 6. SEISMIC ENERGY AND STRESS-RELEASE ESTIMATE

FOR SEISMIC EVENTS AT ZIEMOWIT COAL MINE

Event number	P-wave energy Ep x 10^6 (J)	S-wave energy Es x 10^6 (J)	Total seismic energy E x 10^6 (J)	Stress drop $\Delta\delta$ (MPa)	Apparent stress δa (MPa)
1	15.0	7.70	23.0	1.02	0.31
2	20.0	20.0	41.0	4.04	0.25
3	34.0	13.0	47.0	1.10	0.80
4	22.0	14.0	36.0	1.21	2.21
5	2.60	2.20	4.90	0.61	0.43
6	19.0	19.0	38.0	1.39	0.26
7	5.70	2.30	8.10	1.08	0.13
8		6.30	6.30	0.62	0.54
9	11.0	18.0	28.0	0.43	1.61
10	15.0	12.0	27.0	1.08	0.34
11	40.0	66.0	110.	5.66	1.18
12	3.40	2.30	5.60	0.32	0.63
13	2.80	3.40	6.20	0.51	0.64
14		61.0	61.0	1.03	1.47
15	0.79	2.10	2.90	1.71	0.06
16	66.0	40.0	110.	1.70	1.39
17	86.0	19.0	100.	2.61	0.35
18	11.0	1.70	13.0	1.54	0.45
19		30.0	30.0	0.77	0.96
20	18.0	31.0	49.0	1.58	1.16
21	48.0	41.0	89.0	1.77	1.78
23	28.0	15.0	44.0	1.01	0.82
24	12.0	9.60	22.0	0.77	1.62
25	0.85	1.10	02.0	2.20	0.05
26	96.0	62.0	160.	1.79	2.22
28	9.90	4.20	14.0	0.72	0.65
29	12.0	14.0	25.0	0.59	0.91
30	14.0	3.60	18.0	0.75	0.54
31	12.0	4.50	17.0	1.67	0.31
32	16.0	11.0	27.0	0.65	0.82

Event number	P-wave energy Ep $\times 10^6$ (J)	S-wave energy Es $\times 10^6$ (J)	Total seismic energy E $\times 10^6$ (J)	Stress drop $\Delta\delta$ (MPa)	Apparent stress δa (MPa)
33	33.0	41.0	74.0	1.14	1.61
34	18.0	7.00	24.0	1.52	1.35
35	14.0	18.0	32.0	0.59	1.41
36	22.0	16.0	37.0	0.96	1.05
37	17.0	4.80	22.0	3.60	0.18
38	12.0	5.40	17.0	0.45	0.78
39	22.0	37.0	59.0	0.57	1.19
40	49.0	22.0	71.0	2.23	0.60
41	11.0	3.30	14.0	0.39	0.59
42		43.0	43.0	0.59	0.67
43	17.0	13.0	30.0	0.91	0.35
44	18.0	13.0	31.0	0.87	0.48
45	290.	94.0	380.	4.37	2.50
46	6.70	4.20	11.0	0.55	0.45
47	9.30	19.0	28.0	2.25	0.24
48	140.	130.	280.	1.80	1.61
49		44.0	44.0	0.98	0.78
50	68.0	47.0	120.	2.78	1.30
51	60.0	36.0	96.0	1.99	0.46
52	11.0	5.60	16.0	0.62	0.33
53		18.0	18.0	0.22	0.49
54		11.0	11.0	0.25	0.82
55	4.80	1.50	6.20	0.58	0.08
56		17.0	17.0	0.43	0.33
57		3.10	3.10	0.19	0.22
58	45.0	12.0	57.0	1.18	0.28
59	14.0	4.10	18.0	1.03	0.13
60	8.80	0.86	9.70	0.43	0.29
61	41.0	64.0	110.	2.41	1.62
62	30.0	120.	150.	2.03	2.02
63	40.0	15.0	55.0	1.30	0.57
65	13.0	7.50	21.0	1.72	0.16
67	120.	580.	700.	3.50	4.10
68	20.0	38.0	58.0	2.79	1.26
69	4.00	5.90	9.90	1.20	0.10

Event number	P-wave energy Ep $\times 10^6$ (J)	S-wave energy Es $\times 10^6$ (J)	Total seismic energy E $\times 10^6$ (J)	Stress drop $\Delta\delta$ (MPa)	Apparent stress δa (MPa)
70	15.0	17.0	32.0	0.76	1.42
71	3.90	18.0	22.0	1.21	0.21
72	4.70	9.00	14.0	1.12	0.44
73	2.70	4.80	7.50	0.84	0.40
74	22.0	72.0	93.0	2.09	0.30
75	2.10	3.50	5.60	0.77	0.20
76	31.0	70.0	100.	1.40	1.00
77	14.0	0.43	15.0	0.49	0.22
78	59.0	180.	240.	0.87	3.30
79	5.10	19.0	24.0	0.49	1.01
80	3.50	3.30	6.80	1.50	0.12
81	55.0	36.0	91.0	2.70	0.53
82	28.0	42.0	69.0	0.44	1.79
83	7.00	9.30	16.0	0.70	0.13
84	30.0	3.00	33.0	2.79	1.27
85	5.60	0.82	6.50	0.90	0.16
86	0.91	0.95	1.90	0.94	0.05
87	9.60	0.55	10.0	1.39	0.43

and *S* waves, for the seismic events at Wujek mine are listed in Table 3 and for those at Ziemowit mine are given in Table 5. The density of the source material of 2700 kg/m^3 was accepted. The values of moment magnitude *M*, defined by Hanks and Kanamori (1979), are also listed in Tables 3 and 5. They range between 1.1 and 2.2 for the events at Wujek mine, and from 1.4 to 2.4 for the events at Ziemowit mine.

Estimates of the source size are heavily model dependent. The radius r_o of the circular fault is inversely proportional to the corner frequency and is proportional to a constant depending on the source model. In mine seismicity studies, following the results from natural earthquake studies, the source size has been estimated by some authors using Brune's (1970, 1971) model. In Polish mines, however, it was found that whenever the size and geometry of underground damage caused by rockburts could be estimated, its radius was considerably smaller than that predicted by Brune's model (e. g., Gibowicz, 1984; Gibowicz *et al.*, 1989). It was also found that the Brune model provides unrealistic estimates of the source size in French coal mines (Revalor *et al.*, 1990). The quasi-dynamic model of Madariaga (1976), on the other hand, provides reasonable results in good agreement with independent observations in mines (e. g., Gibowicz, 1984; Gibowicz *et al.*, 1989; 1990), and this model was used to estimate the source radius at Wujek and Ziemowit mines (Tables 3 and 5). The corner frequency of *P* waves ranges there from 6 to 20 Hz and the corner frequency of *S* waves ranges between 4 and 13 Hz.

The radiated seismic energy of either *P* or *S* waves can be estimated directly fromthe integral J_c, expressing the energy flux of either *P* or *S* waves. The loss of energy from attenuation is accounted for in the calculation of the energy flux. The values of the seismic energies E_p and E_s of the *P* and *S* pulses were readily calculated by applying individual values, divided by the RMS averages (e. g., Boatwright and Fletcher, 1984), of the radiation coefficient corresponding to various seismic sensors. The values of E_p and E_s for the selected seismic events at Wujek mine are listed in Table 4, together with the values of the total seismic energy $E = E_p + E_s$. Similarly, the values of the energy for the events at Ziemowit mine are presented in Table 6.

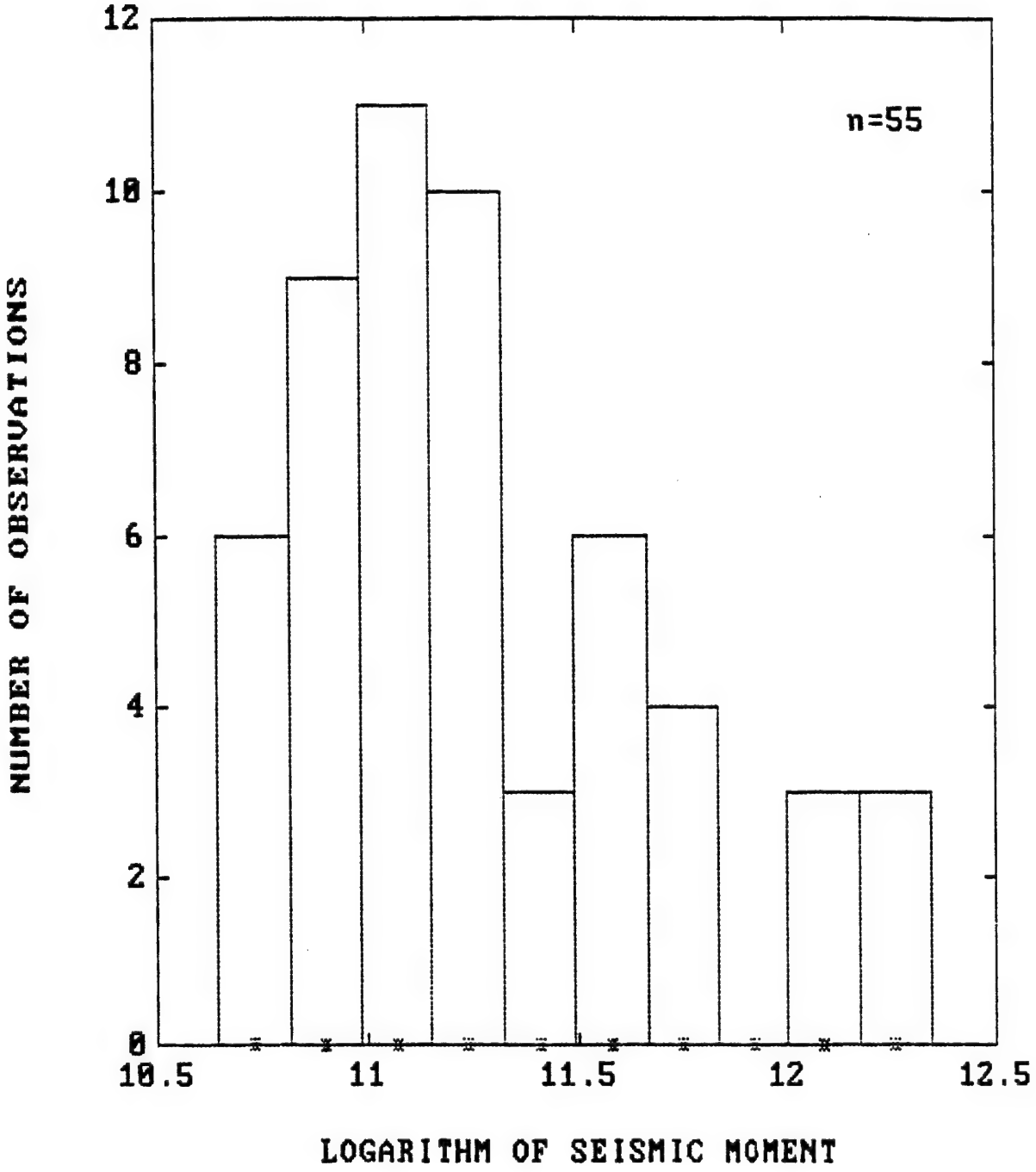

Fig.13. Histogram of the logarithm of seismic moment of the 55 selected seismic events at Wujek coal mine.

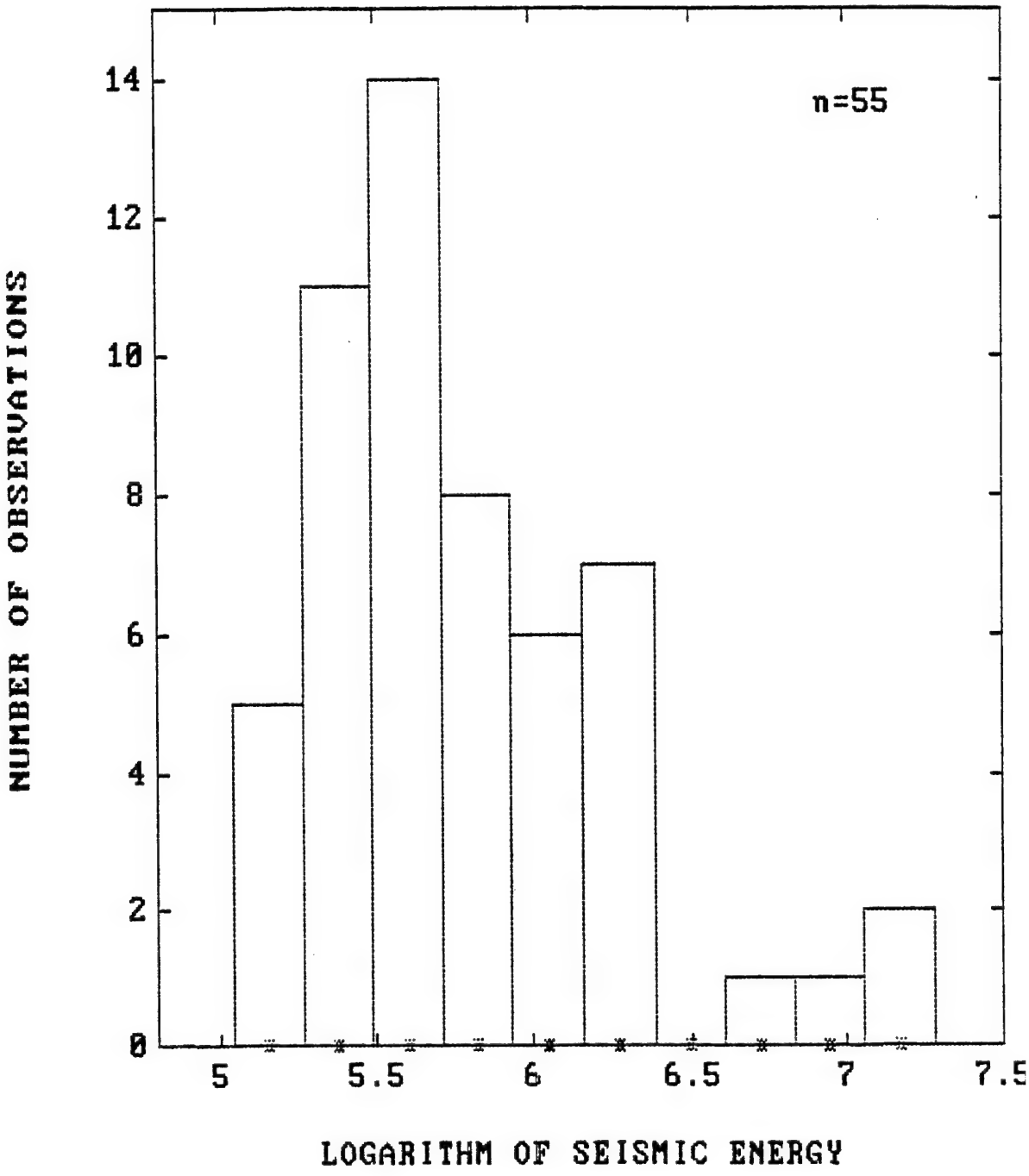

Fig.14. Histogram of the logarithm of seismic energy for selected seismic events at Wujek coal mine.

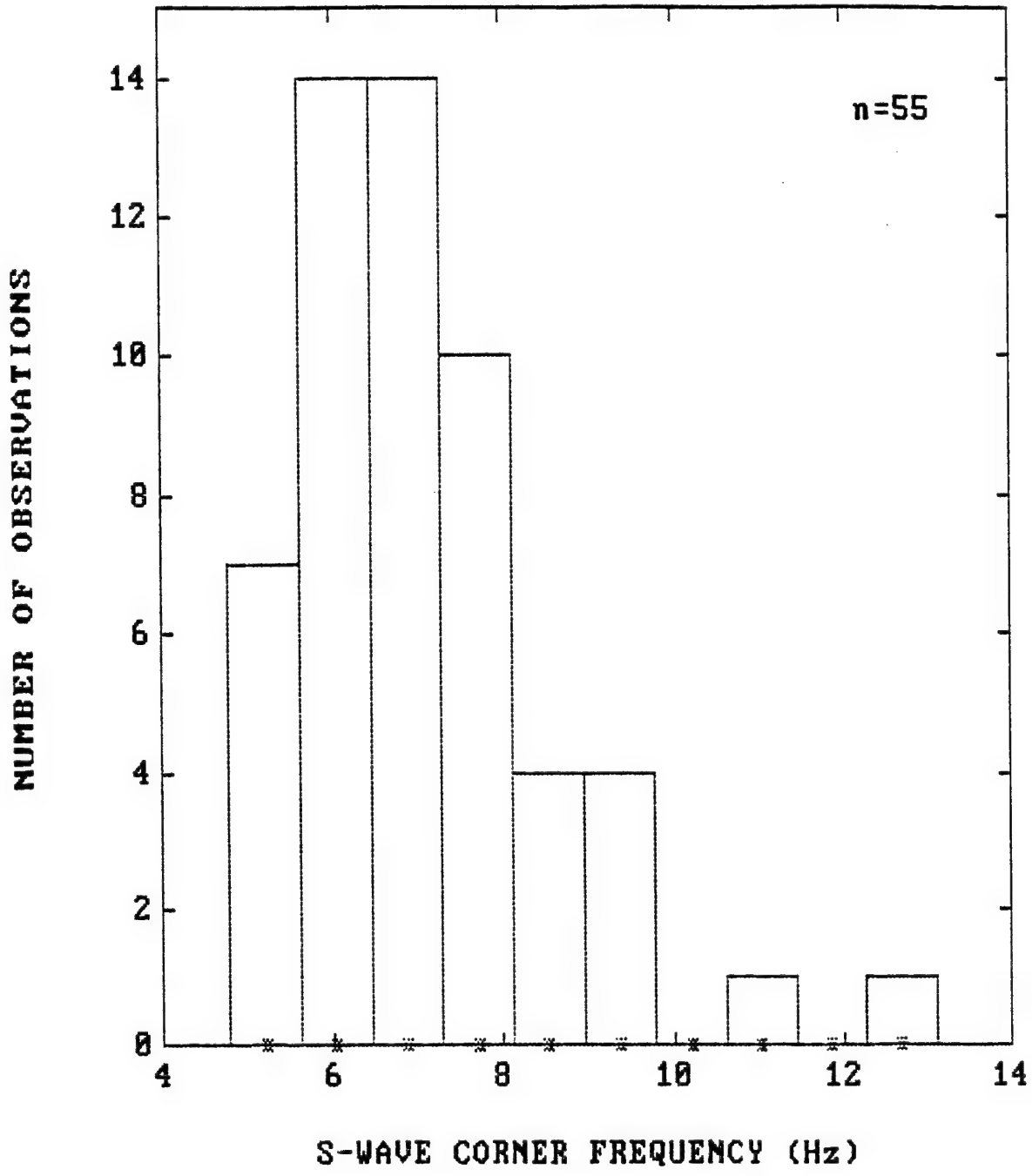

Fig. 15. Histogram of S-wave corner frequency for selected seismic events at Wujek coal mine.

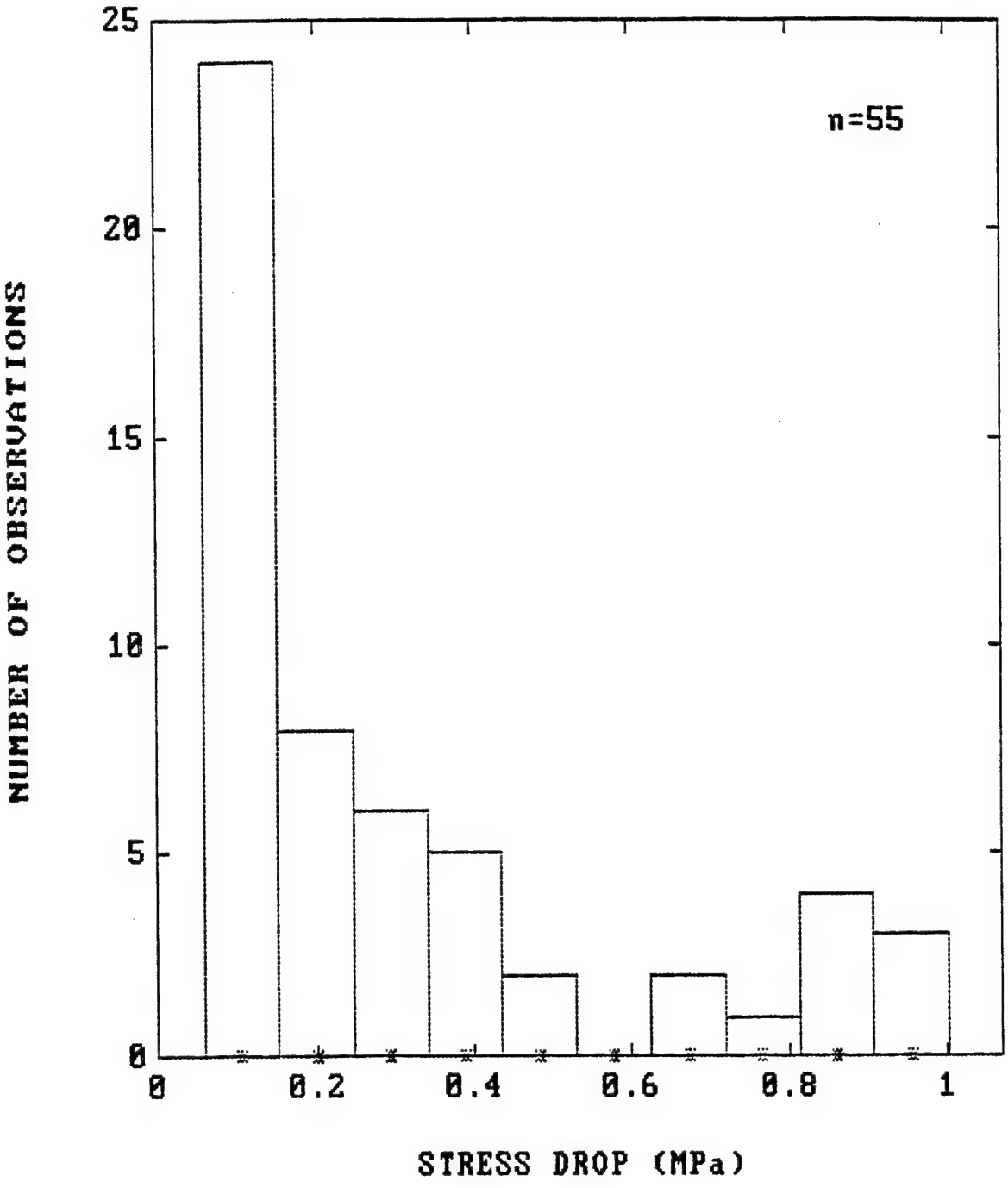

Fig. 16. Histogram of stress drop values for selected seismic events at Wujek coal mine.

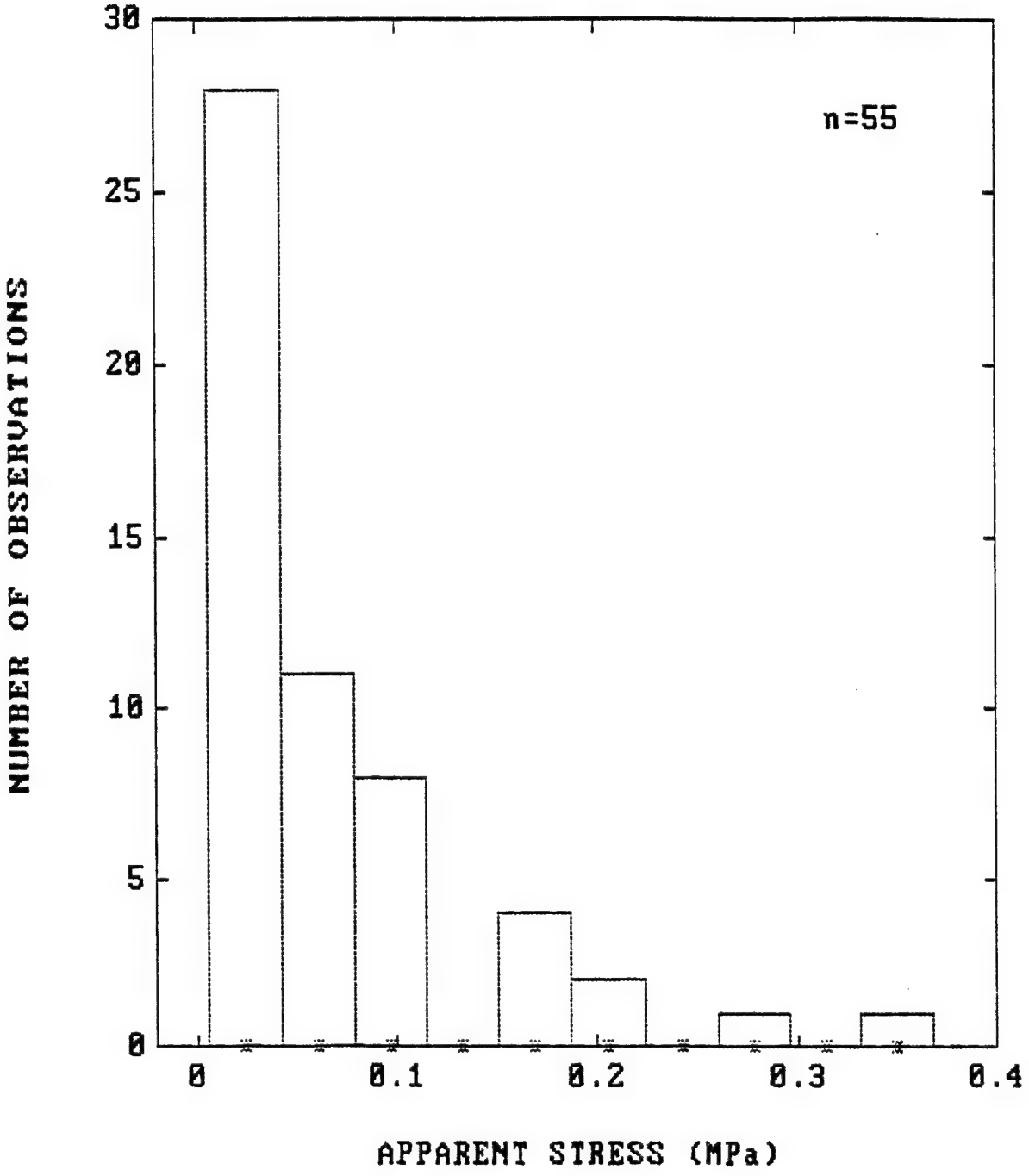

Fig. 17. Histogram of apparent stress values for selected seismic events at Wujek coal mine.

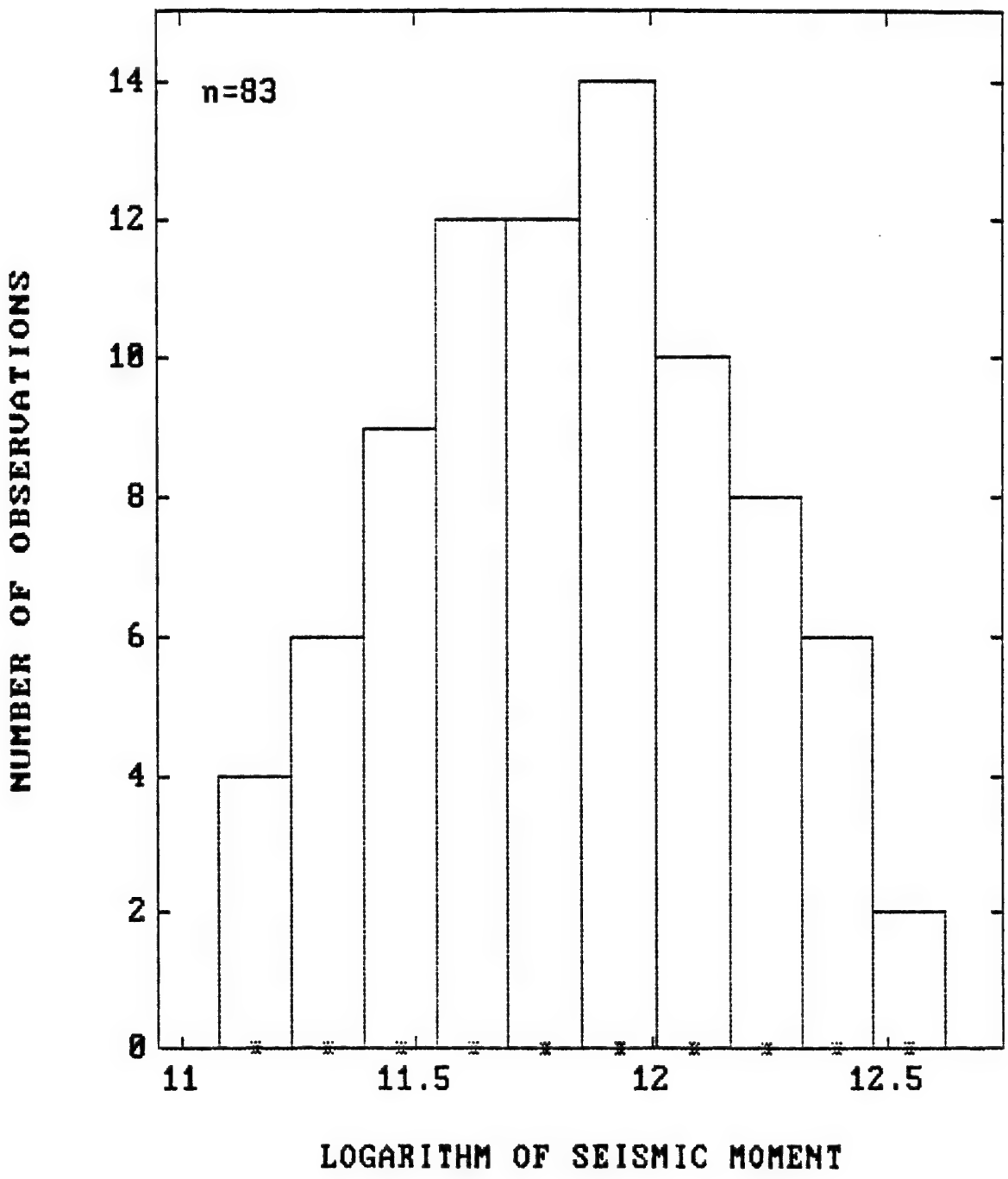

Fig.18. Histogram of the logarithm of seismic moment for the 83 selected seismic events at Ziemowit coal mine.

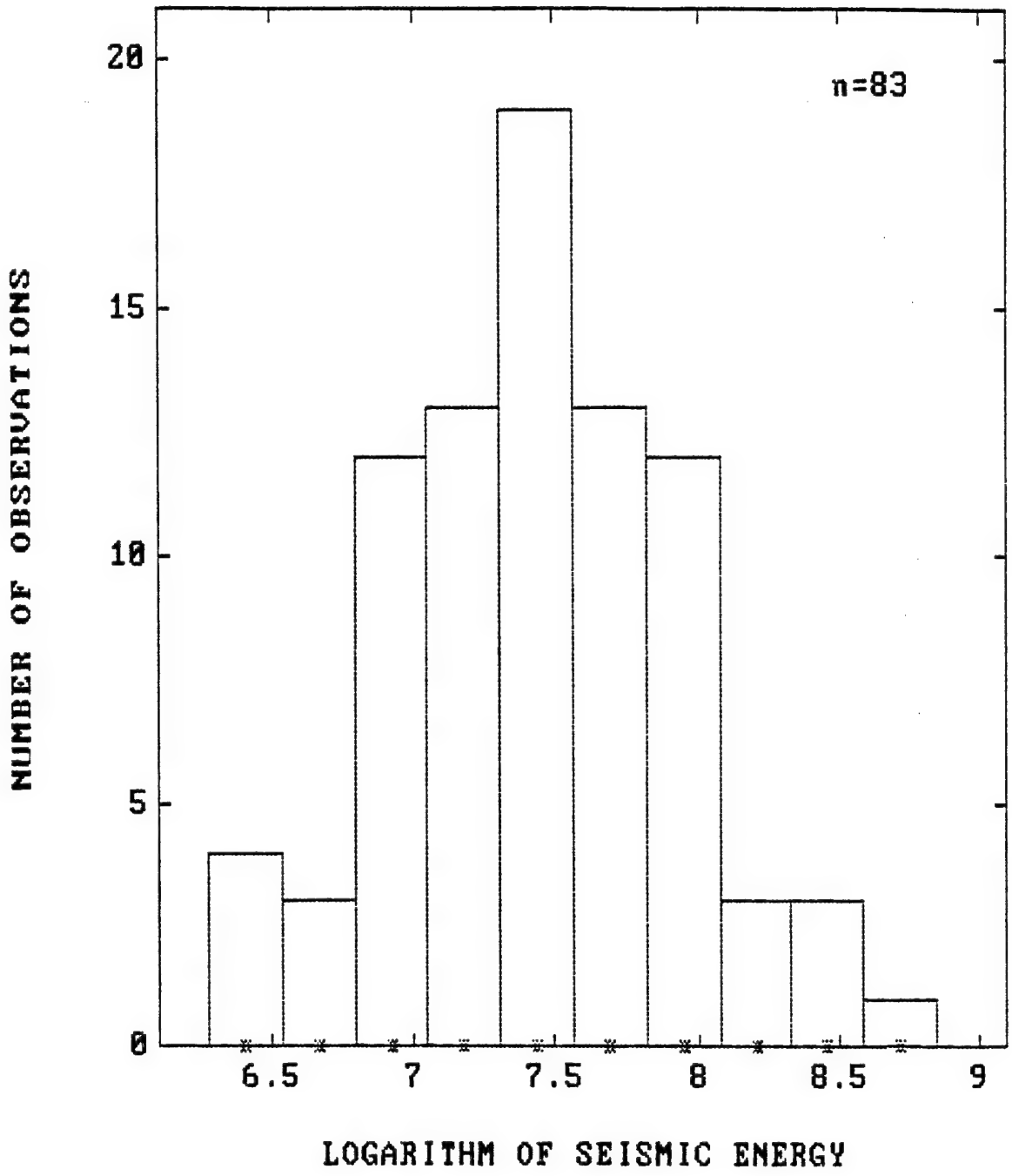

Fig.19. Histogram of the logarithm of seismic energy for selected seismic events at Ziemowit coal mine.

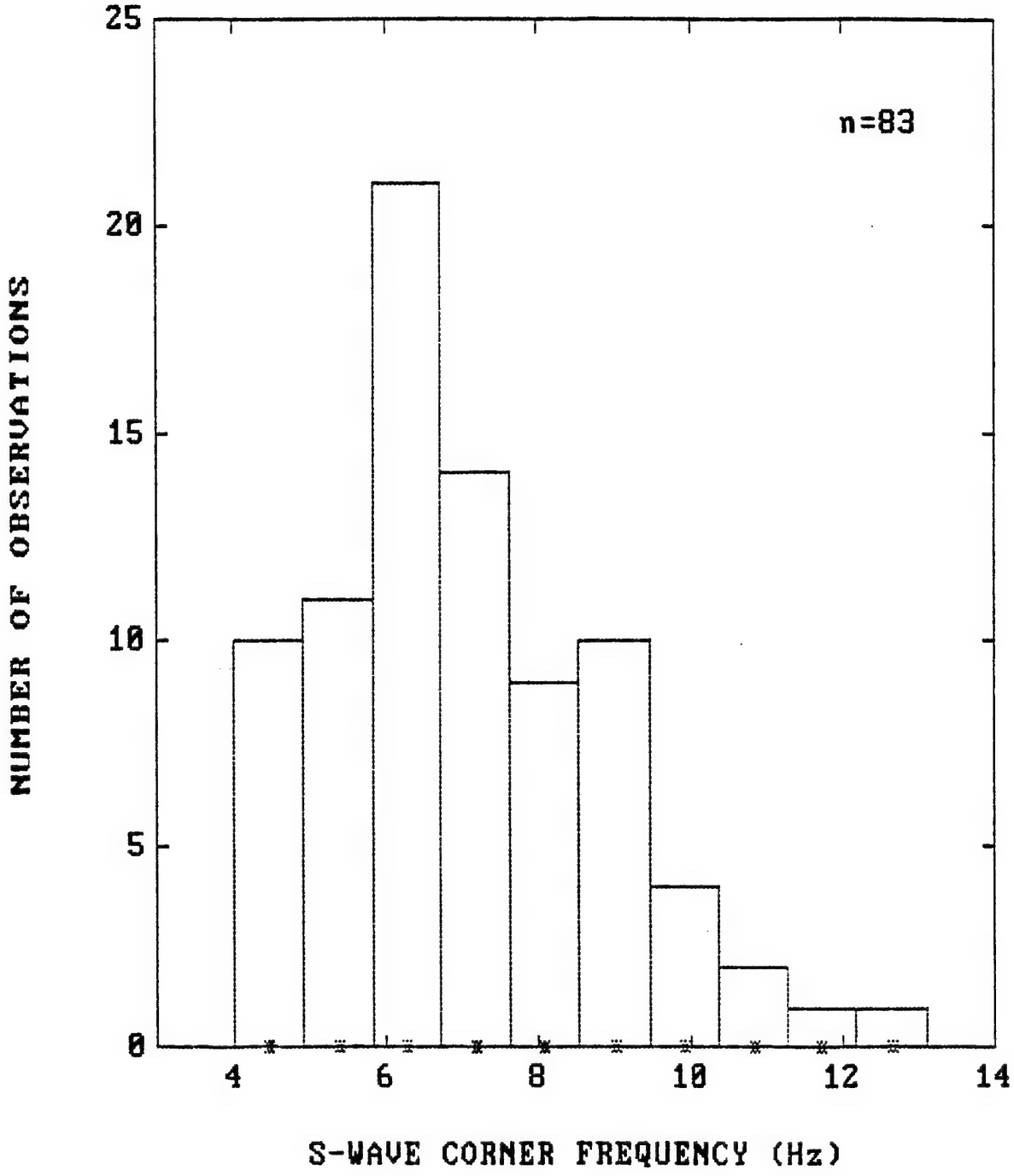

Fig. 20. Histogram of S-wave corner frequency for selected seismic events at Ziemowit coal mine.

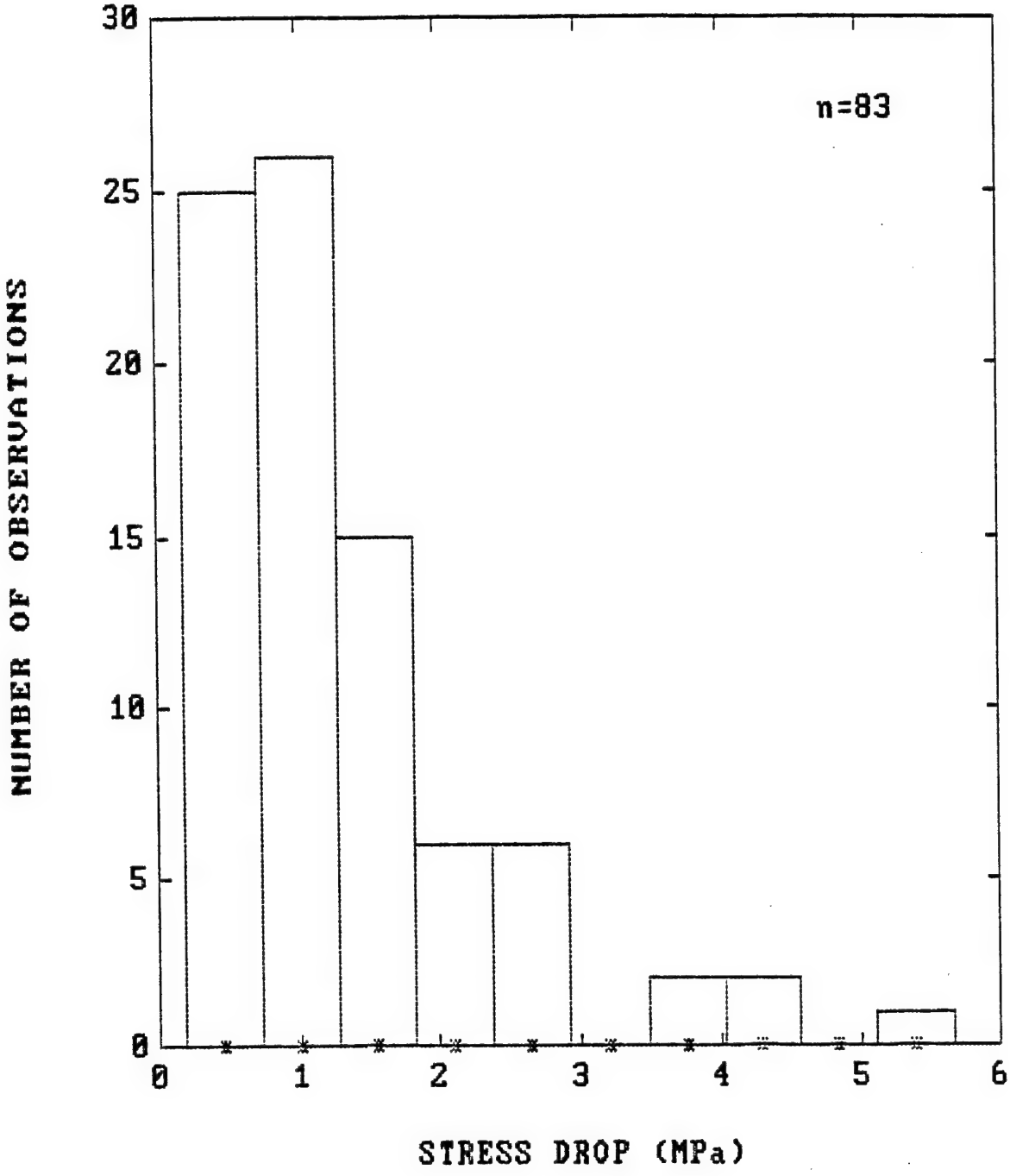

Fig.21. Histogram of stress drop values for selected seismic events at Ziemowit coal mine.

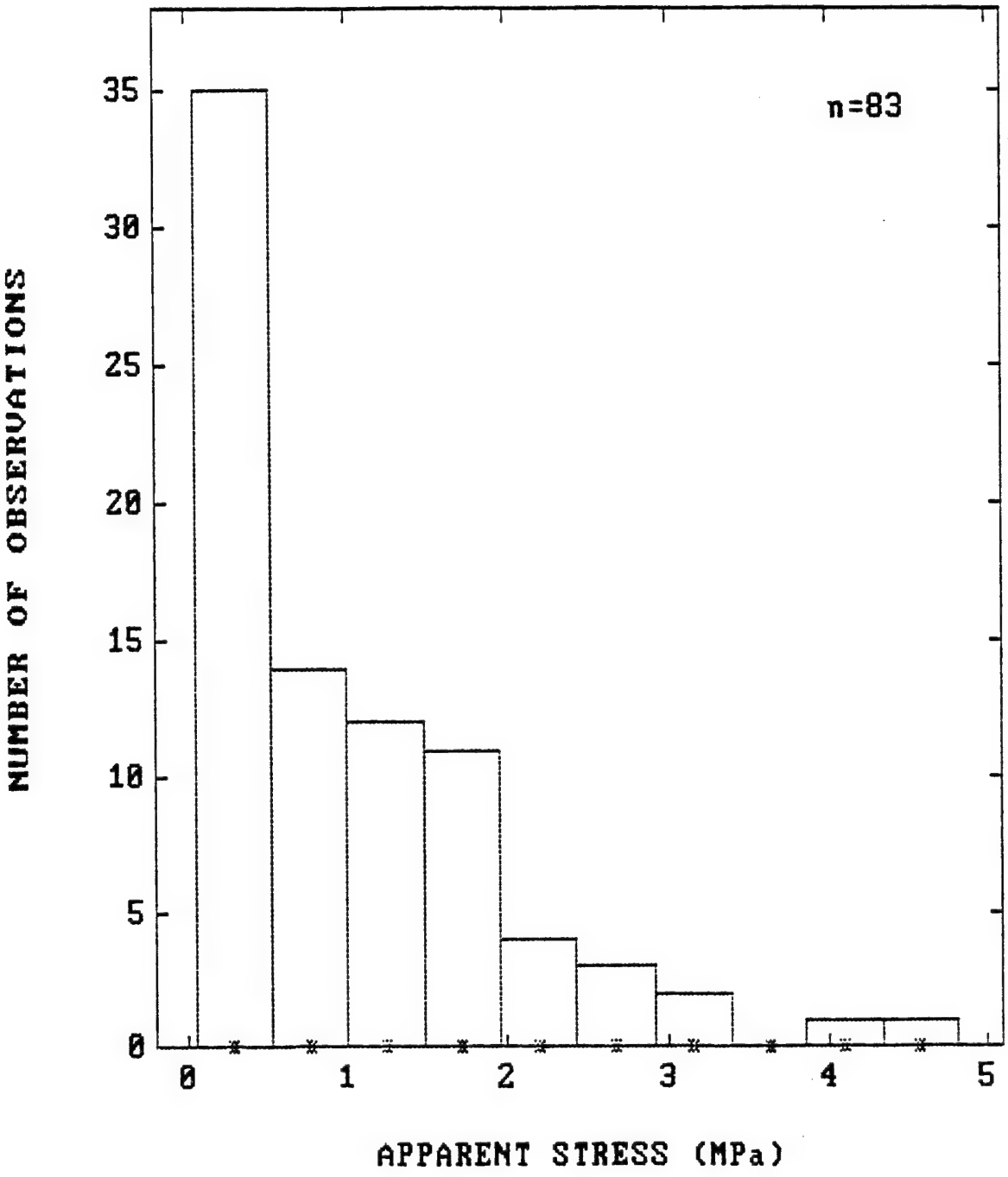

Fig. 22. Histogram of apparent stress values for selected seismic events at Ziemowit coal mine.

Two estimates of stress release are applied here: the modified Brune (1970, 1971) stress drop, based on the source radius from the model of Madariaga (1976) and called here the stress drop $\Delta\sigma$ and the apparent stress σ_a, an independent parameter because of the *P*-wave contribution to the seismic energy, occasionally considered as an estimate of the dynamic stress drop (Boatwright, 1984). The values of the two estimates of stress release for the seismic events at Wujek coal mine are listed in Table 4 and those for the events at Ziemowit coal mine are listed in Table 6.

The selected, well recorded, seismic events at Wujek mine are characterized by a narrow range of seismic moment values from 4.4×10^{10} to 2.3×10^{12} N·m, with the dominant values around the value of 10^{11} N·m (Fig. 13). The seismic energy ranges between 1×10^{5} to 2×10^{7} J, with the dominant values of about 4×10^{5} J (Fig. 14). The *S*-wave corner frequencies are between 5 and 13 Hz, mostly between 6 and 8 Hz (Fig. 15), and the corresponding values of source radius range from 40 to 100 m. The stress drop is characterized by low values, ranging from 0.06 to 1.0 MPa, typical for seimic events induced by mining. In most cases the stress drop values are in the range from 0.1 to 0.2 MPa (Fig. 16). The apparent stress shows even lower values, ranging from 0.006 to 0.37 MPa, but in most cases not exceeding 0.1 MPa (Fig. 17).

The seismic events at Ziemowit mine are also characterized by a narrow range of seismic moment values from 1.2×10^{11} to 4.2×10^{12} N·m, with the dominant values ranging between 5×10^{11} and 1×10^{12} N·m (Fig. 18). The seismic energy, however, here is more than by one order of magnitude higher than that observed at Wujek mine for the events with similar seismic moments. The energy ranges from 2×10^{6} to 7×10^{8} J, with the dominant values of about 3×10^{7} J (Fig. 19). The *S*-wave corner frequencies are in the same range from 4 to 13 Hz (Fig.20) as those observed at Wujek mine. Similarly, the source radius ranges between 38 and 100 m. The stress drop here is about five times higher than that at Wujek mine, and it ranges from 0.2 to 5.7 MPa. Its values in most cases are contained in a range between 0.5 and 1 MPa (Fig. 21). The apparent stress is again much higher, by about one order of magnitude, than that at Wujek mine, ranging from 0.05 to 4.8 MPa, with dominant values concentrated around the value of 0.3 MPa (Fig. 22).

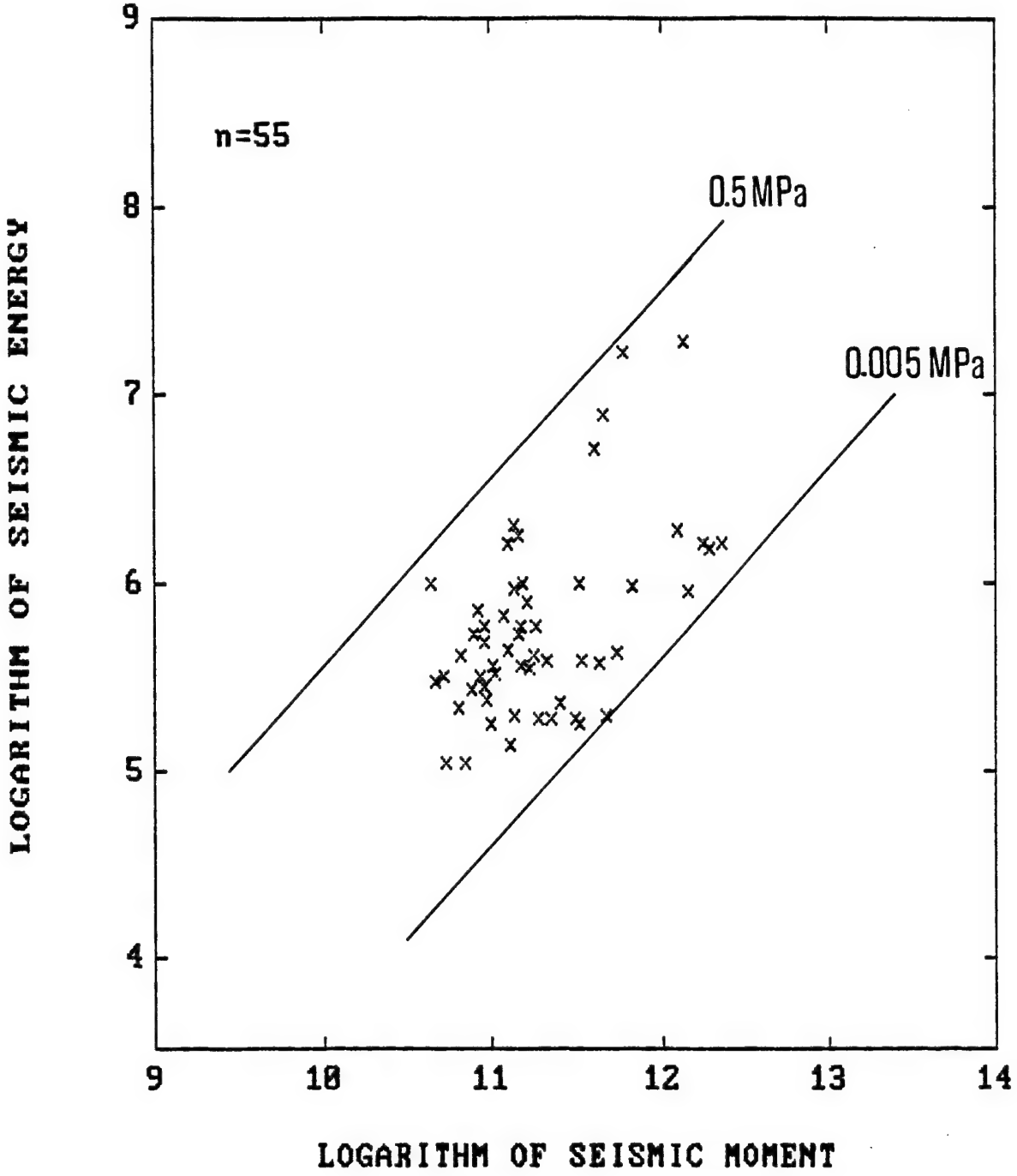

Fig. 23. Logarithm of seismic energy versus logarithm of seismic moment for selected seismic events at Wujek coal mine. The straight lines show the constant values of apparent stress.

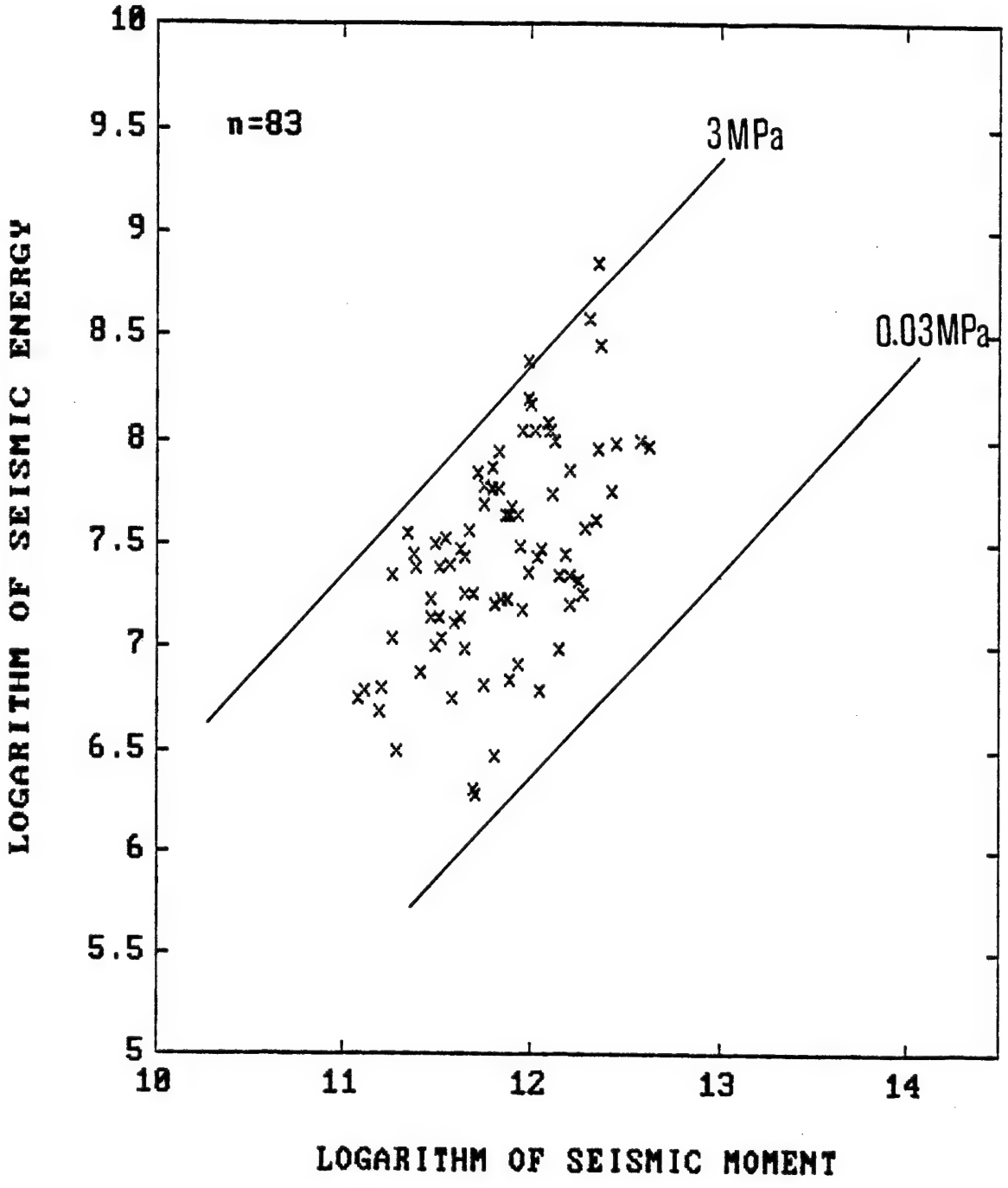

Fig. 24. Logarithm of seismic energy versus logarithm of seismic moment for selected seismic events at Ziemowit coal mine. The straight lines show the constant values of apparent stress.

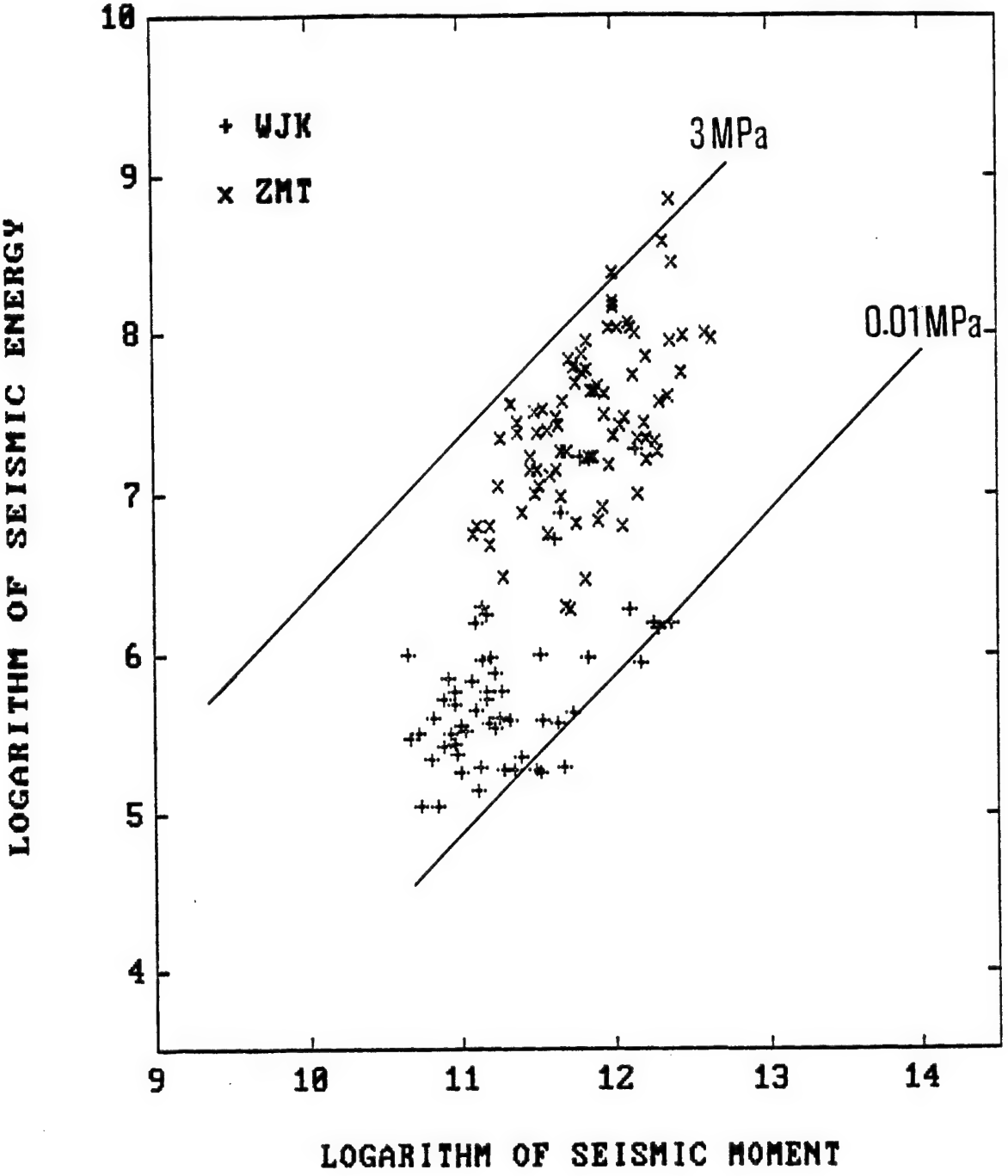

Fig. 25. Logarithm of seismic energy versus logarithm of seismic moment for selected seismic events at Wujek and Ziemowit coal mines. The straight lines show the constant values of apparent stress.

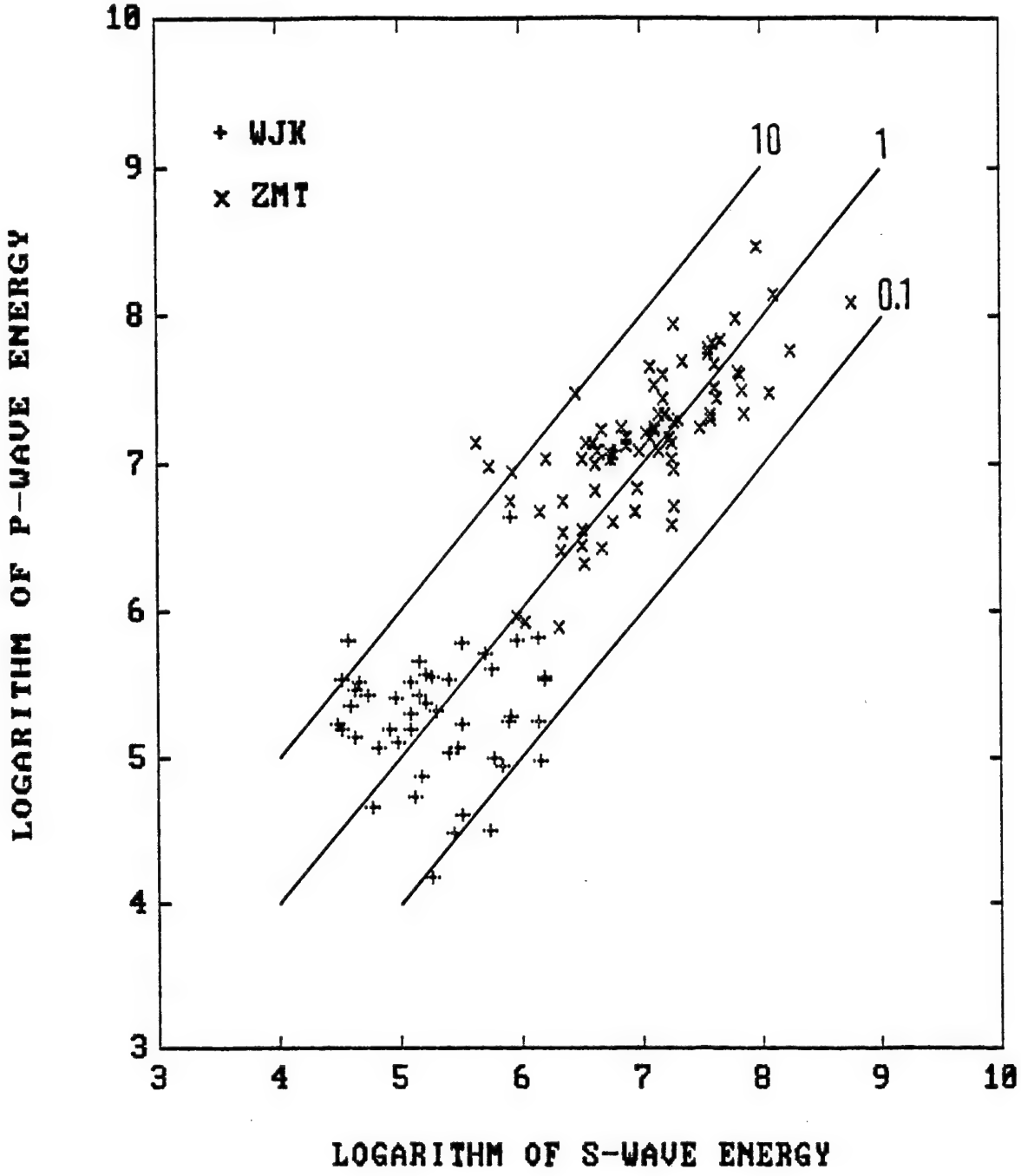

Fig. 26. Logarithm of P-wave energy versus logarithm of S-wave energy for selected seimic events at Wujek (WJK) and Ziemowit (ZMT) coal mines. The ratio of P-wave energy over S-wave energy is shown by straight lines.

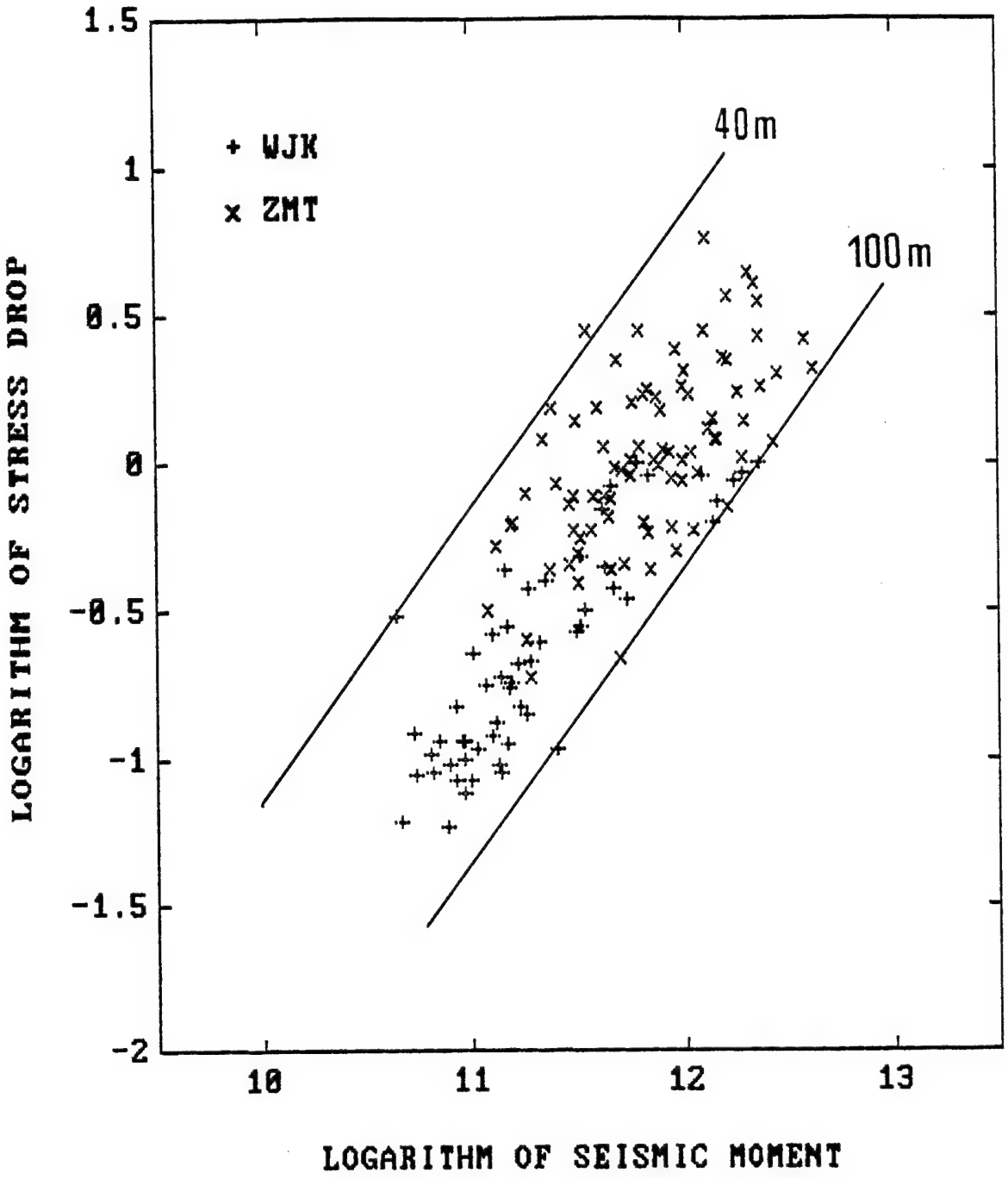

Fig.27. Logarithm of stress drop versus logarithm of seismic moment for selected seismic events at Wujek and Ziemowit coal mines. The straight lines show the constant values of source radius.

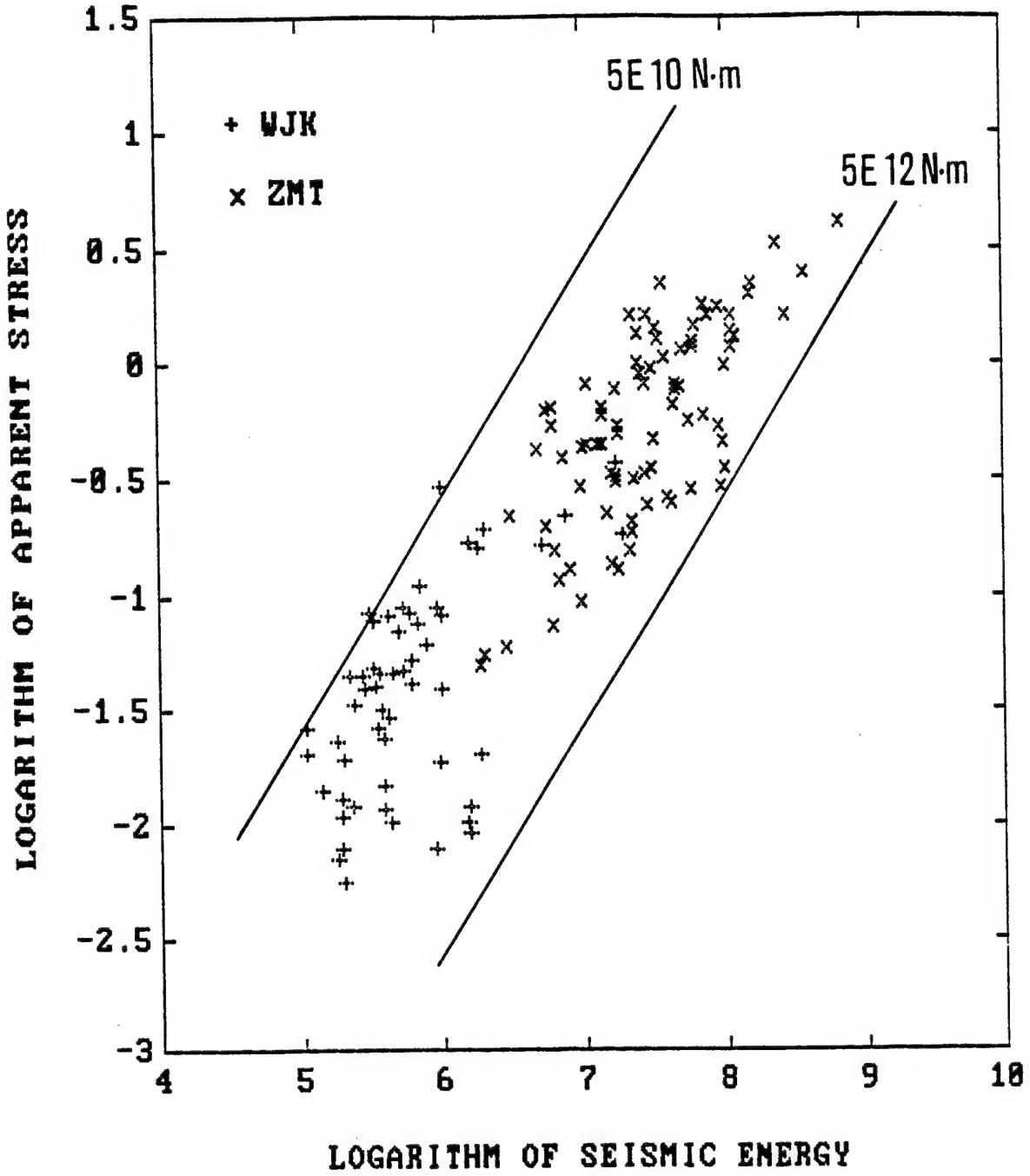

Fig. 28. Logarithm of apparent stress versus logarithm of seismic energy for selected seismic events at Wujek and Ziemowit coal mines. Constant values of seismic moment are indicated by straigt lines.

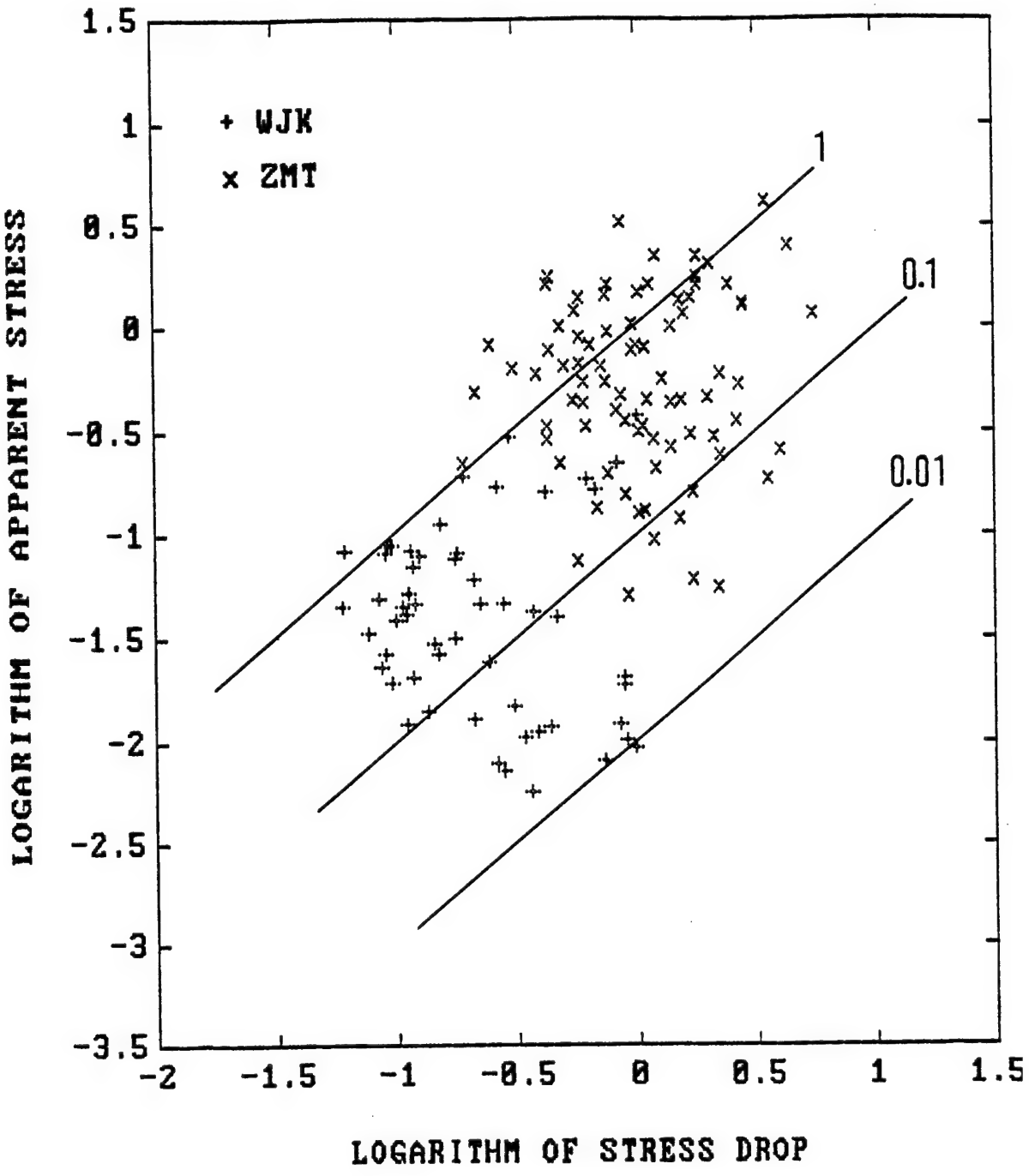

Fig. 29. Logarithm of apparent stress versus logarithm of stress drop for selected seismic events at Wujek and Ziemowit coal mines. The ratio of apparent stress over stress drop is shown by straight lines.

Seismic energy versus seismic moment for the events at Wujek mine is shown on a logarithmic scale in Fig. 23 and for the events at Ziemowit mine is shown in Fig. 24. The energy values are bounded by the lines of constant apparent stress to show that the energy for a given seismic moment can var considerably. As a result of the narrow range of the values of seismic moment, the correlation coefficients for these relations are low: 0.52 for the events from Wujek mine and 0.56 for the events from Ziemowit mine. The same data from the both mines are shown in Fig. 25, and the correlation coefficient in this case is 0.72. The slope of a regression line, describing an average relation between the logarithm of seismic energy and seismic moment, is 1.8. It should be noted that the ratio of the seismic energy of a given seismic event over the average energy corresponding to the same level of seismic moment is used at some gold mines in South Africa as an indicator of rock mass properties (Mendecki, 1993). The high values of the energy ratio, corresponding to relatively compact sources, would characterize undisturbed media, whereas the low energy ratio would be associated with highly fractured rock masses.

P-wave energy E_p versus *S*-wave energy E_s for the seismic events from the both mines is shown in Fig. 26, where the values of the ratio E_p / E_s are also indicated by straight lines. The ratio of *S*-wave to *P*-wave energy ranges from about 0.1 to 20; for about half of our events the ratio is smaller than one. A similar situation has been found in a coal mine in Germany, where two thirds of the selected events were characterized by low values of the ratio E_s / E_p (Gibowicz *et al.*, 1990), and during the shaft excavation at the Underground Research Laboratory in Canada, where 40 percent of the selected events were also characterized by energy depletion in *S* waves (Gibowicz *et al.*, 1991). There is definite evidence from natural ewarthquakes, on the other hand, that the energy radiated in *P* waves is a small fraction of that in *S* waves (e. g., Boatwright and Fletcher, 1984).

Stress drop versus seismic moment for the selected events from the both mines is shown on a logarithmic scale in Fig. 27, where the contours of constant source radius are also marked. The correlation coefficient between the logarithm of stress drop and the logarithm of seismic moment is 0.83, and the slope of a regression line between

these values is 0.84. Thus, the stress drop seems to be moment dependent, roughly along the line of the average source radius of about 60-70 m. Apparent stress versus seismic energy for the all selected events is shown on a logarithmic scale in Fig. 28, where the data are bounded by contours of constant seismic moment. The correlation coefficient here is 0.89, and the regression slope is 0.93. The display, on a logarithmic scale, of the apparent stress against stress drop is shown in Fig. 29, where the values of their ratio are indicated by straight lines. There is no evident correlation here and the apparent stress is in most cases smaller than the stress drop.

4.3 Scaling relations

It has been shown that the far-field displacement spectrum is characterized by frequency-invariant amplitudes below the corner frequency and a decay of amplitudes at frequencies above the corner frequency. The corner period, the reciprocal of the corner frequency, is proportional to the source duration and is related to the source dimensions. A source scaling relation describes the manner in which the source duration or the source dimension increases with increasing seismic moment.

In studies of large earthquakes occurring in seismic regions of the world, it has been found that stress drop is roughly independent of the seismic moment (Kanamori and Anderson, 1975), which means that seismic moment is proportional to the third power of source radius. A constant stress drop scaling relation has been confirmed by innumerable studies and has become an accepted model for large and moderate earthquakes. The constant stress drop pattern was also reported for small volcanic events in Italy (De Natale *et al.*, 1987), for the aftershocks with magnitudes down to 2 near the Norwegian coast (Chael and Kromer, 1988), and for microearthquakes with magnitudes less than about 2 observed at Anza, California (Frankel and Wennerberg, 1989). The constancy of stress drop has been found for some seismic evnts in gold mines in South Africa (Spottiswoode, 1984) and in coal mines in Poland (Gibowicz *et al.*, 1977).

In contrast to these results, there is growing evidence of a breakdown in similarity between large and small earthquakes (e.g., Dysart *et al.*, 1988; Chun *et al.*, 1989; Glassmoyer and Borchardt, 1990). Generally, a marked decrease in stress drop with decreasing seismic moment, for seismic moment below about 10^{13} N·m ($M < 3$), is reported. Another manifestation of this apparent breakdown in similarity is the divergence of the scaling of peak acceleration and ground velocity from that expected from theoretical considerations following the similarity relation (McGarr, 1986).

It seems that the most convincing evidence of the breakdown in scaling relations for small seismic events comes from studies of mine-induced seismicity, based on underground seismic networks. A decreasing stress drop with decreasing seismic moment has been observed for small mine tremors with the moment from about 10^{11} to 10^{13} N·m in Polish copper mines (Gibowicz, 1985), in the Western Deep Levels gold mine in South Africa (Bicknell and McGarr, 1990; Cichowicz *et al.*, 1990), and in a German coal mine in the Ruhr basin (Gibowicz *et al.*, 1990). The scaling relation between seismic moment and source radius for seismic events, with moment magnitude from -3.6 to -1.9, induced by the excavation of a shaft in granite at Lac du Bonnet, Canada, indicates also a decrease in stress drop with decreasing seismic moment (Gibowicz *et al.*, 1991). A similar stress drop dependence on seismic moment and a nonsimilar frequency-magnitude distribution was found for small seismic events at Strathcona mine, Ontario (Urbancic *et al.*, 1992, 1993; Trifu *et al.*, 1993). Furthermore, Urbancic *et al.* (1992) noted that this dependence disappeared when multiple data sets were combined, supporting the idea that a constant stress drop model may fit widely dispersed observations.

The nonsimilar behavior of small earthquakes has been widely interpreted as a source effect, involving either an upper limit to the radiated frequency, that is, the presence of a characteristic fault length, or the dependence of stress on the seismic moment. The change in spectra scaling can also be explained by attenuation effects or by any process that limits high frequencies, whether it is due to the source, the propagation path, the local site, or the recording

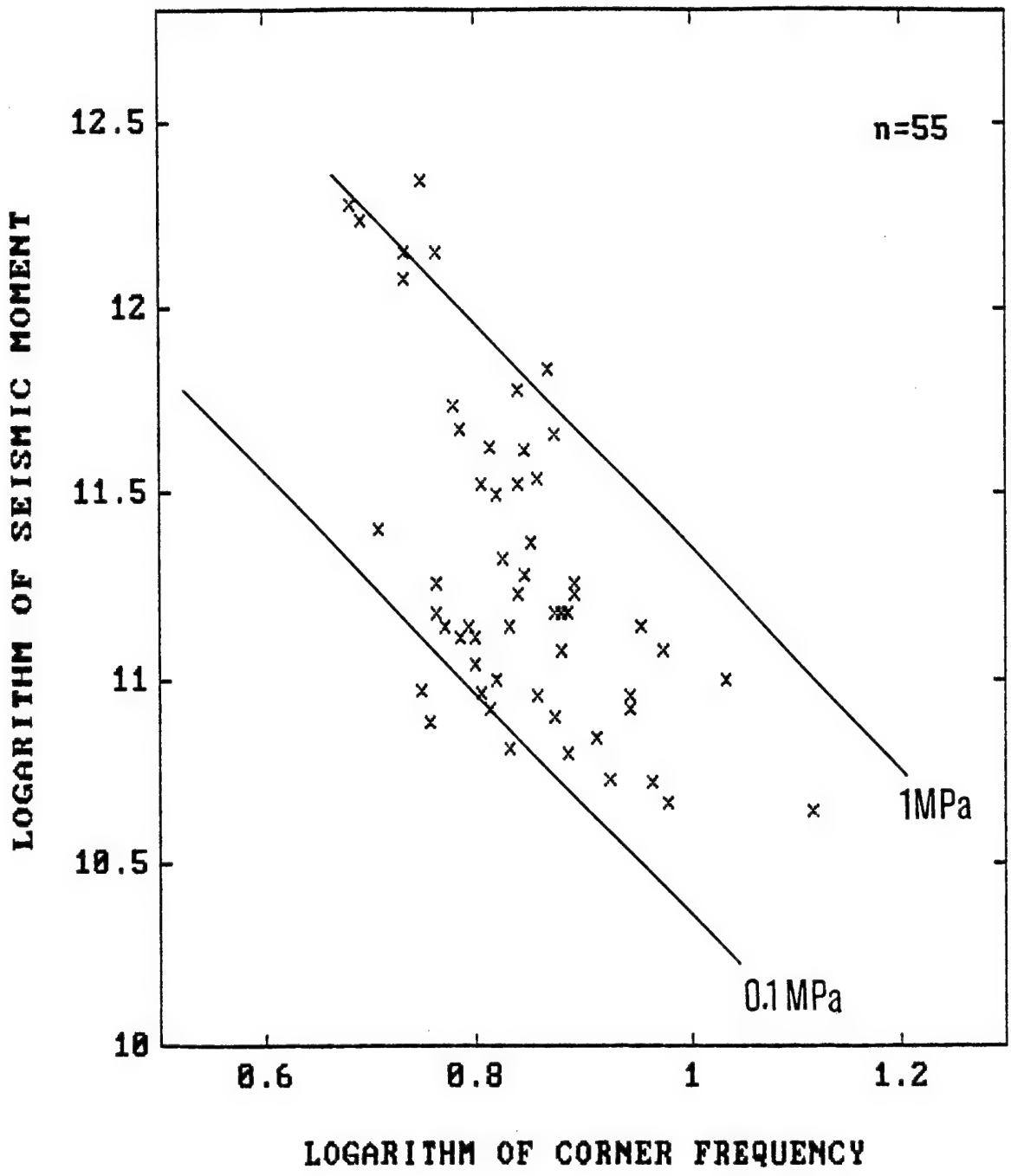

Fig. 30. Logarithm of seismic moment versus logarithm of S-wave corner frequency for selected seismic events at Wujek coal mine. The lines of constant stress drop are indicated.

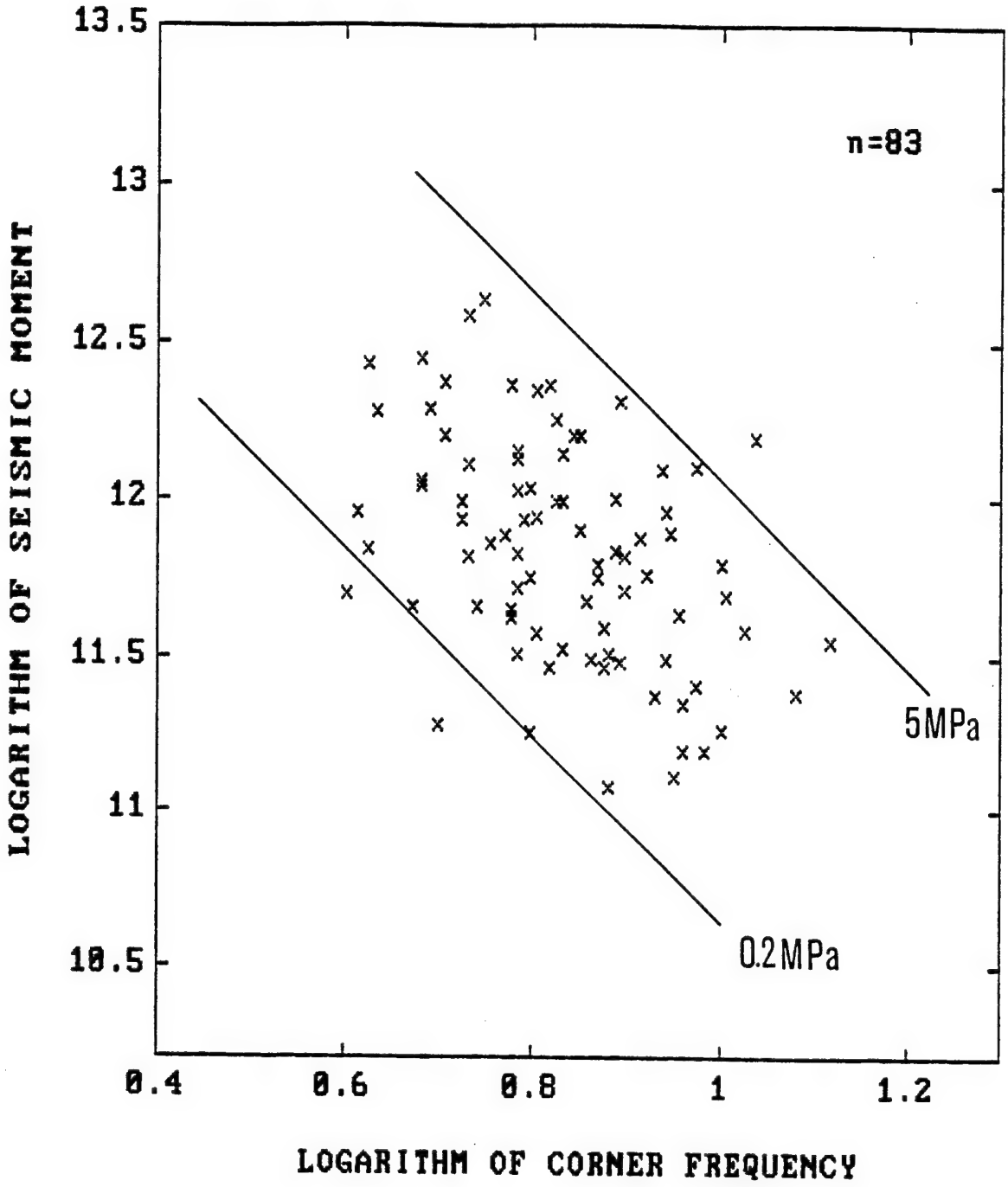

Fig. 31. Logarithm of seismic moment versus logarithm of S-wave corner frequency for selected seismic events at Ziemowit coal mine. The lines of constant stress drop are indicated.

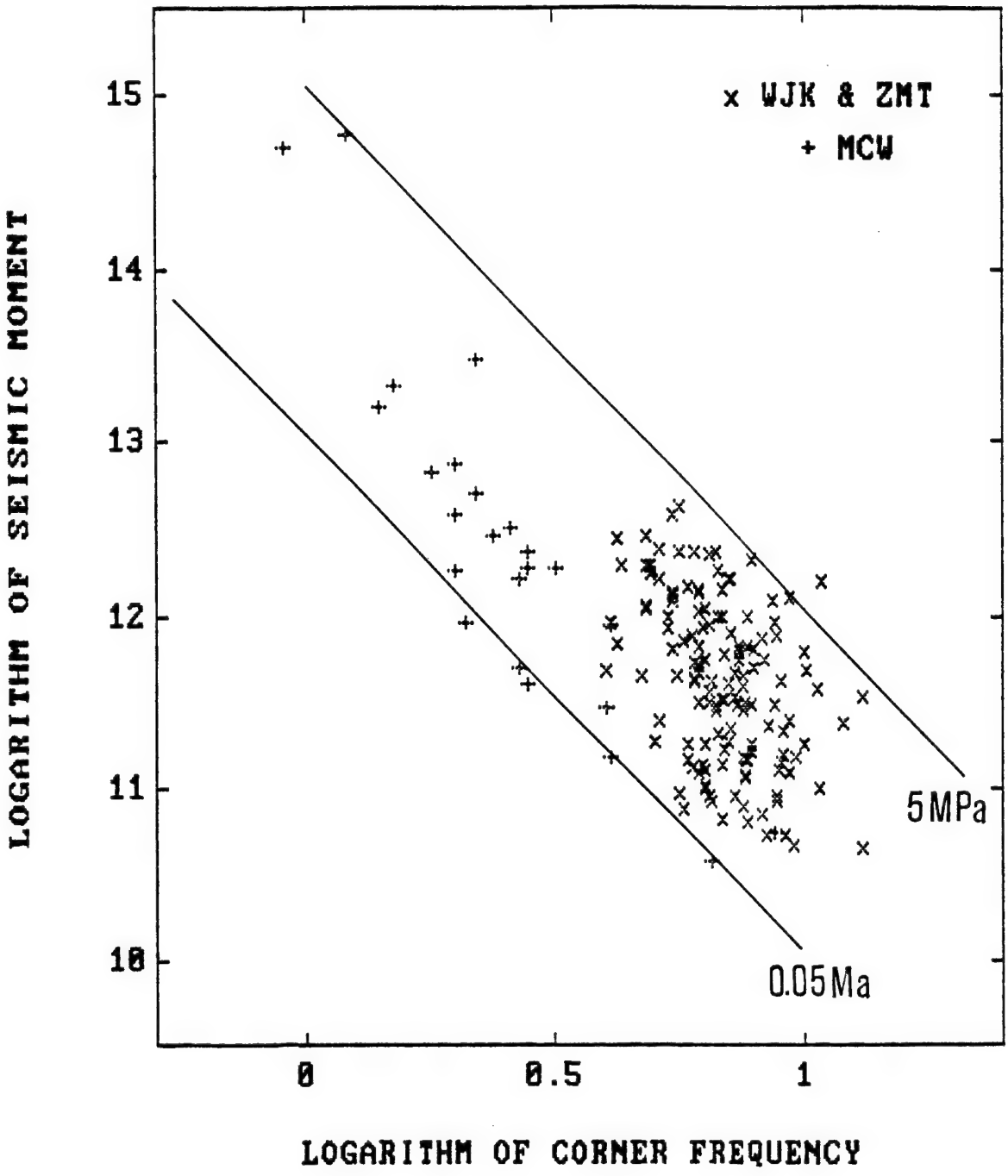

Fig. 32. Logarithm of seismic moment versus logarithm of S-wave corner frequency for selected seismic events at Wujek (WJK), Ziemowit (ZMT), and Miechowice (MCW) coal mines. The lines of constant stress drop are indicated.

instrument. This effect of finite bandwidth has been recognized for some time. Boore (1986) has shown that a moment-independent filter that attenuates high frequencies, regardless of its origin, produces marked changes in the scaling expected from the usual analysis of self-similar models.

Seismic moment versus corner frequency of *S* waves, bounded by the contours of constant stress drop, is displayed on a logarithmic scale for the selected seismic events at Wujek mine in Fig. 30 and for the events at Ziemowit mine in Fig. 31. The correlation coefficient for the events at Wujek mine is -0.60 and at Ziemowit mine it is -0.44. As a result of a narrow range of the observed values, the relationships are rather inconclusive, though the relations shown in Fig. 27 imply that stress drop here is dependent on seismic moment. To enlarge the range of the observed values, 24 data for the seismic events from Miechowice coal mine in the Upper Silesia Coal Basin (Gibowicz *et al.*, 1977) were added to those obtained from Wujek and Ziemowit mines. They are presented in Fig. 32. The correlation coefficient for this set of data is -0.70 and the data imply a constant stress drop model. The situation here is most probably similar to that observed by Urbancic *et al.* (1992) at Strathcona mine in Ontario, where the stress drop dependence on seismic moment was found locally, but it disappeared when multiple data sets were combined.

4.4 P-wave corner frequency versus S-wave corner frequency

It should be noted that corner frequencies calculated from underground records are much more reliable than those obtained from surface records (e. g., Malin *et al.*, 1988). In general, the corner frequencies of *P* waves are expected to be greater than those of *S* waves; their ratio greater than one is an intrinsic property of earthquake sources (Hanks, 1981). It could happen, however, that the apparent value of the ratio of the corner frequency of *P* wave over that of *S* wave is smaller than one when the observations are made at low values of the angle between the normal to the fault plane and the takeoff direction of seismic waves (Gibowicz *et al.*, 1990). The number of published observations is limited and it is interesting to compare the well-determined values of corner frequencies of *P* and *S* waves.

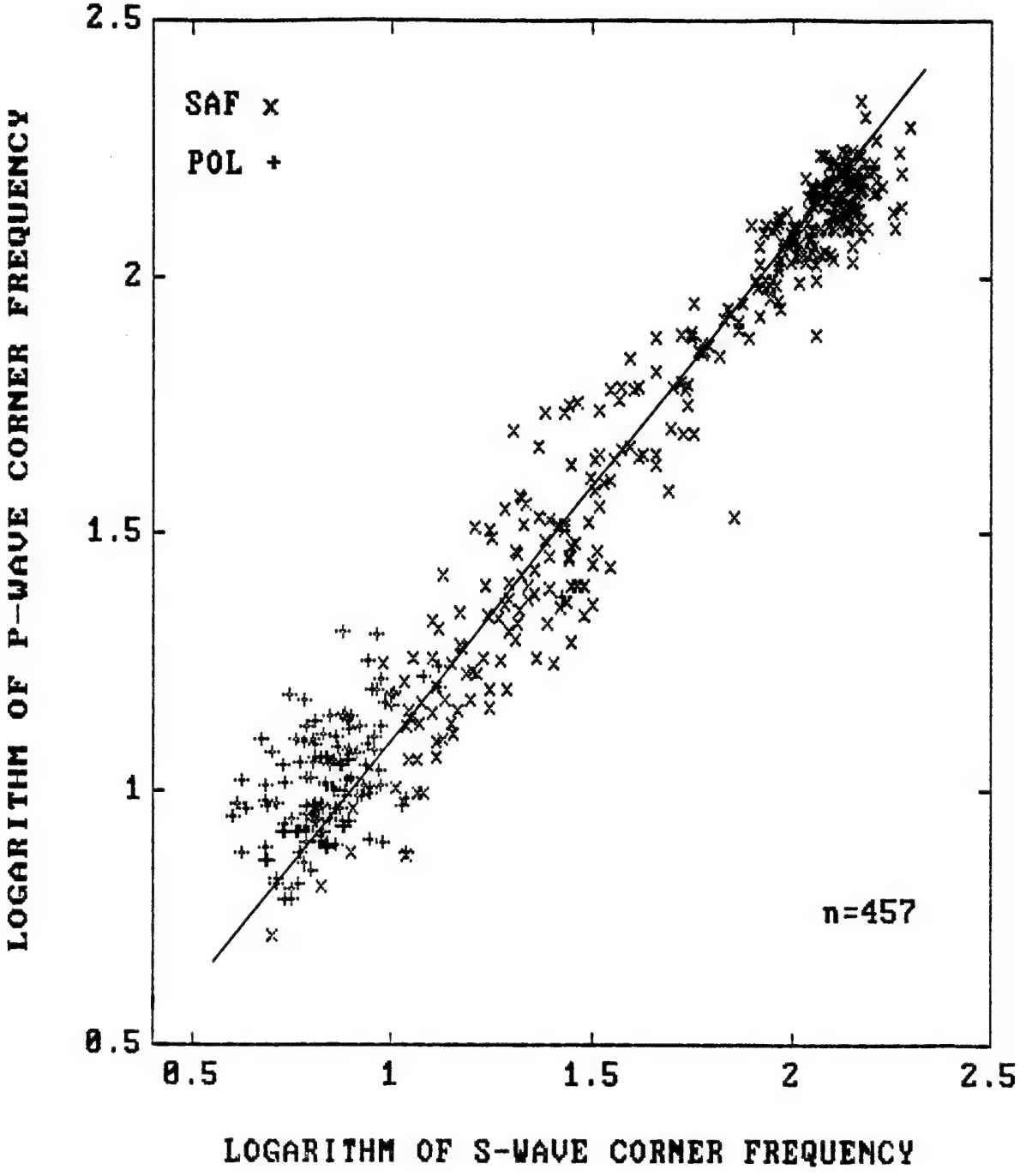

Fig.33. Logarithm of P - wave versus logarithm of S-wave corner frequency for seismic events from Polish (POL) coal and South African (SAF) gold mines.

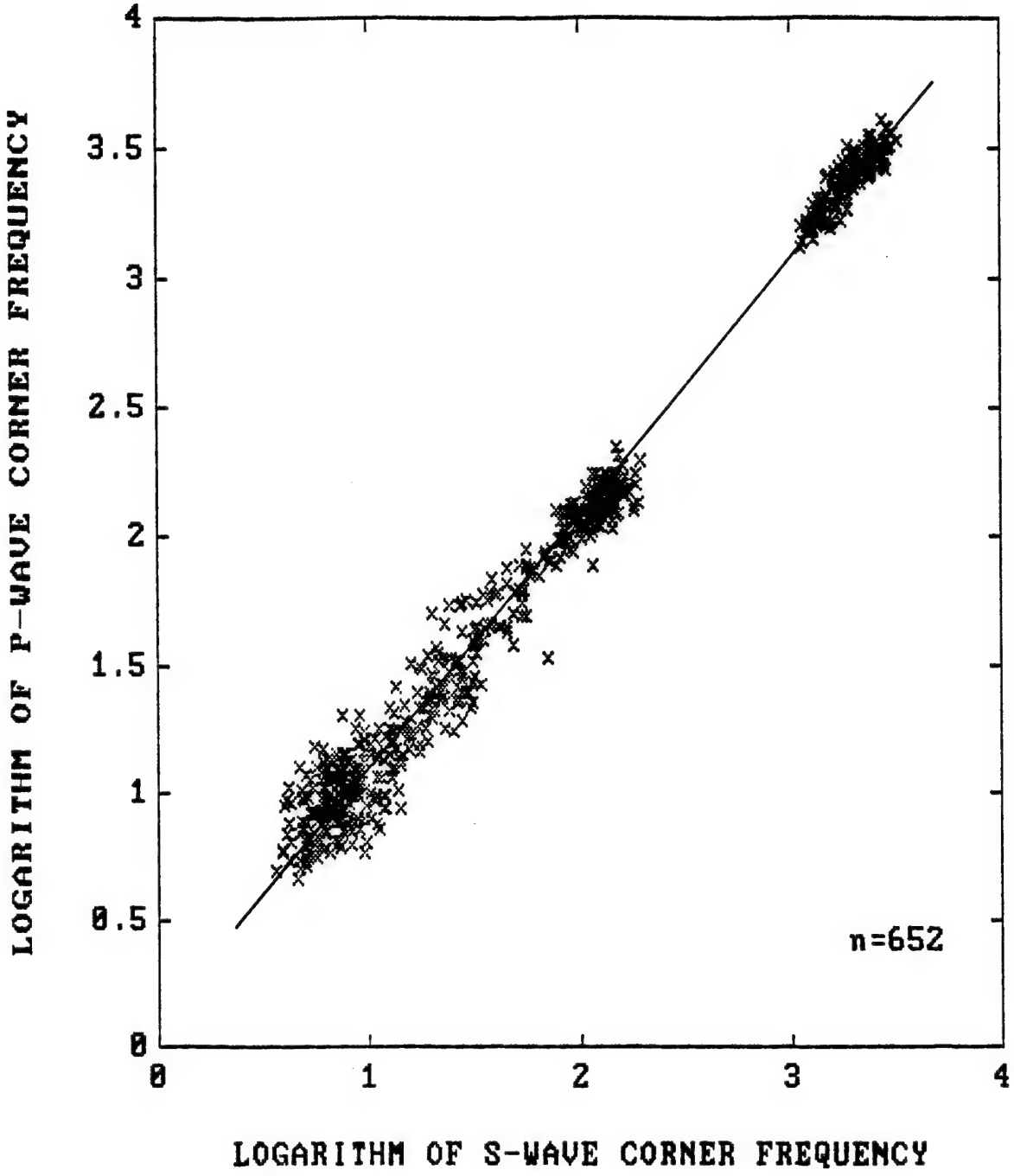

Fig. 34. Logarithm of P-wave corner frequency versus logarithm of S-wave corner frequency for 652 seismic events from Polish, German, South African, and Canadian underground mines.

Since the range of the observed values of corner frequencies at Wujek and Ziemowit coal mines is highly limited, another set of well-determined observations from gold mines in South Africa was added. The set contains 244 observations from seismic events in the Carletonville and 75 observations from events in the Orange Free State mining areas. In the Carletonville area, 217 are new observations (Gibowicz, 1994) and 27 are the observations already published (Spottiswoode, 1984; Bicknell and McGarr, 1990). Similarly, 73 observations from the Orange Free State area are new (Gibowicz, 1994) and 2 were published (McGarr *et al.*, 1990). The observed frequencies in South Africa range from 5 to 220 Hz. *P*-wave corner frequency versus *S*-wave corner frequency for seismic events from Polish coal and South African gold mines is displayed on a logarithmic scale in Fig. 33. The correlation coefficient here is 0.98 and the slope of a regression line is very close to one. The corner frequency of *P* waves is on the average about 30 percent higher than that of *S* waves and the regression analysis of the observations provides the following result: $f_p = 1.31\ f_s$.

The range of observations was further enlarged by taking into account the values found at the Underground Research Laboratory in Manitoba, where the observed frequencies ranged from about 1100 to 4000 Hz (Gibowicz *et al.*, 1991). Additional observations from the Rhur coal basin in Germany (Gibowicz *et al.*, 1990) were also added. Altogether, observations from 652 seismic events in mines were collected, and they are displayed in Fig. 34. The relation is similar to that shown in Fig. 33. The correlation coefficient here is 0.99 and the slope of a regression line is one. The corner frequencies of *P* waves are about 25 percent greater than those of *S* waves, and the relation between these two parameters is described by $f_p = 1.25\ f_s$.

V. MOMENT TENSOR INVERSION

5.1 The method

There are various methods of inversion for moment tensor components. The inversion can be done in the time or frequency domain, and different data can be used separately or in combination. These problems were recently reviewed by Gibowicz (1993).

In many applications a point source approximation may be quite satisfactory. If the source dimensions are small in comparison to the observed wavelengths of seismic waves, and assuming that all components of the time dependent seismic moment tensor M_{ij} have the same time dependence $s(t)$, the case known as synchronous source (Silver and Jordan, 1982), the displacement $u_k(\mathbf{x}, t)$ can be written as

$$u_k(\mathbf{x}, t) = M_{ij} \, [G_{ki,j} * s(t)], \tag{1}$$

where $G_{ki,j}$ are the Greeen's functions containing the propagation effects between the source and the receiver and the comma between indices denotes partial derivatives with respect to the coordinates after the comma, $s(t)$ is often called the source time function, and the asterisk * denotes the temporal convolution. Thus the displacement u_k is a linear function of the moment tensor elements and the terms in the square brackets.

The displacement in the frequency domain, corresponding to the formulation in (1), can be written as

$$u_k(\mathbf{x}, f) = M_{ij}(f) G_{ki,j}(f) \tag{2}$$

for each frequency f. Both approaches (1) and (2) lead to linear inversions in the time or frequency domain, respectively, for which a number of fast computational algorithms are available.

Both equations either (1) or (2) can be written in a matrix form as

$$\mathbf{u} = \mathbb{G}\ \mathbf{m}, \tag{3}$$

where in the time domain, the vector $\mathbf{u}$ consists of n sampled values of the observed ground displacement at various stations, $\mathbb{G}$ is a $n \times 6$ matrix containing the Green's functions calculated using an appropriate algorithm and earth model, and $\mathbf{m} = (M_{11}, M_{12}, M_{22}, M_{13}, M_{23}, M_{33})$ is a vector containing the six moment tensor elements to be determined. In the frequency domain, equations (3) are written separately for each frequency. A detailed description of the procedure for regional and local seismograms is given by Oncescu (1986). The application of moment-tensor inversion to microseismic events is described by O'Connell and Johnson (1988).

The frequency domain approach is used more commonly for two reasons. First, in the time domain the source time function $s(t)$ must be specified in advance, since the matrix $\mathbb{G}$ in the time domain contains the Green's functions derivatives convolved with the source time function. Secondly, in the frequency domain it is possible to use spectral amplitude data for different frequencies, and for each recording station there may be more data entries than in the time domain. In the case of the Upper Silesian data, the time domain approach seems to be more reasonable. All seismometers used in the mines are vertical instruments only and it is not possible to perform rotation of components for proper identification of seismic phases.

The main difficulty in the moment tensor inversion is a proper calculation of Green's functions for geologically complex media. The Green's function is in general different for different displacement components and takes different values for particular stations. The simplest approach in the time domain is to use directly the source radiation formulation for *P*, *SV* or *SH* waves. This approach was used by

Fitch *et al.* (1980), De Natale *et al.* (1987), Wiejacz (1991, 1992), and others, and is used here. The displacement amplitudes of the first arrivals of *P* and *SV* waves are given by (e. g., Fitch *et al.*, 1980; De Natale *et al.*, 1987)

$$\mathbf{u}^{P}(\mathbf{x},t) = \frac{1}{4\pi\rho\alpha^{3}r}\left[\bar{\gamma}\, M\, \dot{s}\left(t - \frac{r}{\alpha}\right)\bar{\gamma}\right]\bar{l}, \tag{4}$$

$$\mathbf{u}^{SV}(\mathbf{x},t) = \frac{1}{4\pi\rho\beta^{3}r}\left[\bar{p}\, M\, \dot{s}\left(t - \frac{r}{\beta}\right)\bar{\gamma}\right]\bar{p}, \tag{5}$$

where $\dot{s}$ is the time derivative of the source time function; ρ is the density of the medium; α and β are the velocities of *P* and *S* waves, respectively; r is the distance between the source and sensor; and $\bar{\gamma}$, $\bar{l}$, and $\bar{p}$ are unitary vectors; $\bar{\gamma}$ is the direction the wave leaves the source, $\bar{l}$ is the direction of propagation of the wave as it arrives at the seismometer, and $\bar{p}$ is perpendicular to $\bar{l}$ in the vertical plane containing $\bar{l}$. Once the displacements **u** are known, the calculation of the unitary vectors $\bar{\gamma}$, $\bar{l}$, and $\bar{p}$ must be performed, which may be done after adoption of a specific velocity model. In our case, in which all seismometers are vertical, it is possible to use only the vertical components of equations (4) and (5).

As for the source time function $s(t)$, two forms are used most commonly: the Haskell (1964) type

$$s(t) = \begin{cases} 0 & \text{for} \quad t<0 \\ t/T & \text{for} \quad 0\le t\le T \\ 1 & \text{for} \quad t>T \end{cases} \tag{6}$$

and the Brune (1970) type

$$s(t) = \begin{cases} 0 & \text{for} \quad t\le 0 \\ 1-\exp(-t/\tau) & \text{for} \quad t>0 \end{cases} \tag{7}$$

where T or τ are parameters associated with the duration of the rupture. The source time function of the Haskell type is used here. Its time derivatives

$$\dot{s}(t) = \begin{cases} 1/T & \text{for} \quad 0<t<T \\ 0 & \text{for} \quad t<0 \text{ and } t>T \end{cases} \tag{8}$$

are simpler to use than the time derivatives of Brune's function, and in practical applications the Haskell function fits the data equally well as the Brune function. The parameter T can be estimated from the time interval between the first onset of the wave and its maximum amplitude.

Finding a moment tensor requires solution of a set of n equations of type (4) or (5). Since the moment tensor has six independent components, there must be at least six such equations, but usually more than that are needed. Additional constraints may be imposed on the solution. The most common constraints require that either the trace of the moment tensor or the trace and the determinator of the tensor vanish. The condition of zero trace automatically excludes the volume change type mechanism, and since zero trace means also that $M_{33} = -(M_{11} + M_{22})$, only five components remain independent. The constraint of zero trace and zero determinator limits the solution to the double-couple source. The null determinator condition is nonlinear, forcing the use of the Lagrange multiplier scheme in order to find the solution (e. g., Oncescu, 1986).

Typically the number of equations (4) and (5) greatly exceeds the number of unknown variables. If we rewrite the set of equations into a $\mathbb{A}\ \mathbf{m} = \mathbf{u}$ form, the best solution of this over-determined problem is normally expected to be such $\mathbf{m}_0$, for which

$$S_2 = \sum_{i=1}^{n} \left(u^{*}_{z(i)} - (\mathbb{A}\ \mathbf{m}_0) \right)^2 = \min, \tag{9}$$

where * is either P or SV. Such solution is commonly referred to as a L_2-norm solution. A series of tests run on synthetic data has shown,

however, that such solutions may be prone to considerable errors; a single erroneous observation, if its value is large, may affect the whole solution. In some cases it is safer therefore to use the L_1-norm solution, which requires that

$$S_1 = \sum_{i=1}^{n} \left| u^{*}_{z(i)} - (\mathbb{A}\, \mathbf{m}_0) \right| = \min. \qquad (10)$$

5.2 Application

The described method has been applied to the seismic data from Ziemowit and Wujek mines. A computer program was written in Microsoft Fortran 5.0 in order to handle the data. The calculations were performed on an IBM-clone 386SX and original IBM PS/VP computers.

First of all, the ground velocity signals have been integrated in order to obtain ground displacement. Then, the appropriate onsets of the direct *P* and *SV* waves have been identified. Their amplitudes and time durations were measured. The time durations of the first onsets of waves were used in two ways. Firstly, they were used to convert the amplitudes, which have been measured in digits, to meters, according to the frequency response curves for the individual channels. This information has been provided by the mines. Secondly, they were used to estimate the rupture duration T in formula (6).

Source locations together with the seismic station positions provided the angular data: source to station azimuths, takeoff angles of the waves, arrival angles at the stations, and the source to station distances. These data, in turn, allow for the calculation of $\bar{l}$, $\bar{p}$, and $\bar{\gamma}$ vectors in formulas (4) and (5). An average *P*-wave velocity of 3800 m/s and a medium density of 2750 kg/m^3 were accepted for the calculations. The calculations were performed twice for each event, using the L_2 and L_1 norms. For each norm, a full moment tensor solution, a no volume change moment tensor solution and a double couple moment tensor solution were found.

The general full moment tensor solutions often contain substantial volume change components and they seem to be of not high quality for two reasons: the number of observations is occasionally as low as eight, and the station coverage of the source is not always adequate, with the stations often spread out at takeoff angles near 90 degrees. The number of independent variables in the no volume change moment tensor solutions is reduced to five, and there appears to be a fair correlation between the L_2-norm and L_1-norm solutions for individual events. The number of independent variables in the double couple moment tensor solutions is down to four. The L_2-norm double couple solutions are usually similar to the L_2-norm no volume change solutions. This is a consequence of the fact that the L_2-norm double couple solutions are calculated by an iterative scheme, to which the no volume change solution serves as a starting point. The L_1-norm double couple solutions often are similar to the L_2-norm solutions, but not always. The most probable reason for this discrepancy may be a substantial deviation of the mechanism from a double couple, or a poor data coverage, or both.

After careful inspection of all solutions, the L_2-norm solutions were accepted for further consideration. Out of 55 processed seismic events from Wujek coal mine, 44 full moment tensor solutions were selected as reasonable. Similarly, out of 83 processed events from Ziemowit coal mine, 72 full moment tensor solutions were taken into account. These moment tensor solutions for the seismic events at Wujek mine are listed in Appendix A and those for the events at Ziemowit mine are presented in Appendix B.

The moment tensor solutions for each seismic event listed in Appendices A and B contain several details. The event numbers at the top are the same as those listed in Tables 1 to 6. Three rows and three columns of numbers is the seismic moment tensor. Its components are in N·m. TO is the estimated rupture time given in seconds. MO is the scalar seismic moment, equal to the greatest eigenvalue of the double couple component of the moment tensor. MT is the so-called total seismic moment, equal to the square root of the half of sum of squares of the eigenvalues of the moment tensor (Silver and Jordan, 1982). Expl., CLVD., and DBCP. stand for explosive, compensated linear

vector dipole, and double couple components. The seismic moment tensor is rotated to a coordinate system formed by its eigenvectors. In such a system, the non-diagonal components of the tensor vanish and the tensor is readily decomposed into the following tensors (e. g., Gibowicz, 1993):

$$\begin{vmatrix} a & 0 & 0 \\ 0 & b & 0 \\ 0 & 0 & c \end{vmatrix} = E \begin{vmatrix} 1 & 0 & 0 \\ 0 & 1 & 0 \\ 0 & 0 & 1 \end{vmatrix} + L \begin{vmatrix} -1 & 0 & 0 \\ 0 & -1 & 0 \\ 0 & 0 & 2 \end{vmatrix} + D \begin{vmatrix} 0 & 0 & 0 \\ 0 & -1 & 0 \\ 0 & 0 & 1 \end{vmatrix}$$

The explosive component is the ratio of E to the sum of absolute values of E, L, and D. Its negative values denote implosion. The compensated linear vector dipole component is the ratio of L to the same sum, and the double couple component is the ratio of D to the sum. The sign of CLVD depends on whether the dipole is compressive or dilatational. Values of the components are given in percent. ΦA, δA, ΦB, and δB are the strikes and dips of nodal planes of the best double couple. These angles are calculated from directions of the main axes and they are given in degrees. The trends and plunges of the main P, T and B axes are also given in degrees. The quality index q depends on three factors $q = 100q_1q_2q_3$ and it is in the range from 0 to 100. The first factor $q_1 = (N - 6)/N$, where N is the number of stations used for the inversion. The second factor q_2 is the maximum ratio of the error to the absolute value of any given moment tensor component. The errors of moment tensor components are calculated as square roots of diagonal components of the covariance matrix. The third factor q_3 is an iteration indicator, used only for double couple solutions which are calculated iteratively. When more than 200 iteration steps are needed, the factor q_3 starts to diminish from 1 down to 0.5. If there are 1000 iteration steps, the procedure stops, initial parameters are taken as final and q_3 is taken equal to 0.5. The final qualification of the solution called normal, reverse or strike slip fault is based on directions of the main axes. If the axis closest to the vertical is the null axis B, the solution is denoted as strike slip, if it is the pressure axis P, the solution is called normal fault, and if it is the tension axis T, the solution is marked as reverse fault. All solutions are also presented graphically on equal-area lower-hemisphere projections.

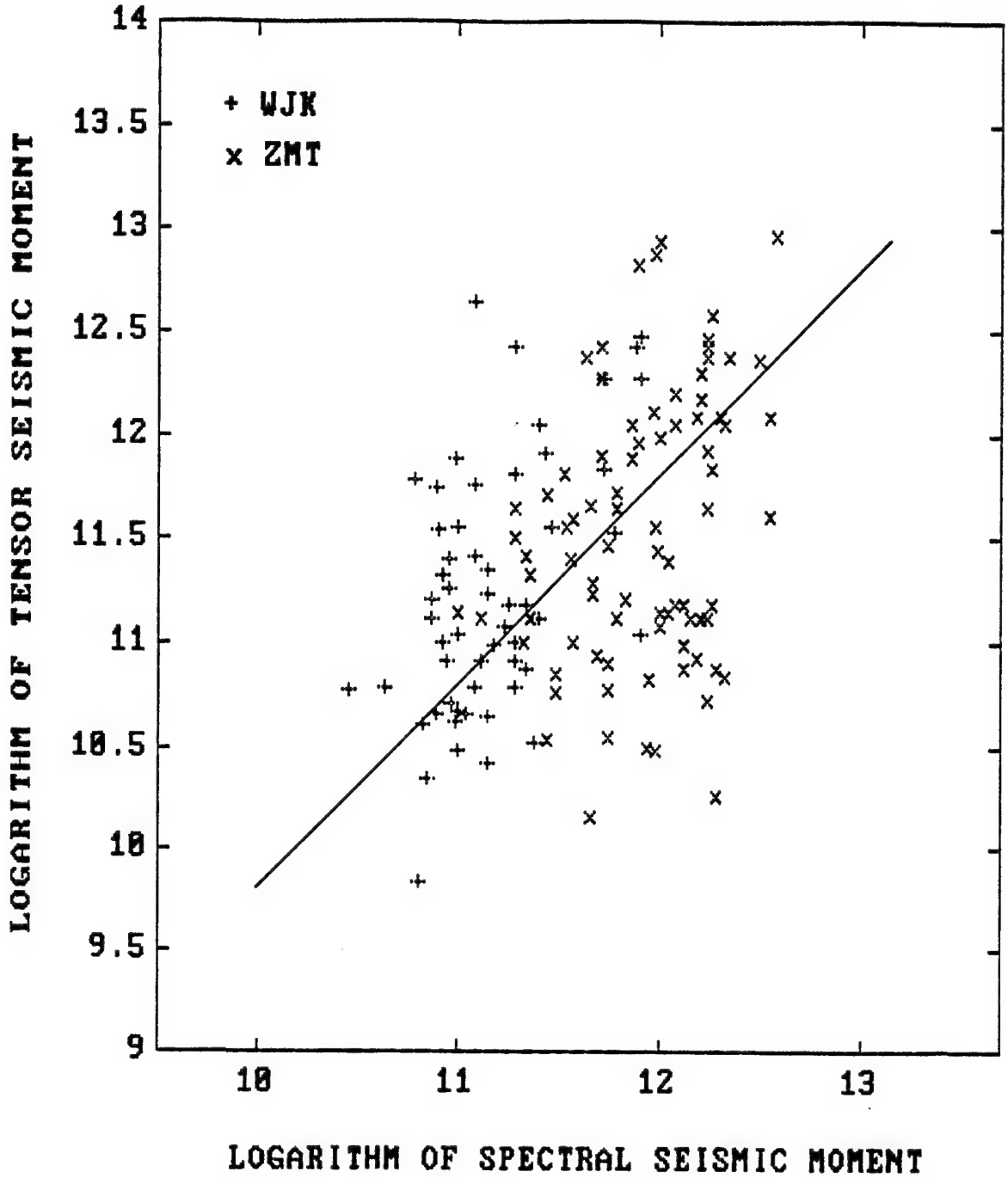

Fig. 35. Logarithm of seismic moment calculated from moment tensor solutions versus logarithn of seismic moment calculated from spectra for selected seismic events at Wujek and Ziemowit coal mines.

5.3 Spectral and moment tensor source parameters

The values of scalar seismic moment calculated as the greatest eigenvalue of the double couple component of general moment tensor solutions versus the values of seismic moment calculated from the spectra of *P* and *S* waves, for selected seismic events observed at both Wujek and Ziemowit coal mines, are shown in Fig. 35. On the average, the values from the moment tensor inversion are lower by a factor of about 0.6 than those estimated from the spectra. The correlation coefficient between these values is only 0.4 and the scattering of data is considerable. Nevertheless, the seismic moment values obtained by the two independent techniques are of the same order of magnitude, and since they are based on records of single vertical components only, the presented results seem to be reasonable.

A comparison of the ratio of *S*-wave over *P*-wave energy with the indicators of either double couple or non-double couple components of the moment tensor solutions is the most interesting for our search of non-shearing components of the seismic source. Out of 55 selected seismic events from Wujek mine, for 6 events the energy of *P* waves could not be estimated (Table 4). Similarly, out of 83 seismic events from Ziemowit mine, for 9 events the energy of *P* waves was not calculated (Table 6). Taking into account that for 11 events at the both mines no reasonable general moment tensor solutions could be obtained, we have finally in hand a set of 38 data from Wujek mine and 63 data from Ziemowit mine, related simultaneously to the energy ratio and to the indicators of moment tensor components.

The logarithm of the ratio of *S*-wave over *P*-wave energy versus the indicator of a double couple component in the general moment tensor solution for the seismic events at both Wujek and Ziemowit mines is shown in Fig. 36. The logarithm of the same ratio versus the indicator of a CLVD component is presented in Fig. 37, and the energy ratio versus the indicator of a volumetric component is shown in Fig. 38. The correlation coefficient in the first case is 0.3 and in the second and third case it is -0.3. These values indicate that the relations between the ratio of *S*- over *P*-wave energy and the indicators of non-

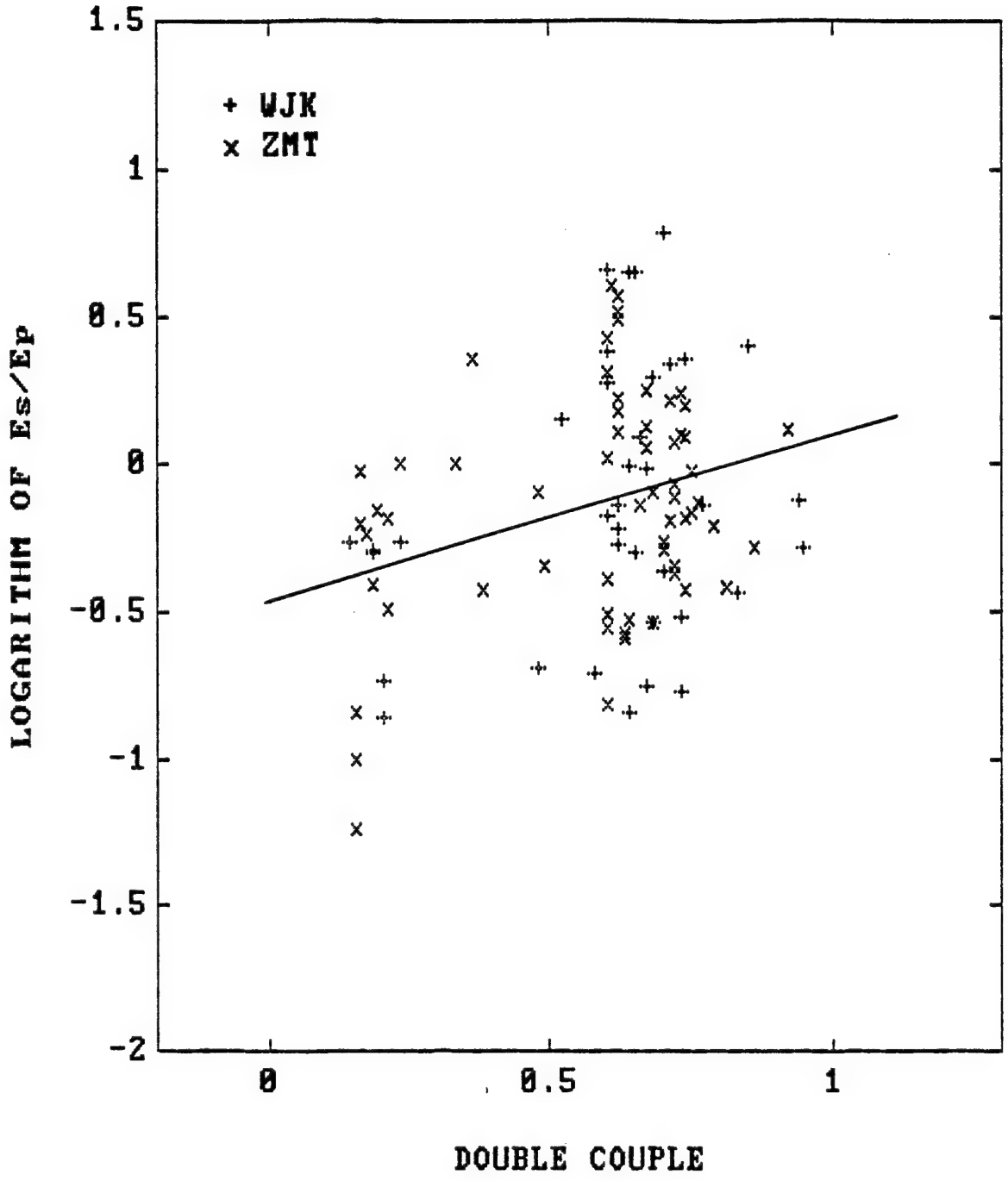

Fig.36. Logarithm of the ratio of S-wave over P-wave energy versus the indicator of a double-couple component in the general moment tensor solution for selected seismic events at Wujek and Ziemowit coal mines.

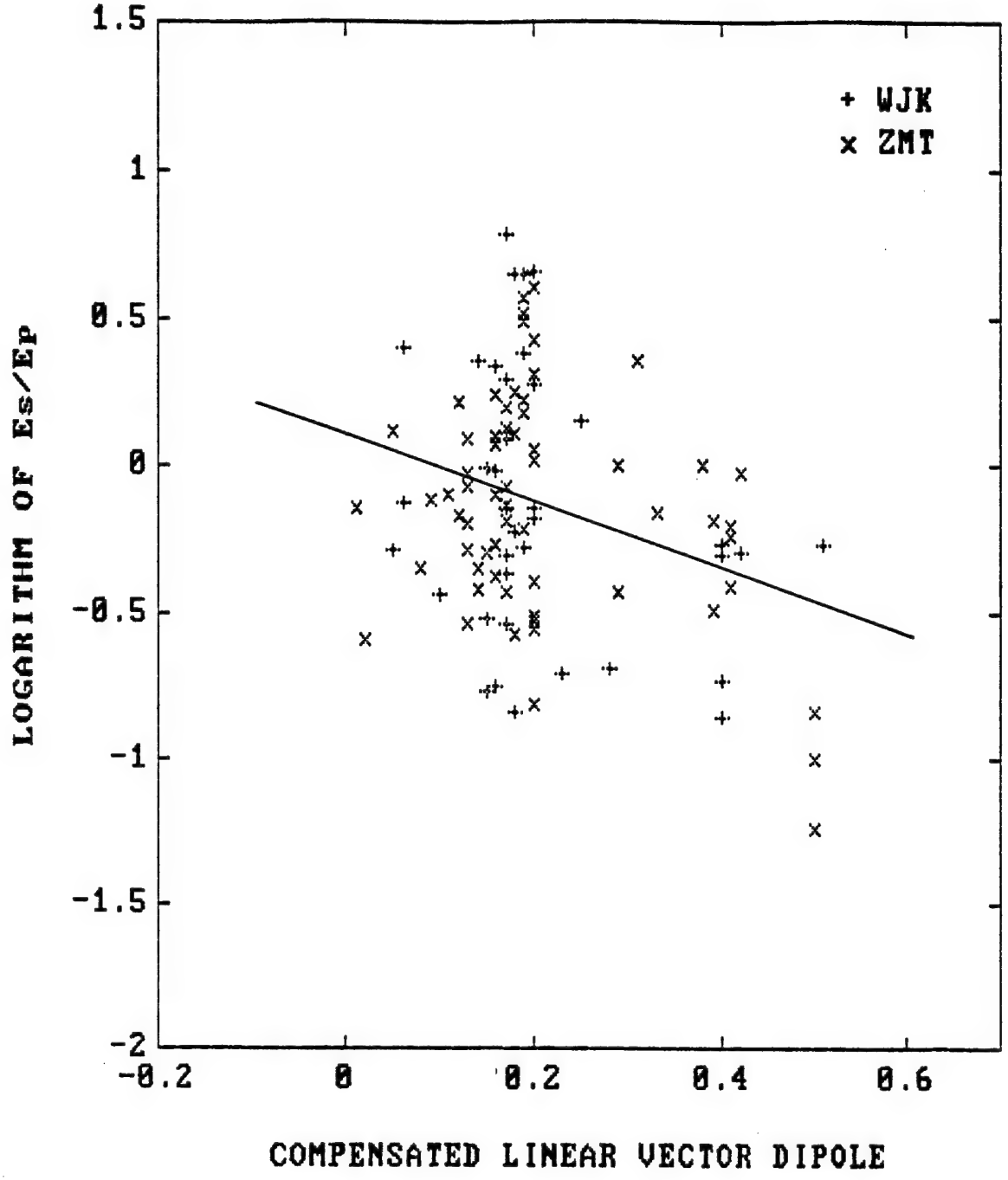

Fig. 37. Logarithm of the ratio of S-wave over P-wave energy versus the indicator of a CLVD component in the general moment tensor solution for selected seismic events at Wujek and Ziemowit coal mines.

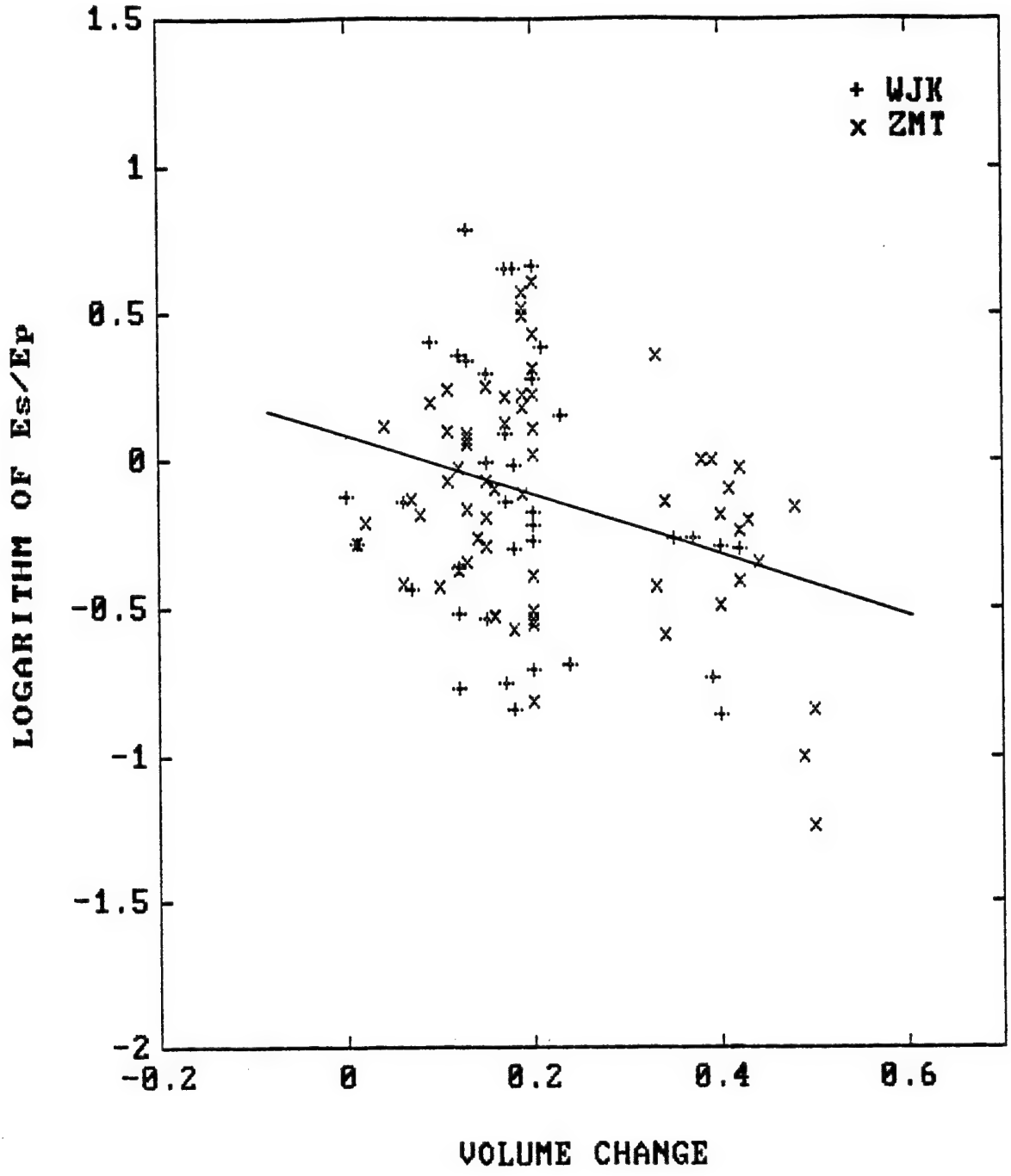

Fig.38. Logarithm of the ratio of S-wave over P-wave energy versus the indicator of a volumetric component in the general moment tensor solution for selected seismic events at Wujek and Ziemowit coal mines.

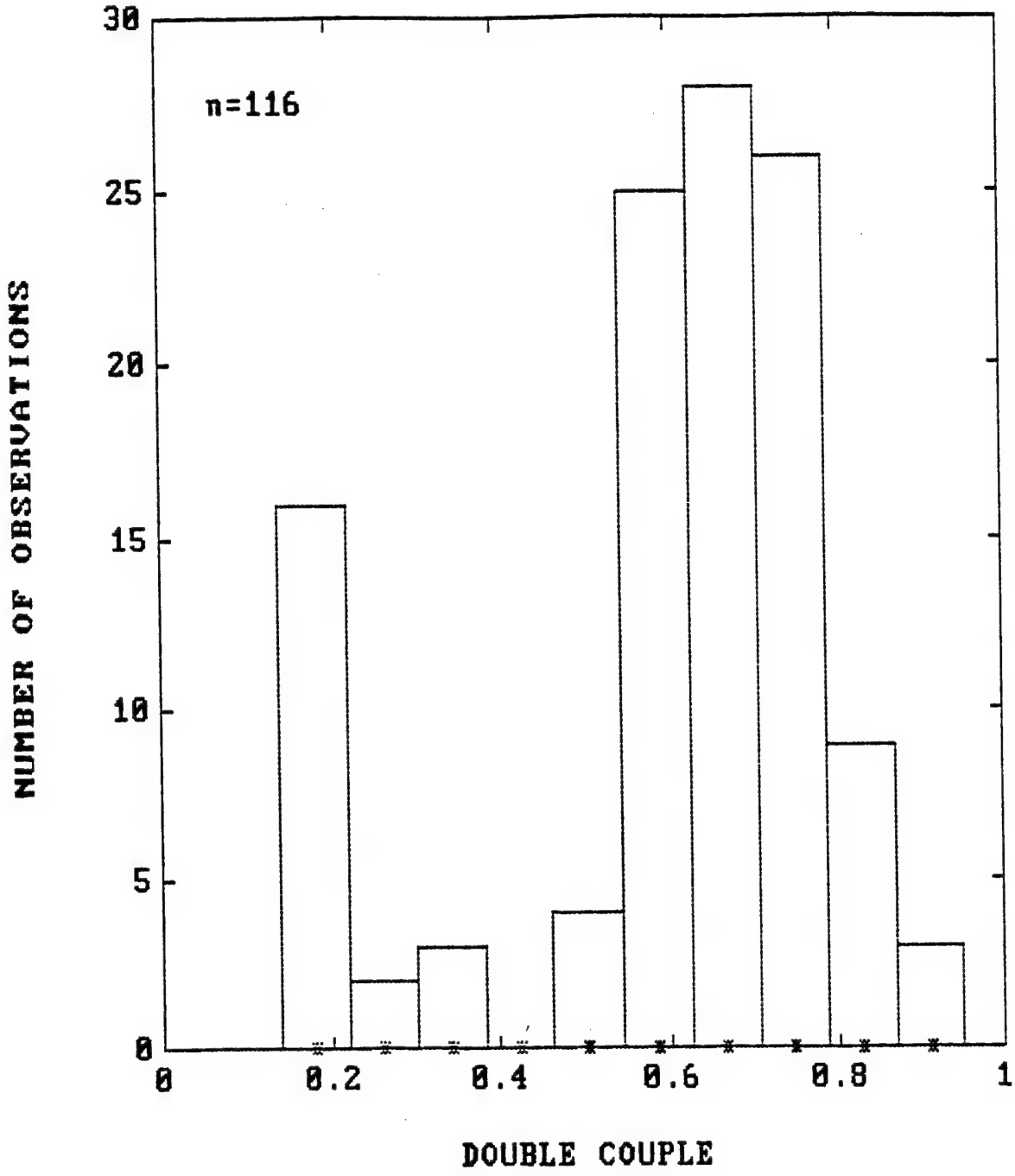

Fig.39. Histogram of the indicator of a double-couple component in the general moment tensor solution for the 116 selected seismic events at Wujek and Ziemowit coal mines.

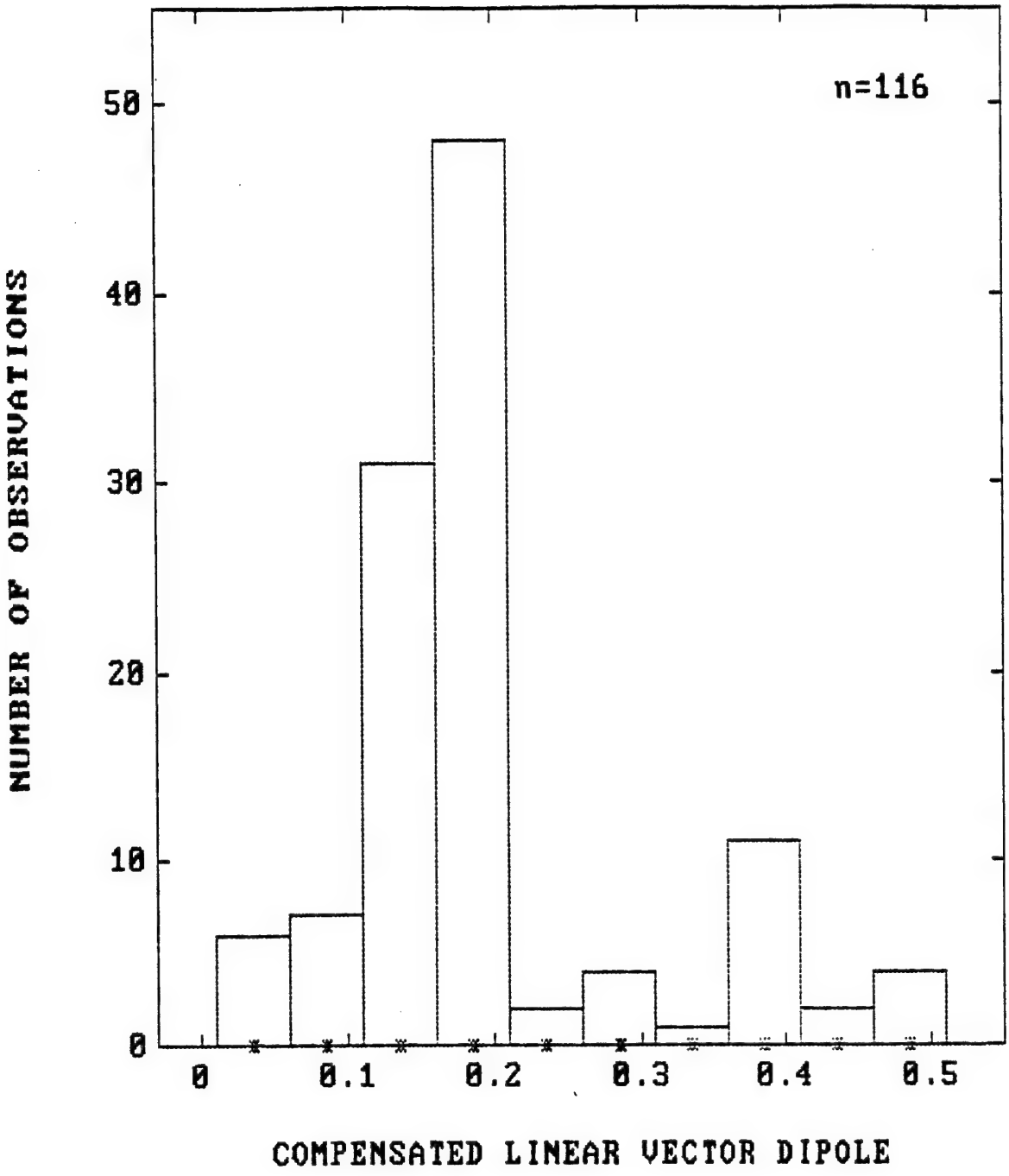

Fig. 40. Histogram of the indicator of a CLVD component in the general moment tensor solution for selected seismic events at Wujek and Ziemowit coal mines.

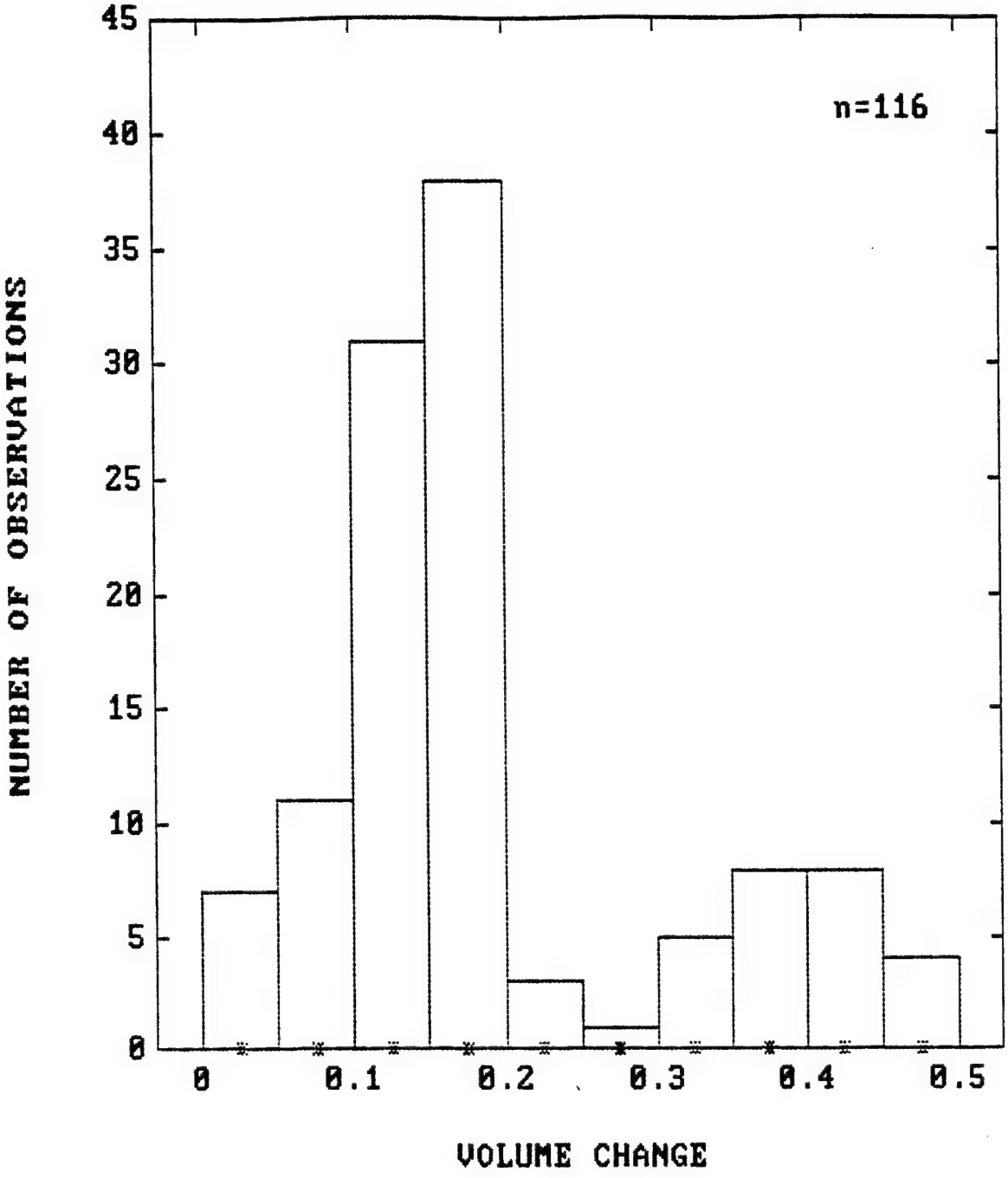

Fig. 41. Histogram of the indicator of a volumetric component in the general moment tensor solution for selected seismic events at Wujek and Ziemowit coal mines.

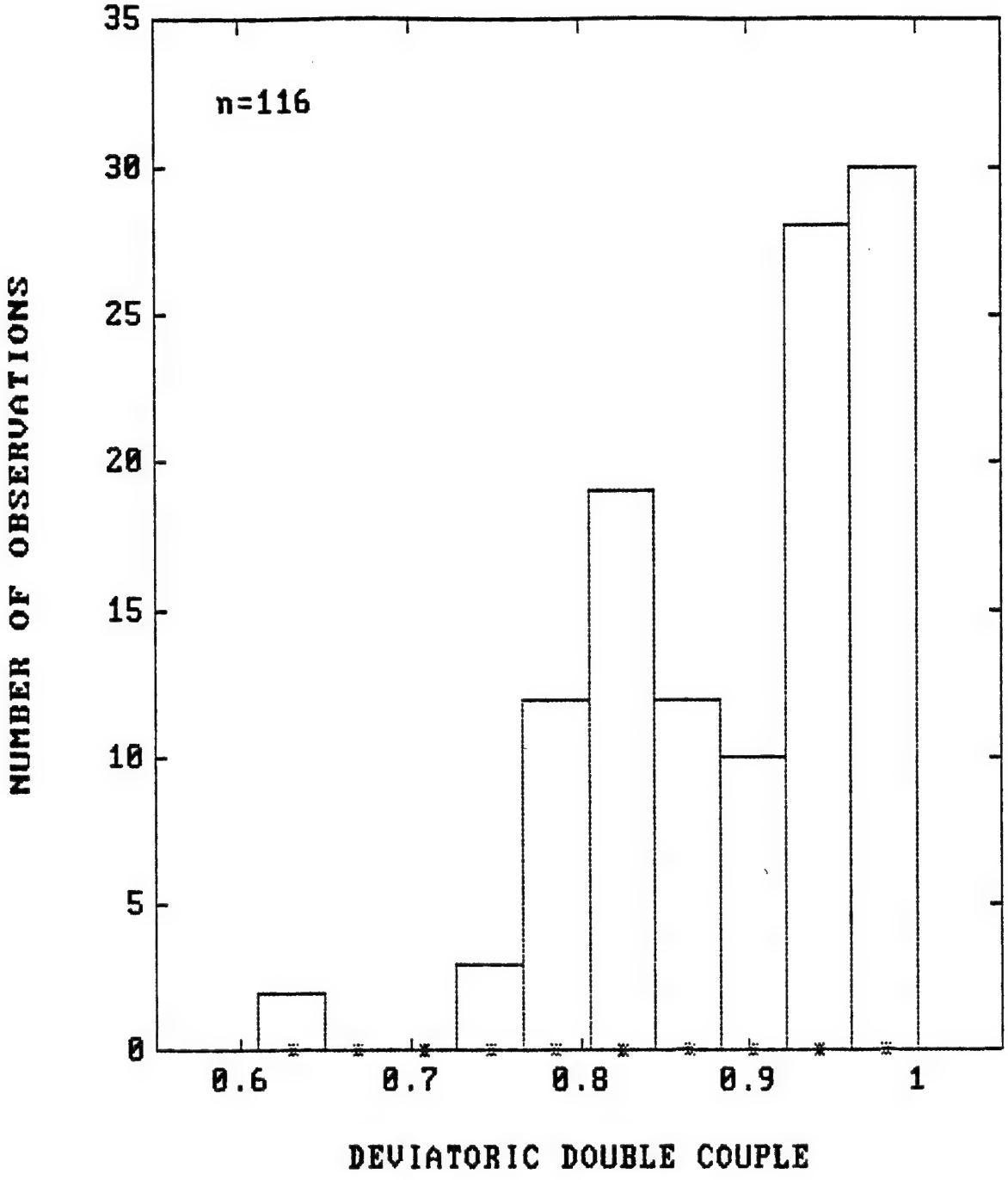

Fig. 42. Histogram of the indicator of a double-couple component in the deviatoric moment tensor solution for selected seismic events at Wujek and Ziemowit mines.

shearing components of the moment tensor are not as straighforward as it was expected. The general tendency, however, points into right direction. On the average, the high values of the *S*- over *P*-wave energy ratio are associated with seismic sources with dominant double couple components.

Histograms of the indicators of a double couple, CLVD, and volumetric components in the general moment tensor solutions are shown in Figs 39, 40, and 41. For about 80 % of seismic events the double couple component forms more than 60 % of the solution. Similarly, for about 80 % of seismic events the CLVD component is smaller than 20 % of the solution, and for about 75 % of the events the volumetric component is also less than 20 % of the general solution. The double couple component in the constrained deviatoric moment tensor solutions is the most dominant part of the source mechanism (Fig. 42). For about 95 % of seismic events the double couple component forms 80 % of the solution, and for about 60 % of the events it corresponds to 90 % of the source mechanism.

VI. CONCLUSIONS

The objective of this research has been to investigate the non-shearing components of the source mechanism of seismic events induced in Polish coal mines. To accomplish this objective we collected and analyzed the available digital data for selected seismic events from Wujek and Ziemowit coal mines in the Upper Silesian Coal Basin. We performed spectral analysis of seismic waves and moment tensor inversion for 55 selected seismic events at Wujek mine, recorded by the underground seismic network composed of 12 vertical seismometers, and for 83 seismic events at Ziemowit mine, recorded by the underground network composed of 16 vertical sensors. The ratio of *P*-wave over *S*-wave energy radiated from seismic events in mines is often anomalously large. We expected to show that seismic events with high *P*-wave energy in comparison to *S*-wave energy are generated by the sources with prominent non-shearing components, as estimated from the moment tensor inversions. Such events usually occur in close vicinity to the mining faces, where favourable conditions for generation of tensile failures or shear failures with tensile components are present.

The selected seismic events from Wujek mine have moment magnitude between 1.1 and 2.2 and seismic energy between $1*10^5$ and $2*10^7$ J, and the seismic events from Ziemowit mine are characterized by moment magnitude from 1.4 to 2.4 and seismic energy from $2*10^6$ to $7*10^8$ J. The source radius is similar at both mines, ranging from 40 to 100 m. The stress drop at Ziemowit mine is about five times higher than that at Wujek mine, ranging from 0.2 to 5.7 MPa. Similarly, the apparent stress at Ziemowit mine is about ten times higher than that at Wujek mine and ranges between 0.05 and 4.8 MPa. The ratio of *S*-wave to *P*-wave energy is at both mines in a similar range of values from about 0.1 to 18. The scaling relations at both mines imply that the self-similarity rule is probably valid there, though the relations are based on a very narrow range of seismic moment values.

Full moment tensor solutions, constrained solutions without isotropic component, and constrained solutions for pure double couple were calculated. The general moment tensor solutions were decomposed into an isotropic part, a compensated linear vector dipole and a double couple. For about 80 % of seismic events the double couple component forms more than 60 % of the solution. Similarly, for about 80 % of seismic events the CLVD component is smaller than 20 % of the solution, and for about 75 % of the events the volumetric component is also less than 20 % of the general solution. The double couple component in the constrained deviatoric moment tensor solutions is the most dominant part of the source mechanism. For about 95 % of seismic events the double couple component forms 80 % of the solution, and for about 60 % of the events it corresponds to 90 % of the source mechanism.

The relations between the ratio of *S*- over *P*-wave energy and the indicators of a double couple component, a compensated linear vector dipole, and an isotropic part in the general solution are not as straighforward as it was expected. Although there is a positive correlation between the energy ratio and the double-couple indicator, and negative correlations between the ratio and the compensated linear vector dipole and volumetric change indicators, the correlation coefficients in all three cases are small. The general tendency, however, points into right direction. On the average, the high values of the *S*- over *P*-wave energy ratio are associated with seismic sources with dominant double couple components. Thus our attempt to correlate the energy ratio, estimated by spectral analysis of seismic waves, with the indicators of non-shearing components of the source, found by moment tensor inversion, was only partly successful. It should be pointed out, however, that only single-component seismograms were available for our study, and that this could well be an important factor in our approach to a search for non-shearing components of the source mechanism of seismic events induced by mining. Unfortunately, all seismic networks in Polish mines are composed of vertical sensors only and no better data than those used here are at present available.

REFERENCES

Bicknell, J., and McGarr, A. (1990). Underground recordings of mine tremors - Implications for earthquake source scaling. *In* "Rockbursts and Seismicity in Mines" (C. Fairhurst, ed.), pp. 109-114. Balkema Rotterdam.

Boatwright, J. (1984). (1984). Seismic estimates of stress release. *J. Geophys. Res.* **89**, 6961-6968.

Boatwright, J., and Fletcher, J. B. (1984). The partition of radiated energy between P and S waves. *Bull. Seism. Soc. Am.* **74**, 361-376.

Boore, D. M. (1986). The effect of finite bandwidth on seismic scaling relations. *In* "Earthquake Source Mechanics" (S. Das, J. Boatwright, C. H. Scholz, eds.), Maurice Ewing Vol. 6, pp. 275-283, Am. Geophys. Union, Washington, D. C.

Brune, J.N. (1970). Tectonic stress and the spectra of seismic shear waves from earthquakes. *J.Geophys.Res.* **75**, 4997-5009.

Brune, J.N. (1971). Correction. *J. Geophys. Res.* **76**, 5002.

Brune, J.N., Archuleta, R., and Hartzell, S. (1979). Far-field S-wave spectra, corner frequencies and pulse shapes. *J. Geophys. Res.* **81**, 2262-2272.

Bukowy, S. (1984). "Variscian Structure of the Silesian-Cracow Region." Silesian University, Katowice, Poland (in Polish with English abstract).

Burdick, L. J. (1978). t^* for *S* waves with a continental ray path. *Bull. Seism. Soc. Am.* **68**, 1013-1030.

Chael, E. P., and Kromer, P. (1988). High-frequency spectral scaling of a main shock/aftershock sequence near the Norwegian coast. *Bull. Seism. Soc. Am.* **78**, 561-570.

Chun, K.-Y., Kokoski, R. J., and West, G. F. (1989). Source spectral characteristics of Miramichi earthquakes: Results from 115 *P*-wave observations. *Bull. Seism. Soc. Am.* **79**, 15-30.

Cichowicz, A., Green, R. W. E., Brink, A. v. Z., Grobler, P., and Mountfort, P. I. (1990). The space and time variation of microevent parameters occurring in front of an active stope. *In* "Rockbursts and Seismicity in Mines" (C. Fairhurst, ed.), pp. 171-175, Balkema, Rotterdam.

De Natale, G., Iannaccone, G., Martini, M., and Zollo, A. (1987). Seismic sources and attenuation properties at the Campi Flegrei volcanic area. *In* "Advances in Volcanic Seismology" (E. A. Okal, ed.), Special Issue, *Pure Appl. Geophys.* **125**, 883-917.

Di Bona, M., and Rovelli, A. (1988). Effects of the bandwidth limitation on stress drops estimated from integrals of the ground motion. *Bull. Seism. Soc. Am.* **78**, 1818-1825.

Dysart, P. S., Snoke, J. A., and Sacks, I. S. (1988). Source parameters and scaling relations for small earthquakes in the Matsushiro region, southwest Honshu, Japan. *Bull. Seism. Soc. Am.* **78**, 571-589.

Ebel, J. E., and Bonjer, K.-P. (1990). Moment tensor inversion of small earthquakes in southwestern Germany for the fault plane solution. *Geophys. J. Int.* **101**, 133-146.

Feignier, B., and Young, R. P. (1992). Moment tensor inversion of induced microseismic events: Evidence of non-shear failures in the $-4<M<-2$ moment magnitude range. *Geophys. Res. Lett.* **19**, 1503-1506.

Fitch, T. J., McCowan, D. W., and Shields, M. W. (1980). Estimation of seismic moment tensor from teleseismic body wave data with application to intraplate and mantle earthquakes. *J. Geophys. Res.* **85**, 3817-3828.

Frankel, A., and Wennerberg, L. (1989). Microearthquake spectra from the Anza, California, seismic network: Site response and source scaling. *Bull. Seism. Soc. Am.* **79**, 581-609.

Fujii, Y., and Sato, K. (1990). Difference in seismic moment tensors between microseismic events associated with a gas outburst and those induced by longwall mining activity. *In* "Rockbursts and Seismicity in Mines" (C. Fairhurst, ed.), pp. 71-75. Balkema, Rotterdam.

Gibowicz, S.J. (1984). The mechanism of large mining tremors in Poland. *In* "Rockbursts and Seismicity in Mines" (N.C.Gay and E.H.Wainwright, eds.), Symp. Ser. No.6, pp. 17-28. S. Afr. Inst. Min. Metal., Johannesburg.

Gibowicz, S. J. (1985). Seismic moment and seismic energy of mining tremors in the Lubin copper basin in Poland. *Acta Geophys. Pol.* **33**, 243-257.

Gibowicz, S. J. (1990a). Keynote lecture: The mechanism of seismic events induced by mining - A review. *In* "Rockbursts and Seismicity in Mines" (C.Fairhurst, ed.), pp. 3-27. Balkema, Rotterdam.

Gibowicz, S. J. (1990b). Seismicity induced by mining. *Adv. Geophys.* **32**, 1-74.

Gibowicz, S. J. (1993). Keynote address: Seismic moment tensor and the mechanism of seismic events in mines. *In* "Rockbursts and Seismicity in Mines" (R. P. Young, ed.), pp. 149-155. Balkema, Rotterdam.

Gibowicz, S. J. (1994). Scaling relations for seismic events induced by mining. In preparation.

Gibowicz, S. J., Cichowicz, A., and Dybeł, T. (1977). Seismic moment and source size of mining tremors in Upper Silesia, Poland. *Acta Geophys. Pol.* **25**, 201-218.

Gibowicz, S.J., Niewiadomski,J., Wiejacz, P., and Domanski, B. (1989). Source study of the Lubin, Poland, mine tremor of 20 June 1987. *Acta Geophys. Pol.* **37**, 111-132.

Gibowicz, S. J., Harjes, H.-P., and Schäfer, M. (1990). Source parameters of seismic events at Heinrich Robert mine, Ruhr basin, Federal Republic of Germany: Evidence for nondouble-couple events. *Bull. Seism. Soc. Am.* **80**, 88-109.

Gibowicz, S. J., Young, R. P., Talebi, S., and Rawlence, D. J.(1991). Source parameters of seismic events at the Underground Research Laboratory in Manitoba, Canada: Scaling relations for the events with moment magnitude smaller than -2. *Bull. Seism. Soc. Am.* **81**, 1157-1182.

Glassmoyer, G., and Borcherdt, R. D. (1990). Source parameters and effects of bandwidth and local geology on high-frequency ground motions observed for aftershocks of the northeastern Ohio earthquake of 31 January 1986. *Bull. Seism. Soc. Am.* **80**, 889-912.

Hanks, T. C. (1981). The corner frequency shift, earthquake source models, and *Q*. *Bull. Seism. Soc. Am.* **71**, 597-612.

Hanks, T. C., and Kanamori, H. (1979). A moment magnitude scale. *J. Geophys. Res.* **84**, 2348-2350.

Haskell, N. A. (1964). Total energy and spectral density of elastic wave radiation from propagating faults. *Bull. Seism. Soc. Am.* **54**, 1811-1841.

Herbich, E. (1981). A tectonic analysis of the fault network of the Upper Silesian Coal Basin. *Rocznik Polish Geol. Soc.* **51**, 383-434 (in Polish with English abstract).

Hinzen, K.-G. (1982). Source parameters of mine tremors in the eastern part of the Ruhr district (West Germany). *J. Geophys.* 51, 105-112.

Kanamori, H., and Anderson, D. L. (1975). Theoretical basis for some empirical relations in seismology. *Bull. Seism. Soc. Am.* **65**, 1073-1096.

Koch, K. (1991a). Moment tensor inversion of local earthquake data – I. Investigation of the method and its numerical stability with model calculations. *Geophys. J. Int.* **106**, 305-319.

Koch, K. (1991b). Moment tensor inversion of local earthquake data – II. Application to aftershocks of the May 1980 Mammoth Lakes earthquakes. *Geophys. J. Int.* **106**, 321-332.

Kotas, A. (1985). Remarks on the structural evolution of the Upper Silesian Coal Basin. *Proc. Confer. Upper Silesian Coal Basin Tectonics*, pp. 17-46, Silesian University, Sosnowiec (in Polish).

Kotas, A., Bula, Z., Gadek, S., Kwarcinski, J., and Malicki, R. (1983). Maps of the coal quality. *In* "Geological Atlas of the Upper Silesian Coal Basin", Part 2, Geological Institute, Warsaw, Poland.

McGarr, A. (1992). An implosive component in the seismic moment tensor of a mining-induced tremor. *Geophys. Res. Lett.* **19**, 1579-1582.

McGarr, A., Bicknell, J., Churcher, J., and Spottiswoode, S. (1990). Comparison of ground motion for tremors and explosions in deep gold mines. *J. Geophys. Res.* **95**, 21,777-21,792.

Madariaga, R. (1976). Dynamics of an expanding circular fault. *Bull. Seism. Soc. Am.* **66**, 639-666.

Malin, P. E., Waller, J. A., Borcherdt, R. D., Cranswick, E., Jensen, E. G., and Van Schack, J. (1988). Vertical seismic profiling of Oroville microearthquakes: Velocity spectra and particle motion as a function of depth. *Bull. Seism. Soc. Am.* **78**, 401-420.

Mendecki, A. J. (1993). Keynote address: Real time quantitative seismology in mines. *In* "Rockburts and Seismicity in Mines" (R. P. Young, ed.), pp. 287-295. Balkema, Rotterdam.

O'Connell, D. R. H., and Johnson, L. R. (1988). Second-order moment tensors of microearthquakes at The Geysers geothermal field, California. *Bull. Seism. Soc. Am.* **78**, 1674-1692.

Oncescu, M.C. (1986). Relative seismic moment tensor determination for Vrancea intermediate depth earthquakes. *In* "Physics of Fracturing and Seismic Energy Release" (J.Kozák and L.Waniek, eds.), Special Issue, *Pure Appl. Geophys.* **124**, 931-940.

Revalor, R., Josien, J. P., Besson, J. L., and Magron, A. (1990). Seismic and seismoacoustic experiments applied to the prediction of rockburts in French coal mines. *In* "Rockburts and Seismicity in Mines" (C. Fairhurst, ed.), pp. 301-306, Balkema, Rotterdam.

Rovelli, A., Cocco, M., Console, R., Alessandrini, B.,and Mazza, S. (1991). Ground motion waveforms and source spectral scaling from close-distance accelerograms in a compressional regime area (Friuli, northeastern Italy). *Bull. Seism. Soc. Am.* **81**, 57-80.

Saikia, C. K., and Herrmann, R. B. (1985). Application of waveform modeling to determine focal mechanisms of four 1982 Miramichi aftershocks. *Bull. Seism. Soc. Am.* **75**, 1021-1040.

Saikia, C. K., and Herrmann, R. B. (1986). Moment-tensor solutions for three 1982 Arkansas swarm earthquakes by waveform modeling. *Bull. Seism. Soc. Am.* **76**, 709-723.

Sato, K., and Fujii, Y. (1989). Source mechanism of a large scale gas outburst at Sunagawa coal mine in Japan. *In* "Seismicity in Mines" (S. J. Gibowicz, ed.), Special Issue, *Pure Appl. Geophys.* **129**, 325-343.

Savage, J. C.(1972). Relation of corner frequency to fault dimensions. *J. Geophys. Res.* **77**, 3788-3795.

Silver, P. G., and Jordan, T. H. (1982). Optimal estimation of scalar seismic moment. *Geophys. J. R. Astr. Soc.* **70**, 755-787.

Smith, R.B., Winkler, P.L., Anderson, J.G., and Scholz, C.H. (1974). Source mechanism of mnicroearthquakes associated with underground mines in eastern Utah. *Bull. Seism. Soc. Am.* **64**, 1295-1317.

Snoke, J. A. (1987). Stable determination of (Brune) stress drops. *Bull. Seism. Soc. Am.* **77**, 530-538.

Snoke, J. A., Linde, A. T., and Sacks, I. S. (1983). Apparent stress: An estimate of the stress drop. *Bull. Seism. Soc. Am.* **73**, 339-348.

Spottiswoode, S. M. (1984). Source mechanisms of mine tremors at Blyvooruitzicht gold mine. *In* "Rockbursts and Seismicity in Mines" (N. C. Gay and E. W. Wainwright,eds.), Symp. Ser. No. 6,pp. 29-37, S. Afr. Inst. Min. Metal., Johannesburg.

Spottiswoode, S.M., and McGarr,A. (1975). Source parameters of tremors in a deep-level gold mine. *Bull. Seism. Soc. Am.* **65**, 93-112.

Trifu, C.-I., Urbancic, T. I., and Young, R. P. (1993). Non-similar frequency-magnitude distribution for M < 1 seismicity. *Geophys. Res. Lett.* **20**, 427-430.

Urbancic, T. I., Feignier, B., and Young, R. P. (1992). Influence of source region properties on scaling relations for M < 0 events. *In* "Induced Seismicity" (A. McGarr, ed.), Special Issue, *Pure Appl. Geophys.* **139**, 721-739.

Urbancic, T. I., Trifu, C.-I., and Young, R. P. (1993). Stress release estimates, scaling behaviour, and source complexities of microseismic events. *In* "Rockbursts and Seismicity in Mines" (R. P. Young, ed.), pp. 255-260. Balkema, Rotterdam.

Wiejacz, P. (1991). Investigation of focal mechanisms of mine tremors by the moment tensor inversion. (In Pol.) Ph.D. Thesis, Inst. Geophys., Pol. Acad. Sci., Warsaw.

Wiejacz, P. (1992). Calculation of seismic moment tensor for mine tremors from the Legnica-Głogów copper basin. *Acta Geophys. Pol.* **40**, 103-122.

APPENDIX A

Moment tensor solutions for selected seismic events

at Wujek coal mine

L2 tensor for : W0201 (510, pods, wb)

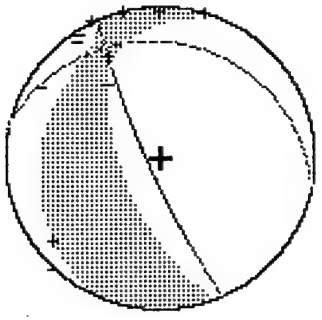

Full solution :

.208E+10	.484E+09	-.531E+10
.484E+09	-.105E+11	-.230E+11
-.531E+10	-.230E+11	-.230E+11

T0= .0573 M0= .296E+11 MT= .405E+11
Expl.= -16.7% CLVD.= -17.4% DBCP.= 65.9%

Full:	ϕA=	155.93	δA=	80.58	ϕB= 280.88 δB= 16.15
	P-axis:	trend=	81.34	plunge=	52.65
	T-axis:	trend=	234.68	plunge=	34.30
	B-axis:	trend=	333.74	plunge=	13.00
	Quality index =		35.5	normal	fault

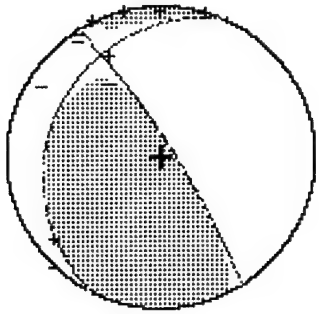

Trace null solution :

.222E+10	-.156E+09	-.104E+11
-.156E+09	-.889E+10	-.141E+11
-.104E+11	-.141E+11	.667E+10

T0= .0573 M0= .188E+11 MT= .193E+11
CLVD.= 4.9% DBCP.= 95.1%

Tr.0:	ϕA=	327.60	δA=	80.08	ϕB= 205.48 δB= 18.20
	P-axis:	trend=	70.54	plunge=	33.37
	T-axis:	trend=	219.70	plunge=	52.51
	B-axis:	trend=	330.30	plunge=	15.11
	Quality index =		35.0	reverse	fault

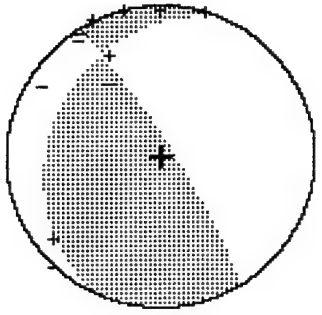

Double couple solution :

.266E+10	-.696E+09	-.985E+10
-.696E+09	-.883E+10	-.139E+11
-.985E+10	-.139E+11	.616E+10

T0= .0573 M0= .188E+11 MT= .188E+11
DBCP.= 100.0%

D.C.:	ϕA=	327.63	δA=	80.06	ϕB= 205.46 δB= 18.22
	P-axis:	trend=	70.58	plunge=	33.34
	T-axis:	trend=	219.71	plunge=	52.54
	B-axis:	trend=	330.34	plunge=	15.11
	Quality index =		24.6	reverse	fault

L2 tensor for : W0202 (510, pods, sw)

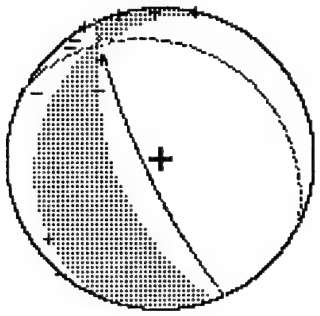

Full solution :

.111E+10	.184E+09	-.470E+10
.184E+09	-.636E+10	-.175E+11
-.470E+10	-.175E+11	-.213E+11

T0= .0507 M0= .240E+11 MT= .332E+11
Expl.= -17.3% CLVD.= -17.5% DBCP.= 65.2%

Full:	ϕA= 155.13	δA= 77.35	ϕB= 295.40	δB= 16.27
	P-axis: trend= 78.38		plunge= 56.47	
	T-axis: trend= 236.59		plunge= 31.60	
	B-axis: trend= 332.85		plunge= 10.06	
	Quality index = 35.6		normal fault	

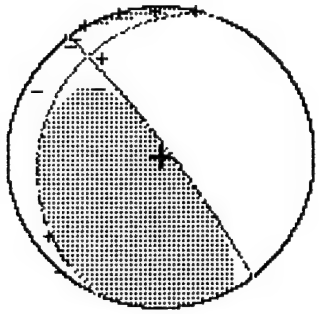

Trace null solution :

.115E+10	-.250E+09	-.832E+10
-.250E+09	-.497E+10	-.990E+10
-.832E+10	-.990E+10	.382E+10

T0= .0507 M0= .132E+11 MT= .137E+11
CLVD.= 6.8% DBCP.= 93.2%

Tr.0:	ϕA= 322.91	δA= 82.55	ϕB= 202.38	δB= 14.43
	P-axis: trend= 63.78		plunge= 36.38	
	T-axis: trend= 218.97		plunge= 50.94	
	B-axis: trend= 324.54		plunge= 12.29	
	Quality index = 34.9		reverse fault	

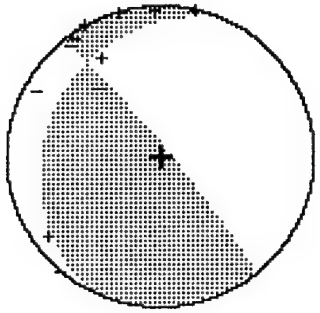

Double couple solution :

.212E+10	-.830E+09	-.819E+10
-.830E+09	-.517E+10	-.932E+10
-.819E+10	-.932E+10	.305E+10

T0= .0507 M0= .132E+11 MT= .132E+11
DBCP.= 100.0%

D.C.:	ϕA= 320.62	δA= 83.09	ϕB= 206.56	δB= 16.55
	P-axis: trend= 63.83		plunge= 36.35	
	T-axis: trend= 214.09		plunge= 49.72	
	B-axis: trend= 322.48		plunge= 14.97	
	Quality index = 34.5		reverse fault	

L2 tensor for : W0203 (501, zaw, zr)

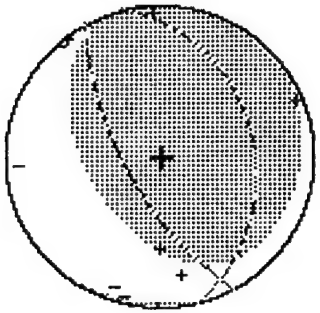

Full solution :

.131E+11	.943E+10	.157E+12
.943E+10	-.324E+11	.185E+12
.157E+12	.185E+12	.590E+12

T0= .0853 M0= .484E+12 MT= .668E+12
Expl.= 39.8% CLVD.= 41.7% DBCP.= 18.4%

Full:	ϕA= 151.27	δA= 63.99	ϕB= 345.63	δB= 26.73
	P-axis: trend= 246.05		plunge= 18.75	
	T-axis: trend= 47.72		plunge= 70.32	
	B-axis: trend= 154.09		plunge= 5.76	
	Quality index = 35.0		reverse fault	

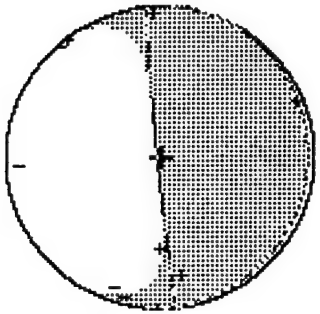

Trace null solution :

.142E+11	-.240E+10	.215E+11
-.240E+10	-.224E+11	.211E+12
.215E+11	.211E+12	.817E+10

T0= .0853 M0= .205E+12 MT= .213E+12
CLVD.= -5.8% DBCP.= 94.2%

Tr.0:	ϕA= 174.15	δA= 87.93	ϕB= 4.16	δB= 2.10
	P-axis: trend= 264.51		plunge= 42.93	
	T-axis: trend= 83.78		plunge= 47.07	
	B-axis: trend= 174.17		plunge= .36	
	Quality index = 32.8		reverse fault	

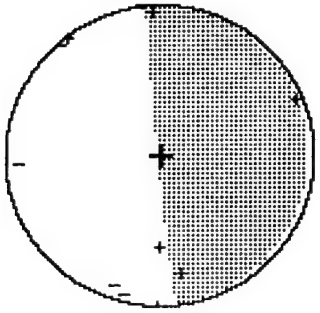

Double couple solution :

.112E+09	-.223E+09	.209E+11
-.223E+09	-.151E+11	.204E+12
.209E+11	.204E+12	.150E+11

T0= .0853 M0= .205E+12 MT= .205E+12
DBCP.= 100.0%

D.C.:	ϕA= 174.16	δA= 87.91	ϕB= 4.16	δB= 2.13
	P-axis: trend= 264.52		plunge= 42.90	
	T-axis: trend= 83.78		plunge= 47.09	
	B-axis: trend= 174.17		plunge= .37	
	Quality index = 23.4		reverse fault	

L2 tensor for : W0204 (510, pods, sw)

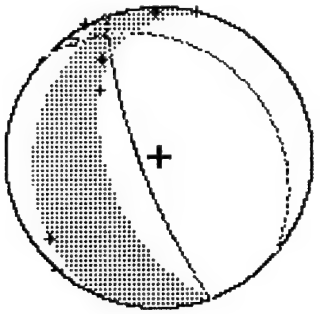

Full solution :

.463E+10	.197E+09	-.151E+11
.197E+09	-.277E+11	-.807E+11
-.151E+11	-.807E+11	-.112E+12

T0= .0693 M0= .116E+12 MT= .159E+12
Expl.= -17.5% CLVD.= -18.4% DBCP.= 64.0%

Full:	∮A= 160.20	δA= 75.57	∮B= 309.97	δB= 16.59
	P-axis:	trend= 81.47	plunge= 58.64	
	T-axis:	trend= 243.46	plunge= 30.09	
	B-axis:	trend= 338.13	plunge= 8.00	
	Quality index = 29.3		normal fault	

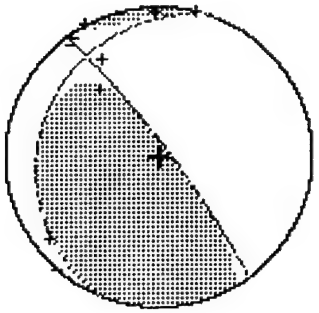

Trace null solution :

.534E+10	-.190E+10	-.356E+11
-.190E+10	-.220E+11	-.437E+11
-.356E+11	-.437E+11	.167E+11

T0= .0693 M0= .584E+11 MT= .598E+11
CLVD.= 4.7% DBCP.= 95.3%

Tr.0:	∮A= 323.40	δA= 82.31	∮B= 201.96	δB= 14.51
	P-axis:	trend= 64.19	plunge= 36.16	
	T-axis:	trend= 219.45	plunge= 51.18	
	B-axis:	trend= 325.08	plunge= 12.23	
	Quality index = 28.6		reverse fault	

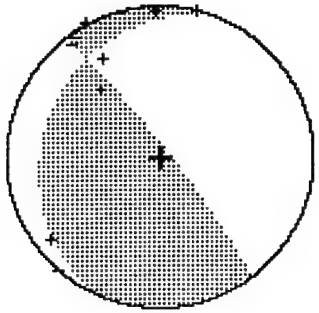

Double couple solution :

.748E+10	-.362E+10	-.348E+11
-.362E+10	-.222E+11	-.425E+11
-.348E+11	-.425E+11	.147E+11

T0= .0693 M0= .584E+11 MT= .584E+11
DBCP.= 100.0%

D.C.:	∮A= 322.57	δA= 82.48	∮B= 203.73	δB= 15.30
	P-axis:	trend= 64.24	plunge= 36.13	
	T-axis:	trend= 217.59	plunge= 50.76	
	B-axis:	trend= 324.35	plunge= 13.25	
	Quality index = 28.4		reverse fault	

L2 tensor for : W0205 (510, pods, wb)

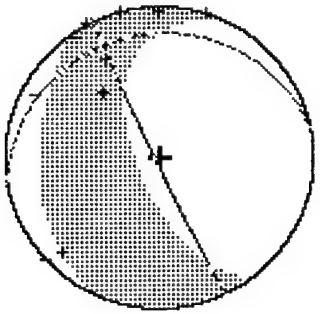

Full solution :

.564E+10	-.191E+10	-.104E+11
-.191E+10	-.149E+11	-.321E+11
-.104E+11	-.321E+11	-.190E+11

T0= .0680 M0= .381E+11 MT= .464E+11
Expl.= -12.1% CLVD.= -17.5% DBCP.= 70.4%

Full:	∮A=	154.36	δA=	86.88	∮B= 258.91	δB= 12.26
	P-axis:	trend=	76.63	plunge=	46.85	
	T-axis:	trend=	233.31	plunge=	40.73	
	B-axis:	trend=	333.71	plunge=	11.84	
	Quality index =		27.9	normal	fault	

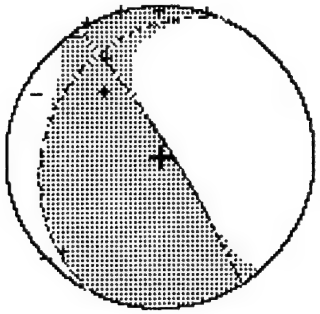

Trace null solution :

.584E+10	-.253E+10	-.152E+11
-.253E+10	-.135E+11	-.236E+11
-.152E+11	-.236E+11	.766E+10

T0= .0680 M0= .290E+11 MT= .305E+11
CLVD.= -7.5% DBCP.= 92.5%

Tr.0:	∮A=	327.49	δA=	81.30	∮B= 207.20	δB= 16.88
	P-axis:	trend=	69.95	plunge=	34.72	
	T-axis:	trend=	220.91	plunge=	51.59	
	B-axis:	trend=	329.74	plunge=	14.35	
	Quality index =		27.3	reverse	fault	

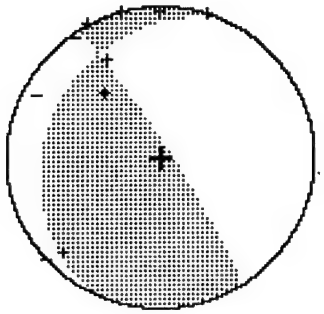

Double couple solution :

.395E+10	-.919E+09	-.155E+11
-.919E+09	-.123E+11	-.220E+11
-.155E+11	-.220E+11	.834E+10

T0= .0680 M0= .290E+11 MT= .290E+11
DBCP.= 100.0%

D.C.:	∮A=	327.12	δA=	81.37	∮B= 206.42	δB= 16.55
	P-axis:	trend=	69.31	plunge=	34.87	
	T-axis:	trend=	220.92	plunge=	51.62	
	B-axis:	trend=	329.29	plunge=	14.01	
	Quality index =		26.8	reverse	fault	

L2 tensor for : W0206 (510, pods, wb)

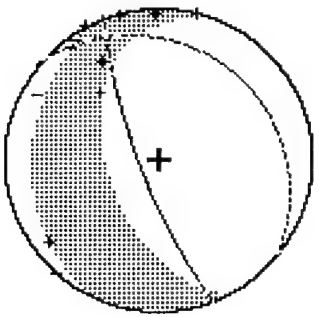

Full solution :

.711E+10	-.109E+10	-.179E+11
-.109E+10	-.296E+11	-.878E+11
-.179E+11	-.878E+11	-.119E+12

T0= .0800 M0= .125E+12 MT= .170E+12
Expl.= -17.0% CLVD.= -18.7% DBCP.= 64.3%

Full:	∮A=	159.26	δA= 75.81	∮B= 308.65	δB= 16.37
	P-axis:	trend=	80.42	plunge= 58.40	
	T-axis:	trend=	242.51	plunge= 30.34	
	B-axis:	trend=	337.22	plunge= 8.00	
	Quality index =		35.6	normal fault	

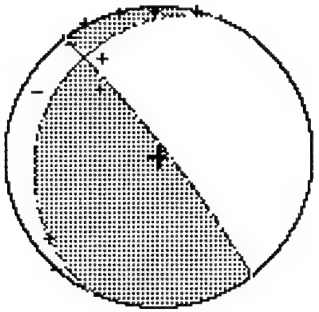

Trace null solution :

.750E+10	-.362E+10	-.387E+11
-.362E+10	-.222E+11	-.474E+11
-.387E+11	-.474E+11	.147E+11

T0= .0800 M0= .643E+11 MT= .644E+11
CLVD.= .2% DBCP.= 99.8%

Tr.0:	∮A=	322.26	δA= 83.25	∮B= 203.72	δB= 13.91
	P-axis:	trend=	63.05	plunge= 37.11	
	T-axis:	trend=	218.74	plunge= 50.31	
	B-axis:	trend=	323.71	plunge= 12.10	
	Quality index =		34.7	reverse fault	

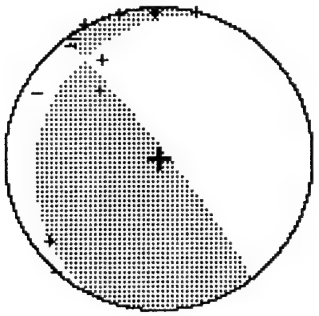

Double couple solution :

.789E+10	-.371E+10	-.388E+11
-.371E+10	-.225E+11	-.471E+11
-.388E+11	-.471E+11	.146E+11

T0= .0800 M0= .643E+11 MT= .643E+11
DBCP.= 100.0%

D.C.:	∮A=	322.03	δA= 83.28	∮B= 204.23	δB= 14.17
	P-axis:	trend=	63.10	plunge= 37.08	
	T-axis:	trend=	218.19	plunge= 50.20	
	B-axis:	trend=	323.52	plunge= 12.42	
	Quality index =		34.7	reverse fault	

L2 tensor for : W0207 (510, pods, wb)

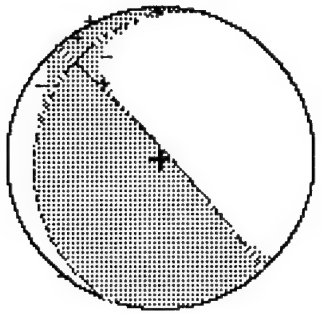

Full solution :

.285E+10	-.380E+10	-.196E+11
-.380E+10	-.882E+10	-.211E+11
-.196E+11	-.211E+11	.546E+10

T0= .0547 M0= .296E+11 MT= .300E+11
Expl.= -.5% CLVD.= -4.5% DBCP.= 95.0%
Full: ∮A= 317.42 δA= 83.80 ∮B= 197.29 δB= 12.20
P-axis: trend= 56.85 plunge= 37.94
T-axis: trend= 215.78 plunge= 50.12
B-axis: trend= 318.57 plunge= 10.47
Quality index = 12.2 reverse fault

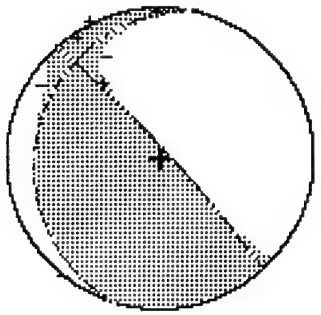

Trace null solution :

.284E+10	-.381E+10	-.196E+11
-.381E+10	-.878E+10	-.208E+11
-.196E+11	-.208E+11	.593E+10

T0= .0547 M0= .291E+11 MT= .298E+11
CLVD.= -4.1% DBCP.= 95.9%
Tr.0: ∮A= 317.22 δA= 83.55 ∮B= 196.29 δB= 12.41
P-axis: trend= 56.70 plunge= 37.67
T-axis: trend= 215.43 plunge= 50.36
B-axis: trend= 318.43 plunge= 10.55
Quality index = 12.2 reverse fault

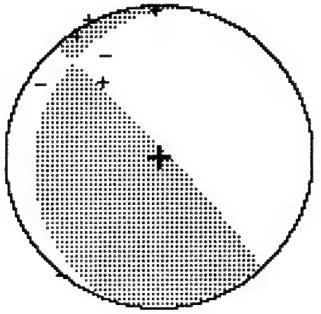

Double couple solution :

.231E+10	-.290E+10	-.196E+11
-.290E+10	-.876E+10	-.199E+11
-.196E+11	-.199E+11	.644E+10

T0= .0547 M0= .291E+11 MT= .291E+11
DBCP.= 100.0%
D.C.: ∮A= 316.69 δA= 83.49 ∮B= 195.66 δB= 12.47
P-axis: trend= 56.20 plunge= 37.61
T-axis: trend= 214.85 plunge= 50.40
B-axis: trend= 317.92 plunge= 10.59
Quality index = 12.1 reverse fault

L2 tensor for : W0208 (510, pods, wb)

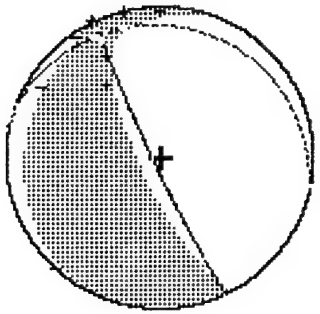

Full solution :

.702E+10	.761E+08	-.351E+11
.761E+08	-.219E+11	-.872E+11
-.351E+11	-.872E+11	-.515E+11

T0= .0747 M0= .102E+12 MT= .128E+12
Expl.= -12.4% CLVD.= -13.6% DBCP.= 74.1%

Full:	$A= 154.71	δA= 84.63	$B= 282.12	δB= 8.79
	P-axis: trend= 72.36		plunge= 49.90	
	T-axis: trend= 238.35		plunge= 39.25	
	B-axis: trend= 334.05		plunge= 6.94	
	Quality index = 12.2		normal fault	

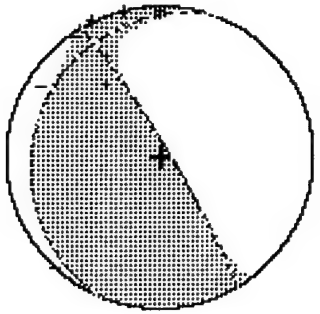

Trace null solution :

.401E+10	-.209E+10	-.203E+11
-.209E+10	-.129E+11	-.328E+11
-.203E+11	-.328E+11	.890E+10

T0= .0747 M0= .396E+11 MT= .403E+11
CLVD.= -3.2% DBCP.= 96.8%

Tr.0:	$A= 328.87	δA= 83.06	$B= 202.49	δB= 11.60
	P-axis: trend= 67.15		plunge= 37.38	
	T-axis: trend= 228.36		plunge= 51.09	
	B-axis: trend= 330.00		plunge= 9.25	
	Quality index = 11.7		reverse fault	

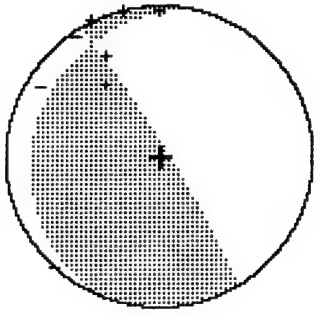

Double couple solution :

.289E+10	-.139E+10	-.205E+11
-.139E+10	-.122E+11	-.320E+11
-.205E+11	-.320E+11	.933E+10

T0= .0747 M0= .396E+11 MT= .396E+11
DBCP.= 100.0%

D.C.:	$A= 328.45	δA= 83.10	$B= 201.09	δB= 11.28
	P-axis: trend= 66.42		plunge= 37.48	
	T-axis: trend= 228.37		plunge= 51.11	
	B-axis: trend= 329.54		plunge= 8.88	
	Quality index = 11.6		reverse fault	

L2 tensor for : W0209 (510, pods, sw)

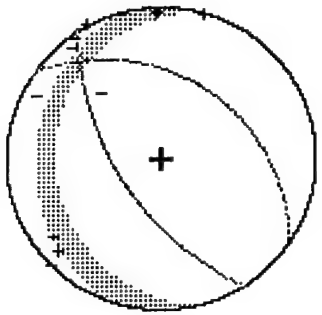

Full solution :

.661E+09	.418E+09	.544E+09
.418E+09	-.829E+10	-.295E+11
.544E+09	-.295E+11	-.954E+11

T0= .0693 M0= .738E+11 MT= .104E+12
Expl.= -19.7% CLVD.= -20.0% DBCP.= 60.3%

Full:	ϕA= 147.84	δA= 58.60	ϕB= 303.64	δB= 33.79
	P-axis:	trend= 91.20	plunge= 72.96	
	T-axis:	trend= 228.33	plunge= 12.66	
	B-axis:	trend= 320.88	plunge= 11.22	
	Quality index = 40.7		normal fault	

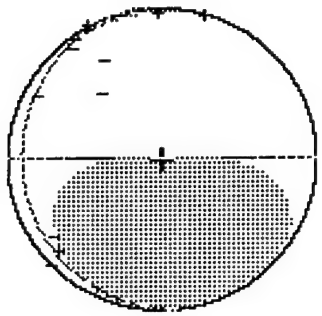

Trace null solution :

.125E+10	-.172E+10	-.163E+11
-.172E+10	-.314E+10	.440E+09
-.163E+11	.440E+09	.188E+10

T0= .0693 M0= .148E+11 MT= .167E+11
CLVD.= 21.4% DBCP.= 78.6%

Tr.0:	ϕA= 270.29	δA= 89.38	ϕB= 174.56	δB= 6.14
	P-axis:	trend= 6.30	plunge= 44.06	
	T-axis:	trend= 174.15	plunge= 45.29	
	B-axis:	trend= 270.36	plunge= 6.11	
	Quality index = 36.4		reverse fault	

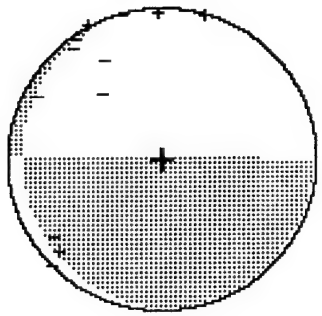

Double couple solution :

-.315E+09	-.158E+10	-.147E+11
-.158E+10	-.162E+08	-.580E+08
-.147E+11	-.580E+08	.332E+09

T0= .0693 M0= .148E+11 MT= .148E+11
DBCP.= 100.0%

D.C.:	ϕA= 270.29	δA= 89.36	ϕB= 174.29	δB= 6.14
	P-axis:	trend= 6.30	plunge= 44.04	
	T-axis:	trend= 174.16	plunge= 45.32	
	B-axis:	trend= 270.36	plunge= 6.10	
	Quality index = 18.3		reverse fault	

L2 tensor for : W0211 (501, zaw, zr)

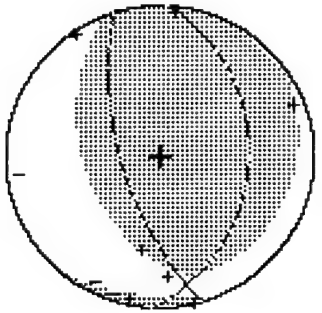

Full solution :

.173E+11	.177E+11	.122E+12
.177E+11	-.437E+11	.183E+12
.122E+12	.183E+12	.567E+12

T0= .0827 M0= .459E+12 MT= .637E+12
Expl.= 39.4% CLVD.= 40.3% DBCP.= 20.2%

Full:	ϕA= 163.38	δA= 62.33	ϕB= 2.32	δB= 29.00	
	P-axis:	trend= 260.05	plunge= 16.86		
	T-axis:	trend= 53.15	plunge= 71.23		
	B-axis:	trend= 167.61	plunge= 8.01		
	Quality index = 39.8		reverse fault		

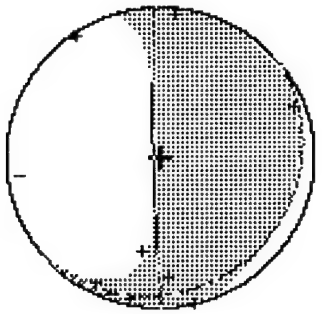

Trace null solution :

.177E+11	.165E+11	.336E+10
.165E+11	-.390E+11	.197E+12
.336E+10	.197E+12	.213E+11

T0= .0827 M0= .192E+12 MT= .201E+12
CLVD.= -7.1% DBCP.= 92.9%

Tr.0:	ϕA= 178.75	δA= 85.72	ϕB= 48.55	δB= 6.62	
	P-axis:	trend= 273.45	plunge= 40.51		
	T-axis:	trend= 83.31	plunge= 49.04		
	B-axis:	trend= 179.13	plunge= 5.03		
	Quality index = 37.2		reverse fault		

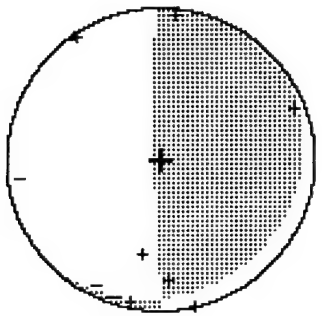

Double couple solution :

.715E+09	.162E+11	.536E+10
.162E+11	-.293E+11	.189E+12
.536E+10	.189E+12	.286E+11

T0= .0827 M0= .192E+12 MT= .192E+12
DBCP.= 100.0%

D.C.:	ϕA= 178.76	δA= 85.69	ϕB= 48.36	δB= 6.63	
	P-axis:	trend= 273.44	plunge= 40.49		
	T-axis:	trend= 83.31	plunge= 49.07		
	B-axis:	trend= 179.14	plunge= 5.03		
	Quality index = 18.5		reverse fault		

L2 tensor for : W0215 (501, przekatna 5)

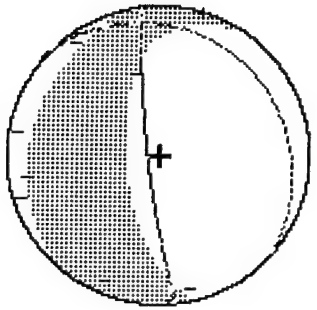

Full solution :

.271E+11	.310E+11	-.115E+11
.310E+11	-.115E+12	-.391E+12
-.115E+11	-.391E+12	-.326E+12

T0= .0667 M0= .462E+12 MT= .604E+12
Expl.= -14.6% CLVD.= -16.9% DBCP.= 68.5%

Full:	ϕA= 172.81	δA= 81.95	ϕB= 309.98	δB= 10.91
	P-axis: trend= 91.41		plunge= 52.50	
	T-axis: trend= 256.31		plunge= 36.53	
	B-axis: trend= 351.77		plunge= 7.32	
	Quality index = 35.4		normal fault	

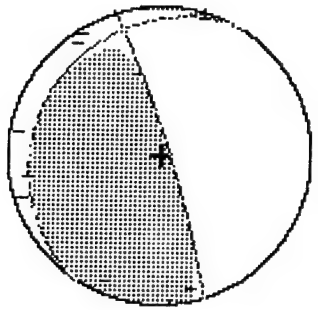

Trace null solution :

.120E+11	.193E+11	-.106E+12
.193E+11	-.983E+11	-.302E+12
-.106E+12	-.302E+12	.863E+11

T0= .0667 M0= .329E+12 MT= .334E+12
CLVD.= 3.0% DBCP.= 97.0%

Tr.0:	ϕA= 342.10	δA= 82.84	ϕB= 211.84	δB= 10.99
	P-axis: trend= 79.53		plunge= 37.30	
	T-axis: trend= 242.59		plunge= 51.46	
	B-axis: trend= 343.15		plunge= 8.30	
	Quality index = 34.8		reverse fault	

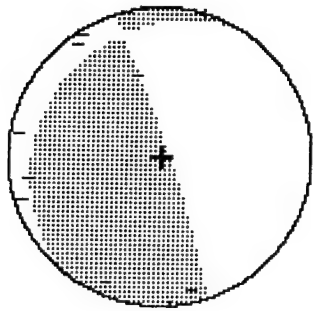

Double couple solution :

.269E+11	.200E+11	-.111E+12
.200E+11	-.105E+12	-.294E+12
-.111E+12	-.294E+12	.778E+11

T0= .0667 M0= .329E+12 MT= .329E+12
DBCP.= 100.0%

D.C.:	ϕA= 340.68	δA= 83.05	ϕB= 216.22	δB= 12.16
	P-axis: trend= 79.55		plunge= 37.28	
	T-axis: trend= 239.43		plunge= 50.97	
	B-axis: trend= 341.90		plunge= 9.93	
	Quality index = 34.9		reverse fault	

L2 tensor for : W0216 (510, pods, wb)

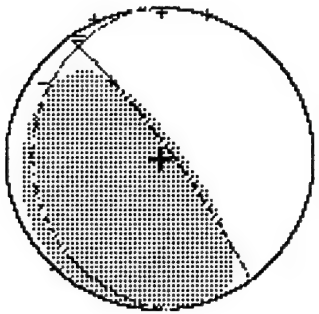

Full solution :

.768E+09	.926E+08	-.131E+11
.926E+08	-.379E+10	-.160E+11
-.131E+11	-.160E+11	.119E+11

T0= .0640 M0= .225E+11 MT= .259E+11
Expl.= 13.0% CLVD.= 17.3% DBCP.= 69.7%

Full:	∮A=	323.47	δA=	80.58	∮B=	176.76	δB= 11.22
	P-axis:	trend=	58.78	plunge=	35.30		
	T-axis:	trend=	226.09	plunge=	54.03		
	B-axis:	trend=	324.48	plunge=	6.05		
	Quality index =		21.2	reverse fault			

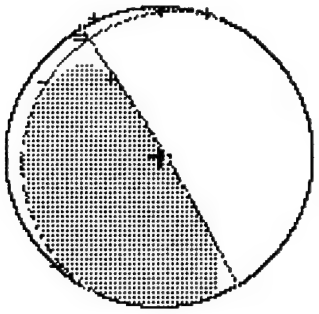

Trace null solution :

.676E+09	.221E+09	-.101E+11
.221E+09	-.398E+10	-.162E+11
-.101E+11	-.162E+11	.330E+10

T0= .0640 M0= .191E+11 MT= .195E+11
CLVD.= 4.1% DBCP.= 95.9%

Tr.0:	∮A=	328.91	δA=	85.64	∮B=	204.90	δB= 7.77
	P-axis:	trend=	64.87	plunge=	40.30		
	T-axis:	trend=	231.98	plunge=	48.97		
	B-axis:	trend=	329.40	plunge=	6.41		
	Quality index =		21.0	reverse fault			

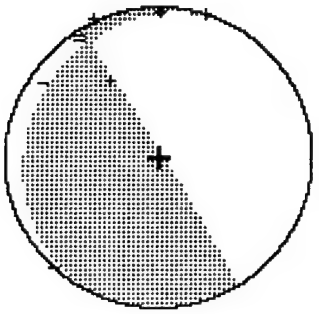

Double couple solution :

.140E+10	-.190E+09	-.100E+11
-.190E+09	-.421E+10	-.158E+11
-.100E+11	-.158E+11	.282E+10

T0= .0640 M0= .191E+11 MT= .191E+11
DBCP.= 100.0%

D.C.:	∮A=	328.11	δA=	85.71	∮B=	208.02	δB= 8.51
	P-axis:	trend=	64.93	plunge=	40.27		
	T-axis:	trend=	230.22	plunge=	48.78		
	B-axis:	trend=	328.67	plunge=	7.33		
	Quality index =		20.7	reverse fault			

L2 tensor for : W0302 (510, pods, sw)

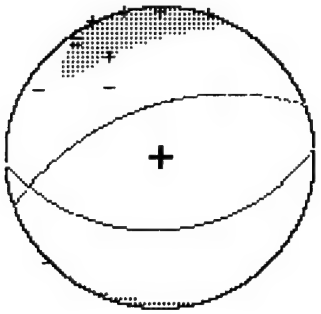

Full solution :

.313E+10	.789E+09	.272E+11
.789E+09	-.177E+11	-.441E+11
.272E+11	-.441E+11	-.258E+12

T0= .0707 M0= .190E+12 MT= .261E+12
Expl.= -21.2% CLVD.= -18.7% DBCP.= 60.1%

Full:	∮A= 250.13	δA= 53.31	∮B= 87.37	δB= 37.96
	P-axis:	trend= 119.74	plunge= 78.52		
	T-axis:	trend= 347.60	plunge= 7.76		
	B-axis:	trend= 256.45	plunge= 8.41		
	Quality index = 29.4		normal	fault	

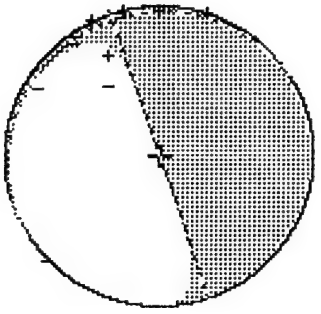

Trace null solution :

-.384E+09	-.735E+10	.425E+11
-.735E+10	.634E+10	.122E+12
.425E+11	.122E+12	-.595E+10

T0= .0707 M0= .127E+12 MT= .130E+12
CLVD.= -3.4% DBCP.= 96.6%

Tr.0:	∮A= 341.07	δA= 89.22	∮B= 238.37	δB= 3.57
	P-axis:	trend= 247.55	plunge= 45.68		
	T-axis:	trend= 74.49	plunge= 44.11		
	B-axis:	trend= 341.12	plunge= 3.48		
	Quality index = 29.1		normal	fault	

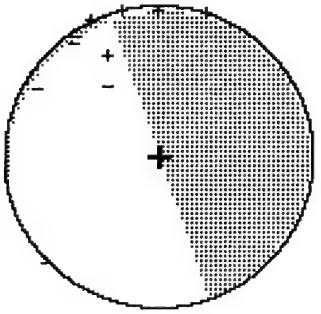

Double couple solution :

-.474E+10	-.540E+10	.418E+11
-.540E+10	.816E+10	.120E+12
.418E+11	.120E+12	-.342E+10

T0= .0707 M0= .127E+12 MT= .127E+12
DBCP.= 100.0%

D.C.:	∮A= 340.83	δA= 89.23	∮B= 239.12	δB= 3.79
	P-axis:	trend= 247.08	plunge= 45.65		
	T-axis:	trend= 74.49	plunge= 44.11		
	B-axis:	trend= 340.88	plunge= 3.71		
	Quality index = 28.9		normal	fault	

L2 tensor for : W0303 (510, pods, wb)

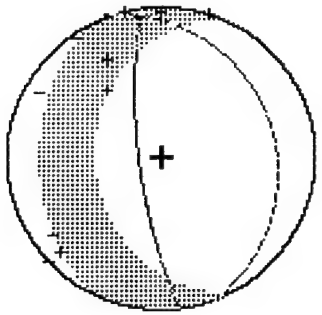

Full solution :

.301E+10	-.937E+08	-.827E+09
-.937E+08	-.113E+11	-.292E+11
-.827E+09	-.292E+11	-.476E+11

T0= .0707 M0= .453E+11 MT= .609E+11
Expl.= -17.4% CLVD.= -20.2% DBCP.= 62.4%

Full:	∯A=	172.80	δA=	73.89	∯B= 338.60 δB= 16.59
	P-axis:	trend=	88.65	plunge=	60.91
	T-axis:	trend=	259.56	plunge=	28.79
	B-axis:	trend=	351.68	plunge=	3.86
	Quality index =		28.3	normal	fault

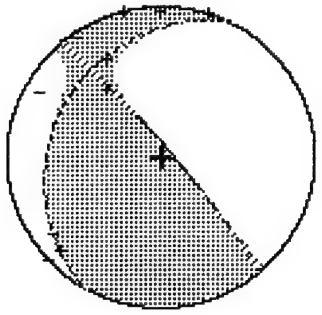

Trace null solution :

.416E+10	-.190E+10	-.116E+11
-.190E+10	-.854E+10	-.130E+11
-.116E+11	-.130E+11	.438E+10

T0= .0707 M0= .186E+11 MT= .190E+11
CLVD.= -4.0% DBCP.= 96.0%

Tr.0:	∯A=	319.71	δA=	82.47	∯B= 208.06 δB= 19.72
	P-axis:	trend=	65.41	plunge=	34.96
	T-axis:	trend=	209.83	plunge=	49.32
	B-axis:	trend=	322.19	plunge=	18.11
	Quality index =		26.2	reverse	fault

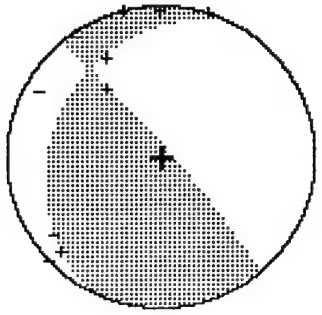

Double couple solution :

.375E+10	-.144E+10	-.117E+11
-.144E+10	-.836E+10	-.124E+11
-.117E+11	-.124E+11	.461E+10

T0= .0707 M0= .186E+11 MT= .186E+11
DBCP.= 100.0%

D.C.:	∯A=	319.17	δA=	82.41	∯B= 207.43 δB= 19.78
	P-axis:	trend=	64.90	plunge=	34.89
	T-axis:	trend=	209.22	plunge=	49.36
	B-axis:	trend=	321.68	plunge=	18.16
	Quality index =		26.1	reverse	fault

L2 tensor for : W0304 (510, pods, wb)

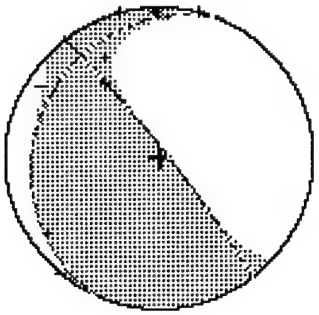

Full solution :

.602E+10	-.425E+10	-.257E+11
-.425E+10	-.129E+11	-.332E+11
-.257E+11	-.332E+11	.710E+10

T0= .0773 M0= .419E+11 MT= .437E+11
Expl.= .1% CLVD.= -6.1% DBCP.= 93.8%

Full:	∮A= 322.23	δA= 84.31	∮B= 204.51	δB= 12.09
	P-axis: trend= 61.86		plunge= 38.41	
	T-axis: trend= 220.56		plunge= 49.60	
	B-axis: trend= 323.30		plunge= 10.63	
	Quality index = 11.4		reverse fault	

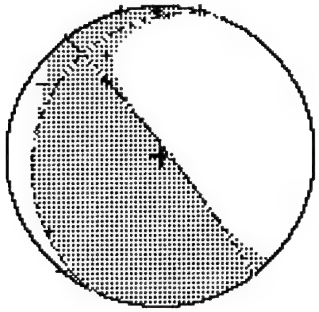

Trace null solution :

.602E+10	-.425E+10	-.256E+11
-.425E+10	-.130E+11	-.332E+11
-.256E+11	-.332E+11	.694E+10

T0= .0773 M0= .420E+11 MT= .437E+11
CLVD.= -6.2% DBCP.= 93.8%

Tr.0:	∮A= 322.27	δA= 84.37	∮B= 204.75	δB= 12.05
	P-axis: trend= 61.90		plunge= 38.47	
	T-axis: trend= 220.62		plunge= 49.55	
	B-axis: trend= 323.33		plunge= 10.62	
	Quality index = 11.4		reverse fault	

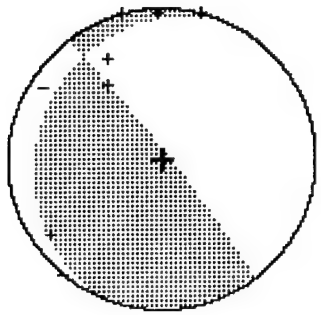

Double couple solution :

.426E+10	-.208E+10	-.255E+11
-.208E+10	-.123E+11	-.315E+11
-.255E+11	-.315E+11	.802E+10

T0= .0773 M0= .420E+11 MT= .420E+11
DBCP.= 100.0%

D.C.:	∮A= 321.97	δA= 84.40	∮B= 203.93	δB= 11.78
	P-axis: trend= 61.35		plunge= 38.55	
	T-axis: trend= 220.64		plunge= 49.57	
	B-axis: trend= 322.99		plunge= 10.33	
	Quality index = 11.1		reverse fault	

L2 tensor for : W0305 (501 osadniki)

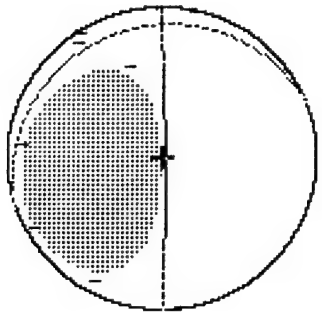

Full solution :

-.298E+11	.145E+11	-.433E+10
.145E+11	-.222E+11	-.103E+12
-.433E+10	-.103E+12	-.113E+09

T0= .0733 M0= .849E+11 MT= .107E+12
Expl.= -15.1% CLVD.= 11.3% DBCP.= 73.6%

Full:	ϕA= 359.53	δA= 86.91	ϕB= 248.66	δB=	8.61
	P-axis: trend=	97.10	plunge=	41.38	
	T-axis: trend=	261.11	plunge=	47.50	
	B-axis: trend=	359.97	plunge=	8.03	
	Quality index =	9.4	reverse	fault	

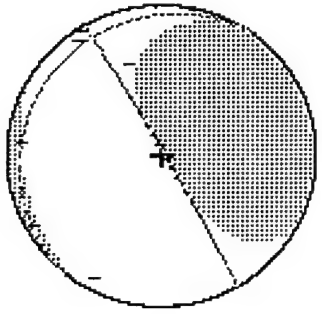

Trace null solution :

-.283E+11	.153E+11	.634E+11
.153E+11	.274E+11	.118E+12
.634E+11	.118E+12	.912E+09

T0= .0733 M0= .122E+12 MT= .138E+12
CLVD.= 23.2% DBCP.= 76.8%

Tr.0:	ϕA= 329.98	δA= 87.32	ϕB= 218.77	δB=	7.38
	P-axis: trend=	232.81	plunge=	47.25	
	T-axis: trend=	66.52	plunge=	41.92	
	B-axis: trend=	330.30	plunge=	6.87	
	Quality index =	15.5	normal	fault	

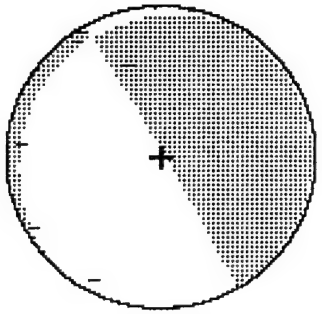

Double couple solution :

-.978E+10	-.236E+10	.607E+11
-.236E+10	.212E+11	.104E+12
.607E+11	.104E+12	-.114E+11

T0= .0733 M0= .122E+12 MT= .122E+12
DBCP.= 100.0%

D.C.:	ϕA= 330.01	δA= 87.29	ϕB= 218.64	δB=	7.41
	P-axis: trend=	232.82	plunge=	47.28	
	T-axis: trend=	66.56	plunge=	41.89	
	B-axis: trend=	330.34	plunge=	6.89	
	Quality index =	10.1	normal	fault	

L2 tensor for : W0306 (510, pods, sw)

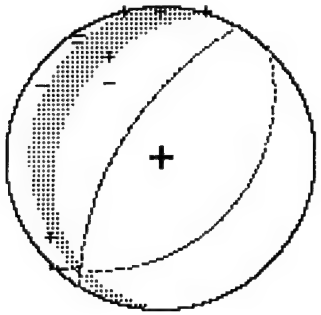

Full solution :

.964E+09	.661E+10	.393E+11
.661E+10	-.362E+11	-.151E+12
.393E+11	-.151E+12	-.516E+12

T0= .0733 M0= .398E+12 MT= .562E+12
Expl.= -19.7% CLVD.= -19.8% DBCP.= 60.5%

Full:	∮A=	211.16	δA=	60.63	
	P-axis:	trend=	104.27	plunge=	73.49
	T-axis:	trend=	306.07	plunge=	15.38
	B-axis:	trend=	214.46	plunge=	5.84
	Quality index =		29.6	normal	fault
				∮B= 44.64	δB= 30.06

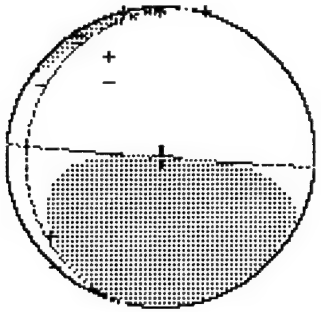

Trace null solution :

.849E+10	-.761E+10	-.595E+11
-.761E+10	-.980E+10	-.293E+10
-.595E+11	-.293E+10	.131E+10

T0= .0733 M0= .559E+11 MT= .608E+11
CLVD.= 15.7% DBCP.= 84.3%

Tr.0:	∮A=	94.47	δA=	88.65	
	P-axis:	trend=	13.07	plunge=	45.71
	T-axis:	trend=	176.26	plunge=	43.04
	B-axis:	trend=	274.27	plunge=	8.49
	Quality index =		27.5	normal	fault
				∮B= 193.42	δB= 8.59

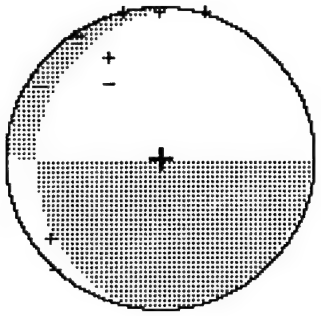

Double couple solution :

.421E+10	-.123E+11	-.544E+11
-.123E+11	-.791E+08	-.641E+09
-.544E+11	-.641E+09	-.413E+10

T0= .0733 M0= .559E+11 MT= .559E+11
DBCP.= 100.0%

D.C.:	∮A=	90.18	δA=	87.83	
	P-axis:	trend=	13.06	plunge=	45.74
	T-axis:	trend=	168.21	plunge=	41.49
	B-axis:	trend=	269.69	plunge=	12.69
	Quality index =		27.1	normal	fault
				∮B= 189.74	δB= 12.88

L2 tensor for : W0307 (510, pods, wb)

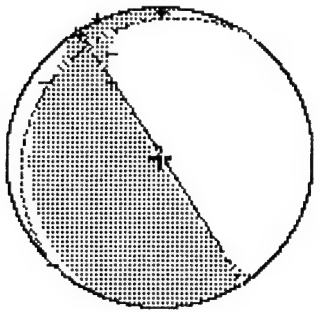

Full solution :

.749E+10	-.512E+10	-.469E+11
-.512E+10	-.254E+11	-.749E+11
-.469E+11	-.749E+11	-.452E+10

T0= .0667 M0= .905E+11 MT= .995E+11
Expl.= -6.1% CLVD.= -8.3% DBCP.= 85.6%

Full:	∮A= 326.90	δA= 87.51	∮B= 220.24	δB= 8.63
	P-axis: trend= 64.75		plunge= 41.94	
	T-axis: trend= 228.34		plunge= 46.87	
	B-axis: trend= 327.26		plunge= 8.26	
	Quality index = 12.3		reverse fault	

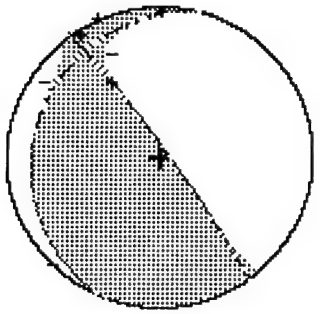

Trace null solution :

.724E+10	-.580E+10	-.460E+11
-.580E+10	-.232E+11	-.609E+11
-.460E+11	-.609E+11	.160E+11

T0= .0667 M0= .781E+11 MT= .792E+11
CLVD.= -2.5% DBCP.= 97.5%

Tr.0:	∮A= 323.62	δA= 83.72	∮B= 200.01	δB= 11.24
	P-axis: trend= 62.00		plunge= 38.04	
	T-axis: trend= 223.23		plunge= 50.43	
	B-axis: trend= 324.65		plunge= 9.29	
	Quality index = 12.3		reverse fault	

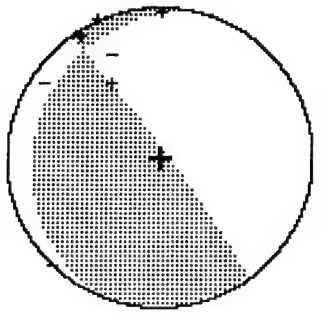

Double couple solution :

.572E+10	-.452E+10	-.461E+11
-.452E+10	-.224E+11	-.596E+11
-.461E+11	-.596E+11	.167E+11

T0= .0667 M0= .781E+11 MT= .781E+11
DBCP.= 100.0%

D.C.:	∮A= 323.28	δA= 83.75	∮B= 198.88	δB= 10.96
	P-axis: trend= 61.39		plunge= 38.12	
	T-axis: trend= 223.24		plunge= 50.46	
	B-axis: trend= 324.27		plunge= 8.97	
	Quality index = 12.3		reverse fault	

L2 tensor for : W0308 (510, pods, sw)

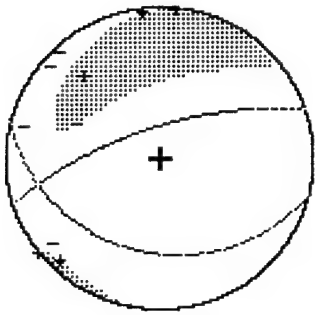

Full solution :

-.137E+10	.618E+10	.279E+11
.618E+10	-.889E+10	-.214E+11
.279E+11	-.214E+11	-.683E+11

T0= .0680 M0= .604E+11 MT= .824E+11
Expl.= -19.8% CLVD.= -17.9% DBCP.= 62.3%

Full:	∮A= 252.08	δA= 67.67	∮B= 104.88	δB= 26.04
	P-axis: trend= 138.92		plunge= 64.68	
	T-axis: trend= 352.49		plunge= 21.51	
	B-axis: trend= 257.39		plunge= 12.71	
	Quality index = 29.5		normal fault	

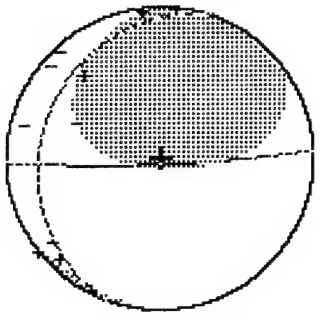

Trace null solution :

-.494E+09	.414E+10	.184E+11
.414E+10	-.570E+10	.178E+10
.184E+11	.178E+10	.619E+10

T0= .0680 M0= .163E+11 MT= .199E+11
CLVD.= 36.1% DBCP.= 63.9%

Tr.0:	∮A= 87.84	δA= 84.22	∮B= 200.29	δB= 14.85
	P-axis: trend= 165.61		plunge= 37.75	
	T-axis: trend= 12.63		plunge= 49.00	
	B-axis: trend= 266.43		plunge= 13.63	
	Quality index = 28.3		reverse fault	

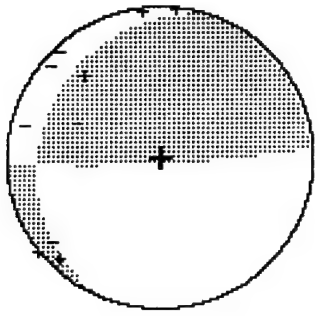

Double couple solution :

-.291E+10	.380E+10	.155E+11
.380E+10	-.353E+09	-.353E+09
.155E+11	-.353E+09	.327E+10

T0= .0680 M0= .163E+11 MT= .163E+11
DBCP.= 100.0%

D.C.:	∮A= 87.29	δA= 84.06	∮B= 201.30	δB= 14.33
	P-axis: trend= 165.63		plunge= 37.73	
	T-axis: trend= 11.49		plunge= 49.31	
	B-axis: trend= 265.92		plunge= 13.00	
	Quality index = 27.1		reverse fault	

L2 tensor for : W0309 (510, pods, wb)

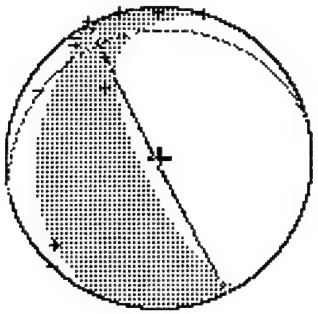

Full solution :

.317E+10	-.109E+10	-.113E+11
-.109E+10	-.122E+11	-.285E+11
-.113E+11	-.285E+11	-.145E+11

T0= .0653 M0= .336E+11 MT= .422E+11
Expl.= -12.6% CLVD.= -14.9% DBCP.= 72.4%

Full:	∮A=	153.33	δA=	87.66	∮B=	255.88	δB= 10.66
	P-axis:	trend=	74.00	plunge=	46.37		
	T-axis:	trend=	233.47	plunge=	41.76		
	B-axis:	trend=	332.90	plunge=	10.40		
	Quality index =		34.2	normal	fault		

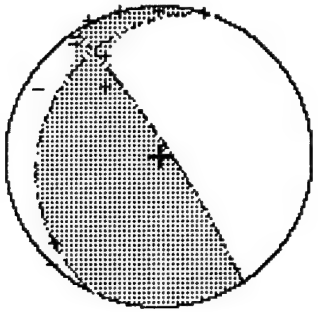

Trace null solution :

.329E+10	-.158E+10	-.151E+11
-.158E+10	-.110E+11	-.217E+11
-.151E+11	-.217E+11	.770E+10

T0= .0653 M0= .280E+11 MT= .283E+11
CLVD.= -1.6% DBCP.= 98.4%

Tr.0:	∮A=	326.66	δA=	81.69	∮B=	202.90	δB= 14.72
	P-axis:	trend=	67.24	plunge=	35.57		
	T-axis:	trend=	222.67	plunge=	51.82		
	B-axis:	trend=	328.45	plunge=	12.07		
	Quality index =		33.8	reverse	fault		

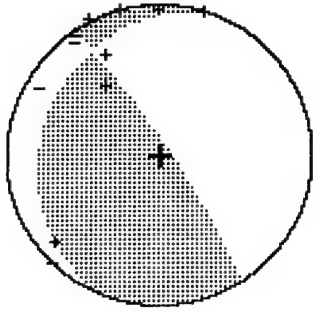

Double couple solution :

.287E+10	-.141E+10	-.153E+11
-.141E+10	-.107E+11	-.214E+11
-.153E+11	-.214E+11	.779E+10

T0= .0653 M0= .280E+11 MT= .280E+11
DBCP.= 100.0%

D.C.:	∮A=	326.29	δA=	81.75	∮B=	201.96	δB= 14.42
	P-axis:	trend=	66.60	plunge=	35.69		
	T-axis:	trend=	222.68	plunge=	51.84		
	B-axis:	trend=	328.02	plunge=	11.74		
	Quality index =		33.7	reverse	fault		

L2 tensor for : W0310 (510, pods, sw)

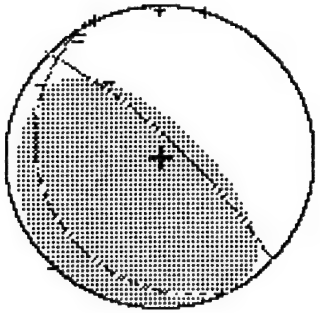

Full solution :

.510E+10	-.703E+09	-.902E+11
-.703E+09	-.140E+11	-.740E+11
-.902E+11	-.740E+11	.116E+12

T0= .0600 M0= .143E+12 MT= .183E+12
Expl.= 24.4% CLVD.= 27.6% DBCP.= 48.0%

Full:	∮A= 313.09	δA= 76.23	∮B= 152.63	δB= 14.58
	P-axis: trend= 47.07		plunge= 31.06	
	T-axis: trend= 216.54		plunge= 58.50	
	B-axis: trend= 314.24		plunge= 4.69	
	Quality index = 22.0		reverse fault	

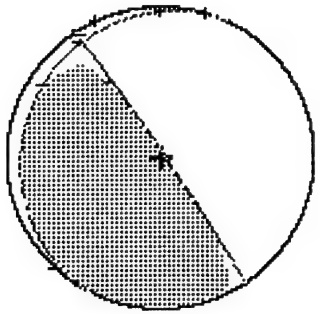

Trace null solution :

.399E+10	.897E+09	-.539E+11
.897E+09	-.164E+11	-.779E+11
-.539E+11	-.779E+11	.124E+11

T0= .0600 M0= .942E+11 MT= .959E+11
CLVD.= 3.5% DBCP.= 96.5%

Tr.0:	∮A= 325.97	δA= 86.74	∮B= 207.11	δB= 6.73
	P-axis: trend= 61.53		plunge= 41.45	
	T-axis: trend= 229.75		plunge= 47.94	
	B-axis: trend= 326.31		plunge= 5.88	
	Quality index = 22.0		reverse fault	

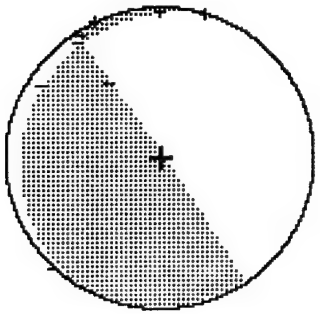

Double couple solution :

.618E+10	-.119E+10	-.530E+11
-.119E+10	-.167E+11	-.765E+11
-.530E+11	-.765E+11	.105E+11

T0= .0600 M0= .942E+11 MT= .942E+11
DBCP.= 100.0%

D.C.:	∮A= 325.63	δA= 86.78	∮B= 208.43	δB= 7.02
	P-axis: trend= 61.51		plunge= 41.46	
	T-axis: trend= 229.05		plunge= 47.86	
	B-axis: trend= 325.98		plunge= 6.23	
	Quality index = 21.8		reverse fault	

L2 tensor for : W0311 (510, pods, wb)

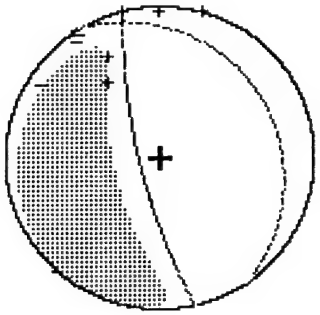

Full solution :

-.666E+09	.183E+11	-.447E+11
.183E+11	-.494E+11	-.303E+12
-.447E+11	-.303E+12	-.377E+12

T0= .0680 M0= .408E+12 MT= .550E+12
Expl.= -17.3% CLVD.= -16.1% DBCP.= 66.7%

Full:	∡A= 166.70	δA= 75.44	∡B= 326.10	δB= 15.50
	P-axis: trend= 84.17		plunge= 59.22	
	T-axis: trend= 252.29		plunge= 30.24	
	B-axis: trend= 345.34		plunge= 5.22	
	Quality index = 21.8		normal fault	

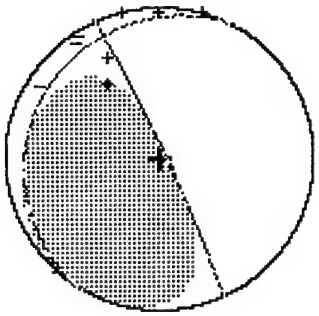

Trace null solution :

-.184E+10	.556E+10	-.275E+11
.556E+10	-.136E+11	-.542E+11
-.275E+11	-.542E+11	.155E+11

T0= .0680 M0= .582E+11 MT= .627E+11
CLVD.= 14.3% DBCP.= 85.7%

Tr.0:	∡A= 335.34	δA= 84.63	∡B= 210.40	δB= 9.33
	P-axis: trend= 72.30		plunge= 39.16	
	T-axis: trend= 236.97		plunge= 49.82	
	B-axis: trend= 336.06		plunge= 7.60	
	Quality index = 20.0		reverse fault	

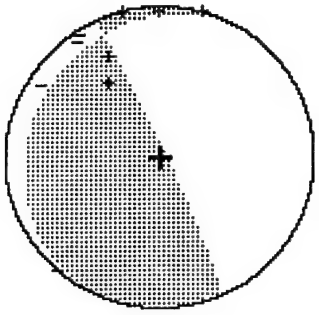

Double couple solution :

.397E+10	.940E+09	-.243E+11
.940E+09	-.148E+11	-.512E+11
-.243E+11	-.512E+11	.108E+11

T0= .0680 M0= .582E+11 MT= .582E+11
DBCP.= 100.0%

D.C.:	∡A= 335.37	δA= 84.60	∡B= 210.36	δB= 9.36
	P-axis: trend= 72.34		plunge= 39.13	
	T-axis: trend= 236.98		plunge= 49.84	
	B-axis: trend= 336.10		plunge= 7.62	
	Quality index = 13.9		reverse fault	

L2 tensor for : W0312 (510, pods, wb)

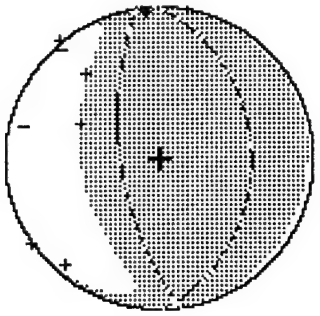

Full solution :

.820E+09	.514E+09	.383E+10
.514E+09	-.949E+09	.160E+11
.383E+10	.160E+11	.464E+11

T0= .0773 M0= .367E+11 MT= .510E+11
Expl.= 42.0% CLVD.= 40.4% DBCP.= 17.7%

Full:	∮A=	172.13	δA=	62.33	∮B= 358.11 δB= 27.80
	P-axis:	trend=	264.19	plunge=	17.29
	T-axis:	trend=	75.57	plunge=	72.53
	B-axis:	trend=	173.43	plunge=	2.46
	Quality index =		21.7	reverse fault	

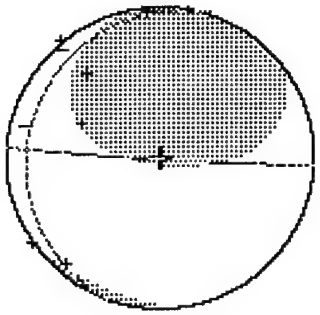

Trace null solution :

.464E+09	.128E+10	.742E+10
.128E+10	-.222E+10	.106E+10
.742E+10	.106E+10	.176E+10

T0= .0773 M0= .635E+10 MT= .787E+10
CLVD.= 38.7% DBCP.= 61.3%

Tr.0:	∮A=	93.66	δA=	87.66	∮B= 198.87 δB= 8.84
	P-axis:	trend=	175.54	plunge=	42.06
	T-axis:	trend=	12.46	plunge=	46.68
	B-axis:	trend=	273.31	plunge=	8.52
	Quality index =		18.6	reverse fault	

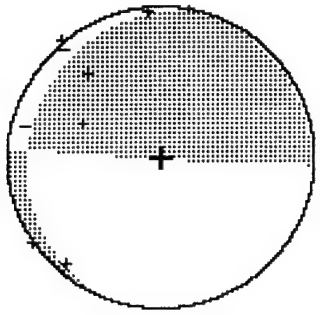

Double couple solution :

-.635E+09	.900E+09	.624E+10
.900E+09	.118E+09	.438E+09
.624E+10	.438E+09	.518E+09

T0= .0773 M0= .635E+10 MT= .635E+10
DBCP.= 100.0%

D.C.:	∮A=	93.65	δA=	87.63	∮B= 199.04 δB= 8.85
	P-axis:	trend=	175.54	plunge=	42.03
	T-axis:	trend=	12.45	plunge=	46.71
	B-axis:	trend=	273.30	plunge=	8.52
	Quality index =		11.6	reverse fault	

L2 tensor for : W0314 (510, pods, wb)

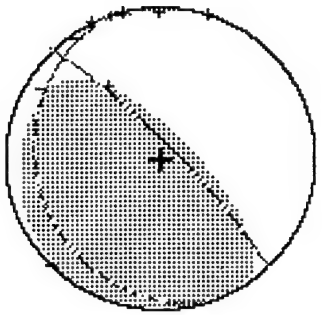

Full solution :

.254E+10	-.326E+09	-.324E+11
-.326E+09	-.643E+10	-.291E+11
-.324E+11	-.291E+11	.340E+11

T0= .0627 M0= .500E+11 MT= .616E+11
Expl.= 19.5% CLVD.= 22.8% DBCP.= 57.7%

Full:	∮A= 315.57	δA= 78.60	∮B= 163.47	δB= 12.85
	P-axis: trend= 50.63		plunge= 33.34	
	T-axis: trend= 218.01		plunge= 56.01	
	B-axis: trend= 316.76		plunge= 5.86	
	Quality index = 12.2		reverse fault	

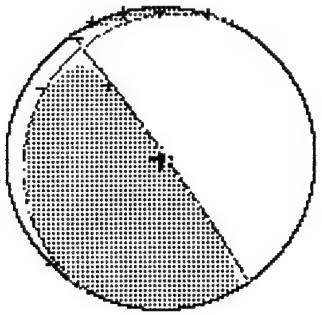

Trace null solution :

.196E+10	-.111E+09	-.172E+11
-.111E+09	-.626E+10	-.237E+11
-.172E+11	-.237E+11	.429E+10

T0= .0627 M0= .294E+11 MT= .298E+11
CLVD.= 2.3% DBCP.= 97.7%

Tr.0:	∮A= 324.84	δA= 86.13	∮B= 207.50	δB= 8.38
	P-axis: trend= 61.77		plunge= 40.68	
	T-axis: trend= 226.92		plunge= 48.35	
	B-axis: trend= 325.34		plunge= 7.42	
	Quality index = 12.0		reverse fault	

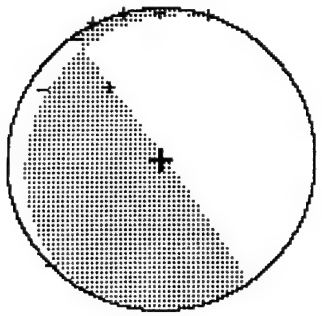

Double couple solution :

.248E+10	-.536E+09	-.170E+11
-.536E+09	-.638E+10	-.234E+11
-.170E+11	-.234E+11	.390E+10

T0= .0627 M0= .294E+11 MT= .294E+11
DBCP.= 100.0%

D.C.:	∮A= 324.50	δA= 86.15	∮B= 208.60	δB= 8.75
	P-axis: trend= 61.83		plunge= 40.65	
	T-axis: trend= 226.14		plunge= 48.27	
	B-axis: trend= 325.03		plunge= 7.85	
	Quality index = 12.0		reverse fault	

L2 tensor for : W0315 (510, pods, wb)

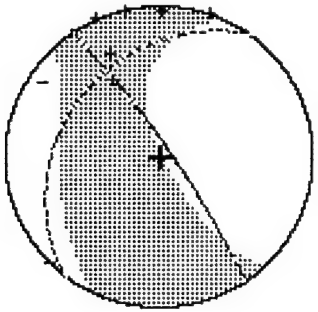

Full solution :

.205E+10	-.107E+10	-.246E+10
-.107E+10	-.460E+10	-.497E+10
-.246E+10	-.497E+10	.463E+09

T0= .0733 M0= .668E+10 MT= .668E+10
Expl.= -5.6% CLVD.= -17.2% DBCP.= 77.2%
Full: ∮A= 325.51 δA= 81.44 ∮B= 216.90 δB= 25.25
P-axis: trend= 75.28 plunge= 32.30
T-axis: trend= 210.15 plunge= 48.14
B-axis: trend= 329.27 plunge= 23.56
Quality index = 8.2 reverse fault

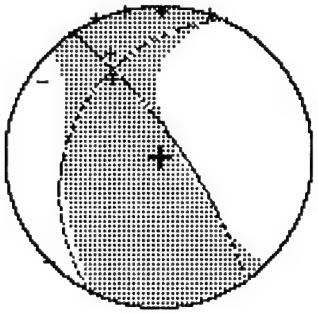

Trace null solution :

.203E+10	-.114E+10	-.237E+10
-.114E+10	-.438E+10	-.359E+10
-.237E+10	-.359E+10	.235E+10

T0= .0733 M0= .503E+10 MT= .585E+10
CLVD.= -15.2% DBCP.= 84.8%
Tr.0: ∮A= 325.06 δA= 74.31 ∮B= 205.81 δB= 29.89
P-axis: trend= 74.88 plunge= 24.95
T-axis: trend= 203.91 plunge= 53.54
B-axis: trend= 332.50 plunge= 24.74
Quality index = 6.8 reverse fault

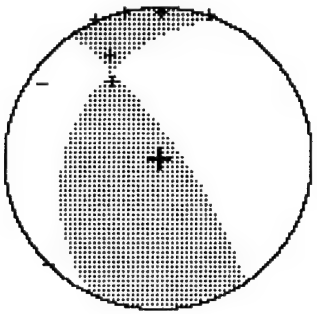

Double couple solution :

.118E+10	-.419E+09	-.272E+10
-.419E+09	-.352E+10	-.284E+10
-.272E+10	-.284E+10	.234E+10

T0= .0733 M0= .503E+10 MT= .503E+10
DBCP.= 100.0%
D.C.: ∮A= 324.64 δA= 74.49 ∮B= 205.24 δB= 29.48
P-axis: trend= 74.22 plunge= 25.25
T-axis: trend= 203.94 plunge= 53.58
B-axis: trend= 331.88 plunge= 24.40
Quality index = 5.7 reverse fault

L2 tensor for : W0401 (510, pods, zr)

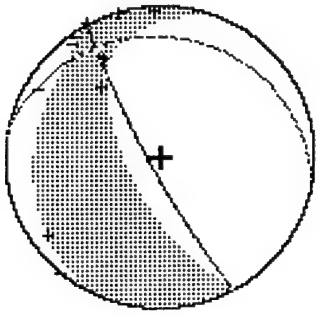

Full solution :

.901E+10	-.117E+10	-.292E+11
-.117E+10	-.301E+11	-.797E+11
-.292E+11	-.797E+11	-.712E+11

T0= .0827 M0= .101E+12 MT= .134E+12
Expl.= -15.0% CLVD.= -16.6% DBCP.= 68.4%

Full:	ϕA= 151.70	δA= 81.56	ϕB= 278.35	δB= 13.97
	P-axis: trend= 74.61		plunge= 52.19	
	T-axis: trend= 232.01		plunge= 35.62	
	B-axis: trend= 330.04		plunge= 11.04	
	Quality index = 29.2		normal fault	

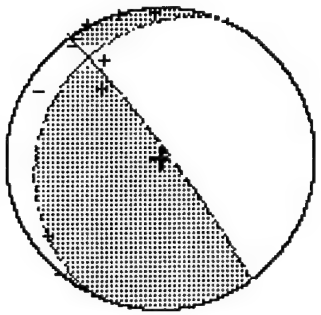

Trace null solution :

.851E+10	-.271E+10	-.411E+11
-.271E+10	-.244E+11	-.527E+11
-.411E+11	-.527E+11	.159E+11

T0= .0827 M0= .700E+11 MT= .703E+11
CLVD.= .7% DBCP.= 99.3%

Tr.0:	ϕA= 323.68	δA= 83.39	ϕB= 205.93	δB= 13.98
	P-axis: trend= 64.62		plunge= 37.21	
	T-axis: trend= 220.03		plunge= 50.14	
	B-axis: trend= 325.12		plunge= 12.26	
	Quality index = 28.8		reverse fault	

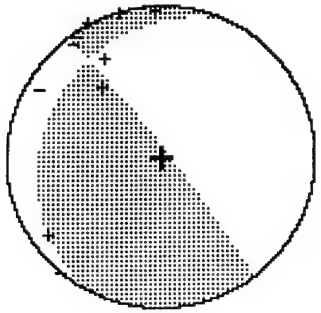

Double couple solution :

.104E+11	-.296E+10	-.419E+11
-.296E+10	-.254E+11	-.515E+11
-.419E+11	-.515E+11	.150E+11

T0= .0827 M0= .700E+11 MT= .700E+11
DBCP.= 100.0%

D.C.:	ϕA= 322.49	δA= 83.64	ϕB= 208.13	δB= 15.12
	P-axis: trend= 64.67		plunge= 37.18	
	T-axis: trend= 217.48		plunge= 49.55	
	B-axis: trend= 324.04		plunge= 13.66	
	Quality index = 28.9		reverse fault	

L2 tensor for : W0402 (501, zaw, wb)

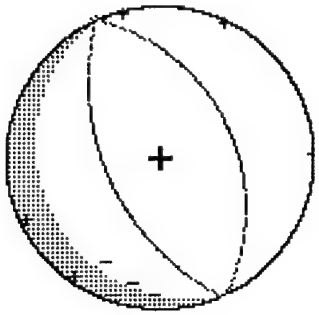

Full solution :

.465E+10	.518E+10	-.644E+11
.518E+10	.397E+10	-.217E+12
-.644E+11	-.217E+12	-.191E+13

T0= .0827 M0= .137E+13 MT= .193E+13
Expl.= -19.8% CLVD.= -19.8% DBCP.= 60.4%

Full:	ϕA= 156.35	δA= 51.61	ϕB= 334.43	δB= 38.40
	P-axis: trend= 73.63		plunge= 83.33	
	T-axis: trend= 245.50		plunge= 6.61	
	B-axis: trend= 335.61		plunge= .94	
	Quality index = 29.9		normal fault	

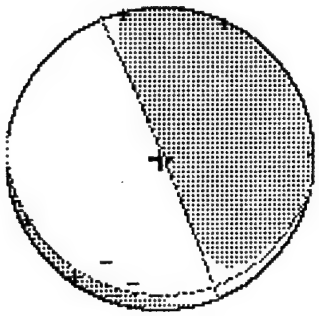

Trace null solution :

.491E+10	.103E+11	.338E+11
.103E+11	.366E+10	.828E+11
.338E+11	.828E+11	-.858E+10

T0= .0827 M0= .890E+11 MT= .903E+11
CLVD.= 2.9% DBCP.= 97.1%

Tr.0:	ϕA= 337.73	δA= 86.87	ϕB= 99.96	δB= 5.86
	P-axis: trend= 252.96		plunge= 47.91	
	T-axis: trend= 63.04		plunge= 41.66	
	B-axis: trend= 157.46		plunge= 4.95	
	Quality index = 27.9		normal fault	

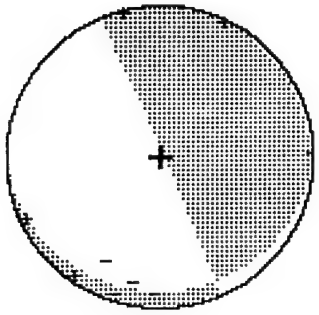

Double couple solution :

.825E+10	.996E+10	.343E+11
.996E+10	.180E+10	.810E+11
.343E+11	.810E+11	-.101E+11

T0= .0827 M0= .890E+11 MT= .890E+11
DBCP.= 100.0%

D.C.:	ϕA= 336.69	δA= 86.74	ϕB= 95.38	δB= 6.76
	P-axis: trend= 252.95		plunge= 47.94	
	T-axis: trend= 61.10		plunge= 41.45	
	B-axis: trend= 156.35		plunge= 5.92	
	Quality index = 27.8		normal fault	

L2 tensor for : W0403 (510, pods, wb)

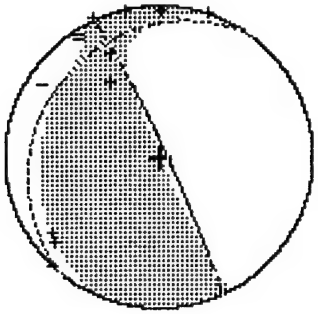

Full solution :

.588E+10	-.130E+10	-.205E+11
-.130E+10	-.246E+11	-.467E+11
-.205E+11	-.467E+11	.175E+10

T0= .0693 M0= .540E+11 MT= .607E+11
Expl.= -7.3% CLVD.= -9.7% DBCP.= 83.0%

Full:	∢A=	335.07	δA=	84.06	∢B= 218.15 δB= 12.95
	P-axis:	trend=	75.40	plunge=	38.02
	T-axis:	trend=	232.46	plunge=	49.67
	B-axis:	trend=	336.28	plunge=	11.47
	Quality index =		40.0	reverse fault	

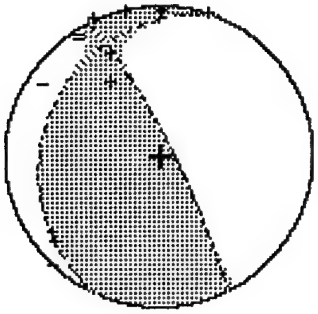

Trace null solution :

.597E+10	-.168E+10	-.234E+11
-.168E+10	-.237E+11	-.418E+11
-.234E+11	-.418E+11	.177E+11

T0= .0693 M0= .518E+11 MT= .525E+11
CLVD.= -2.2% DBCP.= 97.8%

Tr.0:	∢A=	332.79	δA=	79.58	∢B= 203.15 δB= 16.08
	P-axis:	trend=	73.21	plunge=	33.47
	T-axis:	trend=	227.98	plunge=	53.84
	B-axis:	trend=	335.05	plunge=	12.11
	Quality index =		39.9	reverse fault	

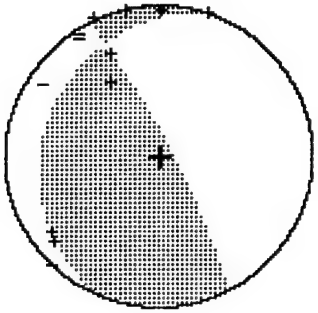

Double couple solution :

.485E+10	-.132E+10	-.237E+11
-.132E+10	-.228E+11	-.411E+11
-.237E+11	-.411E+11	.179E+11

T0= .0693 M0= .518E+11 MT= .518E+11
DBCP.= 100.0%

D.C.:	∢A=	332.41	δA=	79.64	∢B= 202.14 δB= 15.79
	P-axis:	trend=	72.56	plunge=	33.59
	T-axis:	trend=	227.99	plunge=	53.86
	B-axis:	trend=	334.60	plunge=	11.79
	Quality index =		39.8	reverse fault	

L2 tensor for : W0405 (510, pods, wb)

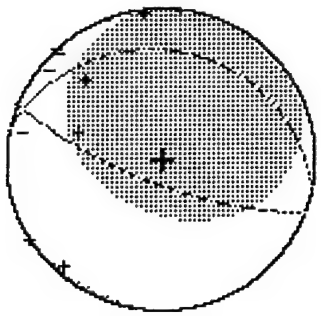

Full solution :

-.465E+09	.600E+10	.397E+11
.600E+10	-.660E+10	.197E+11
.397E+11	.197E+11	.715E+11

T0= .0893 M0= .677E+11 MT= .833E+11
Expl.= 34.8% CLVD.= 51.0% DBCP.= 14.2%

Full:	∮A= 111.36	δA= 71.01	∮B= 280.57	δB= 19.31
	P-axis: trend= 198.57		plunge= 25.93	
	T-axis: trend= 27.06		plunge= 63.82	
	B-axis: trend= 290.21		plunge= 3.36	
	Quality index = 34.8		reverse fault	

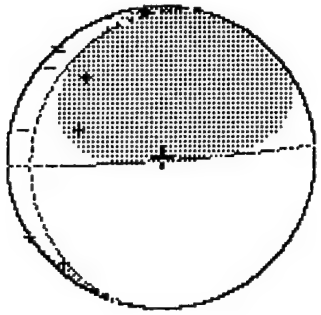

Trace null solution :

-.785E+09	.697E+10	.427E+11
.697E+10	-.813E+10	-.473E+09
.427E+11	-.473E+09	.892E+10

T0= .0893 M0= .399E+11 MT= .441E+11
CLVD.= 18.8% DBCP.= 81.2%

Tr.0:	∮A= 86.15	δA= 86.32	∮B= 196.23	δB= 10.60
	P-axis: trend= 166.90		plunge= 40.52	
	T-axis: trend= 6.62		plunge= 47.77	
	B-axis: trend= 265.50		plunge= 9.93	
	Quality index = 33.7		reverse fault	

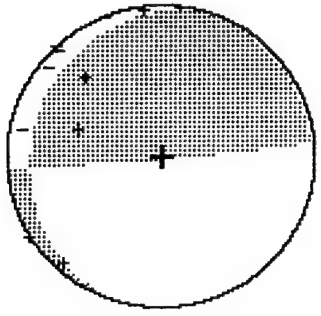

Double couple solution :

-.418E+10	.680E+10	.389E+11
.680E+10	-.102E+10	-.255E+10
.389E+11	-.255E+10	.519E+10

T0= .0893 M0= .399E+11 MT= .399E+11
DBCP.= 100.0%

D.C.:	∮A= 85.63	δA= 86.21	∮B= 197.46	δB= 10.11
	P-axis: trend= 166.92		plunge= 40.49	
	T-axis: trend= 5.53		plunge= 47.98	
	B-axis: trend= 265.00		plunge= 9.35	
	Quality index = 33.4		reverse fault	

L2 tensor for : W0407 (510, pods, wb)

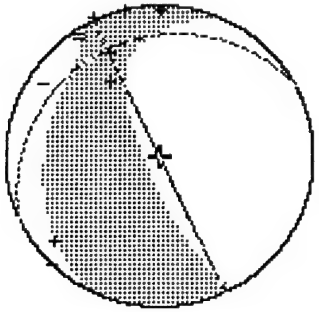

Full solution :

.888E+10	-.359E+09	-.184E+11
-.359E+09	-.294E+11	-.526E+11
-.184E+11	-.526E+11	-.199E+11

T0= .0733 M0= .614E+11 MT= .757E+11
Expl.= -11.9% CLVD.= -15.1% DBCP.= 73.1%

Full:	§A= 334.22	δA= 89.79	§B= 243.44	δB= 14.91
	P-axis: trend= 78.60		plunge= 42.90	
	T-axis: trend= 229.74		plunge= 43.30	
	B-axis: trend= 334.28		plunge= 14.91	
	Quality index = 27.9		reverse fault	

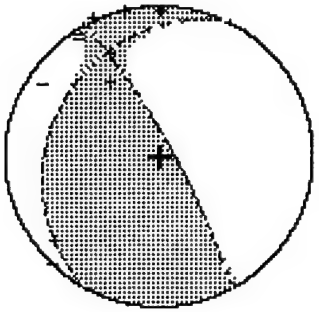

Trace null solution :

.889E+10	-.130E+10	-.252E+11
-.130E+10	-.270E+11	-.410E+11
-.252E+11	-.410E+11	.182E+11

T0= .0733 M0= .529E+11 MT= .538E+11
CLVD.= -2.9% DBCP.= 97.1%

Tr.0:	§A= 330.88	δA= 79.34	§B= 207.86	δB= 19.06
	P-axis: trend= 74.15		plunge= 32.51	
	T-axis: trend= 222.09		plunge= 53.05	
	B-axis: trend= 333.90		plunge= 15.61	
	Quality index = 27.6		reverse fault	

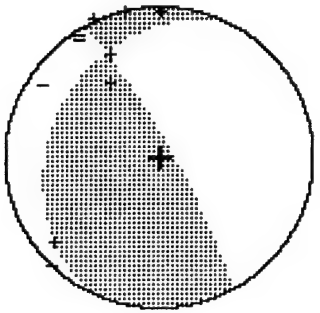

Double couple solution :

.751E+10	-.684E+09	-.257E+11
-.684E+09	-.259E+11	-.401E+11
-.257E+11	-.401E+11	.184E+11

T0= .0733 M0= .529E+11 MT= .529E+11
DBCP.= 100.0%

D.C.:	§A= 330.52	δA= 79.42	§B= 207.13	δB= 18.75
	P-axis: trend= 73.55		plunge= 32.66	
	T-axis: trend= 222.11		plunge= 53.08	
	B-axis: trend= 333.45		plunge= 15.30	
	Quality index = 27.4		reverse fault	

L2 tensor for : W0516 (510, pods, zr)

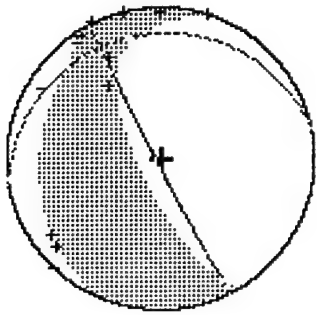

Full solution :

.260E+11	-.852E+10	-.823E+11
-.852E+10	-.981E+11	-.216E+12
-.823E+11	-.216E+12	-.129E+12

T0= .0907 M0= .259E+12 MT= .330E+12
Expl.= -13.4% CLVD.= -15.7% DBCP.= 70.8%

Full:	∮A= 152.70	δA= 86.59	∮B= 258.93	δB= 12.02
	P-axis: trend= 74.71		plunge= 47.19	
	T-axis: trend= 231.99		plunge= 40.51	
	B-axis: trend= 332.01		plunge= 11.51	
	Quality index = 39.7		normal fault	

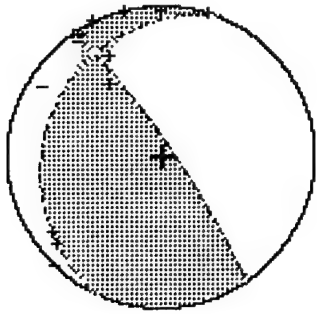

Trace null solution :

.271E+11	-.128E+11	-.116E+12
-.128E+11	-.875E+11	-.158E+12
-.116E+12	-.158E+12	.605E+11

T0= .0907 M0= .210E+12 MT= .211E+12
CLVD.= -1.3% DBCP.= 98.7%

Tr.0:	∮A= 325.68	δA= 81.28	∮B= 203.26	δB= 15.97
	P-axis: trend= 67.24		plunge= 34.93	
	T-axis: trend= 220.24		plunge= 51.91	
	B-axis: trend= 327.76		plunge= 13.27	
	Quality index = 39.3		reverse fault	

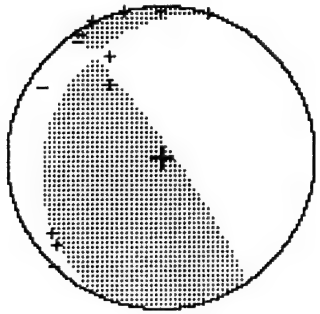

Double couple solution :

.249E+11	-.123E+11	-.118E+12
-.123E+11	-.867E+11	-.156E+12
-.118E+12	-.156E+12	.617E+11

T0= .0907 M0= .210E+12 MT= .210E+12
DBCP.= 100.0%

D.C.:	∮A= 325.11	δA= 81.21	∮B= 202.42	δB= 15.98
	P-axis: trend= 66.63		plunge= 34.87	
	T-axis: trend= 219.68		plunge= 51.99	
	B-axis: trend= 327.20		plunge= 13.24	
	Quality index = 39.2		reverse fault	

L2 tensor for : W0518 (510, pods, sw)

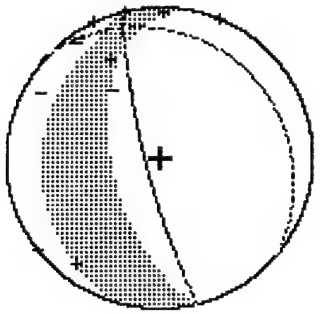

Full solution :

.199E+10	.133E+09	-.714E+10
.133E+09	-.273E+11	-.597E+11
-.714E+10	-.597E+11	-.689E+11

T0= .0693 M0= .798E+11 MT= .111E+12
Expl.= -17.8% CLVD.= -18.4% DBCP.= 63.8%

Full:	♀A= 166.00	δA= 79.83	♀B= 309.82	δB= 12.53
	P-axis: trend= 84.99		plunge= 54.60	
	T-axis: trend= 249.69		plunge= 34.43	
	B-axis: trend= 344.69		plunge= 7.24	
	Quality index = 34.7		normal fault	

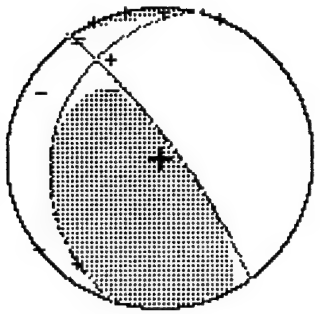

Trace null solution :

.301E+10	-.278E+10	-.249E+11
-.278E+10	-.219E+11	-.275E+11
-.249E+11	-.275E+11	.189E+11

T0= .0693 M0= .407E+11 MT= .425E+11
CLVD.= 8.4% DBCP.= 91.6%

Tr.0:	♀A= 323.82	δA= 77.24	♀B= 196.03	δB= 20.28
	P-axis: trend= 66.81		plunge= 30.47	
	T-axis: trend= 214.07		plunge= 55.03	
	B-axis: trend= 327.42		plunge= 15.50	
	Quality index = 33.1		reverse fault	

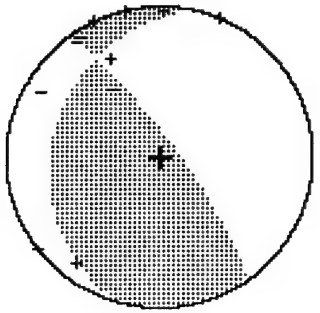

Double couple solution :

.433E+10	-.474E+10	-.227E+11
-.474E+10	-.213E+11	-.271E+11
-.227E+11	-.271E+11	.170E+11

T0= .0693 M0= .407E+11 MT= .407E+11
DBCP.= 100.0%

D.C.:	♀A= 324.05	δA= 77.16	♀B= 195.66	δB= 20.15
	P-axis: trend= 66.85		plunge= 30.44	
	T-axis: trend= 214.52		plunge= 55.18	
	B-axis: trend= 327.62		plunge= 15.26	
	Quality index = 32.8		reverse fault	

L2 tensor for : W0519 (510, pods, wb)

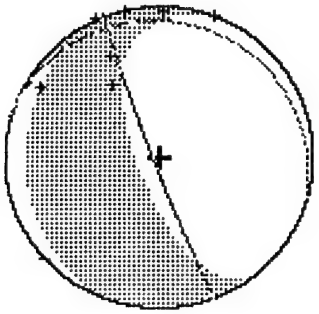

Full solution :

.307E+10	-.133E+10	-.103E+11
-.133E+10	-.930E+10	-.316E+11
-.103E+11	-.316E+11	-.181E+11

T0= .0653 M0= .363E+11 MT= .446E+11
Expl.= -11.8% CLVD.= -15.5% DBCP.= 72.6%

Full:	ϕA= 158.85	δA= 85.88	ϕB= 285.03	δB= 6.95
	P-axis: trend= 74.87		plunge= 48.82	
	T-axis: trend= 243.63		plunge= 40.63	
	B-axis: trend= 338.44		plunge= 5.59	
	Quality index = 12.1		normal fault	

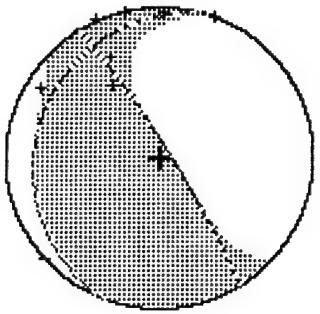

Trace null solution :

.280E+10	-.232E+10	-.927E+10
-.232E+10	-.682E+10	-.152E+11
-.927E+10	-.152E+11	.402E+10

T0= .0653 M0= .176E+11 MT= .189E+11
CLVD.= -9.4% DBCP.= 90.6%

Tr.0:	ϕA= 328.14	δA= 82.04	ϕB= 199.79	δB= 12.69
	P-axis: trend= 66.83		plunge= 36.30	
	T-axis: trend= 226.73		plunge= 51.97	
	B-axis: trend= 329.52		plunge= 9.83	
	Quality index = 11.6		reverse fault	

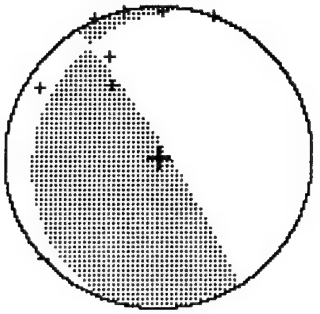

Double couple solution :

.121E+10	-.939E+09	-.933E+10
-.939E+09	-.593E+10	-.139E+11
-.933E+10	-.139E+11	.472E+10

T0= .0653 M0= .176E+11 MT= .176E+11
DBCP.= 100.0%

D.C.:	ϕA= 327.49	δA= 82.13	ϕB= 197.75	δB= 12.20
	P-axis: trend= 65.71		plunge= 36.47	
	T-axis: trend= 226.74		plunge= 51.99	
	B-axis: trend= 328.78		plunge= 9.26	
	Quality index = 11.5		reverse fault	

L2 tensor for : W0601 (510, pods, wb)

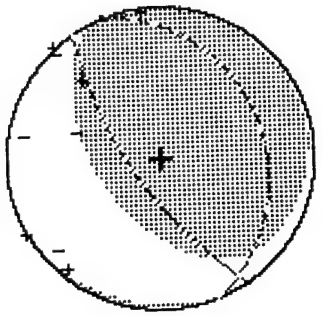

Full solution :

.999E+09	.115E+10	.132E+11
.115E+10	-.114E+10	.161E+11
.132E+11	.161E+11	.382E+11

T0= .0707 M0= .342E+11 MT= .467E+11
Expl.= 37.3% CLVD.= 39.7% DBCP.= 23.0%

Full:	∮A= 146.66	δA= 68.84	∮B= 338.60	δB= 21.59
	P-axis: trend= 240.03		plunge= 23.72	
	T-axis: trend= 49.09		plunge= 65.89	
	B-axis: trend= 148.24		plunge= 4.07	
	Quality index = 34.4		reverse fault	

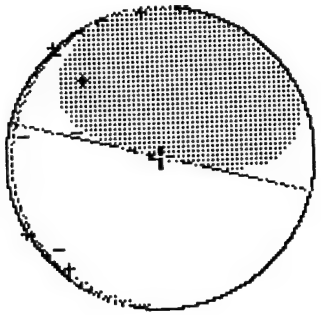

Trace null solution :

.713E+09	.168E+10	.159E+11
.168E+10	-.192E+10	.434E+10
.159E+11	.434E+10	.120E+10

T0= .0707 M0= .152E+11 MT= .167E+11
CLVD.= 16.9% DBCP.= 83.1%

Tr.0:	∮A= 284.61	δA= 89.87	∮B= 191.96	δB= 2.86
	P-axis: trend= 191.74		plunge= 45.06	
	T-axis: trend= 17.46		plunge= 44.80	
	B-axis: trend= 284.61		plunge= 2.86	
	Quality index = 32.0		normal fault	

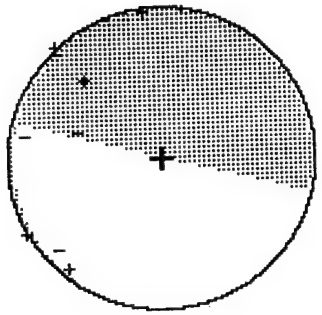

Double couple solution :

-.305E+09	.678E+09	.147E+11
.678E+09	.374E+09	.383E+10
.147E+11	.383E+10	-.689E+08

T0= .0707 M0= .152E+11 MT= .152E+11
DBCP.= 100.0%

D.C.:	∮A= 284.61	δA= 89.87	∮B= 192.00	δB= 2.86
	P-axis: trend= 191.75		plunge= 45.06	
	T-axis: trend= 17.45		plunge= 44.80	
	B-axis: trend= 284.61		plunge= 2.85	
	Quality index = 22.5		normal fault	

L2 tensor for : W0602 (510, pods, wb)

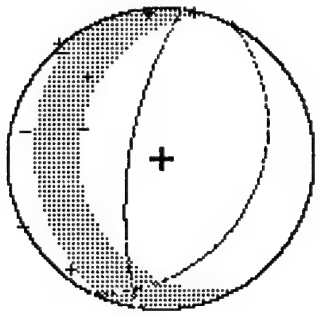

Full solution :

.255E+10	-.145E+10	-.271E+10
-.145E+10	-.100E+11	-.323E+11
-.271E+10	-.323E+11	-.719E+11

T0= .0693 M0= .607E+11 MT= .832E+11
Expl.= -18.4% CLVD.= -20.2% DBCP.= 61.4%

Full:	ϕA= 188.58	δA= 67.35	ϕB= 27.54	δB= 23.81
	P-axis: trend= 84.95		plunge= 66.81	
	T-axis: trend= 284.32		plunge= 22.00	
	B-axis: trend= 191.49		plunge= 6.95	
	Quality index = 29.1		normal fault	

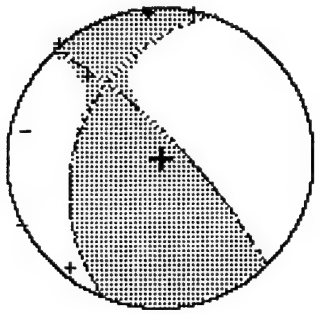

Trace null solution :

.318E+10	-.268E+10	-.675E+10
-.268E+10	-.821E+10	-.533E+10
-.675E+10	-.533E+10	.504E+10

T0= .0693 M0= .112E+11 MT= .115E+11
CLVD.= -4.5% DBCP.= 95.5%

Tr.0:	ϕA= 316.01	δA= 74.57	ϕB= 201.00	δB= 33.14
	P-axis: trend= 68.53		plunge= 23.82	
	T-axis: trend= 191.95		plunge= 51.28	
	B-axis: trend= 324.64		plunge= 28.53	
	Quality index = 24.6		reverse fault	

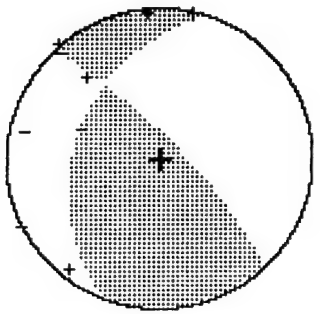

Double couple solution :

.287E+10	-.236E+10	-.693E+10
-.236E+10	-.783E+10	-.502E+10
-.693E+10	-.502E+10	.496E+10

T0= .0693 M0= .112E+11 MT= .112E+11
DBCP.= 100.0%

D.C.:	ϕA= 315.62	δA= 74.77	ϕB= 200.55	δB= 32.72
	P-axis: trend= 67.92		plunge= 24.15	
	T-axis: trend= 191.98		plunge= 51.32	
	B-axis: trend= 324.01		plunge= 28.19	
	Quality index = 24.7		reverse fault	

L2 tensor for : W0604 (510, pods, zr)

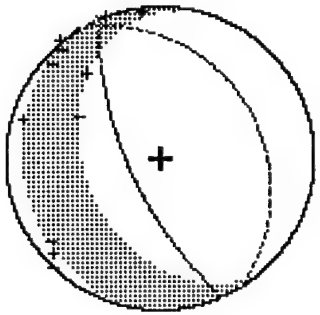

Full solution :

.474E+11	-.657E+11	-.352E+12
-.657E+11	-.222E+12	-.109E+13
-.352E+12	-.109E+13	-.255E+13

T0= .1150 M0= .214E+13 MT= .296E+13
Expl.= -18.4% CLVD.= -19.5% DBCP.= 62.1%

Full:	∮A= 156.35	δA= 67.13	∮B= 327.88	δB= 23.10
	P-axis: trend= 72.54		plunge= 67.71	
	T-axis: trend= 243.83		plunge= 22.06	
	B-axis: trend= 335.06		plunge= 3.05	
	Quality index = 41.2		normal fault	

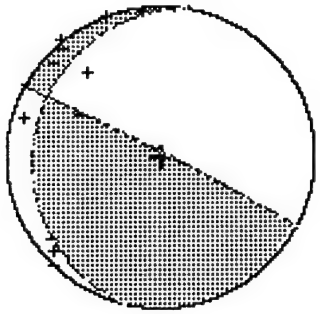

Trace null solution :

.517E+11	-.102E+12	-.594E+12
-.102E+12	-.122E+12	-.302E+12
-.594E+12	-.302E+12	.705E+11

T0= .1150 M0= .682E+12 MT= .682E+12
CLVD.= .2% DBCP.= 99.8%

Tr.0:	∮A= 297.52	δA= 87.01	∮B= 192.46	δB= 11.38
	P-axis: trend= 37.80		plunge= 41.02	
	T-axis: trend= 196.15		plunge= 46.90	
	B-axis: trend= 298.10		plunge= 10.97	
	Quality index = 40.1		reverse fault	

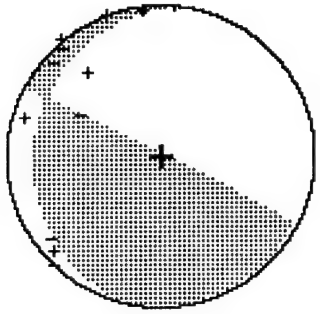

Double couple solution :

.493E+11	-.103E+12	-.596E+12
-.103E+12	-.117E+12	-.297E+12
-.596E+12	-.297E+12	.682E+11

T0= .1150 M0= .682E+12 MT= .682E+12
DBCP.= 100.0%

D.C.:	∮A= 297.01	δA= 87.08	∮B= 192.07	δB= 11.20
	P-axis: trend= 37.16		plunge= 41.12	
	T-axis: trend= 195.82		plunge= 46.86	
	B-axis: trend= 297.57		plunge= 10.80	
	Quality index = 40.0		reverse fault	

L2 tensor for : W0606 (501, zaw, wb)

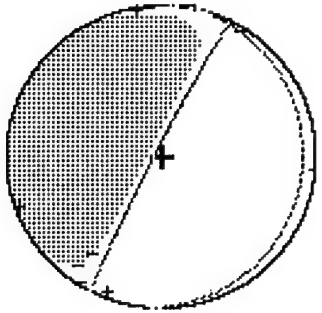

Full solution :

-.472E+11	.280E+10	.333E+12
.280E+10	.717E+10	-.640E+12
.333E+12	-.640E+12	-.229E+12

T0= .0667 M0= .740E+12 MT= .814E+12
Expl.= -9.3% CLVD.= -5.8% DBCP.= 84.8%

Full:	∮A= 207.09	δA= 85.62	∮B= 3.84	δB= 4.76
	P-axis:	trend= 119.13	plunge= 49.35	
	T-axis:	trend= 295.34	plunge= 40.59	
	B-axis:	trend= 26.95	plunge= 1.87	
	Quality index = 27.2		normal fault	

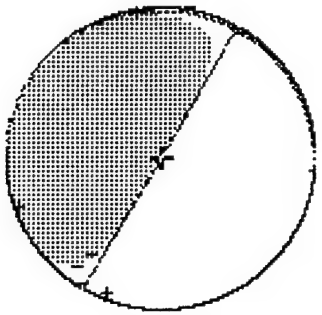

Trace null solution :

-.487E+11	.614E+10	.367E+12
.614E+10	.764E+10	-.641E+12
.367E+12	-.641E+12	.411E+11

T0= .0667 M0= .725E+12 MT= .740E+12
CLVD.= 4.1% DBCP.= 95.9%

Tr.0:	∮A= 29.97	δA= 88.97	∮B= 274.29	δB= 2.36
	P-axis:	trend= 122.07	plunge= 43.94	
	T-axis:	trend= 297.81	plunge= 45.99	
	B-axis:	trend= 30.01	plunge= 2.13	
	Quality index = 27.2		reverse fault	

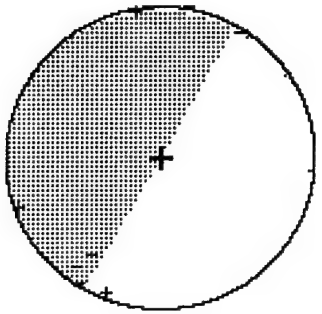

Double couple solution :

-.347E+11	.281E+11	.356E+12
.281E+11	.935E+10	-.631E+12
.356E+12	-.631E+12	.254E+11

T0= .0667 M0= .725E+12 MT= .725E+12
DBCP.= 100.0%

D.C.:	∮A= 29.47	δA= 89.00	∮B= 278.65	δB= 2.82
	P-axis:	trend= 122.06	plunge= 43.94	
	T-axis:	trend= 296.79	plunge= 45.94	
	B-axis:	trend= 29.52	plunge= 2.64	
	Quality index = 27.0		reverse fault	

L2 tensor for : W0607 (501, zaw, zr)

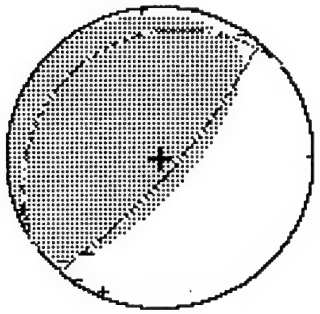

Full solution :

-.649E+11	.194E+11	.461E+12
.194E+11	.524E+10	-.574E+12
.461E+12	-.574E+12	.704E+12

T0= .0493 M0= .890E+12 MT= .114E+13
Expl.= 23.2% CLVD.= 25.0% DBCP.= 51.8%
Full: $A= 40.87 δA= 76.51 $B= 233.43 δB= 13.81
P-axis: trend= 133.34 plunge= 31.44
T-axis: trend= 306.86 plunge= 58.39
B-axis: trend= 41.57 plunge= 2.89
Quality index = 20.5 reverse fault

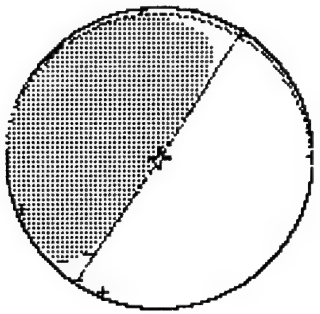

Trace null solution :

-.590E+11	.119E+11	.338E+12
.119E+11	.537E+10	-.526E+12
.338E+12	-.526E+12	.536E+11

T0= .0493 M0= .613E+12 MT= .628E+12
CLVD.= 4.8% DBCP.= 95.2%
Tr.0: $A= 33.07 δA= 88.21 $B= 273.33 δB= 3.61
P-axis: trend= 126.11 plunge= 43.12
T-axis: trend= 299.83 plunge= 46.71
B-axis: trend= 33.17 plunge= 3.14
Quality index = 19.8 reverse fault

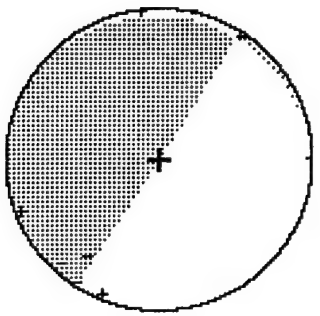

Double couple solution :

-.457E+11	.331E+11	.328E+12
.331E+11	.796E+10	-.515E+12
.328E+12	-.515E+12	.377E+11

T0= .0493 M0= .613E+12 MT= .613E+12
DBCP.= 100.0%
D.C.: $A= 32.63 δA= 88.23 $B= 276.37 δB= 3.99
P-axis: trend= 126.10 plunge= 43.12
T-axis: trend= 298.95 plunge= 46.65
B-axis: trend= 32.75 plunge= 3.58
Quality index = 19.6 reverse fault

L2 tensor for : W0608 (510, pods, sw)

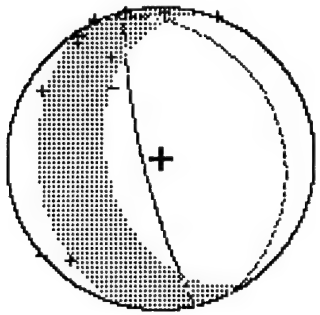

Full solution :

.160E+11	-.122E+11	-.330E+11
-.122E+11	-.715E+11	-.189E+12
-.330E+11	-.189E+12	-.252E+12

T0= .0613 M0= .267E+12 MT= .357E+12
Expl.= -16.7% CLVD.= -19.5% DBCP.= 63.8%

Full:	$A= 166.61	δA= 77.41	$B= 332.98	δB= 12.94
	P-axis: trend= 80.60		plunge= 57.48	
	T-axis: trend= 254.08		plunge= 32.35	
	B-axis: trend= 345.95		plunge= 2.95	
	Quality index = 35.5		normal fault	

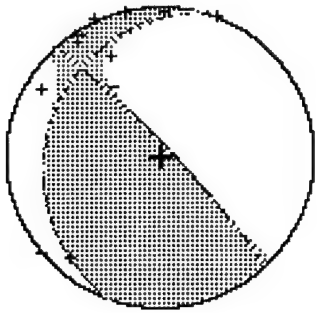

Trace null solution :

.188E+11	-.208E+11	-.897E+11
-.208E+11	-.545E+11	-.899E+11
-.897E+11	-.899E+11	.357E+11

T0= .0613 M0= .135E+12 MT= .137E+12
CLVD.= -3.6% DBCP.= 96.4%

Tr.0:	$A= 316.47	δA= 81.71	$B= 198.23	δB= 17.12
	P-axis: trend= 59.41		plunge= 35.02	
	T-axis: trend= 209.51		plunge= 51.06	
	B-axis: trend= 318.69		plunge= 14.87	
	Quality index = 34.7		reverse fault	

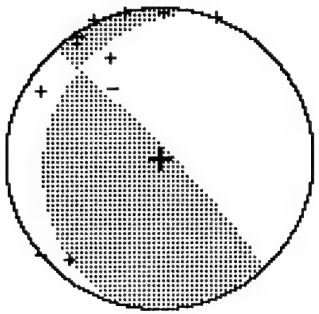

Double couple solution :

.159E+11	-.171E+11	-.901E+11
-.171E+11	-.527E+11	-.866E+11
-.901E+11	-.866E+11	.368E+11

T0= .0613 M0= .135E+12 MT= .135E+12
DBCP.= 100.0%

D.C.:	$A= 316.06	δA= 81.80	$B= 197.43	δB= 16.74
	P-axis: trend= 58.70		plunge= 35.19	
	T-axis: trend= 209.53		plunge= 51.08	
	B-axis: trend= 318.20		plunge= 14.49	
	Quality index = 34.6		reverse fault	

L2 tensor for : W0609 (510, pods, wb)

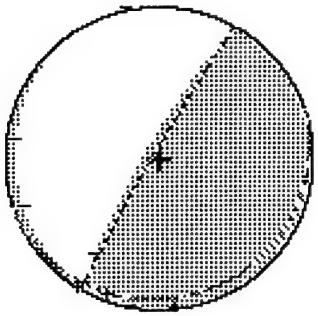

Full solution :

-.364E+11	-.533E+11	-.107E+13
-.533E+11	.294E+12	.192E+13
-.107E+13	.192E+13	.780E+12

T0= .0480 M0= .227E+13 MT= .273E+13
Expl.= 14.5% CLVD.= 14.5% DBCP.= 71.0%

Full:	∮A= 210.10	δA= 86.60	∮B= 72.24	δB= 4.58
	P-axis: trend= 303.00		plunge= 41.52	
	T-axis: trend= 116.83		plunge= 48.32	
	B-axis: trend= 210.28		plunge= 3.07	
	Quality index = 22.2		reverse fault	

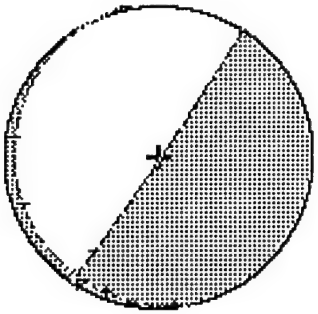

Trace null solution :

-.324E+11	-.501E+11	-.102E+13
-.501E+11	.239E+12	.153E+13
-.102E+13	.153E+13	-.207E+12

T0= .0480 M0= .185E+13 MT= .185E+13
CLVD.= -.2% DBCP.= 99.8%

Tr.0:	∮A= 33.49	δA= 86.82	∮B= 167.65	δB= 4.56
	P-axis: trend= 306.95		plunge= 48.08	
	T-axis: trend= 120.39		plunge= 41.73	
	B-axis: trend= 213.31		plunge= 3.27	
	Quality index = 22.1		normal fault	

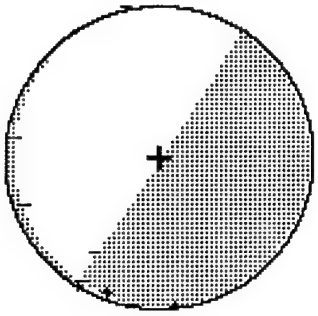

Double couple solution :

-.181E+11	-.587E+11	-.100E+13
-.587E+11	.224E+12	.154E+13
-.100E+13	.154E+13	-.206E+12

T0= .0480 M0= .185E+13 MT= .185E+13
DBCP.= 100.0%

D.C.:	∮A= 32.95	δA= 86.79	∮B= 172.89	δB= 4.19
	P-axis: trend= 305.80		plunge= 48.14	
	T-axis: trend= 120.39		plunge= 41.73	
	B-axis: trend= 212.79		plunge= 2.69	
	Quality index = 22.1		normal fault	

L2 tensor for : W0610 (504, zaw, zr)

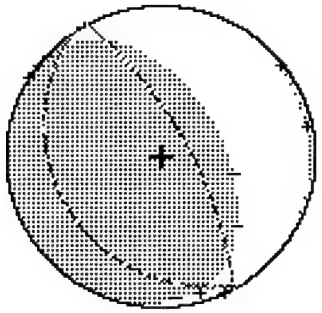

Full solution :

-.889E+10	.127E+11	-.148E+12
.127E+11	.219E+11	-.291E+12
-.148E+12	-.291E+12	.615E+12

T0= .0773 M0= .544E+12 MT= .747E+12
Expl.= 38.9% CLVD.= 41.2% DBCP.= 19.9%
Full: ∮A= 331.35 δA= 68.95 ∮B= 148.00 δB= 21.08
P-axis: trend= 60.42 plunge= 23.94
T-axis: trend= 243.45 plunge= 66.03
B-axis: trend= 150.92 plunge= 1.12
Quality index = 29.4 reverse fault

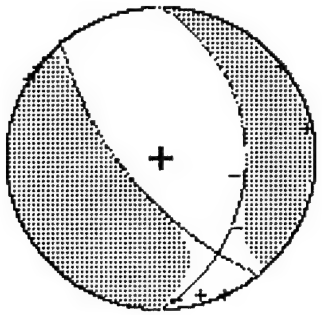

Trace null solution :

-.290E+09	.425E+10	-.574E+10
.425E+10	.917E+10	-.466E+10
-.574E+10	-.466E+10	-.888E+10

T0= .0773 M0= .120E+11 MT= .124E+11
CLVD.= 6.2% DBCP.= 93.8%
Tr.0: ∮A= 140.47 δA= 64.27 ∮B= 359.31 δB= 31.75
P-axis: trend= 16.56 plunge= 65.27
T-axis: trend= 244.60 plunge= 17.11
B-axis: trend= 149.10 plunge= 17.29
Quality index = 1.5 normal fault

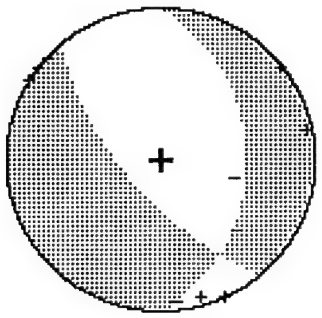

Double couple solution :

.181E+09	.375E+10	-.588E+10
.375E+10	.868E+10	-.437E+10
-.588E+10	-.437E+10	-.886E+10

T0= .0773 M0= .120E+11 MT= .120E+11
DBCP.= 100.0%
D.C.: ∮A= 140.01 δA= 64.40 ∮B= 358.58 δB= 31.50
P-axis: trend= 16.58 plunge= 65.29
T-axis: trend= 243.97 plunge= 17.30
B-axis: trend= 148.48 plunge= 17.08
Quality index = 1.5 normal fault

L2 tensor for : W0611 (504, pods, zr)

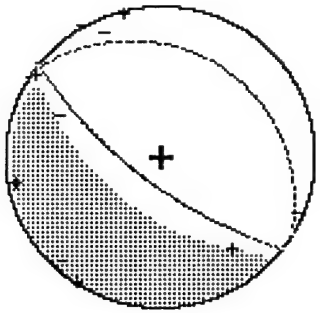

Full solution :

.809E+09	-.210E+10	-.764E+11
-.210E+10	-.517E+10	-.649E+11
-.764E+11	-.649E+11	-.167E+12

T0= .0547 M0= .155E+12 MT= .214E+12
Expl.= -17.5% CLVD.= -17.2% DBCP.= 65.3%

Full:	ϕA=	127.76	δA=	70.36	ϕB= 301.54	δB= 19.75
	P-axis:	trend=	41.21	plunge=	64.58	
	T-axis:	trend=	216.12	plunge=	25.33	
	B-axis:	trend=	307.05	plunge=	1.97	
	Quality index =		29.3	normal fault		

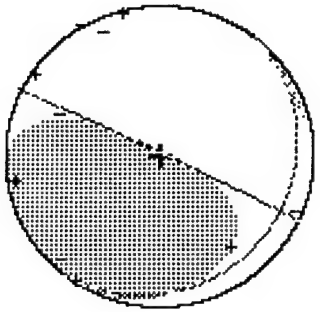

Trace null solution :

-.369E+10	.470E+10	-.273E+11
.470E+10	-.406E+09	-.143E+11
-.273E+11	-.143E+11	.410E+10

T0= .0547 M0= .287E+11 MT= .314E+11
CLVD.= 16.7% DBCP.= 83.3%

Tr.0:	ϕA=	295.50	δA=	88.30	ϕB= 37.60	δB= 8.06
	P-axis:	trend=	17.91	plunge=	42.78	
	T-axis:	trend=	213.54	plunge=	46.15	
	B-axis:	trend=	115.27	plunge=	7.88	
	Quality index =		25.8	reverse fault		

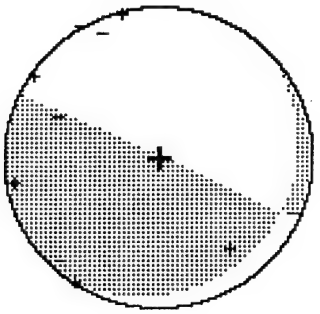

Double couple solution :

-.428E+10	.168E+10	-.257E+11
.168E+10	.249E+10	-.121E+11
-.257E+11	-.121E+11	.179E+10

T0= .0547 M0= .287E+11 MT= .287E+11
DBCP.= 100.0%

D.C.:	ϕA=	294.93	δA=	88.20	ϕB= 38.65	δB= 7.56
	P-axis:	trend=	17.86	plunge=	42.74	
	T-axis:	trend=	212.45	plunge=	46.32	
	B-axis:	trend=	114.70	plunge=	7.34	
	Quality index =		25.9	reverse fault		

L2 tensor for : W0614 (uskok Klodnicki)

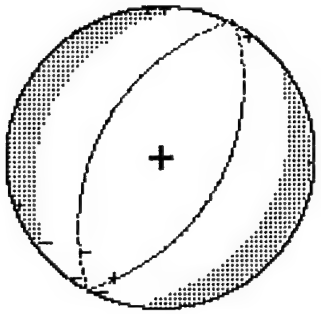

Full solution :

.111E+11	-.629E+11	-.142E+11
-.629E+11	.921E+11	-.246E+11
-.142E+11	-.246E+11	-.191E+13

T0= .1480 M0= .135E+13 MT= .189E+13
Expl.= -19.6% CLVD.= -18.9% DBCP.= 61.5%

Full:	ϕA= 207.80	δA= 45.42	ϕB= 29.27	δB= 44.59
	P-axis: trend= 58.09	plunge= 89.15		
	T-axis: trend= 298.53	plunge= .42		
	B-axis: trend= 208.52	plunge= .74		
	Quality index = 35.0	normal fault		

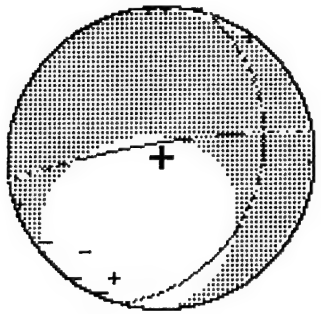

Trace null solution :

-.240E+10	-.468E+11	.181E+12
-.468E+11	.948E+11	.308E+11
.181E+12	.308E+11	-.924E+11

T0= .1480 M0= .146E+12 MT= .211E+12
CLVD.= -22.1% DBCP.= 77.9%

Tr.0:	ϕA= 260.97	δA= 80.04	ϕB= 15.51	δB= 22.92
	P-axis: trend= 194.25	plunge= 50.68		
	T-axis: trend= 333.80	plunge= 31.94		
	B-axis: trend= 77.22	plunge= 20.42		
	Quality index = 23.5	normal fault		

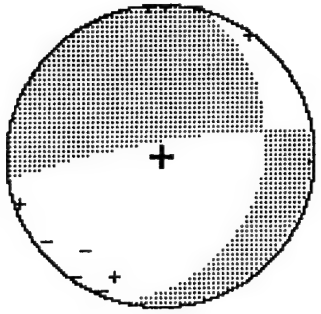

Double couple solution :

.302E+11	-.549E+11	.129E+12
-.549E+11	.173E+11	-.122E+11
.129E+12	-.122E+11	-.475E+11

T0= .1480 M0= .146E+12 MT= .146E+12
DBCP.= 100.0%

D.C.:	ϕA= 260.64	δA= 79.89	ϕB= 16.06	δB= 22.55
	P-axis: trend= 193.53	plunge= 51.00		
	T-axis: trend= 333.86	plunge= 31.94		
	B-axis: trend= 76.93	plunge= 19.93		
	Quality index = 23.0	normal fault		

L2 tensor for : W0616 (501, zaw, wb)

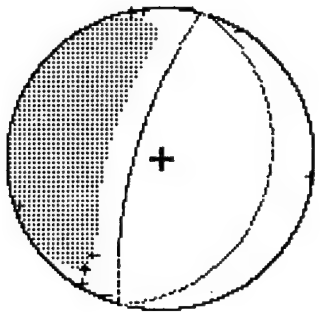

Full solution :

-.674E+10	-.186E+10	.302E+11
-.186E+10	.534E+09	-.108E+12
.302E+11	-.108E+12	-.168E+12

T0= .0507 M0= .164E+12 MT= .217E+12
Expl.= -17.8% CLVD.= -15.6% DBCP.= 66.6%

Full:	∮A=	195.42	δA=	71.57	∮B=	14.97	δB= 18.43
	P-axis:	trend=	105.64	plunge=	63.43		
	T-axis:	trend=	285.30	plunge=	26.57		
	B-axis:	trend=	15.37	plunge=	.13		
	Quality index =		28.0	normal	fault		

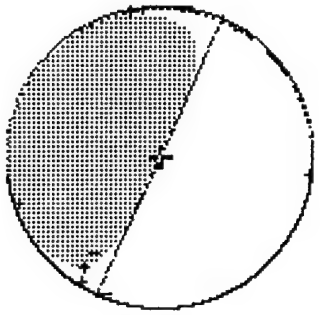

Trace null solution :

-.704E+10	-.271E+09	.403E+11
-.271E+09	.917E+09	-.918E+11
.403E+11	-.918E+11	.612E+10

T0= .0507 M0= .974E+11 MT= .100E+12
CLVD.= 6.1% DBCP.= 93.9%

Tr.0:	∮A=	23.86	δA=	89.10	∮B=	264.14	δB= 1.82
	P-axis:	trend=	115.42	plunge=	44.08		
	T-axis:	trend=	292.26	plunge=	45.88		
	B-axis:	trend=	23.89	plunge=	1.58		
	Quality index =		26.6	reverse	fault		

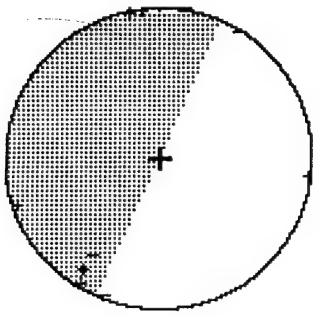

Double couple solution :

-.248E+10	.293E+10	.393E+11
.293E+10	-.580E+09	-.890E+11
.393E+11	-.890E+11	.306E+10

T0= .0507 M0= .974E+11 MT= .974E+11
DBCP.= 100.0%

D.C.:	∮A=	23.86	δA=	89.10	∮B=	264.10	δB= 1.82
	P-axis:	trend=	115.41	plunge=	44.08		
	T-axis:	trend=	292.26	plunge=	45.88		
	B-axis:	trend=	23.89	plunge=	1.58		
	Quality index =		13.1	reverse	fault		

APPENDIX B

Moment tensor solutions for selected seismic events

at Ziemowit coal mine

L2 tensor for : #1

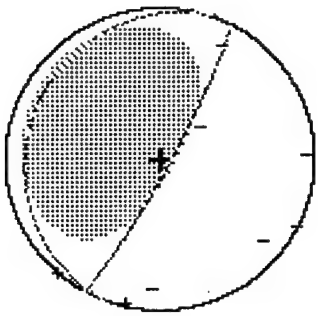

Full solution :

-.125E+11	-.629E+09	.348E+11
-.629E+09	-.152E+11	-.626E+11
.348E+11	-.626E+11	.309E+11

T0= .0600 M0= .698E+11 MT= .761E+11
Expl.= .9% CLVD.= 13.0% DBCP.= 86.0%

Full:	∮A=	28.51	δA= 81.29	∮B= 200.86	δB= 8.79
	P-axis:	trend= 117.49		plunge= 36.28	
	T-axis:	trend= 299.90		plunge= 53.69	
	B-axis:	trend= 208.34		plunge= 1.15	
	Quality index =	10.0		reverse fault	

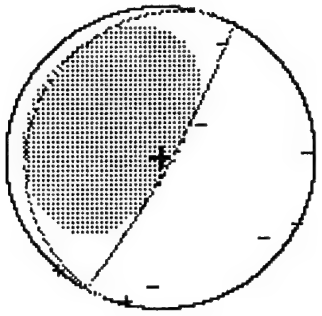

Trace null solution :

-.129E+11	-.230E+09	.335E+11
-.230E+09	-.156E+11	-.597E+11
.335E+11	-.597E+11	.284E+11

T0= .0600 M0= .650E+11 MT= .728E+11
CLVD.= 12.9% DBCP.= 87.1%

Tr.0:	∮A=	28.85	δA= 81.25	∮B= 201.86	δB= 8.82
	P-axis:	trend= 117.91		plunge= 36.24	
	T-axis:	trend= 300.13		plunge= 53.74	
	B-axis:	trend= 208.68		plunge= 1.06	
	Quality index =	9.8		reverse fault	

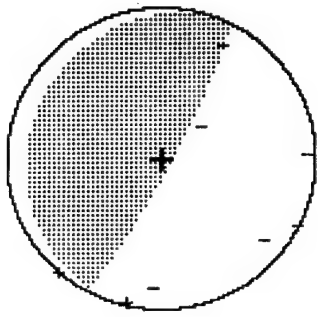

Double couple solution :

-.336E+10	.748E+10	.295E+11
.748E+10	-.162E+11	-.545E+11
.295E+11	-.545E+11	.196E+11

T0= .0600 M0= .650E+11 MT= .650E+11
DBCP.= 100.0%

D.C.:	∮A=	28.24	δA= 81.23	∮B= 201.08	δB= 8.84
	P-axis:	trend= 117.28		plunge= 36.22	
	T-axis:	trend= 299.55		plunge= 53.76	
	B-axis:	trend= 208.07		plunge= 1.08	
	Quality index =	10.4		reverse fault	

L2 tensor for : #2

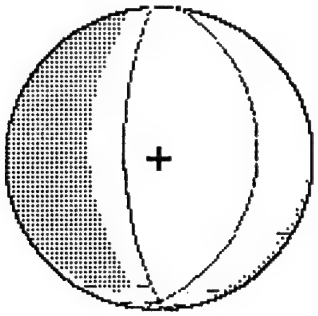

Full solution :

-.316E+11	-.584E+11	-.137E+12
-.584E+11	.329E+11	-.105E+13
-.137E+12	-.105E+13	-.234E+13

T0= .0667 M0= .196E+13 MT= .272E+13
Expl.= -39.1% CLVD.= -37.9% DBCP.= 22.9%

Full:	ϕA=	178.14	δA=	65.84	ϕB=	6.66 δB= 24.40
P-axis:	trend=	81.23	plunge=	68.96		
T-axis:	trend=	270.80	plunge=	20.77		
B-axis:	trend=	179.58	plunge=	3.20		
Quality index =	12.4	normal fault				

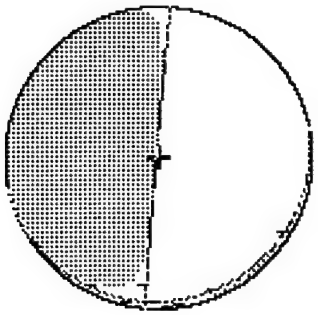

Trace null solution :

-.198E+11	-.508E+11	.778E+11
-.508E+11	.320E+11	-.931E+12
.778E+11	-.931E+12	-.122E+11

T0= .0667 M0= .922E+12 MT= .936E+12
CLVD.= 2.8% DBCP.= 97.2%

Tr.0:	ϕA=	184.69	δA=	89.20	ϕB=	78.85 δB= 2.92
P-axis:	trend=	91.84	plunge=	45.73		
T-axis:	trend=	277.46	plunge=	44.13		
B-axis:	trend=	184.73	plunge=	2.81		
Quality index =	12.4	normal fault				

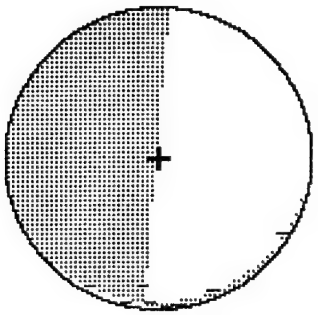

Double couple solution :

.752E+10	-.466E+11	.746E+11
-.466E+11	.190E+11	-.918E+12
.746E+11	-.918E+12	-.265E+11

T0= .0667 M0= .922E+12 MT= .922E+12
DBCP.= 100.0%

D.C.:	ϕA=	184.69	δA=	89.17	ϕB=	78.28 δB= 2.92
P-axis:	trend=	91.85	plunge=	45.76		
T-axis:	trend=	277.45	plunge=	44.11		
B-axis:	trend=	184.73	plunge=	2.80		
Quality index =	8.5	normal fault				

L2 tensor for : #3

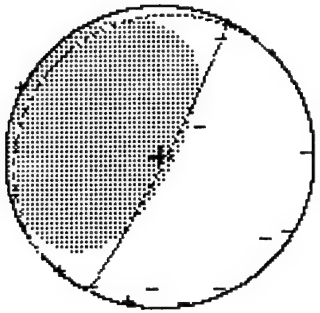

Full solution :

-.103E+11	-.287E+10	.342E+11
-.287E+10	.838E+09	-.690E+11
.342E+11	-.690E+11	.321E+11

T0= .0633 M0= .807E+11 MT= .848E+11
Expl.= 5.8% CLVD.= 13.7% DBCP.= 80.6%

Full:	ϕA=	27.32	δA=	84.27	ϕB= 228.23	δB= 6.14
	P-axis:	trend=	119.31	plunge=	39.23	
	T-axis:	trend=	294.88	plunge=	50.69	
	B-axis:	trend=	27.54	plunge=	2.18	
	Quality index =		51.2	reverse fault		

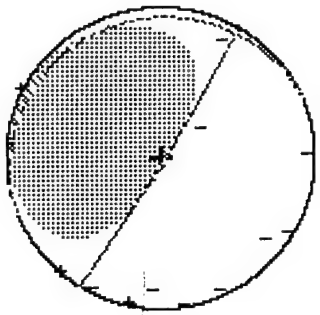

Trace null solution :

-.113E+11	-.164E+10	.289E+11
-.164E+10	-.254E+10	-.495E+11
.289E+11	-.495E+11	.139E+11

T0= .0633 M0= .528E+11 MT= .587E+11
CLVD.= 12.4% DBCP.= 87.6%

Tr.0:	ϕA=	31.39	δA=	85.68	ϕB= 247.97	δB= 5.37
	P-axis:	trend=	124.37	plunge=	40.60	
	T-axis:	trend=	297.93	plunge=	49.22	
	B-axis:	trend=	31.63	plunge=	3.19	
	Quality index =		50.0	reverse fault		

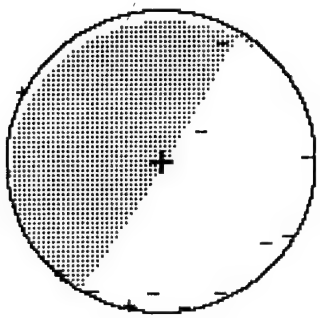

Double couple solution :

-.475E+10	.486E+10	.270E+11
.486E+10	-.316E+10	-.446E+11
.270E+11	-.446E+11	.791E+10

T0= .0633 M0= .528E+11 MT= .528E+11
DBCP.= 100.0%

D.C.:	ϕA=	31.39	δA=	85.68	ϕB= 247.93	δB= 5.37
	P-axis:	trend=	124.36	plunge=	40.60	
	T-axis:	trend=	297.93	plunge=	49.22	
	B-axis:	trend=	31.63	plunge=	3.18	
	Quality index =		35.0	reverse fault		

L2 tensor for : #4

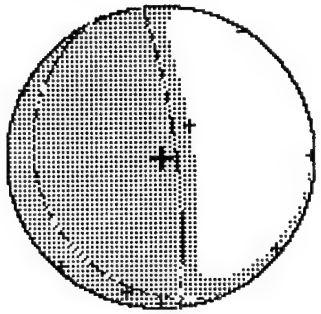

Full solution :

.380E+10	-.794E+10	-.103E+11
-.794E+10	.549E+10	-.137E+12
-.103E+11	-.137E+12	.126E+12

T0= .0483 M0= .164E+12 MT= .210E+12
Expl.= 15.3% CLVD.= 13.5% DBCP.= 71.2%

Full:	∮A= 353.48	δA= 77.93	∮B= 157.74	δB= 12.53
	P-axis: trend= 80.64		plunge= 32.85	
	T-axis: trend= 267.85		plunge= 56.95	
	B-axis: trend= 172.77		plunge= 3.30	
	Quality index = 12.4		reverse fault	

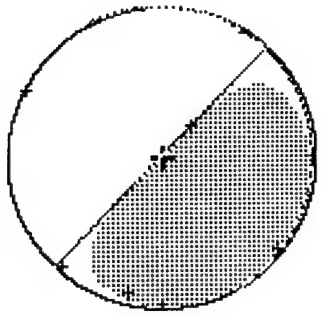

Trace null solution :

-.627E+09	-.484E+10	-.646E+11
-.484E+10	-.442E+10	.679E+11
-.646E+11	.679E+11	.505E+10

T0= .0483 M0= .901E+11 MT= .940E+11
CLVD.= 6.5% DBCP.= 93.5%

Tr.0:	∮A= 223.41	δA= 89.56	∮B= 331.62	δB= 1.39
	P-axis: trend= 312.10		plunge= 44.55	
	T-axis: trend= 134.74		plunge= 45.42	
	B-axis: trend= 43.40		plunge= 1.32	
	Quality index = 11.4		reverse fault	

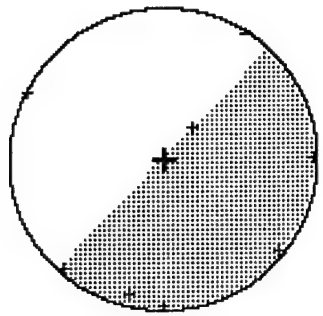

Double couple solution :

.143E+10	.570E+09	-.619E+11
.570E+09	-.280E+10	.654E+11
-.619E+11	.654E+11	.137E+10

T0= .0483 M0= .901E+11 MT= .901E+11
DBCP.= 100.0%

D.C.:	∮A= 223.41	δA= 89.56	∮B= 331.68	δB= 1.39
	P-axis: trend= 312.10		plunge= 44.55	
	T-axis: trend= 134.74		plunge= 45.42	
	B-axis: trend= 43.40		plunge= 1.32	
	Quality index = 8.1		reverse fault	

L2 tensor for : #5

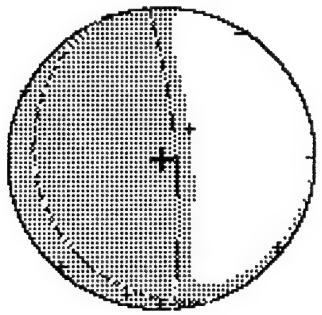

Full solution :

.173E+10	-.360E+10	-.343E+10
-.360E+10	.216E+10	-.695E+11
-.343E+10	-.695E+11	.617E+11

T0= .0467 M0= .822E+11 MT= .105E+12
Expl.= 14.9% CLVD.= 13.4% DBCP.= 71.7%

Full:	ϕA=	355.26	δA=	78.29	ϕB= 160.74	δB= 12.08
	P-axis:	trend=	82.72	plunge=	33.23	
	T-axis:	trend=	269.13	plunge=	56.61	
	B-axis:	trend=	174.65	plunge=	2.95	
	Quality index =		12.3	reverse fault		

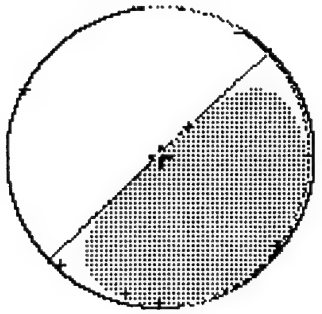

Trace null solution :

-.515E+09	-.196E+10	-.311E+11
-.196E+10	-.251E+10	.300E+11
-.311E+11	.300E+11	.302E+10

T0= .0467 M0= .415E+11 MT= .434E+11
CLVD.= 6.7% DBCP.= 93.3%

Tr.0:	ϕA=	225.92	δA=	89.16	ϕB= 350.19	δB= 1.50
	P-axis:	trend=	314.70	plunge=	44.14	
	T-axis:	trend=	137.18	plunge=	45.83	
	B-axis:	trend=	45.90	plunge=	1.24	
	Quality index =		11.3	reverse fault		

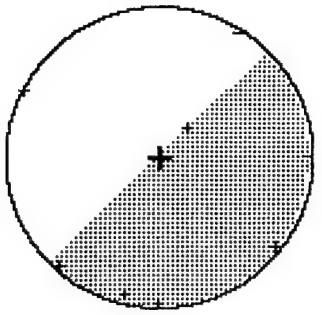

Double couple solution :

.317E+09	.582E+09	-.295E+11
.582E+09	-.146E+10	.291E+11
-.295E+11	.291E+11	.114E+10

T0= .0467 M0= .415E+11 MT= .415E+11
DBCP.= 100.0%

D.C.:	ϕA=	225.35	δA=	89.21	ϕB= 347.89	δB= 1.47
	P-axis:	trend=	314.13	plunge=	44.20	
	T-axis:	trend=	136.60	plunge=	45.77	
	B-axis:	trend=	45.33	plunge=	1.24	
	Quality index =		11.3	reverse fault		

L2 tensor for : #6

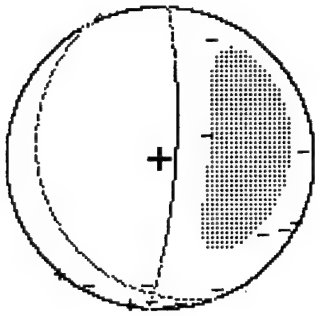

Full solution :

-.370E+11	.248E+11	-.356E+11
.248E+11	-.638E+11	.229E+12
-.356E+11	.229E+12	-.290E+12

T0= .0883 M0= .315E+12 MT= .405E+12
Expl.= -38.3% CLVD.= -28.8% DBCP.= 32.8%

Full:	∮A= 3.64	δA= 77.05	∮B= 158.45	δB= 14.26
	P-axis: trend= 281.57		plunge= 57.54	
	T-axis: trend= 88.64		plunge= 31.80	
	B-axis: trend= 182.29		plunge= 5.86	
	Quality index = 52.4		normal fault	

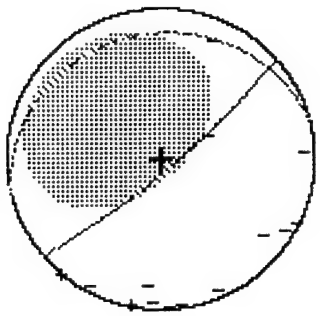

Trace null solution :

-.214E+11	-.632E+10	.439E+11
-.632E+10	-.130E+11	-.426E+11
.439E+11	-.426E+11	.344E+11

T0= .0883 M0= .540E+11 MT= .684E+11
CLVD.= 18.7% DBCP.= 81.3%

Tr.0:	∮A= 49.64	δA= 79.60	∮B= 255.97	δB= 11.57
	P-axis: trend= 144.01		plunge= 34.41	
	T-axis: trend= 313.33		plunge= 55.12	
	B-axis: trend= 50.57		plunge= 5.02	
	Quality index = 45.9		reverse fault	

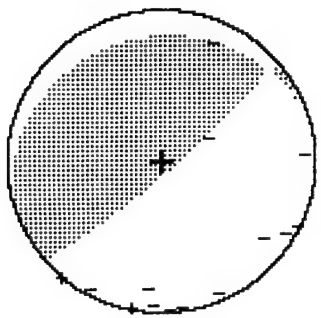

Double couple solution :

-.157E+11	.876E+10	.374E+11
.876E+10	-.345E+10	-.335E+11
.374E+11	-.335E+11	.191E+11

T0= .0883 M0= .540E+11 MT= .540E+11
DBCP.= 100.0%

D.C.:	∮A= 49.15	δA= 79.58	∮B= 255.72	δB= 11.61
	P-axis: trend= 143.57		plunge= 34.39	
	T-axis: trend= 312.75		plunge= 55.13	
	B-axis: trend= 50.09		plunge= 5.08	
	Quality index = 46.6		reverse fault	

L2 tensor for : #7

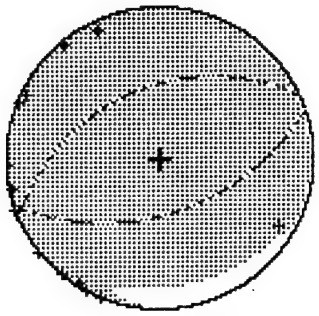

Full solution :

.200E+10	.611E+10	.725E+11
.611E+10	.685E+10	.206E+11
.725E+11	.206E+11	.907E+12

T0= .0550 M0= .646E+12 MT= .908E+12
Expl.= 20.2% CLVD.= 19.7% DBCP.= 60.0%

Full:	∮A=	71.97	δA= 48.86	∮B= 246.23	δB= 41.28
	P-axis:	trend= 159.29		plunge= 3.79	
	T-axis:	trend= 16.26		plunge= 85.25	
	B-axis:	trend= 249.48		plunge= 2.85	
	Quality index =	50.0		reverse fault	

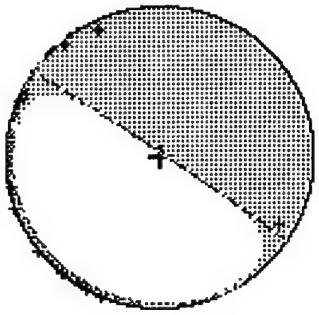

Trace null solution :

.580E+10	.398E+10	.103E+12
.398E+10	.841E+10	.694E+11
.103E+12	.694E+11	-.142E+11

T0= .0550 M0= .123E+12 MT= .125E+12
CLVD.= -3.2% DBCP.= 96.8%

Tr.0:	∮A=	304.09	δA= 87.18	∮B= 147.81	δB= 3.08
	P-axis:	trend= 212.79		plunge= 47.81	
	T-axis:	trend= 35.27		plunge= 42.17	
	B-axis:	trend= 304.15		plunge= 1.24	
	Quality index =	49.7		normal fault	

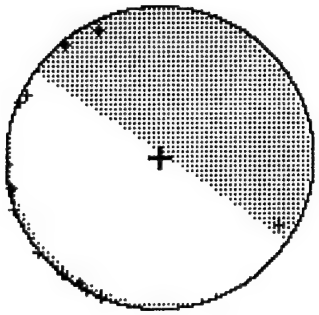

Double couple solution :

.768E+10	.657E+10	.101E+12
.657E+10	.538E+10	.686E+11
.101E+12	.686E+11	-.131E+11

T0= .0550 M0= .123E+12 MT= .123E+12
DBCP.= 100.0%

D.C.:	∮A=	304.21	δA= 86.95	∮B= 135.87	δB= 3.11
	P-axis:	trend= 213.55		plunge= 48.05	
	T-axis:	trend= 34.81		plunge= 41.95	
	B-axis:	trend= 304.24		plunge= .63	
	Quality index =	49.5		normal fault	

L2 tensor for : #8

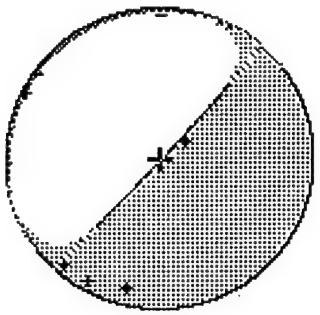

Full solution :

.468E+09	.106E+10	-.215E+11
.106E+10	-.232E+09	.235E+11
-.215E+11	.235E+11	-.643E+10

T0= .0400 M0= .322E+11 MT= .344E+11
Expl.= -6.4% CLVD.= -10.1% DBCP.= 83.5%

Full:	ϕA=	42.51	δA=	87.54	ϕB= 233.23	δB= 2.50
	P-axis:	trend=	312.03		plunge= 47.45	
	T-axis:	trend=	132.96		plunge= 42.54	
	B-axis:	trend=	42.53		plunge= .46	
	Quality index =		10.5		normal fault	

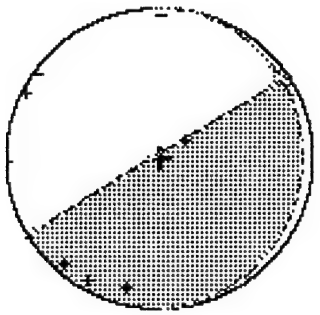

Trace null solution :

.469E+08	.128E+10	-.188E+11
.128E+10	-.140E+10	.115E+11
-.188E+11	.115E+11	.136E+10

T0= .0400 M0= .221E+11 MT= .221E+11
CLVD.= -.6% DBCP.= 99.4%

Tr.0:	ϕA=	238.42	δA=	88.15	ϕB= 358.60	δB= 3.67
	P-axis:	trend=	325.35		plunge= 43.07	
	T-axis:	trend=	151.69		plunge= 46.76	
	B-axis:	trend=	58.31		plunge= 3.17	
	Quality index =		9.5		reverse fault	

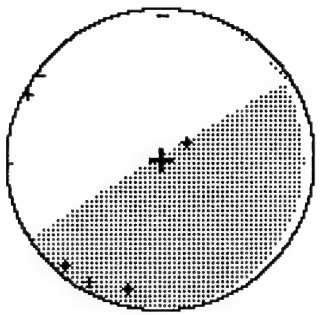

Double couple solution :

.576E+08	.118E+10	-.187E+11
.118E+10	-.148E+10	.115E+11
-.187E+11	.115E+11	.142E+10

T0= .0400 M0= .221E+11 MT= .221E+11
DBCP.= 100.0%

D.C.:	ϕA=	238.42	δA=	88.15	ϕB= 358.62	δB= 3.66
	P-axis:	trend=	325.35		plunge= 43.07	
	T-axis:	trend=	151.68		plunge= 46.75	
	B-axis:	trend=	58.32		plunge= 3.16	
	Quality index =		4.8		reverse fault	

L2 tensor for : #9

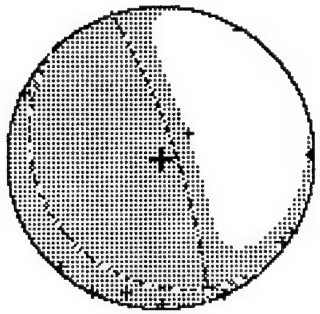

Full solution :

.259E+10	-.620E+10	-.186E+11
-.620E+10	.637E+10	-.670E+11
-.186E+11	-.670E+11	.660E+11

T0= .0400 M0= .842E+11 MT= .104E+12
Expl.= 16.9% CLVD.= 12.5% DBCP.= 70.6%

Full:	∮A= 341.35	δA= 77.62	∮B= 138.94	δB= 13.35
	P-axis: trend= 67.12		plunge= 32.44	
	T-axis: trend= 257.93		plunge= 57.09	
	B-axis: trend= 160.26		plunge= 4.93	
	Quality index = 52.7		reverse fault	

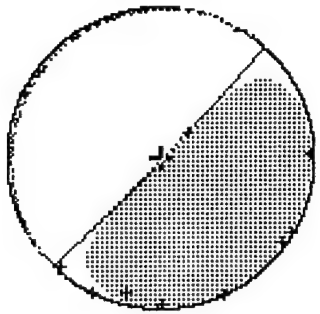

Trace null solution :

.164E+10	-.527E+10	-.391E+11
-.527E+10	.254E+10	.408E+11
-.391E+11	.408E+11	-.418E+10

T0= .0400 M0= .552E+11 MT= .569E+11
CLVD.= 4.9% DBCP.= 95.1%

Tr.0:	∮A= 43.83	δA= 87.08	∮B= 219.16	δB= 2.93
	P-axis: trend= 314.08		plunge= 47.92	
	T-axis: trend= 133.61		plunge= 42.08	
	B-axis: trend= 223.82		plunge= .24	
	Quality index = 52.1		normal fault	

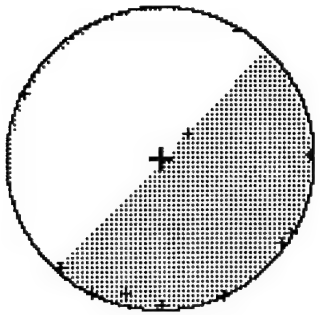

Double couple solution :

.246E+10	-.279E+10	-.381E+11
-.279E+10	.314E+10	.396E+11
-.381E+11	.396E+11	-.560E+10

T0= .0400 M0= .552E+11 MT= .552E+11
DBCP.= 100.0%

D.C.:	∮A= 43.83	δA= 87.09	∮B= 219.16	δB= 2.92
	P-axis: trend= 314.08		plunge= 47.91	
	T-axis: trend= 133.61		plunge= 42.09	
	B-axis: trend= 223.82		plunge= .24	
	Quality index = 36.8		normal fault	

L2 tensor for : #10

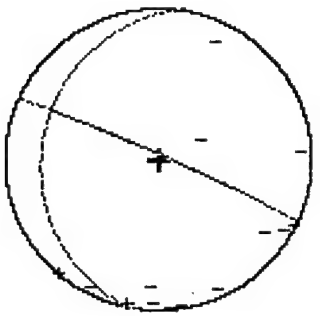

Full solution :

-.260E+11	.821E+10	.160E+11
.821E+10	-.264E+11	.970E+10
.160E+11	.970E+10	-.258E+11

T0= .0750 M0= .379E+11 MT= .390E+11
Expl.= -41.2% CLVD.= 11.2% DBCP.= 47.6%

Full:	∮A=	293.95	δA=	86.10	∮B=	190.17	δB=	15.96
P-axis:	trend=	187.96	plunge=	46.71				
T-axis:	trend=	38.05	plunge=	39.18				
B-axis:	trend=	295.03	plunge=	15.45				
Quality index =	49.5	normal fault						

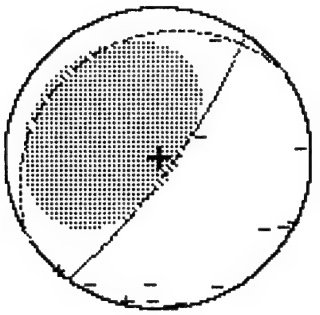

Trace null solution :

-.227E+11	.296E+10	.324E+11
.296E+10	-.142E+11	-.512E+11
.324E+11	-.512E+11	.370E+11

T0= .0750 M0= .584E+11 MT= .687E+11
CLVD.= 15.7% DBCP.= 84.3%

Tr.0:	∮A=	35.43	δA=	77.37	∮B=	236.39	δB=	13.49
P-axis:	trend=	129.43	plunge=	32.21				
T-axis:	trend=	299.15	plunge=	57.37				
B-axis:	trend=	36.48	plunge=	4.67				
Quality index =	51.8	reverse fault						

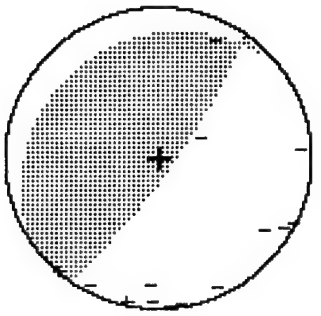

Double couple solution :

-.125E+11	.133E+11	.292E+11
.133E+11	-.123E+11	-.438E+11
.292E+11	-.438E+11	.249E+11

T0= .0750 M0= .584E+11 MT= .584E+11
DBCP.= 100.0%

D.C.:	∮A=	34.81	δA=	77.36	∮B=	235.60	δB=	13.49
P-axis:	trend=	128.78	plunge=	32.20				
T-axis:	trend=	298.57	plunge=	57.39				
B-axis:	trend=	35.85	plunge=	4.63				
Quality index =	51.0	reverse fault						

L2 tensor for : #12

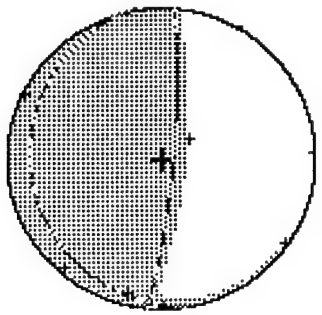

Full solution :

.172E+10	-.410E+10	.113E+11
-.410E+10	-.689E+08	-.994E+11
.113E+11	-.994E+11	.710E+11

T0= .0617 M0= .112E+12 MT= .141E+12
Expl.= 12.8% CLVD.= 12.4% DBCP.= 74.8%

Full:	∮A=	5.19	δA=	80.30	∮B= 171.02	δB= 10.00
	P-axis:	trend=	93.08	plunge=	35.25	
	T-axis:	trend=	278.17	plunge=	54.64	
	B-axis:	trend=	184.78	plunge=	2.40	
	Quality index =		12.4	reverse fault		

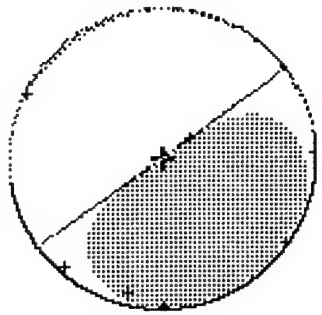

Trace null solution :

.702E+09	-.298E+10	-.179E+11
-.298E+10	-.169E+10	.129E+11
-.179E+11	.129E+11	.990E+09

T0= .0617 M0= .203E+11 MT= .223E+11
CLVD.= 11.8% DBCP.= 88.2%

Tr.0:	∮A=	54.01	δA=	88.89	∮B= 260.83	δB= 1.24
	P-axis:	trend=	323.44	plunge=	46.11	
	T-axis:	trend=	144.56	plunge=	43.89	
	B-axis:	trend=	54.02	plunge=	.56	
	Quality index =		10.5	normal fault		

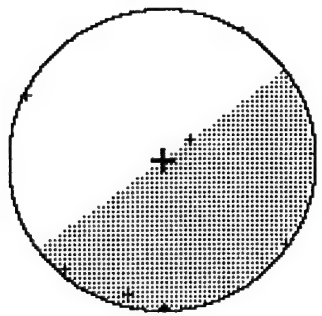

Double couple solution :

.701E+09	-.311E+09	-.164E+11
-.311E+09	.820E+08	.119E+11
-.164E+11	.119E+11	-.783E+09

T0= .0617 M0= .203E+11 MT= .203E+11
DBCP.= 100.0%

D.C.:	∮A=	54.01	δA=	88.89	∮B= 260.86	δB= 1.24
	P-axis:	trend=	323.44	plunge=	46.10	
	T-axis:	trend=	144.56	plunge=	43.89	
	B-axis:	trend=	54.02	plunge=	.56	
	Quality index =		7.6	normal fault		

L2 tensor for : #13

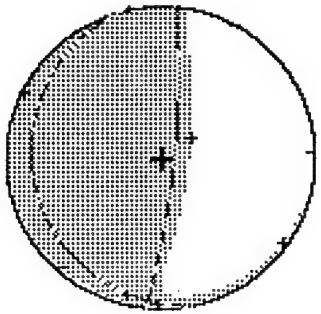

Full solution :

.213E+10	-.476E+10	.116E+11
-.476E+10	.204E+08	-.862E+11
.116E+11	-.862E+11	.678E+11

T0= .0550 M0= .994E+11 MT= .127E+12
Expl.= 13.5% CLVD.= 12.9% DBCP.= 73.5%

Full:	∮A= 5.81	δA= 79.48	∮B= 168.47	δB= 11.01
	P-axis: trend= 93.01		plunge= 34.40	
	T-axis: trend= 279.87		plunge= 55.41	
	B-axis: trend= 185.21		plunge= 3.21	
	Quality index = 12.4		reverse fault	

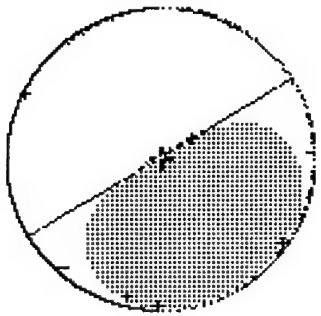

Trace null solution :

.303E+09	-.295E+10	-.181E+11
-.295E+10	-.261E+10	.110E+11
-.181E+11	.110E+11	.231E+10

T0= .0550 M0= .190E+11 MT= .215E+11
CLVD.= 13.8% DBCP.= 86.2%

Tr.0:	∮A= 238.71	δA= 89.88	∮B= .00	δB= .21
	P-axis: trend= 328.89		plunge= 44.88	
	T-axis: trend= 148.54		plunge= 45.12	
	B-axis: trend= 238.71		plunge= .18	
	Quality index = 10.5		reverse fault	

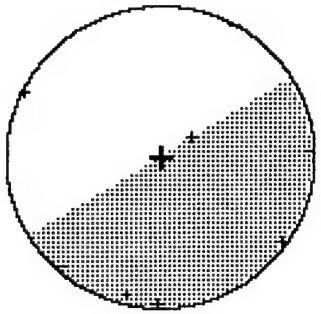

Double couple solution :

-.110E+09	.897E+07	-.162E+11
.897E+07	.298E+08	.985E+10
-.162E+11	.985E+10	.804E+08

T0= .0550 M0= .190E+11 MT= .190E+11
DBCP.= 100.0%

D.C.:	∮A= 238.71	δA= 89.88	∮B= .00	δB= .21
	P-axis: trend= 328.89		plunge= 44.88	
	T-axis: trend= 148.54		plunge= 45.12	
	B-axis: trend= 238.71		plunge= .18	
	Quality index = 5.2		reverse fault	

L2 tensor for : #14

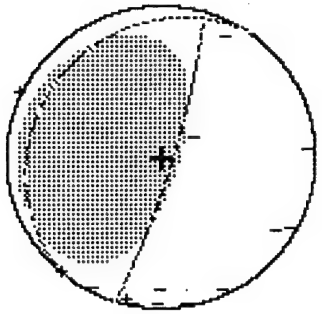

Full solution :

-.206E+11	.629E+10	.281E+11
.629E+10	-.152E+11	-.104E+12
.281E+11	-.104E+12	.581E+11

T0= .0783 M0= .117E+12 MT= .118E+12
Expl.= 4.1% CLVD.= 13.2% DBCP.= 82.7%
Full: ∮A= 16.92 δA= 80.15 ∮B= 217.07 δB= 10.48
P-axis: trend= 110.02 plunge= 35.05
T-axis: trend= 282.51 plunge= 54.72
B-axis: trend= 17.53 plunge= 3.54
Quality index = 54.3 reverse fault

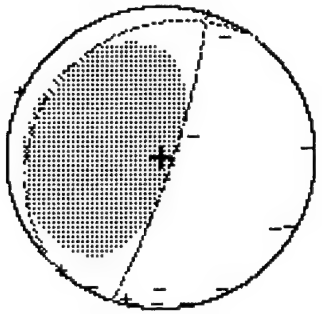

Trace null solution :

-.215E+11	.720E+10	.237E+11
.720E+10	-.191E+11	-.829E+11
.237E+11	-.829E+11	.406E+11

T0= .0783 M0= .836E+11 MT= .934E+11
CLVD.= 12.7% DBCP.= 87.3%
Tr.0: ∮A= 18.02 δA= 79.78 ∮B= 221.21 δB= 11.10
P-axis: trend= 111.75 plunge= 34.64
T-axis: trend= 282.65 plunge= 55.02
B-axis: trend= 18.79 plunge= 4.28
Quality index = 53.4 reverse fault

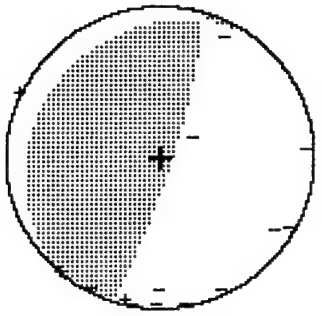

Double couple solution :

-.617E+10	.134E+11	.223E+11
.134E+11	-.230E+11	-.749E+11
.223E+11	-.749E+11	.292E+11

T0= .0783 M0= .836E+11 MT= .836E+11
DBCP.= 100.0%
D.C.: ∮A= 17.43 δA= 79.77 ∮B= 220.51 δB= 11.10
P-axis: trend= 111.15 plunge= 34.63
T-axis: trend= 282.08 plunge= 55.03
B-axis: trend= 18.20 plunge= 4.26
Quality index = 52.4 reverse fault

L2 tensor for : #15

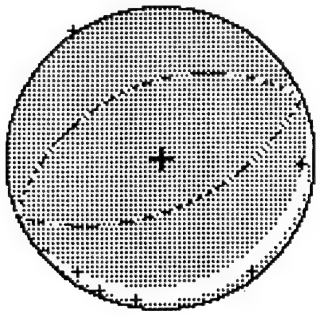

Full solution :

.110E+12	-.454E+11	.133E+13
-.454E+11	.210E+11	-.560E+12
.133E+13	-.560E+12	.126E+14

T0= .0467 M0= .905E+13 MT= .128E+14
Expl.= 20.0% CLVD.= 20.0% DBCP.= 60.1%

Full:	ϕA=	67.17	δA=	51.51	ϕB=	247.17	δB=	38.49
P-axis:	trend=	157.17	plunge=	6.51				
T-axis:	trend=	337.19	plunge=	83.49				
B-axis:	trend=	68.63	plunge=	.13				
Quality index =	12.4	reverse fault						

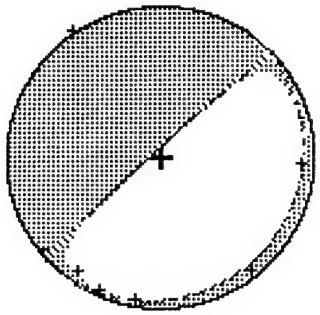

Trace null solution :

.656E+11	-.551E+11	.565E+12
-.551E+11	.779E+11	-.524E+12
.565E+12	-.524E+12	-.144E+12

T0= .0467 M0= .774E+12 MT= .783E+12
CLVD.= -2.2% DBCP.= 97.8%

Tr.0:	ϕA=	227.11	δA=	85.04	ϕB=	38.51	δB=	5.02
P-axis:	trend=	137.93	plunge=	49.96				
T-axis:	trend=	316.41	plunge=	40.03				
B-axis:	trend=	47.04	plunge=	.75				
Quality index =	11.8	normal fault						

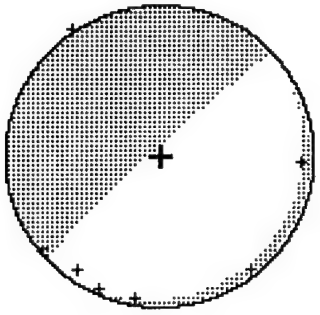

Double couple solution :

.615E+11	-.672E+11	.559E+12
-.672E+11	.718E+11	-.518E+12
.559E+12	-.518E+12	-.133E+12

T0= .0467 M0= .774E+12 MT= .774E+12
DBCP.= 100.0%

D.C.:	ϕA=	227.11	δA=	85.04	ϕB=	38.52	δB=	5.01
P-axis:	trend=	137.93	plunge=	49.95				
T-axis:	trend=	316.42	plunge=	40.04				
B-axis:	trend=	47.04	plunge=	.74				
Quality index =	5.9	normal fault						

L2 tensor for : #16

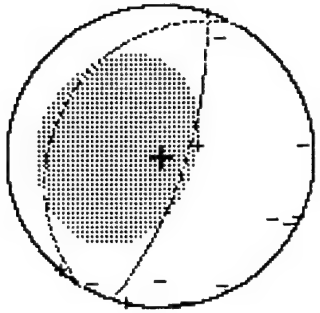

Full solution :

-.151E+11	.277E+10	.724E+10
.277E+10	-.152E+11	-.307E+11
.724E+10	-.307E+11	.350E+11

T0= .0567 M0= .364E+11 MT= .430E+11
Expl.= 1.9% CLVD.= 18.9% DBCP.= 79.2%
Full: §A= 17.87 δA= 70.24 §B= 209.94 δB= 20.17
P-axis: trend= 111.10 plunge= 25.13
T-axis: trend= 281.06 plunge= 64.53
B-axis: trend= 19.27 plunge= 3.89
Quality index = 46.0 reverse fault

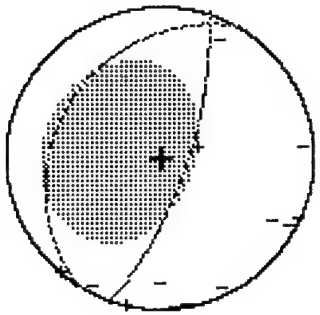

Trace null solution :

-.153E+11	.306E+10	.633E+10
.306E+10	-.161E+11	-.269E+11
.633E+10	-.269E+11	.314E+11

T0= .0567 M0= .302E+11 MT= .389E+11
CLVD.= 19.2% DBCP.= 80.8%
Tr.0: §A= 18.71 δA= 69.02 §B= 211.51 δB= 21.46
P-axis: trend= 112.31 plunge= 23.89
T-axis: trend= 280.71 plunge= 65.67
B-axis: trend= 20.38 plunge= 4.34
Quality index = 45.1 reverse fault

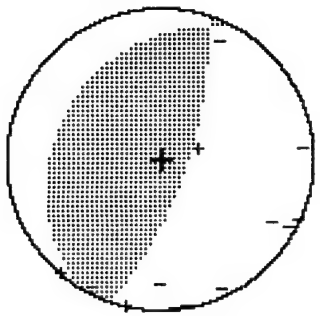

Double couple solution :

-.344E+10	.791E+10	.634E+10
.791E+10	-.167E+11	-.215E+11
.634E+10	-.215E+11	.201E+11

T0= .0567 M0= .302E+11 MT= .302E+11
DBCP.= 100.0%
D.C.: §A= 18.68 δA= 69.01 §B= 211.42 δB= 21.47
P-axis: trend= 112.26 plunge= 23.88
T-axis: trend= 280.72 plunge= 65.69
B-axis: trend= 20.34 plunge= 4.32
Quality index = 31.7 reverse fault

L2 tensor for : #18

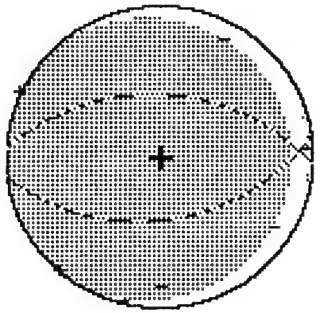

Full solution :

-.445E+11	.172E+11	-.186E+12
.172E+11	.361E+11	-.751E+12
-.186E+12	-.751E+12	.840E+13

T0= .0467 M0= .599E+13 MT= .844E+13
Expl.= 19.8% CLVD.= 20.0% DBCP.= 60.2%

Full:	ϕA= 272.66	δA= 46.27	ϕB= 82.42	δB= 44.19
	P-axis:	trend= 357.64	plunge= 1.05	
	T-axis:	trend= 256.15	plunge= 84.76	
	B-axis:	trend= 87.73	plunge= 5.14	
	Quality index = 12.3		reverse fault	

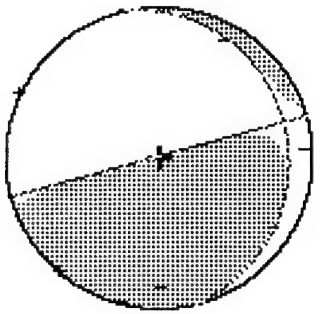

Trace null solution :

.450E+11	.661E+11	-.472E+12
.661E+11	-.528E+11	.127E+12
-.472E+12	.127E+12	.778E+10

T0= .0467 M0= .489E+12 MT= .496E+12
CLVD.= 2.3% DBCP.= 97.7%

Tr.0:	ϕA= 254.52	δA= 89.88	ϕB= 345.26	δB= 9.51
	P-axis:	trend= 335.16	plunge= 44.09	
	T-axis:	trend= 173.92	plunge= 44.34	
	B-axis:	trend= 74.50	plunge= 9.51	
	Quality index = 10.1		reverse fault	

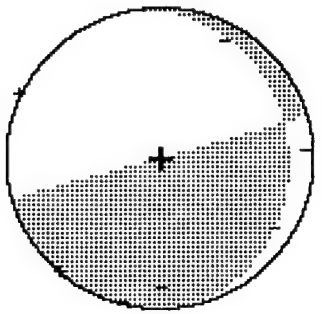

Double couple solution :

.401E+11	.698E+11	-.465E+12
.698E+11	-.417E+11	.129E+12
-.465E+12	.129E+12	.158E+10

T0= .0467 M0= .489E+12 MT= .489E+12
DBCP.= 100.0%

D.C.:	ϕA= 254.54	δA= 89.91	ϕB= 345.10	δB= 9.51
	P-axis:	trend= 335.17	plunge= 44.12	
	T-axis:	trend= 173.94	plunge= 44.31	
	B-axis:	trend= 74.52	plunge= 9.51	
	Quality index = 7.2		reverse fault	

L2 tensor for : #19

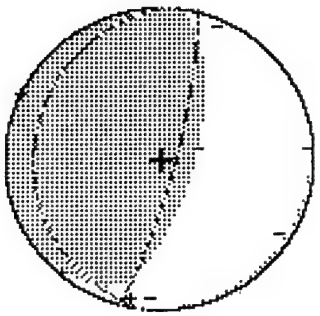

Full solution :

.523E+08	-.471E+10	.280E+11
-.471E+10	.362E+10	-.959E+11
.280E+11	-.959E+11	.954E+11

T0= .0600 M0= .121E+12 MT= .158E+12
Expl.= 14.3% CLVD.= 15.2% DBCP.= 70.4%

Full:	ϕA= 14.86	δA= 77.90	ϕB= 185.80	δB= 12.25
	P-axis: trend= 103.24		plunge= 32.88	
	T-axis: trend= 287.34		plunge= 57.06	
	B-axis: trend= 194.45		plunge= 1.87	
	Quality index = 12.1		reverse fault	

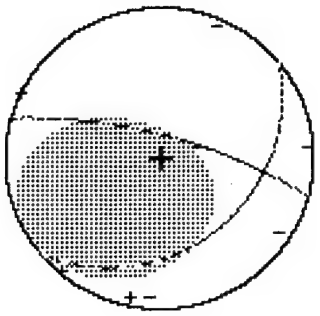

Trace null solution :

-.539E+10	.298E+10	-.811E+10
.298E+10	-.204E+10	-.580E+10
-.811E+10	-.580E+10	.743E+10

T0= .0600 M0= .933E+10 MT= .123E+11
CLVD.= 20.0% DBCP.= 80.0%

Tr.0:	ϕA= 284.85	δA= 73.35	ϕB= 50.83	δB= 26.98
	P-axis: trend= 358.17		plunge= 25.32	
	T-axis: trend= 222.81		plunge= 56.38	
	B-axis: trend= 98.40		plunge= 20.59	
	Quality index = 5.8		reverse fault	

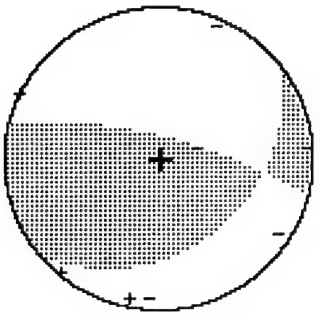

Double couple solution :

-.605E+10	.175E+10	-.678E+10
.175E+10	.128E+10	-.274E+10
-.678E+10	-.274E+10	.477E+10

T0= .0600 M0= .933E+10 MT= .933E+10
DBCP.= 100.0%

D.C.:	ϕA= 284.25	δA= 73.32	ϕB= 50.24	δB= 27.01
	P-axis: trend= 357.55		plunge= 25.28	
	T-axis: trend= 222.25		plunge= 56.40	
	B-axis: trend= 97.78		plunge= 20.61	
	Quality index = 5.7		reverse fault	

L2 tensor for : #20

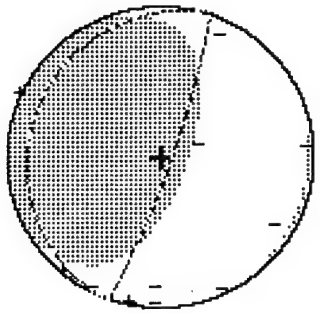

Full solution :

-.824E+10	-.547E+10	.325E+11
-.547E+10	.622E+10	-.928E+11
.325E+11	-.928E+11	.743E+11

T0= .0650 M0= .112E+12 MT= .135E+12
Expl.= 11.3% CLVD.= 16.0% DBCP.= 72.7%

Full:	∮A=	19.38	δA= 80.69	∮B= 200.36	δB= 9.31
	P-axis:	trend= 109.51		plunge= 35.69	
	T-axis:	trend= 289.18		plunge= 54.31	
	B-axis:	trend= 19.40		plunge= .16	
	Quality index =	48.7		reverse fault	

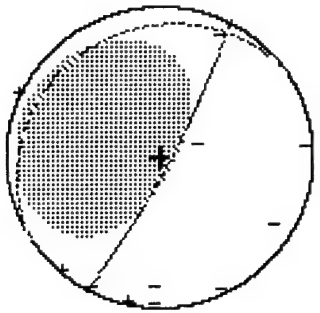

Trace null solution :

-.118E+11	-.135E+09	.153E+11
-.135E+09	-.456E+10	-.328E+11
.153E+11	-.328E+11	.163E+11

T0= .0650 M0= .328E+11 MT= .391E+11
CLVD.= 16.3% DBCP.= 83.7%

Tr.0:	∮A=	27.78	δA= 81.38	∮B= 236.63	δB= 9.82
	P-axis:	trend= 121.92		plunge= 36.21	
	T-axis:	trend= 292.18		plunge= 53.39	
	B-axis:	trend= 28.49		plunge= 4.67	
	Quality index =	45.5		reverse fault	

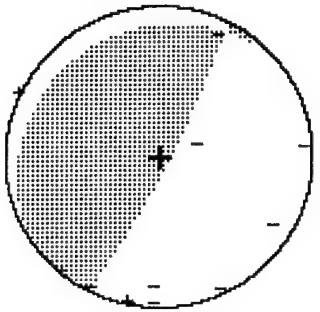

Double couple solution :

-.418E+10	.549E+10	.139E+11
.549E+10	-.553E+10	-.280E+11
.139E+11	-.280E+11	.971E+10

T0= .0650 M0= .328E+11 MT= .328E+11
DBCP.= 100.0%

D.C.:	∮A=	27.17	δA= 81.36	∮B= 235.81	δB= 9.82
	P-axis:	trend= 121.27		plunge= 36.20	
	T-axis:	trend= 291.60		plunge= 53.41	
	B-axis:	trend= 27.87		plunge= 4.63	
	Quality index =	44.4		reverse fault	

L2 tensor for : #21

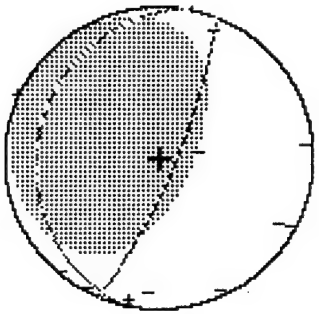

Full solution :

-.101E+11	-.607E+10	.425E+11
-.607E+10	-.951E+10	-.933E+11
.425E+11	-.933E+11	.100E+12

T0= .0717 M0= .125E+12 MT= .149E+12
Expl.= 11.0% CLVD.= 16.8% DBCP.= 72.2%
Full: ∮A= 22.44 δA= 76.33 ∮B= 192.32 δB= 13.88
P-axis: trend= 110.44 plunge= 31.29
T-axis: trend= 295.72 plunge= 58.60
B-axis: trend= 201.87 plunge= 2.35
Quality index = 48.0 reverse fault

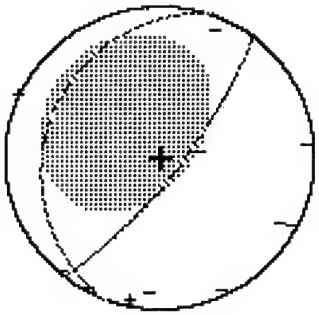

Trace null solution :

-.129E+11	-.142E+10	.247E+11
-.142E+10	-.184E+11	-.270E+11
.247E+11	-.270E+11	.314E+11

T0= .0717 M0= .351E+11 MT= .456E+11
CLVD.= 19.5% DBCP.= 80.5%
Tr.0: ∮A= 37.56 δA= 73.70 ∮B= 200.25 δB= 17.03
P-axis: trend= 123.54 plunge= 28.53
T-axis: trend= 314.87 plunge= 61.00
B-axis: trend= 216.16 plunge= 4.80
Quality index = 42.6 reverse fault

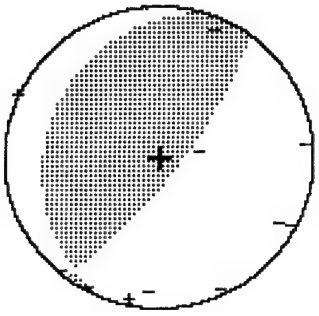

Double couple solution :

-.396E+10	.823E+10	.184E+11
.823E+10	-.149E+11	-.230E+11
.184E+11	-.230E+11	.188E+11

T0= .0717 M0= .351E+11 MT= .351E+11
DBCP.= 100.0%
D.C.: ∮A= 36.93 δA= 73.68 ∮B= 199.52 δB= 17.06
P-axis: trend= 122.88 plunge= 28.51
T-axis: trend= 314.28 plunge= 61.01
B-axis: trend= 215.51 plunge= 4.83
Quality index = 42.0 reverse fault

L2 tensor for : #23

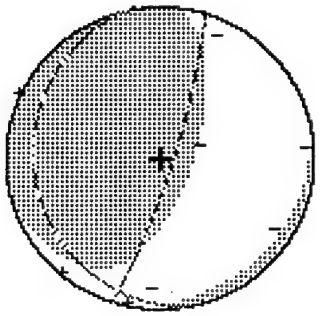

Full solution :

.156E+10	-.121E+11	.369E+11
-.121E+11	.539E+10	-.929E+11
.369E+11	-.929E+11	.897E+11

T0= .0550 M0= .119E+12 MT= .153E+12
Expl.= 13.8% CLVD.= 16.1% DBCP.= 70.1%

Full:	∮A= 17.66	δA= 79.29	∮B= 171.15	δB= 11.93
	P-axis: trend= 103.14		plunge= 34.09	
	T-axis: trend= 294.26		plunge= 55.41	
	B-axis: trend= 196.67		plunge= 5.20	
	Quality index = 11.9		reverse fault	

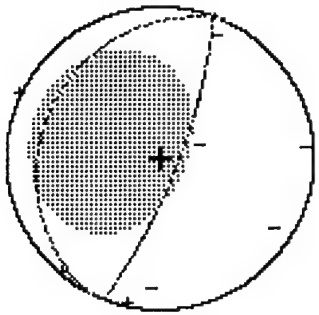

Trace null solution :

-.657E+10	-.387E+09	.468E+10
-.387E+09	-.477E+10	-.132E+11
.468E+10	-.132E+11	.113E+11

T0= .0550 M0= .128E+11 MT= .171E+11
CLVD.= 20.2% DBCP.= 79.8%

Tr.0:	∮A= 20.86	δA= 75.06	∮B= 206.11	δB= 15.00
	P-axis: trend= 111.97		plunge= 30.05	
	T-axis: trend= 288.94		plunge= 59.92	
	B-axis: trend= 21.21		plunge= 1.31	
	Quality index = 5.2		reverse fault	

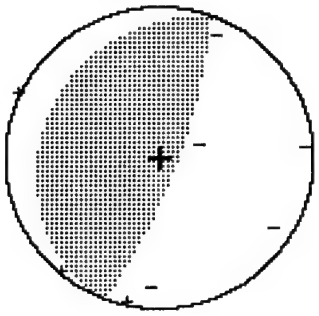

Double couple solution :

-.954E+09	.230E+10	.378E+10
.230E+10	-.545E+10	-.105E+11
.378E+10	-.105E+11	.640E+10

T0= .0550 M0= .128E+11 MT= .128E+11
DBCP.= 100.0%

D.C.:	∮A= 20.25	δA= 75.05	∮B= 205.36	δB= 15.01
	P-axis: trend= 111.33		plunge= 30.04	
	T-axis: trend= 288.39		plunge= 59.93	
	B-axis: trend= 20.60		plunge= 1.28	
	Quality index = 5.8		reverse fault	

L2 tensor for : #24

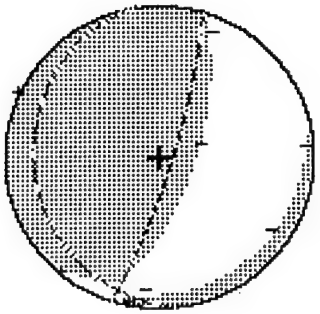

Full solution :

.206E+10	-.402E+10	.125E+11
-.402E+10	.369E+10	-.319E+11
.125E+11	-.319E+11	.342E+11

T0= .0517 M0= .423E+11 MT= .570E+11
Expl.= 15.8% CLVD.= 16.1% DBCP.= 68.1%

Full:	ϕA= 17.38	δA= 78.66	ϕB= 173.34	δB= 12.39
	P-axis: trend= 103.13		plunge= 33.48	
	T-axis: trend= 293.73		plunge= 56.07	
	B-axis: trend= 196.39		plunge= 4.91	
	Quality index = 12.1		reverse fault	

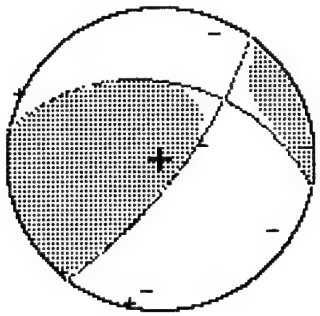

Trace null solution :

-.766E+09	.396E+09	.273E+09
.396E+09	.190E+09	-.770E+09
.273E+09	-.770E+09	.576E+09

T0= .0517 M0= .110E+10 MT= .114E+10
CLVD.= 5.8% DBCP.= 94.2%

Tr.0:	ϕA= 36.82	δA= 71.80	ϕB= 280.98	δB= 37.03
	P-axis: trend= 150.90		plunge= 20.10	
	T-axis: trend= 268.56		plunge= 51.75	
	B-axis: trend= 48.21		plunge= 30.99	
	Quality index = .1		reverse fault	

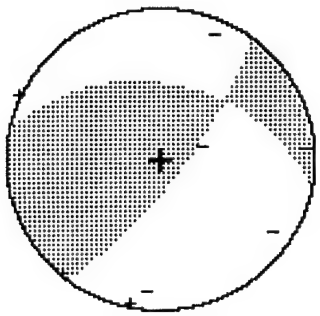

Double couple solution :

-.742E+09	.423E+09	.297E+09
.423E+09	.192E+09	-.707E+09
.297E+09	-.707E+09	.550E+09

T0= .0517 M0= .110E+10 MT= .110E+10
DBCP.= 100.0%

D.C.:	ϕA= 36.86	δA= 71.76	ϕB= 280.97	δB= 37.04
	P-axis: trend= 150.94		plunge= 20.07	
	T-axis: trend= 268.58		plunge= 51.79	
	B-axis: trend= 48.27		plunge= 30.98	
	Quality index = .1		reverse fault	

L2 tensor for : #25

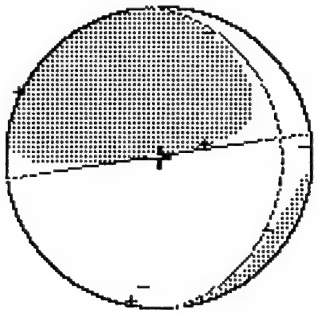

Full solution :

-.439E+10	-.136E+11	.612E+11
-.136E+11	-.207E+10	-.102E+11
.612E+11	-.102E+11	-.263E+10

T0= .0450 M0= .584E+11 MT= .636E+11
Expl.= -4.0% CLVD.= 4.5% DBCP.= 91.5%

Full:	∮A= 261.36	δA= 89.51	∮B= 353.63	δB= 12.15
	P-axis: trend= 183.33		plunge= 44.21	
	T-axis: trend= 339.57		plunge= 43.25	
	B-axis: trend= 81.25		plunge= 12.14	
	Quality index = 9.9		normal fault	

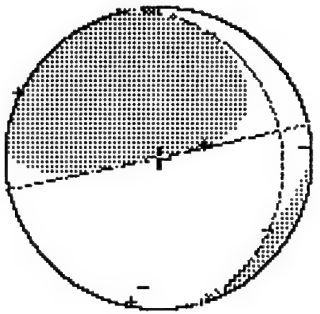

Trace null solution :

-.376E+10	-.147E+11	.638E+11
-.147E+11	-.137E+10	-.167E+11
.638E+11	-.167E+11	.513E+10

T0= .0450 M0= .633E+11 MT= .677E+11
CLVD.= 9.3% DBCP.= 90.7%

Tr.0:	∮A= 77.61	δA= 89.32	∮B= 344.39	δB= 11.94
	P-axis: trend= 179.15		plunge= 43.11	
	T-axis: trend= 335.80		plunge= 44.44	
	B-axis: trend= 77.75		plunge= 11.92	
	Quality index = 10.1		reverse fault	

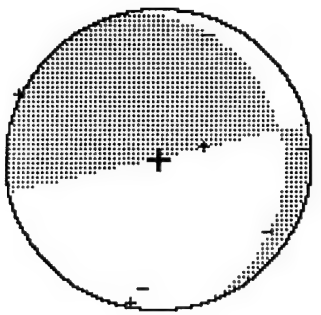

Double couple solution :

-.628E+10	-.111E+11	.603E+11
-.111E+11	.559E+10	-.143E+11
.603E+11	-.143E+11	.690E+09

T0= .0450 M0= .633E+11 MT= .633E+11
DBCP.= 100.0%

D.C.:	∮A= 76.73	δA= 89.68	∮B= 345.17	δB= 11.50
	P-axis: trend= 177.94		plunge= 43.55	
	T-axis: trend= 335.41		plunge= 44.18	
	B-axis: trend= 76.80		plunge= 11.49	
	Quality index = 10.0		reverse fault	

L2 tensor for : #26

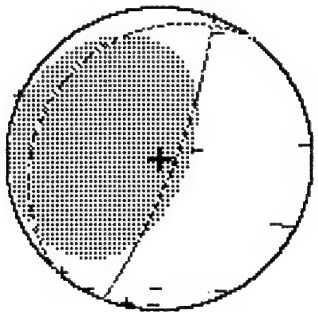

Full solution :

-.265E+11	.114E+10	.341E+11
.114E+10	-.552E+10	-.108E+12
.341E+11	-.108E+12	.970E+11

T0= .0800 M0= .134E+12 MT= .146E+12
Expl.= 8.4% CLVD.= 17.4% DBCP.= 74.3%

Full:	∮A= 21.04	δA= 77.38	∮B= 219.63	δB= 13.29
	P-axis: trend= 114.55		plunge= 32.26	
	T-axis: trend= 285.52		plunge= 57.42	
	B-axis: trend= 21.96		plunge= 4.10	
	Quality index = 51.0		reverse fault	

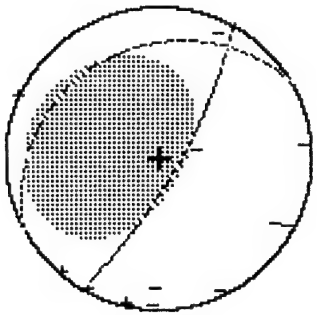

Trace null solution :

-.292E+11	.506E+10	.200E+11
.506E+10	-.148E+11	-.518E+11
.200E+11	-.518E+11	.440E+11

T0= .0800 M0= .540E+11 MT= .679E+11
CLVD.= 18.4% DBCP.= 81.6%

Tr.0:	∮A= 29.52	δA= 74.17	∮B= 240.81	δB= 18.35
	P-axis: trend= 127.09		plunge= 28.57	
	T-axis: trend= 286.25		plunge= 59.77	
	B-axis: trend= 32.11		plunge= 9.05	
	Quality index = 47.4		reverse fault	

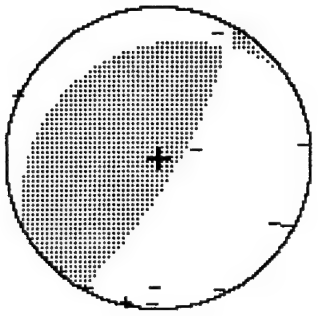

Double couple solution :

-.140E+11	.163E+11	.202E+11
.163E+11	-.140E+11	-.406E+11
.202E+11	-.406E+11	.280E+11

T0= .0800 M0= .540E+11 MT= .540E+11
DBCP.= 100.0%

D.C.:	∮A= 29.47	δA= 74.16	∮B= 240.63	δB= 18.34
	P-axis: trend= 127.00		plunge= 28.57	
	T-axis: trend= 286.25		plunge= 59.79	
	B-axis: trend= 32.05		plunge= 9.01	
	Quality index = 32.7		reverse fault	

L2 tensor for : #28

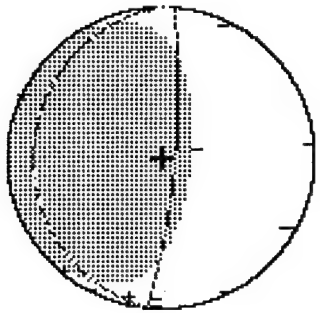

Full solution :

-.447E+10	-.650E+09	.519E+10
-.650E+09	.198E+10	-.596E+11
.519E+10	-.596E+11	.509E+11

T0= .0517 M0= .699E+11 MT= .866E+11
Expl.= 12.2% CLVD.= 15.6% DBCP.= 72.2%
Full: ϕA= 4.91 δA= 78.91 ϕB= 184.43 δB= 11.09
P-axis: trend= 94.83 plunge= 33.91
T-axis: trend= 275.02 plunge= 56.09
B-axis: trend= 184.89 plunge= .09
Quality index = 52.2 reverse fault

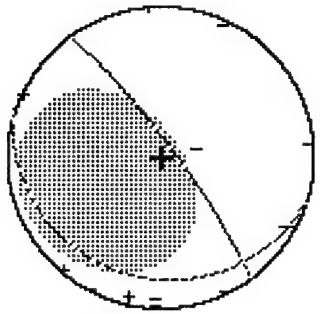

Trace null solution :

-.578E+10	.114E+10	-.684E+10
.114E+10	-.177E+10	-.115E+11
-.684E+10	-.115E+11	.755E+10

T0= .0517 M0= .115E+11 MT= .151E+11
CLVD.= 19.8% DBCP.= 80.2%
Tr.0: ϕA= 323.56 δA= 79.92 ϕB= 107.77 δB= 12.36
P-axis: trend= 47.39 plunge= 34.54
T-axis: trend= 242.34 plunge= 54.54
B-axis: trend= 142.30 plunge= 7.08
Quality index = 45.7 reverse fault

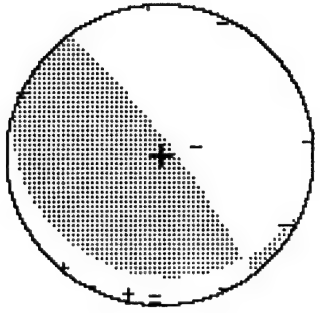

Double couple solution :

-.278E+10	-.228E+10	-.623E+10
-.228E+10	-.116E+10	-.870E+10
-.623E+10	-.870E+10	.393E+10

T0= .0517 M0= .115E+11 MT= .115E+11
DBCP.= 100.0%
D.C.: ϕA= 323.04 δA= 79.91 ϕB= 107.42 δB= 12.35
P-axis: trend= 46.91 plunge= 34.53
T-axis: trend= 241.78 plunge= 54.55
B-axis: trend= 141.78 plunge= 7.04
Quality index = 46.2 reverse fault

L2 tensor for : #29

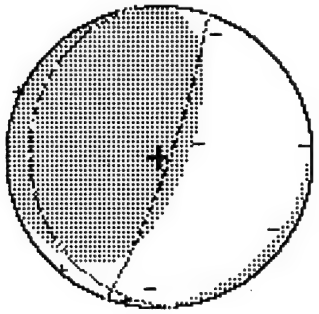

Full solution :

-.795E+08	-.102E+11	.348E+11
-.102E+11	.451E+10	-.858E+11
.348E+11	-.858E+11	.727E+11

T0= .0567 M0= .106E+12 MT= .133E+12
Expl.= 12.7% CLVD.= 15.7% DBCP.= 71.7%

Full:	%A= 19.22	δA= 80.64	%B= 174.77	δB= 10.26
P-axis:	trend= 105.55	plunge= 35.51		
T-axis:	trend= 294.33	plunge= 54.17		
B-axis:	trend= 198.53	plunge= 4.17		
Quality index = 11.8	reverse fault			

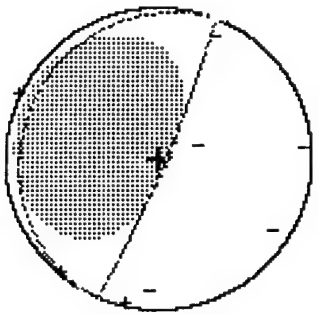

Trace null solution :

-.618E+10	-.131E+10	.890E+10
-.131E+10	-.288E+10	-.219E+11
.890E+10	-.219E+11	.906E+10

T0= .0567 M0= .210E+11 MT= .250E+11
CLVD.= 16.2% DBCP.= 83.8%

Tr.0:	%A= 22.42	δA= 83.16	%B= 207.20	δB= 6.86
P-axis:	trend= 112.94	plunge= 38.16		
T-axis:	trend= 291.77	plunge= 51.83		
B-axis:	trend= 22.49	plunge= .57		
Quality index = 8.6	reverse fault			

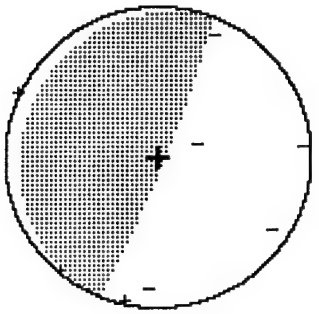

Double couple solution :

-.824E+09	.186E+10	.757E+10
.186E+10	-.416E+10	-.190E+11
.757E+10	-.190E+11	.498E+10

T0= .0567 M0= .210E+11 MT= .210E+11
DBCP.= 100.0%

D.C.:	%A= 21.82	δA= 83.14	%B= 206.34	δB= 6.88
P-axis:	trend= 112.31	plunge= 38.14		
T-axis:	trend= 291.21	plunge= 51.85		
B-axis:	trend= 21.89	plunge= .54		
Quality index = 8.9	reverse fault			

L2 tensor for : #30

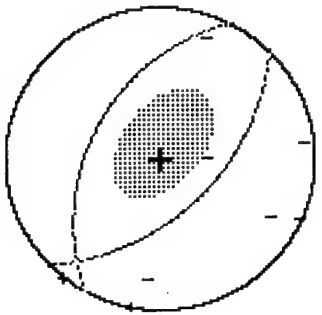

Full solution :

-.321E+10	.195E+10	.733E+09
.195E+10	-.427E+10	-.752E+08
.733E+09	-.752E+08	.166E+10

T0= .0517 M0= .402E+10 MT= .447E+10
Expl.= -34.3% CLVD.= -2.4% DBCP.= 63.3%
Full: ∮A= 45.92 δA= 49.52 ∮B= 208.64 δB= 41.79
P-axis: trend= 127.86 plunge= 3.91
T-axis: trend= 13.78 plunge= 80.49
B-axis: trend= 218.45 plunge= 8.66
Quality index = 3.2 reverse fault

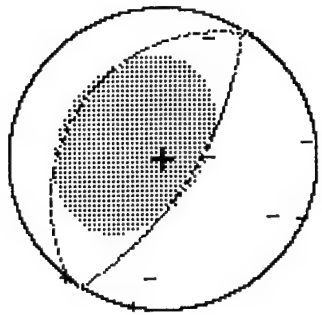

Trace null solution :

-.283E+10	.114E+10	.210E+10
.114E+10	-.358E+10	-.371E+10
.210E+10	-.371E+10	.640E+10

T0= .0517 M0= .587E+10 MT= .710E+10
CLVD.= 16.9% DBCP.= 83.1%
Tr.0: ∮A= 32.08 δA= 64.13 ∮B= 216.40 δB= 25.94
P-axis: trend= 123.50 plunge= 19.11
T-axis: trend= 298.02 plunge= 70.81
B-axis: trend= 32.91 plunge= 1.70
Quality index = 6.2 reverse fault

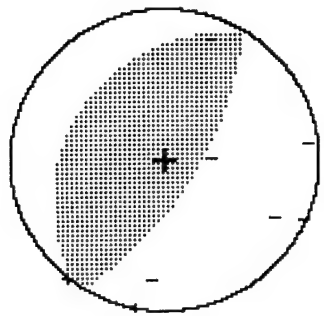

Double couple solution :

-.141E+10	.213E+10	.183E+10
.213E+10	-.320E+10	-.314E+10
.183E+10	-.314E+10	.461E+10

T0= .0517 M0= .587E+10 MT= .587E+10
DBCP.= 100.0%
D.C.: ∮A= 31.47 δA= 64.12 ∮B= 215.73 δB= 25.94
P-axis: trend= 122.86 plunge= 19.10
T-axis: trend= 297.45 plunge= 70.82
B-axis: trend= 32.28 plunge= 1.68
Quality index = 7.4 reverse fault

L2 tensor for : #31

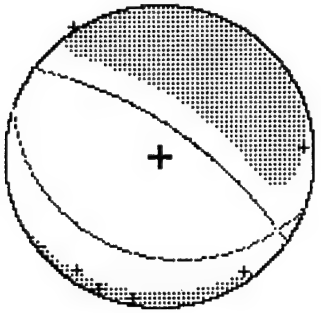

Full solution :

.652E+11	.281E+11	.263E+12
.281E+11	-.305E+11	.236E+12
.263E+12	.236E+12	-.632E+12

T0= .0500 M0= .573E+12 MT= .759E+12
Expl.= -32.8% CLVD.= -29.1% DBCP.= 38.1%

Full:	$A= 304.99	δA= 67.64	$B= 110.39	δB= 23.03
	P-axis: trend= 225.23		plunge= 66.89	
	T-axis: trend= 30.66		plunge= 22.44	
	B-axis: trend= 122.83		plunge= 5.24	
	Quality index = 12.0		normal fault	

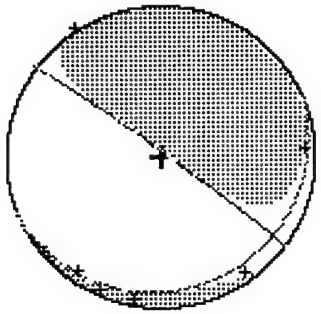

Trace null solution :

.679E+11	.275E+11	.305E+12
.275E+11	-.317E+11	.223E+12
.305E+12	.223E+12	-.361E+11

T0= .0500 M0= .371E+12 MT= .383E+12
CLVD.= 5.3% DBCP.= 94.7%

Tr.0:	$A= 306.37	δA= 86.42	$B= 67.56	δB= 6.89
	P-axis: trend= 222.63		plunge= 48.26	
	T-axis: trend= 30.84		plunge= 41.14	
	B-axis: trend= 126.00		plunge= 5.88	
	Quality index = 11.8		normal fault	

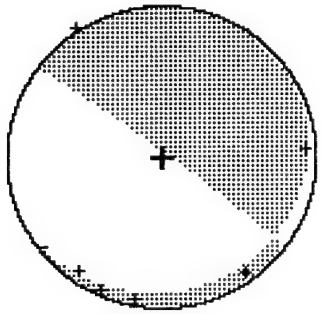

Double couple solution :

.660E+11	.107E+11	.293E+12
.107E+11	-.201E+11	.219E+12
.293E+12	.219E+12	-.459E+11

T0= .0500 M0= .371E+12 MT= .371E+12
DBCP.= 100.0%

D.C.:	$A= 306.37	δA= 86.42	$B= 67.58	δB= 6.88
	P-axis: trend= 222.62		plunge= 48.26	
	T-axis: trend= 30.85		plunge= 41.14	
	B-axis: trend= 126.01		plunge= 5.87	
	Quality index = 8.4		normal fault	

L2 tensor for : #32

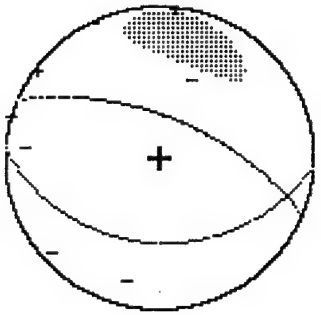

Full solution :

-.551E+09	-.732E+08	.661E+10
-.732E+08	-.427E+10	.583E+10
.661E+10	.583E+10	-.293E+11

T0= .0450 M0= .227E+11 MT= .307E+11
Expl.= -47.5% CLVD.= -33.3% DBCP.= 19.2%

Full:	ϕA= 291.91	δA= 59.99	ϕB= 94.10	δB= 31.25
	P-axis: trend= 225.02		plunge= 73.38	
	T-axis: trend= 15.25		plunge= 14.53	
	B-axis: trend= 107.31		plunge= 7.90	
	Quality index = 6.6		normal fault	

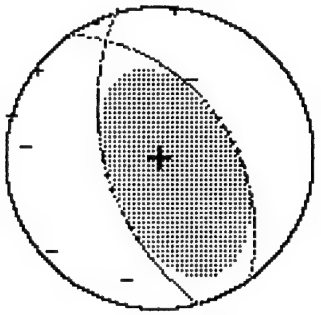

Trace null solution :

-.213E+10	-.287E+10	-.974E+09
-.287E+10	-.650E+10	.225E+10
-.974E+09	.225E+10	.862E+10

T0= .0450 M0= .807E+10 MT= .865E+10
CLVD.= 9.4% DBCP.= 90.6%

Tr.0:	ϕA= 164.66	δA= 51.47	ϕB= 323.53	δB= 40.48
	P-axis: trend= 245.09		plunge= 5.59	
	T-axis: trend= 127.60		plunge= 78.03	
	B-axis: trend= 336.13		plunge= 10.55	
	Quality index = .1		reverse fault	

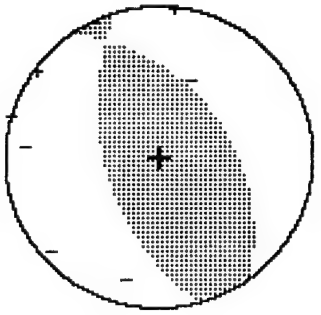

Double couple solution :

-.129E+10	-.322E+10	-.669E+09
-.322E+10	-.636E+10	.201E+10
-.669E+09	.201E+10	.765E+10

T0= .0450 M0= .807E+10 MT= .807E+10
DBCP.= 100.0%

D.C.:	ϕA= 164.68	δA= 51.47	ϕB= 323.57	δB= 40.48
	P-axis: trend= 245.12		plunge= 5.59	
	T-axis: trend= 127.59		plunge= 78.04	
	B-axis: trend= 336.16		plunge= 10.54	
	Quality index = .1		reverse fault	

L2 tensor for : #33

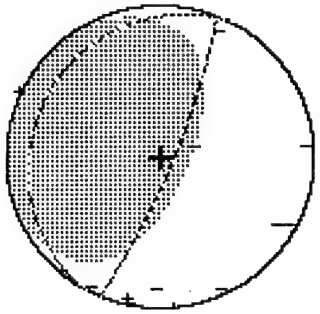

Full solution :

-.104E+11	-.337E+10	.358E+11
-.337E+10	.153E+10	-.905E+11
.358E+11	-.905E+11	.809E+11

T0= .0567 M0= .113E+12 MT= .135E+12
Expl.= 11.1% CLVD.= 16.2% DBCP.= 72.7%

Full:	∮A=	22.43	δA=	78.98	∮B= 208.25	δB= 11.08
	P-axis:	trend=	113.39		plunge= 33.97	
	T-axis:	trend=	291.02		plunge= 56.01	
	B-axis:	trend=	22.65		plunge= 1.10	
	Quality index =		48.2		reverse fault	

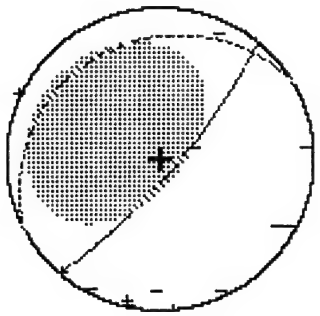

Trace null solution :

-.136E+11	.890E+09	.190E+11
.890E+09	-.818E+10	-.257E+11
.190E+11	-.257E+11	.218E+11

T0= .0567 M0= .308E+11 MT= .372E+11
CLVD.= 16.9% DBCP.= 83.1%

Tr.0:	∮A=	40.29	δA=	76.23	∮B= 241.08	δB= 14.69
	P-axis:	trend=	134.55		plunge= 31.04	
	T-axis:	trend=	303.30		plunge= 58.46	
	B-axis:	trend=	41.52		plunge= 5.01	
	Quality index =		42.8		reverse fault	

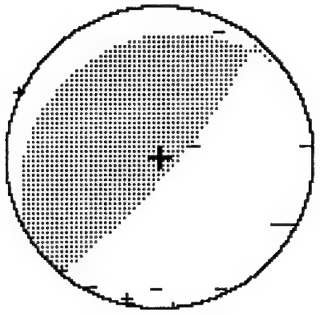

Double couple solution :

-.839E+10	.746E+10	.168E+11
.746E+10	-.578E+10	-.213E+11
.168E+11	-.213E+11	.142E+11

T0= .0567 M0= .308E+11 MT= .308E+11
DBCP.= 100.0%

D.C.:	∮A=	39.66	δA=	76.22	∮B= 240.27	δB= 14.68
	P-axis:	trend=	133.88		plunge= 31.04	
	T-axis:	trend=	302.72		plunge= 58.48	
	B-axis:	trend=	40.88		plunge= 4.97	
	Quality index =		43.0		reverse fault	

L2 tensor for : #34

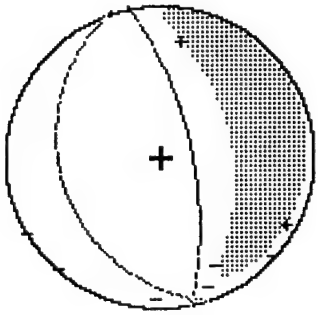

Full solution :

-.102E+10	.276E+10	.124E+11
.276E+10	-.777E+10	.948E+11
.124E+11	.948E+11	-.220E+12

T0= .0400 M0= .183E+12 MT= .255E+12
Expl.= -41.8% CLVD.= -40.6% DBCP.= 17.6%

Full:	§A= 348.20	δA= 65.82	§B= 161.85	δB= 24.31
	P-axis:	trend= 263.37	plunge= 69.07		
	T-axis:	trend= 76.23	plunge= 20.78		
	B-axis:	trend= 167.13	plunge= 2.38		
	Quality index = 12.4		normal fault		

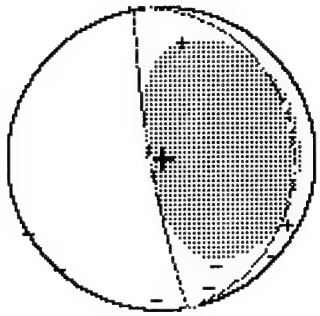

Trace null solution :

-.317E+10	.505E+07	.270E+10
.505E+07	-.285E+10	.154E+11
.270E+10	.154E+11	.602E+10

T0= .0400 M0= .147E+11 MT= .165E+11
CLVD.= 13.1% DBCP.= 86.9%

Tr.0:	§A= 170.01	δA= 82.09	§B= 348.70	δB= 7.91
	P-axis:	trend= 259.85	plunge= 37.09		
	T-axis:	trend= 80.22	plunge= 52.91		
	B-axis:	trend= 349.98	plunge= .18		
	Quality index = 10.8		reverse fault		

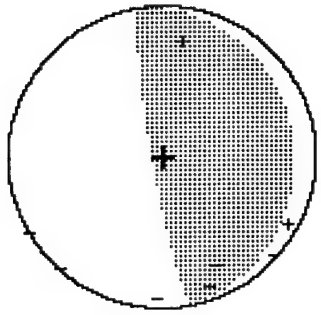

Double couple solution :

-.136E+09	-.727E+09	.245E+10
-.727E+09	-.388E+10	.139E+11
.245E+10	.139E+11	.402E+10

T0= .0400 M0= .147E+11 MT= .147E+11
DBCP.= 100.0%

D.C.:	§A= 170.02	δA= 82.07	§B= 348.78	δB= 7.93
	P-axis:	trend= 259.87	plunge= 37.07		
	T-axis:	trend= 80.22	plunge= 52.93		
	B-axis:	trend= 350.00	plunge= .17		
	Quality index = 7.2		reverse fault		

L2 tensor for : #35

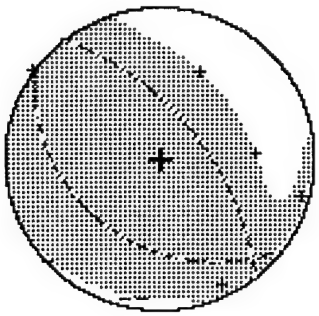

Full solution :

-.475E+10	-.706E+10	-.237E+11
-.706E+10	.820E+10	-.634E+11
-.237E+11	-.634E+11	.233E+12

T0= .0417 M0= .178E+12 MT= .246E+12
Expl.= 19.8% CLVD.= 18.4% DBCP.= 61.8%

Full:	ϕA= 321.22 δA= 59.04	ϕB= 126.92 δB= 31.76
	P-axis: trend= 45.79	plunge= 13.74
	T-axis: trend= 251.73	plunge= 74.79
	B-axis: trend= 137.36	plunge= 6.40
	Quality index = 12.2	reverse fault

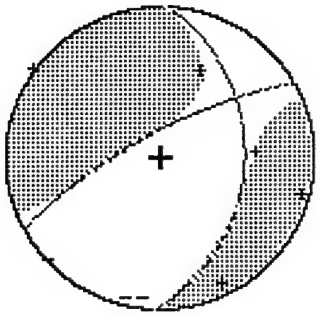

Trace null solution :

.326E+09	-.550E+10	.668E+10
-.550E+10	.456E+10	-.308E+10
.668E+10	-.308E+10	-.489E+10

T0= .0417 M0= .948E+10 MT= .103E+11
CLVD.= 10.9% DBCP.= 89.1%

Tr.0:	ϕA= 241.27 δA= 72.53	ϕB= 1.58 δB= 31.94
	P-axis: trend= 184.89	plunge= 54.32
	T-axis: trend= 310.76	plunge= 22.82
	B-axis: trend= 52.51	plunge= 25.83
	Quality index = 5.8	normal fault

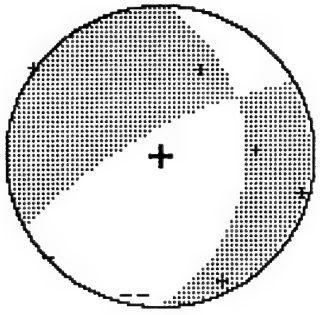

Double couple solution :

.231E+09	-.425E+10	.668E+10
-.425E+10	.461E+10	-.219E+10
.668E+10	-.219E+10	-.484E+10

T0= .0417 M0= .948E+10 MT= .948E+10
DBCP.= 100.0%

D.C.:	ϕA= 241.21 δA= 72.50	ϕB= 1.58 δB= 31.95
	P-axis: trend= 184.86	plunge= 54.35
	T-axis: trend= 310.71	plunge= 22.79
	B-axis: trend= 52.44	plunge= 25.82
	Quality index = 3.7	normal fault

L2 tensor for : #36

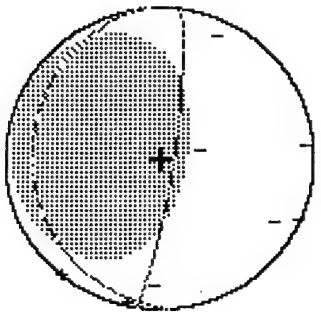

Full solution :

-.112E+11	-.317E+10	.954E+10
-.317E+10	-.472E+10	-.535E+11
.954E+10	-.535E+11	.414E+11

T0= .0633 M0= .625E+11 MT= .657E+11
Expl.= 7.1% CLVD.= 17.3% DBCP.= 75.6%

Full:	∮A=	8.31	δA=	78.66	∮B=	176.61 δB= 11.57
	P-axis:	trend=	96.33	plunge=	33.62	
	T-axis:	trend=	281.29	plunge=	56.28	
	B-axis:	trend=	187.86	plunge=	2.29	
	Quality index =		10.5	reverse fault		

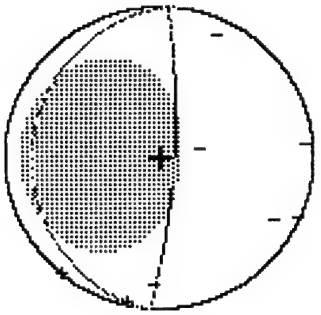

Trace null solution :

-.134E+11	.149E+09	.148E+10
.149E+09	-.764E+10	-.335E+11
.148E+10	-.335E+11	.211E+11

T0= .0633 M0= .298E+11 MT= .383E+11
CLVD.= 19.1% DBCP.= 80.9%

Tr.0:	∮A=	3.21	δA=	78.41	∮B=	187.45 δB= 11.62
	P-axis:	trend=	93.93	plunge=	33.40	
	T-axis:	trend=	272.12	plunge=	56.58	
	B-axis:	trend=	3.38	plunge=	.83	
	Quality index =		8.3	reverse fault		

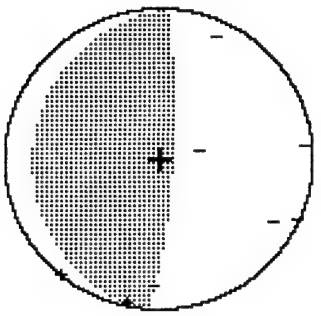

Double couple solution :

-.850E+08	.109E+10	.144E+10
.109E+10	-.117E+11	-.274E+11
.144E+10	-.274E+11	.118E+11

T0= .0633 M0= .298E+11 MT= .298E+11
DBCP.= 100.0%

D.C.:	∮A=	3.21	δA=	78.39	∮B=	187.41 δB= 11.64
	P-axis:	trend=	93.92	plunge=	33.39	
	T-axis:	trend=	272.12	plunge=	56.60	
	B-axis:	trend=	3.38	plunge=	.83	
	Quality index =		6.1	reverse fault		

L2 tensor for : #37

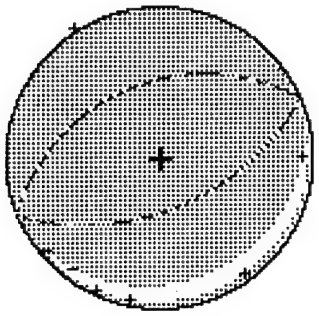

Full solution :

.342E+12	-.135E+12	.416E+13
-.135E+12	.666E+11	-.170E+13
.416E+13	-.170E+13	.378E+14

T0= .0417 M0= .271E+14 MT= .383E+14
Expl.= 20.0% CLVD.= 20.0% DBCP.= 60.1%

Full:	∮A= 67.80	δA= 51.75	∮B= 247.82	δB= 38.25
	P-axis: trend= 157.81		plunge= 6.75	
	T-axis: trend= 337.75		plunge= 83.25	
	B-axis: trend= 68.11		plunge= .03	
	Quality index = 12.4		reverse fault	

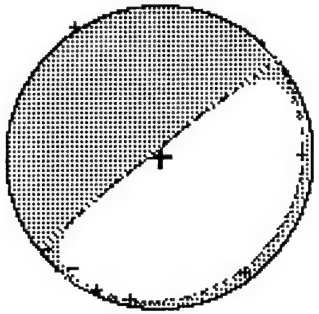

Trace null solution :

.228E+12	-.165E+12	.213E+13
-.165E+12	.225E+12	-.169E+13
.213E+13	-.169E+13	-.453E+12

T0= .0417 M0= .272E+13 MT= .275E+13
CLVD.= -2.4% DBCP.= 97.6%

Tr.0:	∮A= 231.44	δA= 85.61	∮B= 41.81	δB= 4.45
	P-axis: trend= 142.25		plunge= 49.39	
	T-axis: trend= 320.75		plunge= 40.60	
	B-axis: trend= 51.38		plunge= .74	
	Quality index = 11.9		normal fault	

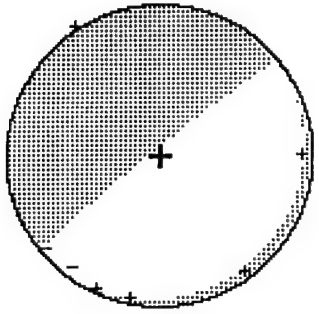

Double couple solution :

.219E+12	-.210E+12	.210E+13
-.210E+12	.195E+12	-.167E+13
.210E+13	-.167E+13	-.415E+12

T0= .0417 M0= .272E+13 MT= .272E+13
DBCP.= 100.0%

D.C.:	∮A= 231.44	δA= 85.61	∮B= 41.82	δB= 4.45
	P-axis: trend= 142.25		plunge= 49.38	
	T-axis: trend= 320.75		plunge= 40.61	
	B-axis: trend= 51.38		plunge= .74	
	Quality index = 5.9		normal fault	

L2 tensor for : #38

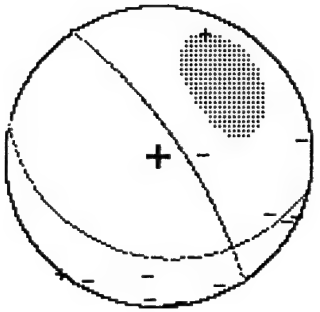

Full solution :

-.628E+10	.572E+10	.802E+10
.572E+10	-.129E+11	.165E+11
.802E+10	.165E+11	-.299E+11

T0= .0683 M0= .303E+11 MT= .356E+11
Expl.= -43.6% CLVD.= -7.7% DBCP.= 48.7%

Full:	∮A= 325.51	δA= 72.83	∮B= 103.93	δB= 22.45
	P-axis: trend= 256.24		plunge= 59.58	
	T-axis: trend= 43.97		plunge= 26.41	
	B-axis: trend= 141.09		plunge= 14.01	
	Quality index = 47.9		normal fault	

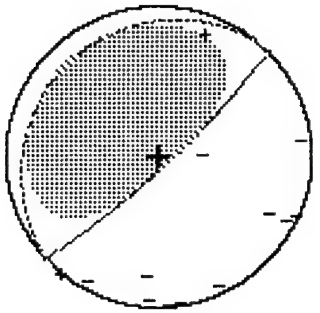

Trace null solution :

-.486E+10	.195E+10	.169E+11
.195E+10	-.505E+10	-.158E+11
.169E+11	-.158E+11	.991E+10

T0= .0683 M0= .231E+11 MT= .248E+11
CLVD.= 9.4% DBCP.= 90.6%

Tr.0:	∮A= 46.79	δA= 80.03	∮B= 223.67	δB= 9.98
	P-axis: trend= 136.33		plunge= 35.03	
	T-axis: trend= 317.46		plunge= 54.96	
	B-axis: trend= 226.70		plunge= .53	
	Quality index = 47.0		reverse fault	

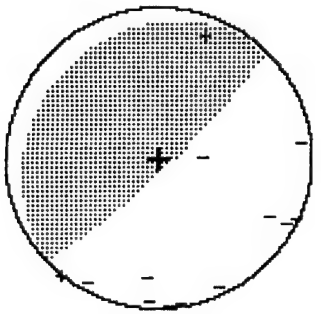

Double couple solution :

-.392E+10	.395E+10	.157E+11
.395E+10	-.398E+10	-.150E+11
.157E+11	-.150E+11	.790E+10

T0= .0683 M0= .231E+11 MT= .231E+11
DBCP.= 100.0%

D.C.:	∮A= 46.28	δA= 80.02	∮B= 223.28	δB= 9.99
	P-axis: trend= 135.83		plunge= 35.02	
	T-axis: trend= 316.92		plunge= 54.98	
	B-axis: trend= 226.19		plunge= .51	
	Quality index = 47.2		reverse fault	

L2 tensor for : #39

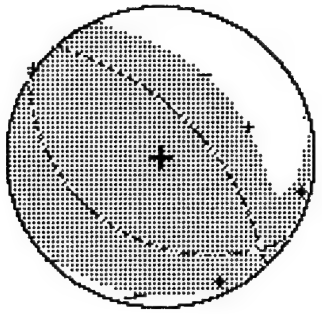

Full solution :

-.606E+10	-.549E+10	-.265E+11
-.549E+10	.712E+10	-.563E+11
-.265E+11	-.563E+11	.225E+12

T0= .0400 M0= .171E+12 MT= .237E+12
Expl.= 19.6% CLVD.= 18.6% DBCP.= 61.8%

Full:	∢A= 316.38	δA= 58.41	∢B= 122.97	δB= 32.30
	P-axis: trend= 41.22		plunge= 13.14	
	T-axis: trend= 246.84		plunge= 75.48	
	B-axis: trend= 132.64		plunge= 6.06	
	Quality index = 12.3		reverse fault	

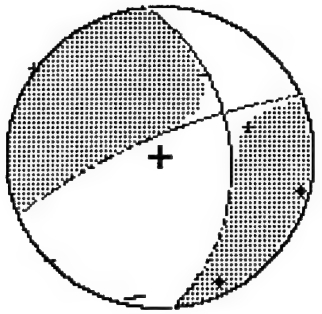

Trace null solution :

-.734E+09	-.436E+10	.501E+10
-.436E+10	.359E+10	-.134E+10
.501E+10	-.134E+10	-.285E+10

T0= .0400 M0= .723E+10 MT= .752E+10
CLVD.= 6.3% DBCP.= 93.7%

Tr.0:	∢A= 246.76	δA= 75.71	∢B= 354.38	δB= 40.09
	P-axis: trend= 195.17		plunge= 45.69	
	T-axis: trend= 308.95		plunge= 21.49	
	B-axis: trend= 55.89		plunge= 36.50	
	Quality index = 6.6		normal fault	

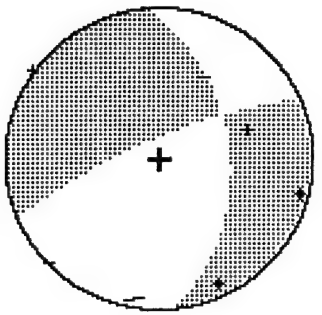

Double couple solution :

-.811E+09	-.395E+10	.503E+10
-.395E+10	.355E+10	-.971E+09
.503E+10	-.971E+09	-.274E+10

T0= .0400 M0= .723E+10 MT= .723E+10
DBCP.= 100.0%

D.C.:	∢A= 246.70	δA= 75.66	∢B= 354.38	δB= 40.09
	P-axis: trend= 195.14		plunge= 45.73	
	T-axis: trend= 308.92		plunge= 21.46	
	B-axis: trend= 55.81		plunge= 36.48	
	Quality index = 3.2		normal fault	

L2 tensor for : #40

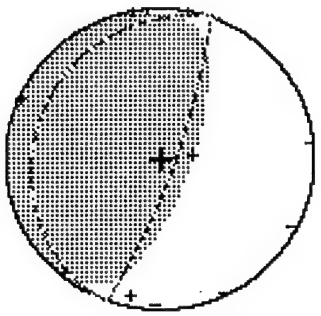

Full solution :

-.233E+11	.316E+10	.253E+12
.316E+10	-.733E+09	-.722E+12
.253E+12	-.722E+12	.682E+12

T0= .0633 M0= .904E+12 MT= .116E+13
Expl.= 13.3% CLVD.= 14.4% DBCP.= 72.3%
Full: ∮A= 19.83 δA= 77.90 ∮B= 203.36 δB= 12.12
P-axis: trend= 110.46 plunge= 32.89
T-axis: trend= 288.87 plunge= 57.10
B-axis: trend= 19.99 plunge= .72
Quality index = 52.7 reverse fault

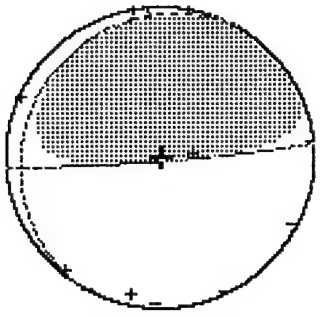

Trace null solution :

-.235E+11	.241E+11	.222E+12
.241E+11	-.172E+11	-.127E+11
.222E+12	-.127E+11	.407E+11

T0= .0633 M0= .219E+12 MT= .227E+12
CLVD.= 5.3% DBCP.= 94.7%
Tr.0: ∮A= 85.71 δA= 85.66 ∮B= 211.55 δB= 7.39
P-axis: trend= 170.15 plunge= 40.37
T-axis: trend= 2.16 plunge= 49.01
B-axis: trend= 265.25 plunge= 5.97
Quality index = 50.4 reverse fault

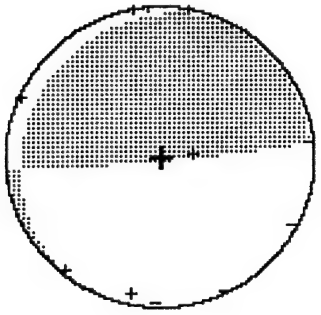

Double couple solution :

-.288E+11	.252E+11	.215E+12
.252E+11	-.408E+10	-.165E+11
.215E+12	-.165E+11	.329E+11

T0= .0633 M0= .219E+12 MT= .219E+12
DBCP.= 100.0%
D.C.: ∮A= 85.14 δA= 85.66 ∮B= 210.99 δB= 7.38
P-axis: trend= 169.60 plunge= 40.37
T-axis: trend= 1.59 plunge= 49.00
B-axis: trend= 264.69 plunge= 5.96
Quality index = 50.1 reverse fault

L2 tensor for : #41

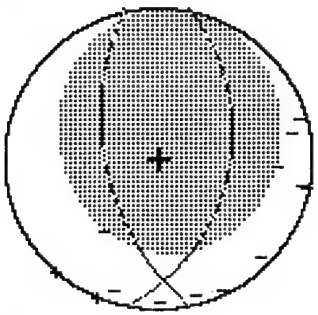

Full solution :

-.634E+09	.192E+10	.185E+11
.192E+10	-.927E+10	.102E+11
.185E+11	.102E+11	.798E+11

T0= .0667 M0= .606E+11 MT= .803E+11
Expl.= 16.5% CLVD.= 19.8% DBCP.= 63.6%

Full:	∮A= 167.76	δA= 52.89	∮B= 11.80	δB= 39.64
	P-axis: trend= 268.42		plunge= 6.77	
	T-axis: trend= 27.33		plunge= 76.21	
	B-axis: trend= 176.98		plunge= 11.96	
	Quality index = 49.2		reverse fault	

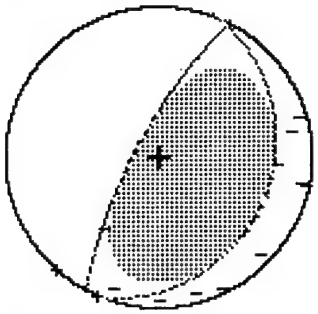

Trace null solution :

-.361E+10	.279E+10	-.871E+10
.279E+10	-.895E+10	.158E+11
-.871E+10	.158E+11	.126E+11

T0= .0667 M0= .201E+11 MT= .214E+11
CLVD.= 9.0% DBCP.= 91.0%

Tr.0:	∮A= 207.86	δA= 73.95	∮B= 21.13	δB= 16.15
	P-axis: trend= 296.35		plunge= 28.93	
	T-axis: trend= 120.58		plunge= 61.01	
	B-axis: trend= 27.34		plunge= 1.79	
	Quality index = 47.7		reverse fault	

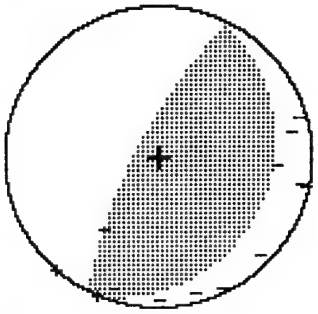

Double couple solution :

-.173E+10	.398E+10	-.794E+10
.398E+10	-.895E+10	.150E+11
-.794E+10	.150E+11	.107E+11

T0= .0667 M0= .201E+11 MT= .201E+11
DBCP.= 100.0%

D.C.:	∮A= 207.25	δA= 73.92	∮B= 20.56	δB= 16.18
	P-axis: trend= 295.75		plunge= 28.90	
	T-axis: trend= 119.97		plunge= 61.03	
	B-axis: trend= 26.74		plunge= 1.79	
	Quality index = 47.4		reverse fault	

L2 tensor for : #42

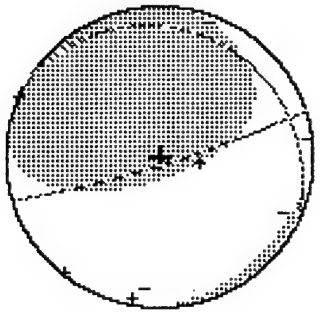

Full solution :

.151E+10	-.170E+11	.989E+11
-.170E+11	-.433E+10	-.386E+11
.989E+11	-.386E+11	.650E+11

T0= .0700 M0= .117E+12 MT= .134E+12
Expl.= 9.5% CLVD.= 16.0% DBCP.= 74.5%

Full:	∮A=	72.96	δA=	82.69	∮B= 296.87	δB= 10.09
	P-axis:	trend=	169.16	plunge=	37.32	
	T-axis:	trend=	334.97	plunge=	51.82	
	B-axis:	trend=	73.85	plunge=	6.92	
	Quality index =		11.1	reverse fault		

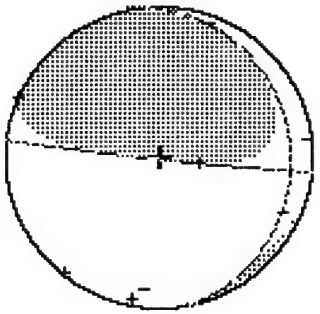

Trace null solution :

-.179E+10	-.112E+11	.822E+11
-.112E+11	-.899E+10	.702E+10
.822E+11	.702E+10	.108E+11

T0= .0700 M0= .804E+11 MT= .839E+11
CLVD.= 6.7% DBCP.= 93.3%

Tr.0:	∮A=	96.23	δA=	87.35	∮B= 348.31	δB= 8.54
	P-axis:	trend=	193.93	plunge=	41.81	
	T-axis:	trend=	357.80	plunge=	47.05	
	B-axis:	trend=	96.61	plunge=	8.12	
	Quality index =		10.4	reverse fault		

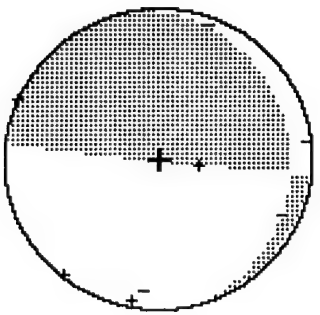

Double couple solution :

-.509E+10	-.118E+11	.789E+11
-.118E+11	-.229E+10	.727E+10
.789E+11	.727E+10	.738E+10

T0= .0700 M0= .804E+11 MT= .804E+11
DBCP.= 100.0%

D.C.:	∮A=	95.65	δA=	87.34	∮B= 347.61	δB= 8.54
	P-axis:	trend=	193.34	plunge=	41.79	
	T-axis:	trend=	357.22	plunge=	47.06	
	B-axis:	trend=	96.03	plunge=	8.11	
	Quality index =		10.4	reverse fault		

L2 tensor for : #43

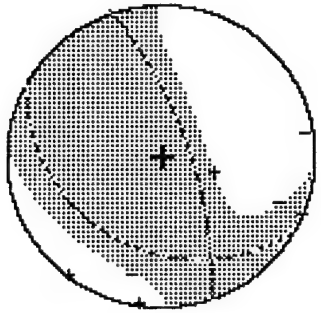

Full solution :

-.141E+11	-.302E+12	-.699E+11
-.302E+12	-.345E+11	-.677E+12
-.699E+11	-.677E+12	.929E+12

T0= .0700 M0= .993E+12 MT= .113E+13
Expl.= 18.7% CLVD.= 9.1% DBCP.= 72.2%

Full:	ϕA= 341.11	δA= 69.27	ϕB= 119.92	δB= 26.70
	P-axis: trend= 58.03		plunge= 22.42	
	T-axis: trend= 277.47		plunge= 61.89	
	B-axis: trend= 154.85		plunge= 16.06	
	Quality index = 11.0		reverse fault	

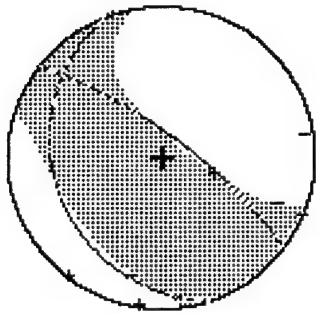

Trace null solution :

-.665E+11	-.225E+12	-.302E+12
-.225E+12	-.137E+12	-.232E+12
-.302E+12	-.232E+12	.204E+12

T0= .0700 M0= .412E+12 MT= .478E+12
CLVD.= -26.9% DBCP.= 73.1%

Tr.0:	ϕA= 306.97	δA= 73.25	ϕB= 161.46	δB= 20.07
	P-axis: trend= 45.87		plunge= 27.41	
	T-axis: trend= 200.91		plunge= 60.23	
	B-axis: trend= 310.24		plunge= 10.72	
	Quality index = 9.2		reverse fault	

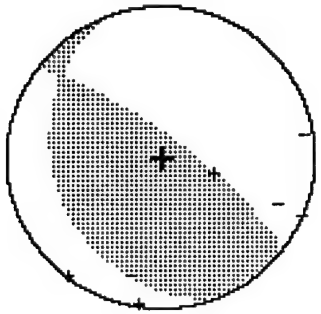

Double couple solution :

-.709E+11	-.129E+12	-.285E+12
-.129E+12	-.152E+12	-.183E+12
-.285E+12	-.183E+12	.223E+12

T0= .0700 M0= .412E+12 MT= .412E+12
DBCP.= 100.0%

D.C.:	ϕA= 306.51	δA= 73.30	ϕB= 160.92	δB= 19.99
	P-axis: trend= 45.36		plunge= 27.47	
	T-axis: trend= 200.56		plunge= 60.20	
	B-axis: trend= 309.75		plunge= 10.66	
	Quality index = 9.5		reverse fault	

L2 tensor for : #44

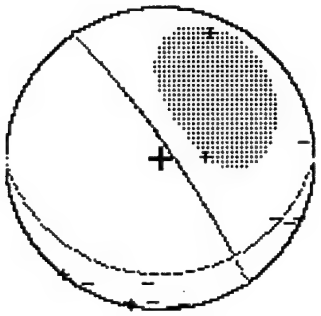

Full solution :

-.102E+11	.939E+10	.223E+11
.939E+10	-.228E+11	.349E+11
.223E+11	.349E+11	-.361E+11

T0= .0817 M0= .461E+11 MT= .526E+11
Expl.= -34.2% CLVD.= .0% DBCP.= 65.8%

Full:	∮A= 325.44	δA= 81.26	∮B= 90.67	δB= 14.93
	P-axis: trend= 249.51		plunge= 52.25	
	T-axis: trend= 44.95		plunge= 35.15	
	B-axis: trend= 143.57		plunge= 12.01	
	Quality index = 49.6		normal fault	

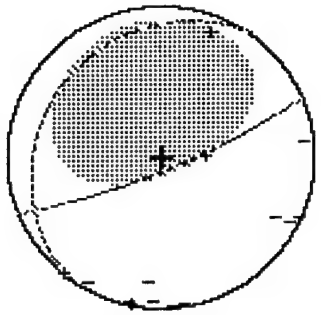

Trace null solution :

-.750E+10	.333E+10	.364E+11
.333E+10	-.138E+11	-.116E+11
.364E+11	-.116E+11	.213E+11

T0= .0817 M0= .362E+11 MT= .426E+11
CLVD.= 15.7% DBCP.= 84.3%

Tr.0:	∮A= 67.85	δA= 78.52	∮B= 216.22	δB= 13.41
	P-axis: trend= 151.95		plunge= 33.17	
	T-axis: trend= 346.69		plunge= 55.95	
	B-axis: trend= 246.45		plunge= 6.85	
	Quality index = 48.3		reverse fault	

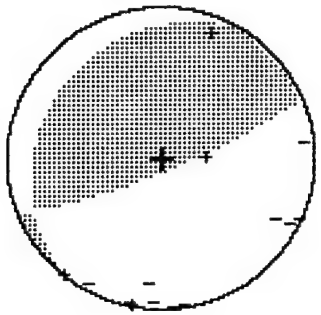

Double couple solution :

-.905E+10	.797E+10	.310E+11
.797E+10	-.499E+10	-.116E+11
.310E+11	-.116E+11	.140E+11

T0= .0817 M0= .362E+11 MT= .362E+11
DBCP.= 100.0%

D.C.:	∮A= 67.88	δA= 78.51	∮B= 216.40	δB= 13.41
	P-axis: trend= 152.01		plunge= 33.16	
	T-axis: trend= 346.68		plunge= 55.97	
	B-axis: trend= 246.49		plunge= 6.82	
	Quality index = 34.3		reverse fault	

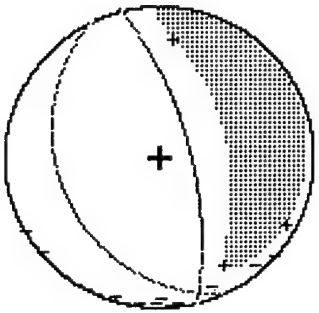

L2 tensor for : #45

Full solution :

-.181E+10	.531E+11	.131E+12
.531E+11	-.617E+11	.937E+12
.131E+12	.937E+12	-.205E+13

T0= .0583 M0= .173E+13 MT= .240E+13
Expl.= -40.3% CLVD.= -38.8% DBCP.= 20.9%

Full:	∮A= 345.67	δA= 66.48	∮B= 155.59	δB= 23.85
	P-axis: trend= 263.43		plunge= 68.27	
	T-axis: trend= 72.59		plunge= 21.38	
	B-axis: trend= 164.05		plunge= 3.72	
	Quality index = 53.1		normal fault	

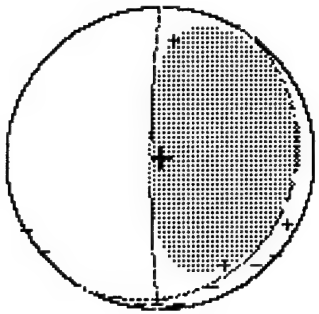

Trace null solution :

-.251E+11	.167E+11	.210E+10
.167E+11	-.440E+11	.248E+12
.210E+10	.248E+12	.691E+11

T0= .0583 M0= .243E+12 MT= .256E+12
CLVD.= 7.8% DBCP.= 92.2%

Tr.0:	∮A= 180.52	δA= 83.56	∮B= 31.21	δB= 7.48
	P-axis: trend= 273.96		plunge= 38.45	
	T-axis: trend= 86.21		plunge= 51.30	
	B-axis: trend= 180.95		plunge= 3.78	
	Quality index = 51.2		reverse fault	

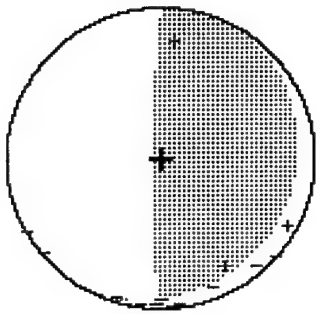

Double couple solution :

-.296E+09	.165E+11	-.339E+09
.165E+11	-.539E+11	.236E+12
-.339E+09	.236E+12	.542E+11

T0= .0583 M0= .243E+12 MT= .243E+12
DBCP.= 100.0%

D.C.:	∮A= 180.52	δA= 83.54	∮B= 31.09	δB= 7.49
	P-axis: trend= 273.95		plunge= 38.42	
	T-axis: trend= 86.22		plunge= 51.32	
	B-axis: trend= 180.95		plunge= 3.78	
	Quality index = 25.6		reverse fault	

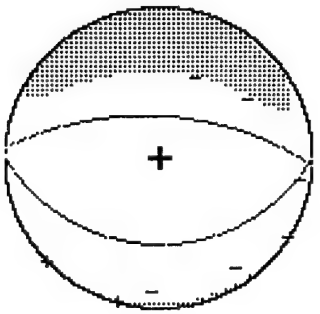

L2 tensor for : #46

Full solution :

.402E+10	-.535E+09	.538E+11
-.535E+09	-.346E+10	.539E+10
.538E+11	.539E+10	-.183E+12

T0= .0617 M0= .140E+12 MT= .194E+12
Expl.= -43.4% CLVD.= -41.0% DBCP.= 15.6%

Full:	∮A= 273.17	δA= 60.02	∮B= 91.02	δB= 29.99
	P-axis: trend= 186.09		plunge= 74.95	
	T-axis: trend= 2.38		plunge= 15.02	
	B-axis: trend= 92.63		plunge= .93	
	Quality index = 12.3		normal fault	

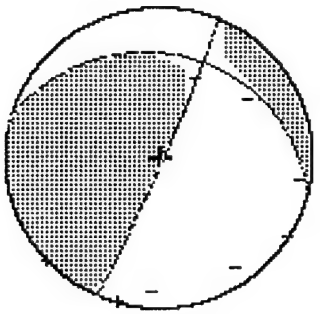

Trace null solution :

-.601E+10	.544E+10	.630E+10
.544E+10	.319E+10	-.169E+11
.630E+10	-.169E+11	.282E+10

T0= .0617 M0= .192E+11 MT= .196E+11
CLVD.= 3.6% DBCP.= 96.4%

Tr.0:	∮A= 23.27	δA= 85.93	∮B= 282.98	δB= 21.73
	P-axis: trend= 132.17		plunge= 37.35	
	T-axis: trend= 271.90		plunge= 45.00	
	B-axis: trend= 24.86		plunge= 21.31	
	Quality index = 10.5		reverse fault	

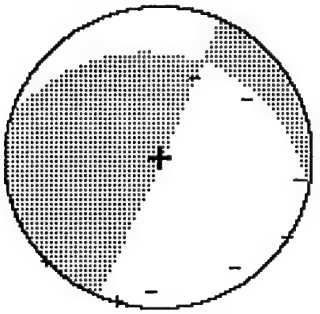

Double couple solution :

-.544E+10	.570E+10	.653E+10
.570E+10	.292E+10	-.164E+11
.653E+10	-.164E+11	.253E+10

T0= .0617 M0= .192E+11 MT= .192E+11
DBCP.= 100.0%

D.C.:	∮A= 23.26	δA= 85.93	∮B= 282.96	δB= 21.69
	P-axis: trend= 132.13		plunge= 37.37	
	T-axis: trend= 271.94		plunge= 45.01	
	B-axis: trend= 24.85		plunge= 21.26	
	Quality index = 7.4		reverse fault	

L2 tensor for : #47

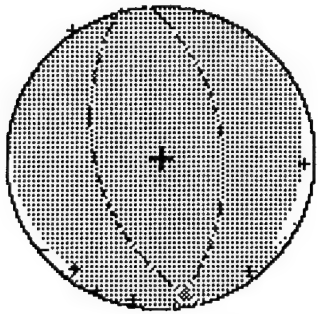

Full solution :

.434E+12	-.106E+12	.391E+13
-.106E+12	-.974E+11	-.798E+12
.391E+13	-.798E+12	.448E+14

T0= .0483 M0= .320E+14 MT= .451E+14
Expl.= 20.0% CLVD.= 19.9% DBCP.= 60.0%

Full:	ϕA= 355.24	δA= 45.38	ϕB= 165.09	δB= 45.07
	P-axis: trend= 80.18		plunge= .15	
	T-axis: trend= 348.47		plunge= 84.90	
	B-axis: trend= 170.20		plunge= 5.09	
	Quality index = 29.9		reverse fault	

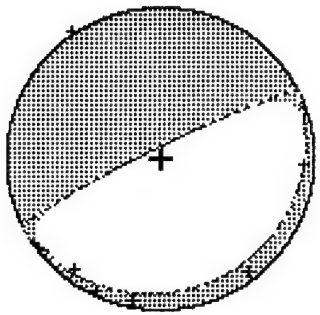

Trace null solution :

.294E+12	-.140E+12	.130E+13
-.140E+12	.859E+11	-.648E+12
.130E+13	-.648E+12	-.379E+12

T0= .0483 M0= .149E+13 MT= .150E+13
CLVD.= -1.0% DBCP.= 99.0%

Tr.0:	ϕA= 243.48	δA= 82.82	ϕB= 63.13	δB= 7.18
	P-axis: trend= 153.53		plunge= 52.18	
	T-axis: trend= 333.44		plunge= 37.82	
	B-axis: trend= 63.48		plunge= .04	
	Quality index = 28.7		normal fault	

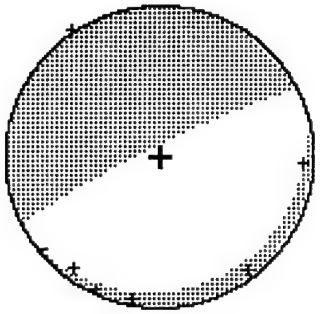

Double couple solution :

.297E+12	-.148E+12	.129E+13
-.148E+12	.742E+11	-.644E+12
.129E+13	-.644E+12	-.371E+12

T0= .0483 M0= .149E+13 MT= .149E+13
DBCP.= 100.0%

D.C.:	ϕA= 243.51	δA= 82.80	ϕB= 63.34	δB= 7.20
	P-axis: trend= 153.53		plunge= 52.20	
	T-axis: trend= 333.49		plunge= 37.80	
	B-axis: trend= 63.51		plunge= .02	
	Quality index = 14.3		normal fault	

L2 tensor for : #48

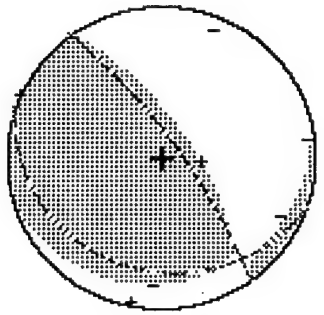

Full solution :

-.160E+12	-.914E+11	-.391E+12
-.914E+11	.557E+11	-.682E+12
-.391E+12	-.682E+12	.701E+12

T0= .0733 M0= .941E+12 MT= .119E+13
Expl.= 12.4% CLVD.= 12.8% DBCP.= 74.8%

Full:	ϕA= 324.06	δA= 76.22	ϕB= 108.99	δB= 16.68
	P-axis: trend= 46.28		plunge= 30.59	
	T-axis: trend= 246.69		plunge= 57.75	
	B-axis: trend= 141.78		plunge= 9.22	
	Quality index = 10.9		reverse fault	

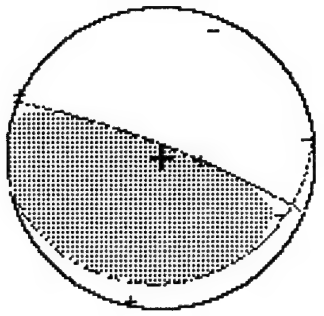

Trace null solution :

-.206E+12	-.170E+11	-.574E+12
-.170E+11	-.147E+09	-.238E+12
-.574E+12	-.238E+12	.206E+12

T0= .0733 M0= .646E+12 MT= .655E+12
CLVD.= 2.4% DBCP.= 97.6%

Tr.0:	ϕA= 291.48	δA= 81.14	ϕB= 81.13	δB= 10.24
	P-axis: trend= 16.98		plunge= 35.94	
	T-axis: trend= 207.62		plunge= 53.58	
	B-axis: trend= 110.68		plunge= 5.09	
	Quality index = 10.1		reverse fault	

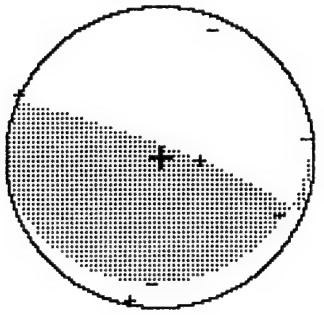

Double couple solution :

-.209E+12	-.248E+11	-.567E+12
-.248E+11	.129E+11	-.233E+12
-.567E+12	-.233E+12	.196E+12

T0= .0733 M0= .646E+12 MT= .646E+12
DBCP.= 100.0%

D.C.:	ϕA= 291.45	δA= 81.12	ϕB= 81.11	δB= 10.26
	P-axis: trend= 16.95		plunge= 35.92	
	T-axis: trend= 207.61		plunge= 53.60	
	B-axis: trend= 110.66		plunge= 5.10	
	Quality index = 5.0		reverse fault	

L2 tensor for : #49

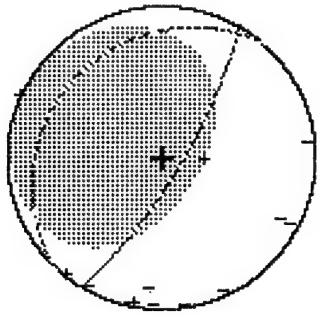

Full solution :

-.192E+11	-.433E+10	.407E+11
-.433E+10	-.424E+10	-.782E+11
.407E+11	-.782E+11	.102E+12

T0= .0767 M0= .115E+12 MT= .132E+12
Expl.= 10.8% CLVD.= 18.7% DBCP.= 70.5%

Full:	∮A= 30.86	δA= 74.45	∮B= 222.67	δB= 15.87
	P-axis: trend= 123.46		plunge= 29.38	
	T-axis: trend= 296.26		plunge= 60.42	
	B-axis: trend= 31.72		plunge= 3.09	
	Quality index = 54.4		reverse fault	

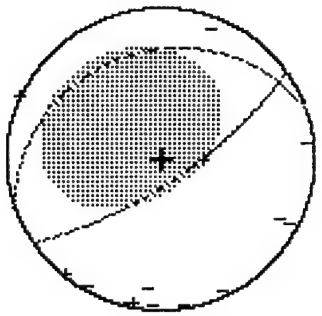

Trace null solution :

-.212E+11	.305E+09	.263E+11
.305E+09	-.144E+11	-.222E+11
.263E+11	-.222E+11	.355E+11

T0= .0767 M0= .358E+11 MT= .463E+11
CLVD.= 19.3% DBCP.= 80.7%

Tr.0:	∮A= 55.64	δA= 70.61	∮B= 251.08	δB= 20.06
	P-axis: trend= 149.74		plunge= 25.43	
	T-axis: trend= 317.16		plunge= 64.03	
	B-axis: trend= 57.39		plunge= 4.94	
	Quality index = 50.2		reverse fault	

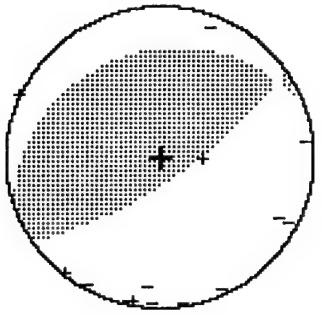

Double couple solution :

-.182E+11	.928E+10	.224E+11
.928E+10	-.422E+10	-.166E+11
.224E+11	-.166E+11	.224E+11

T0= .0767 M0= .358E+11 MT= .358E+11
DBCP.= 100.0%

D.C.:	∮A= 55.70	δA= 70.59	∮B= 251.21	δB= 20.09
	P-axis: trend= 149.82		plunge= 25.41	
	T-axis: trend= 317.17		plunge= 64.04	
	B-axis: trend= 57.46		plunge= 4.97	
	Quality index = 35.5		reverse fault	

L2 tensor for : #52

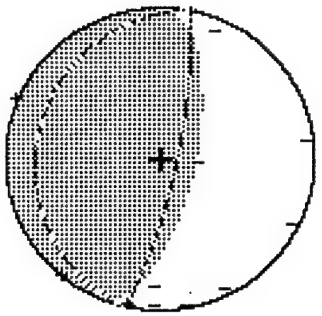

Full solution :

-.308E+10	-.458E+09	.447E+11
-.458E+09	.678E+10	-.218E+12
.447E+11	-.218E+12	.230E+12

T0= .0717 M0= .275E+12 MT= .364E+12
Expl.= 14.7% CLVD.= 15.3% DBCP.= 70.0%

Full:	∮A= 11.94	δA= 76.65	∮B= 193.76	δB= 13.36
	P-axis: trend= 102.29		plunge= 31.65	
	T-axis: trend= 281.37		plunge= 58.35	
	B-axis: trend= 12.03		plunge= .41	
	Quality index = 49.6		reverse fault	

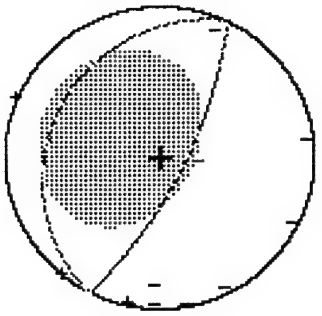

Trace null solution :

-.775E+10	-.602E+08	.627E+10
-.602E+08	-.753E+10	-.128E+11
.627E+10	-.128E+11	.153E+11

T0= .0717 M0= .144E+11 MT= .194E+11
CLVD.= 20.6% DBCP.= 79.4%

Tr.0:	∮A= 26.40	δA= 70.66	∮B= 207.09	δB= 19.34
	P-axis: trend= 116.58		plunge= 25.66	
	T-axis: trend= 296.03		plunge= 64.34	
	B-axis: trend= 26.47		plunge= .21	
	Quality index = 42.0		reverse fault	

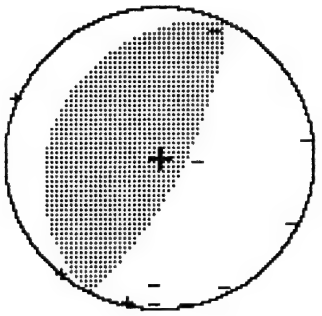

Double couple solution :

-.181E+10	.360E+10	.496E+10
.360E+10	-.718E+10	-.101E+11
.496E+10	-.101E+11	.898E+10

T0= .0717 M0= .144E+11 MT= .144E+11
DBCP.= 100.0%

D.C.:	∮A= 26.35	δA= 70.64	∮B= 206.94	δB= 19.36
	P-axis: trend= 116.50		plunge= 25.64	
	T-axis: trend= 296.03		plunge= 64.35	
	B-axis: trend= 26.41		plunge= .18	
	Quality index = 28.4		reverse fault	

L2 tensor for : #53

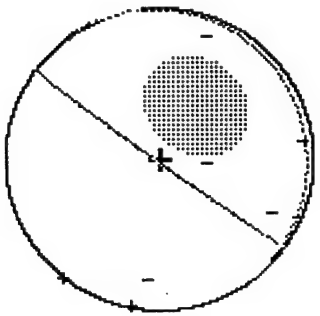

Full solution :

-.119E+11	.336E+10	.133E+11
.336E+10	-.146E+11	.946E+10
.133E+11	.946E+10	-.667E+10

T0= .0583 M0= .163E+11 MT= .219E+11
Expl.= -26.3% CLVD.= 13.8% DBCP.= 59.9%

Full:	∮A= 125.82	δA= 87.43	∮B= 323.17	δB= 2.69
	P-axis: trend= 216.58		plunge= 42.43	
	T-axis: trend= 34.98		plunge= 47.56	
	B-axis: trend= 125.85		plunge= .80	
	Quality index = 6.3		reverse fault	

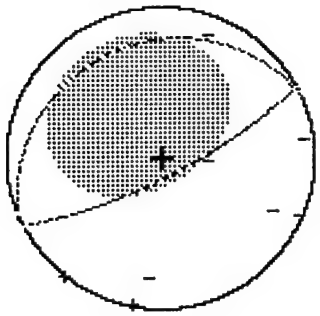

Trace null solution :

-.980E+10	-.108E+10	.210E+11
-.108E+10	-.106E+11	-.110E+11
.210E+11	-.110E+11	.204E+11

T0= .0583 M0= .223E+11 MT= .296E+11
CLVD.= 20.1% DBCP.= 79.9%

Tr.0:	∮A= 63.18	δA= 74.06	∮B= 246.14	δB= 15.96
	P-axis: trend= 153.84		plunge= 29.06	
	T-axis: trend= 332.00		plunge= 60.93	
	B-axis: trend= 63.41		plunge= .78	
	Quality index = 8.0		reverse fault	

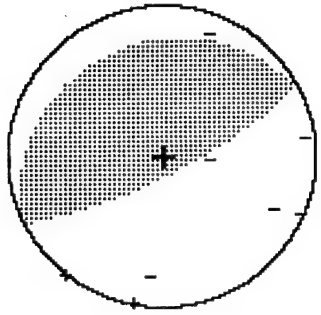

Double couple solution :

-.965E+10	.455E+10	.169E+11
.455E+10	-.214E+10	-.860E+10
.169E+11	-.860E+10	.118E+11

T0= .0583 M0= .223E+11 MT= .223E+11
DBCP.= 100.0%

D.C.:	∮A= 63.23	δA= 74.05	∮B= 246.30	δB= 15.97
	P-axis: trend= 153.91		plunge= 29.04	
	T-axis: trend= 332.00		plunge= 60.94	
	B-axis: trend= 63.46		plunge= .81	
	Quality index = 6.1		reverse fault	

L2 tensor for : #54

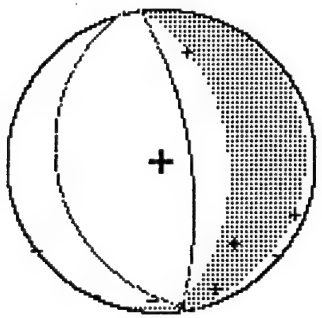

Full solution :

.602E+09	.973E+09	.395E+10
.973E+09	-.528E+10	.511E+11
.395E+10	.511E+11	-.106E+12

T0= .0433 M0= .911E+11 MT= .128E+12
Expl.= -40.9% CLVD.= -41.3% DBCP.= 17.8%

Full:	ϕA=	352.19	δA=	67.59	ϕB=	166.47 δB= 22.51
	P-axis:	trend=	266.21	plunge=	67.34	
	T-axis:	trend=	80.52	plunge=	22.56	
	B-axis:	trend=	171.36	plunge=	2.02	
	Quality index =		12.3	normal fault		

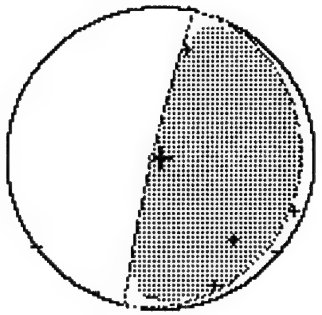

Trace null solution :

-.369E+09	.379E+09	-.304E+10
.379E+09	-.208E+10	.131E+11
-.304E+10	.131E+11	.245E+10

T0= .0433 M0= .135E+11 MT= .137E+11
CLVD.= 2.0% DBCP.= 98.0%

Tr.0:	ϕA=	193.01	δA=	85.14	ϕB=	11.24 δB= 4.86
	P-axis:	trend=	282.87	plunge=	40.14	
	T-axis:	trend=	103.17	plunge=	49.86	
	B-axis:	trend=	13.00	plunge=	.15	
	Quality index =		10.5	reverse fault		

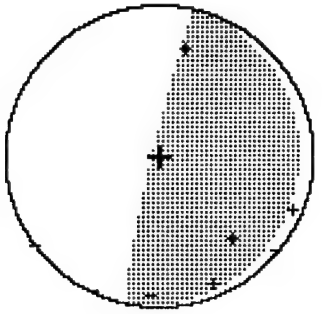

Double couple solution :

-.535E+08	.373E+09	-.297E+10
.373E+09	-.225E+10	.130E+11
-.297E+10	.130E+11	.230E+10

T0= .0433 M0= .135E+11 MT= .135E+11
DBCP.= 100.0%

D.C.:	ϕA=	192.79	δA=	85.11	ϕB=	5.99 δB= 4.93
	P-axis:	trend=	282.25	plunge=	40.11	
	T-axis:	trend=	103.43	plunge=	49.89	
	B-axis:	trend=	12.74	plunge=	.58	
	Quality index =		10.5	reverse fault		

L2 tensor for : #55

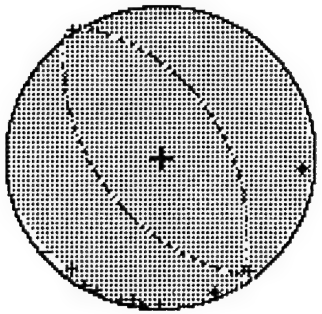

Full solution :

.121E+11	-.669E+10	.776E+11
-.669E+10	.328E+10	-.141E+11
.776E+11	-.141E+11	.131E+13

T0= .0617 M0= .928E+12 MT= .131E+13
Expl.= 20.3% CLVD.= 19.8% DBCP.= 59.9%

Full:	∮A= 142.16	δA= 46.52	∮B= 328.50	δB= 43.66
	P-axis: trend= 235.25		plunge= 1.43	
	T-axis: trend= 349.52		plunge= 86.52	
	B-axis: trend= 145.17		plunge= 3.17	
	Quality index = 50.0		reverse fault	

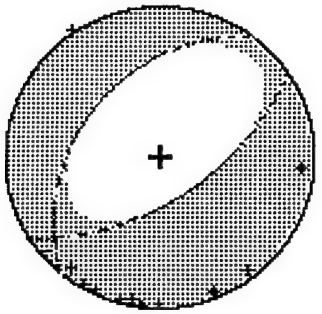

Trace null solution :

.743E+10	-.602E+10	-.572E+10
-.602E+10	.658E+10	.160E+10
-.572E+10	.160E+10	-.140E+11

T0= .0617 M0= .141E+11 MT= .148E+11
CLVD.= -9.9% DBCP.= 90.1%

Tr.0:	∮A= 56.81	δA= 56.43	∮B= 218.36	δB= 34.98
	P-axis: trend= 358.90		plunge= 76.02	
	T-axis: trend= 139.30		plunge= 10.86	
	B-axis: trend= 230.98		plunge= 8.70	
	Quality index = 47.3		normal fault	

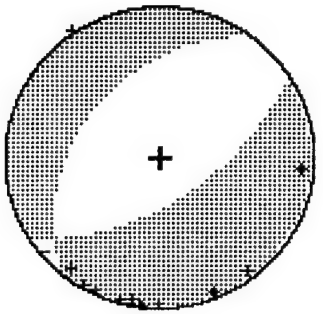

Double couple solution :

.699E+10	-.668E+10	-.527E+10
-.668E+10	.575E+10	.176E+10
-.527E+10	.176E+10	-.127E+11

T0= .0617 M0= .141E+11 MT= .141E+11
DBCP.= 100.0%

D.C.:	∮A= 56.85	δA= 56.43	∮B= 218.43	δB= 34.97
	P-axis: trend= 358.89		plunge= 76.03	
	T-axis: trend= 139.36		plunge= 10.86	
	B-axis: trend= 231.04		plunge= 8.68	
	Quality index = 33.4		normal fault	

-P

L2 tensor for : #56

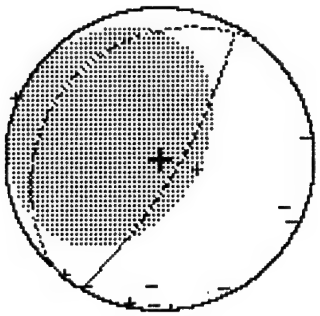

Full solution :

-.140E+11	-.396E+10	.298E+11
-.396E+10	-.294E+10	-.572E+11
.298E+11	-.572E+11	.751E+11

T0= .0733 M0= .843E+11 MT= .970E+11
Expl.= 10.8% CLVD.= 19.0% DBCP.= 70.3%

Full:	∮A= 30.55	δA= 74.47	∮B= 221.11	δB= 15.78
	P-axis: trend= 122.87		plunge= 29.42	
	T-axis: trend= 296.45		plunge= 60.43	
	B-axis: trend= 31.31		plunge= 2.75	
	Quality index = 53.6		reverse fault	

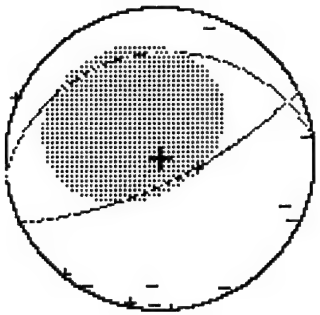

Trace null solution :

-.153E+11	-.118E+10	.198E+11
-.118E+10	-.109E+11	-.130E+11
.198E+11	-.130E+11	.262E+11

T0= .0733 M0= .245E+11 MT= .329E+11
CLVD.= 20.4% DBCP.= 79.6%

Tr.0:	∮A= 64.49	δA= 69.75	∮B= 262.24	δB= 21.17
	P-axis: trend= 159.40		plunge= 24.50	
	T-axis: trend= 323.99		plunge= 64.70	
	B-axis: trend= 66.68		plunge= 5.93	
	Quality index = 46.6		reverse fault	

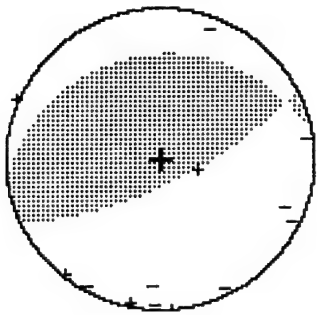

Double couple solution :

-.148E+11	.468E+10	.162E+11
.468E+10	-.104E+10	-.897E+10
.162E+11	-.897E+10	.158E+11

T0= .0733 M0= .245E+11 MT= .245E+11
DBCP.= 100.0%

D.C.:	∮A= 63.96	δA= 69.74	∮B= 261.79	δB= 21.20
	P-axis: trend= 158.90		plunge= 24.48	
	T-axis: trend= 323.40		plunge= 64.71	
	B-axis: trend= 66.17		plunge= 5.96	
	Quality index = 46.6		reverse fault	

L2 tensor for : #57

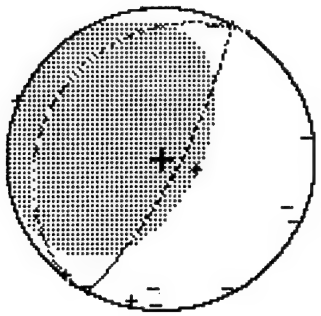

Full solution :

-.575E+10	-.197E+10	.200E+11
-.197E+10	-.549E+07	-.405E+11
.200E+11	-.405E+11	.505E+11

T0= .0667 M0= .578E+11 MT= .710E+11
Expl.= 12.5% CLVD.= 17.7% DBCP.= 69.8%

Full:	∮A= 27.93	δA= 75.46	∮B= 214.81	δB= 14.64
	P-axis: trend= 119.35		plunge= 30.44	
	T-axis: trend= 295.51		plunge= 59.50	
	B-axis: trend= 28.37		plunge= 1.68	
	Quality index = 51.5		reverse fault	

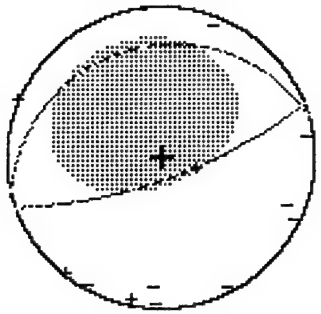

Trace null solution :

-.679E+10	-.142E+08	.124E+11
-.142E+08	-.582E+10	-.483E+10
.124E+11	-.483E+10	.126E+11

T0= .0667 M0= .135E+11 MT= .172E+11
CLVD.= 19.0% DBCP.= 81.0%

Tr.0:	∮A= 70.19	δA= 72.06	∮B= 254.78	δB= 17.99
	P-axis: trend= 161.31		plunge= 27.05	
	T-axis: trend= 337.99		plunge= 62.91	
	B-axis: trend= 70.62		plunge= 1.35	
	Quality index = 45.1		reverse fault	

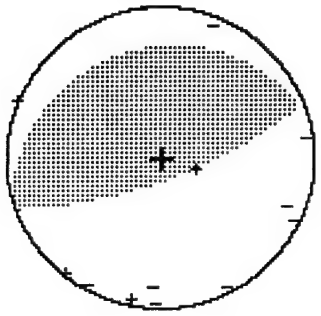

Double couple solution :

-.716E+10	.233E+10	.102E+11
.233E+10	-.745E+09	-.389E+10
.102E+11	-.389E+10	.790E+10

T0= .0667 M0= .135E+11 MT= .135E+11
DBCP.= 100.0%

D.C.:	∮A= 69.65	δA= 72.04	∮B= 254.32	δB= 18.01
	P-axis: trend= 160.80		plunge= 27.03	
	T-axis: trend= 337.41		plunge= 62.93	
	B-axis: trend= 70.10		plunge= 1.37	
	Quality index = 45.1		reverse fault	

L2 tensor for : #58

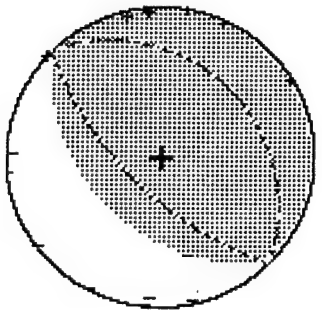

Full solution :

-.643E+10	.350E+10	.584E+12
.350E+10	.375E+10	.593E+12
.584E+12	.593E+12	.205E+13

T0= .1070 M0= .167E+13 MT= .234E+13
Expl.= 18.4% CLVD.= 18.5% DBCP.= 63.2%

Full:	∮A= 134.73	δA= 64.52	∮B= 313.82	δB= 25.49
	P-axis: trend= 224.43		plunge= 19.52	
	T-axis: trend= 45.56		plunge= 70.48	
	B-axis: trend= 314.56		plunge= .35	
	Quality index = 53.2		reverse fault	

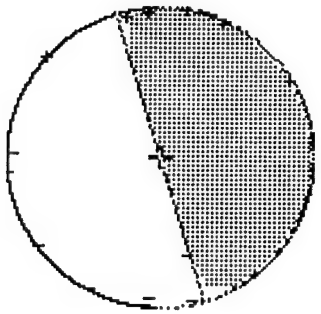

Trace null solution :

-.137E+11	.336E+10	.316E+12
.336E+10	.168E+11	.103E+13
.316E+12	.103E+13	-.305E+10

T0= .1070 M0= .107E+13 MT= .107E+13
CLVD.= 1.2% DBCP.= 98.8%

Tr.0:	∮A= 342.88	δA= 89.75	∮B= .00	δB= .40
	P-axis: trend= 252.57		plunge= 45.25	
	T-axis: trend= 73.19		plunge= 44.75	
	B-axis: trend= 342.88		plunge= .31	
	Quality index = 53.0		normal fault	

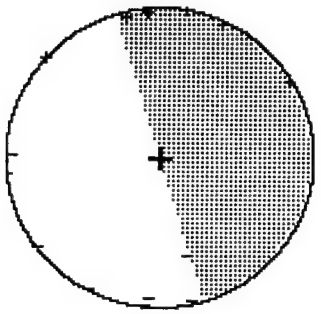

Double couple solution :

-.242E+10	-.210E+10	.315E+12
-.210E+10	.119E+11	.102E+13
.315E+12	.102E+13	-.946E+10

T0= .1070 M0= .107E+13 MT= .107E+13
DBCP.= 100.0%

D.C.:	∮A= 342.88	δA= 89.75	∮B= .00	δB= .40
	P-axis: trend= 252.57		plunge= 45.25	
	T-axis: trend= 73.19		plunge= 44.75	
	B-axis: trend= 342.88		plunge= .31	
	Quality index = 37.5		normal fault	

L2 tensor for : #59

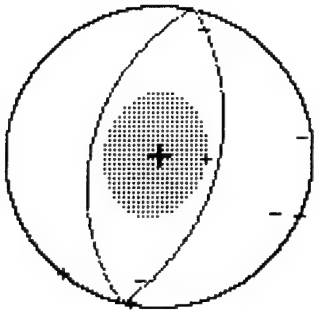

Full solution :

-.709E+10	.138E+10	.145E+09
.138E+10	-.126E+11	-.598E+09
.145E+09	-.598E+09	.733E+10

T0= .0583 M0= .615E+10 MT= .115E+11
Expl.= -19.7% CLVD.= 12.7% DBCP.= 67.6%

Full:	∮A=	13.40	δA=	46.74	∮B= 193.37 δB= 43.26
	P-axis:	trend=	103.39	plunge=	1.74
	T-axis:	trend=	283.75	plunge=	88.26
	B-axis:	trend=	193.39	plunge=	.01
	Quality index =		.1	reverse fault	

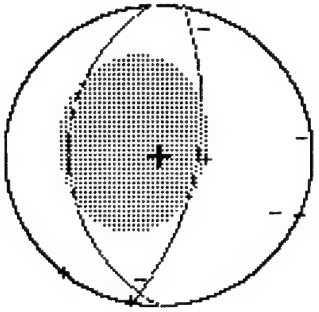

Trace null solution :

-.640E+10	-.841E+08	.296E+10
-.841E+08	-.113E+11	-.839E+10
.296E+10	-.839E+10	.177E+11

T0= .0583 M0= .136E+11 MT= .179E+11
CLVD.= 19.8% DBCP.= 80.2%

Tr.0:	∮A=	9.59	δA=	60.56	∮B= 179.20 δB= 29.85
	P-axis:	trend=	95.81	plunge=	15.41
	T-axis:	trend=	292.82	plunge=	73.92
	B-axis:	trend=	187.05	plunge=	4.48
	Quality index =		6.3	reverse fault	

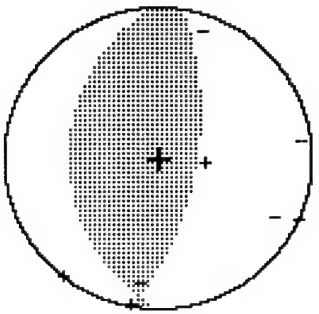

Double couple solution :

.277E+08	.901E+09	.176E+10
.901E+09	-.117E+11	-.682E+10
.176E+10	-.682E+10	.116E+11

T0= .0583 M0= .136E+11 MT= .136E+11
DBCP.= 100.0%

D.C.:	∮A=	9.57	δA=	60.55	∮B= 179.19 δB= 29.86
	P-axis:	trend=	95.80	plunge=	15.40
	T-axis:	trend=	292.82	plunge=	73.93
	B-axis:	trend=	187.04	plunge=	4.48
	Quality index =		5.3	reverse fault	

L2 tensor for : #61

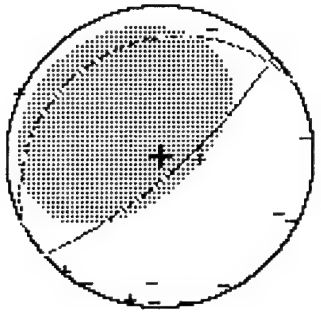

Full solution :

-.228E+11	.106E+10	.638E+11
.106E+10	-.117E+11	-.629E+11
.638E+11	-.629E+11	.925E+11

T0= .0767 M0= .112E+12 MT= .127E+12
Expl.= 9.1% CLVD.= 16.5% DBCP.= 74.4%

Full:	∮A=	48.55	δA= 74.01	∮B= 241.23	δB= 16.37
	P-axis:	trend= 141.41		plunge= 28.92	
	T-axis:	trend= 313.40		plunge= 60.84	
	B-axis:	trend= 49.52		plunge= 3.41	
	Quality index =	54.3		reverse fault	

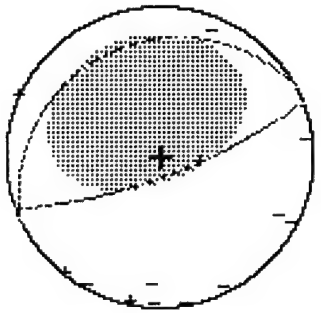

Trace null solution :

-.244E+11	.423E+10	.533E+11
.423E+10	-.199E+11	-.184E+11
.533E+11	-.184E+11	.443E+11

T0= .0767 M0= .578E+11 MT= .683E+11
CLVD.= 16.0% DBCP.= 84.0%

Tr.0:	∮A=	69.56	δA= 73.91	∮B= 243.32	δB= 16.18
	P-axis:	trend= 158.16		plunge= 28.89	
	T-axis:	trend= 342.10		plunge= 61.05	
	B-axis:	trend= 249.08		plunge= 1.67	
	Quality index =	52.5		reverse fault	

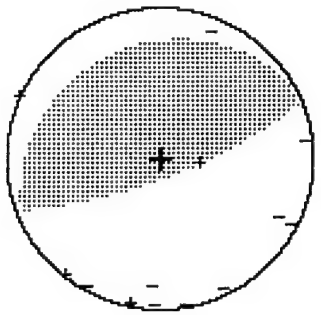

Double couple solution :

-.257E+11	.115E+11	.458E+11
.115E+11	-.506E+10	-.170E+11
.458E+11	-.170E+11	.308E+11

T0= .0767 M0= .578E+11 MT= .578E+11
DBCP.= 100.0%

D.C.:	∮A=	69.03	δA= 73.89	∮B= 242.84	δB= 16.19
	P-axis:	trend= 157.64		plunge= 28.87	
	T-axis:	trend= 341.55		plunge= 61.07	
	B-axis:	trend= 248.55		plunge= 1.66	
	Quality index =	52.5		reverse fault	

L2 tensor for : #62

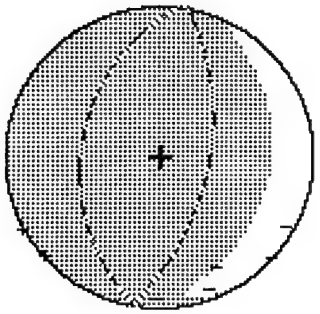

Full solution :

.138E+12	-.454E+11	.137E+13
-.454E+11	-.154E+12	-.454E+13
.137E+13	-.454E+13	.307E+14

T0= .0533 M0= .222E+14 MT= .313E+14
Expl.= 19.8% CLVD.= 19.6% DBCP.= 60.6%

Full:	∮A= 10.49	δA= 53.50	∮B= 188.17	δB= 36.52
	P-axis: trend= 99.50		plunge= 8.50	
	T-axis: trend= 287.05		plunge= 81.43	
	B-axis: trend= 189.67		plunge= 1.11	
	Quality index = 12.4		reverse fault	

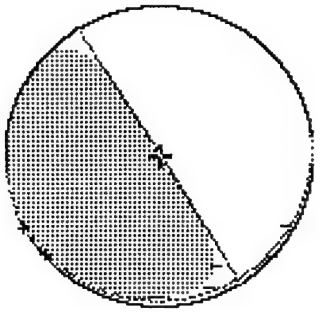

Trace null solution :

-.518E+12	-.655E+11	-.460E+13
-.655E+11	.963E+11	-.738E+13
-.460E+13	-.738E+13	.421E+12

T0= .0533 M0= .857E+13 MT= .871E+13
CLVD.= 3.0% DBCP.= 97.0%

Tr.0:	∮A= 327.94	δA= 89.08	∮B= 82.49	δB= 2.21
	P-axis: trend= 55.97		plunge= 44.05	
	T-axis: trend= 239.98		plunge= 45.88	
	B-axis: trend= 147.91		plunge= 2.01	
	Quality index = 12.3		reverse fault	

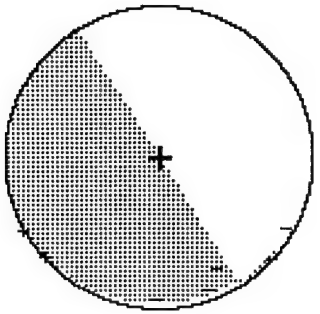

Double couple solution :

-.347E+12	-.254E+12	-.454E+13
-.254E+12	.726E+11	-.726E+13
-.454E+13	-.726E+13	.274E+12

T0= .0533 M0= .857E+13 MT= .857E+13
DBCP.= 100.0%

D.C.:	∮A= 327.94	δA= 89.08	∮B= 82.52	δB= 2.20
	P-axis: trend= 55.97		plunge= 44.05	
	T-axis: trend= 239.97		plunge= 45.88	
	B-axis: trend= 147.91		plunge= 2.00	
	Quality index = 6.1		reverse fault	

L2 tensor for : #63

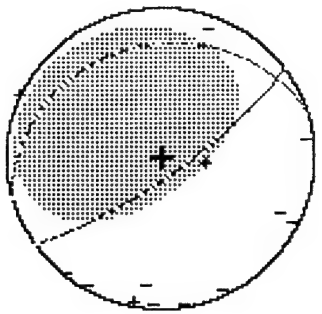

Full solution :

-.137E+11	-.118E+10	.398E+11
-.118E+10	-.454E+10	-.338E+11
.398E+11	-.338E+11	.553E+11

T0= .0733 M0= .660E+11 MT= .756E+11
Expl.= 9.7% CLVD.= 16.8% DBCP.= 73.5%

Full:	∮A= 54.58	δA= 73.97	∮B= 253.40	δB= 16.89
	P-axis: trend= 148.91		plunge= 28.77	
	T-axis: trend= 316.80		plunge= 60.68	
	B-axis: trend= 56.07		plunge= 5.17	
	Quality index = 51.4		reverse fault	

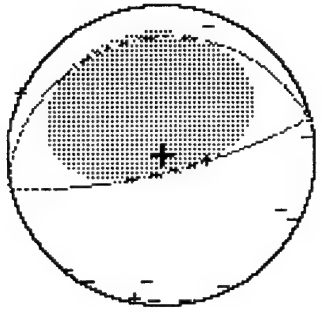

Trace null solution :

-.145E+11	.988E+09	.332E+11
.988E+09	-.932E+10	-.835E+10
.332E+11	-.835E+10	.238E+11

T0= .0733 M0= .347E+11 MT= .400E+11
CLVD.= 14.7% DBCP.= 85.3%

Tr.0:	∮A= 76.23	δA= 75.30	∮B= 258.37	δB= 14.71
	P-axis: trend= 166.67		plunge= 30.30	
	T-axis: trend= 345.46		plunge= 59.69	
	B-axis: trend= 76.36		plunge= .53	
	Quality index = 49.7		reverse fault	

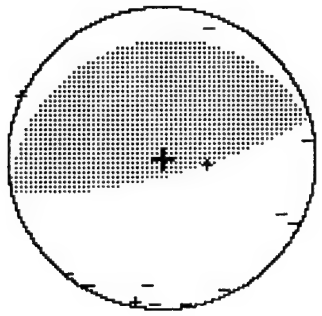

Double couple solution :

-.161E+11	.381E+10	.292E+11
.381E+10	-.892E+09	-.756E+10
.292E+11	-.756E+10	.170E+11

T0= .0733 M0= .347E+11 MT= .347E+11
DBCP.= 100.0%

D.C.:	∮A= 75.66	δA= 75.30	∮B= 257.79	δB= 14.71
	P-axis: trend= 166.10		plunge= 30.30	
	T-axis: trend= 344.91		plunge= 59.70	
	B-axis: trend= 75.80		plunge= .52	
	Quality index = 49.7		reverse fault	

L2 tensor for : #65

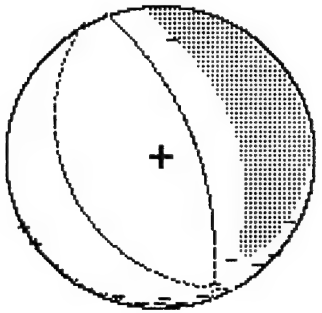

Full solution :

.287E+10	.427E+11	.135E+12
.427E+11	-.272E+11	.634E+12
.135E+12	.634E+12	-.176E+13

T0= .0683 M0= .140E+13 MT= .195E+13
Expl.= -42.4% CLVD.= -40.7% DBCP.= 16.9%

Full:	∮A=	339.89	δA=	62.98	∮B=	150.83 δB= 27.31
	P-axis:	trend=	259.26	plunge=	71.72	
	T-axis:	trend=	66.81	plunge=	17.88	
	B-axis:	trend=	158.00	plunge=	3.69	
	Quality index =		56.1	normal fault		

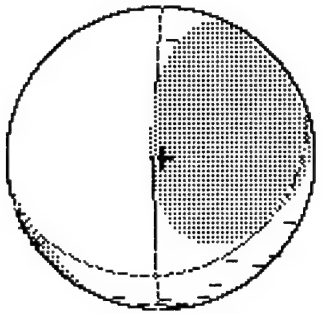

Trace null solution :

-.183E+11	.197E+11	.753E+10
.197E+11	-.236E+10	.809E+11
.753E+10	.809E+11	.207E+11

T0= .0683 M0= .744E+11 MT= .858E+11
CLVD.= 14.7% DBCP.= 85.3%

Tr.0:	∮A=	180.69	δA=	85.56	∮B=	73.54 δB= 14.77
	P-axis:	trend=	283.49	plunge=	38.97	
	T-axis:	trend=	75.89	plunge=	47.61	
	B-axis:	trend=	181.80	plunge=	14.05	
	Quality index =		53.3	reverse fault		

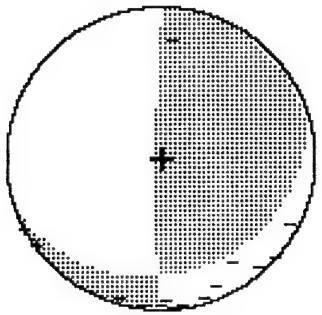

Double couple solution :

-.436E+09	.182E+11	.552E+09
.182E+11	-.108E+11	.713E+11
.552E+09	.713E+11	.112E+11

T0= .0683 M0= .744E+11 MT= .744E+11
DBCP.= 100.0%

D.C.:	∮A=	180.69	δA=	85.53	∮B=	73.44 δB= 14.76
	P-axis:	trend=	283.47	plunge=	38.95	
	T-axis:	trend=	75.90	plunge=	47.63	
	B-axis:	trend=	181.81	plunge=	14.04	
	Quality index =		26.0	reverse fault		

L2 tensor for : #70

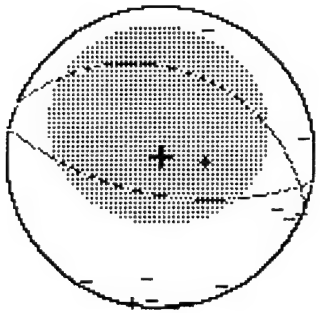

Full solution :

-.796E+10	-.136E+10	.218E+11
-.136E+10	-.880E+10	.165E+09
.218E+11	.165E+09	.613E+11

T0= .0650 M0= .493E+11 MT= .591E+11
Expl.= 13.0% CLVD.= 20.4% DBCP.= 66.6%

Full:	ϕA= 100.59	δA= 60.70	ϕB= 289.44	δB= 29.59
	P-axis: trend= 193.79		plunge= 15.59	
	T-axis: trend= 359.41		plunge= 73.93	
	B-axis: trend= 102.73		plunge= 3.80	
	Quality index = 48.4		reverse fault	

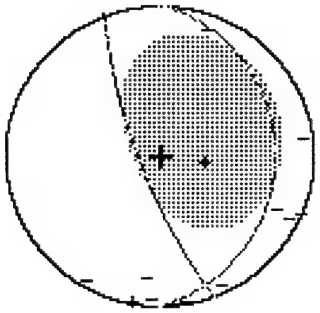

Trace null solution :

-.893E+10	.141E+10	.139E+11
.141E+10	-.154E+11	.299E+11
.139E+11	.299E+11	.243E+11

T0= .0650 M0= .327E+11 MT= .393E+11
CLVD.= 16.6% DBCP.= 83.4%

Tr.0:	ϕA= 159.40	δA= 74.93	ϕB= .10	δB= 16.06
	P-axis: trend= 253.97		plunge= 29.71	
	T-axis: trend= 61.53		plunge= 59.70	
	B-axis: trend= 160.87		plunge= 5.42	
	Quality index = 47.4		reverse fault	

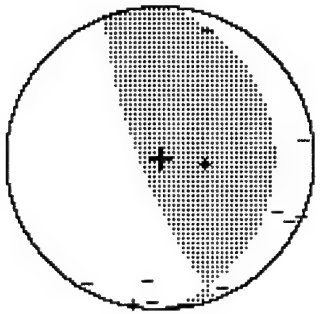

Double couple solution :

-.442E+08	-.322E+10	.109E+11
-.322E+10	-.163E+11	.260E+11
.109E+11	.260E+11	.164E+11

T0= .0650 M0= .327E+11 MT= .327E+11
DBCP.= 100.0%

D.C.:	ϕA= 158.85	δA= 74.90	ϕB= 359.60	δB= 16.10
	P-axis: trend= 253.44		plunge= 29.68	
	T-axis: trend= 60.93		plunge= 59.73	
	B-axis: trend= 160.33		plunge= 5.44	
	Quality index = 46.7		reverse fault	

L2 tensor for : #73

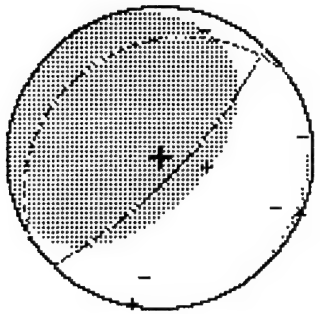

Full solution :

-.142E+11	-.109E+11	.111E+12
-.109E+11	.856E+10	-.134E+12
.111E+12	-.134E+12	.239E+12

T0= .0450 M0= .243E+12 MT= .318E+12
Expl.= 15.0% CLVD.= 17.9% DBCP.= 67.1%

Full:	∮A= 43.88	δA= 73.17	∮B= 237.21	δB= 17.27
	P-axis: trend= 137.02		plunge= 28.07	
	T-axis: trend= 308.04		plunge= 61.63	
	B-axis: trend= 45.02		plunge= 3.75	
	Quality index = 21.0		reverse fault	

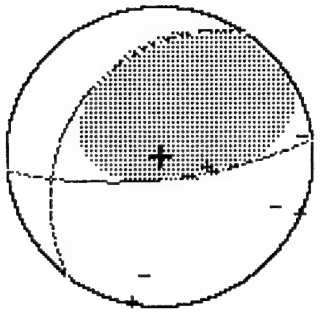

Trace null solution :

-.295E+11	.227E+11	.551E+11
.227E+11	-.160E+11	.866E+10
.551E+11	.866E+10	.455E+11

T0= .0450 M0= .643E+11 MT= .723E+11
CLVD.= 13.2% DBCP.= 86.8%

Tr.0:	∮A= 84.19	δA= 71.28	∮B= 215.64	δB= 27.10
	P-axis: trend= 158.90		plunge= 23.74	
	T-axis: trend= 22.07		plunge= 58.91	
	B-axis: trend= 257.54		plunge= 18.87	
	Quality index = 17.5		reverse fault	

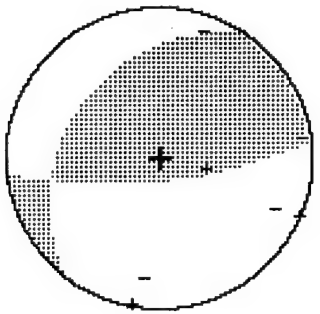

Double couple solution :

-.322E+11	.240E+11	.484E+11
.240E+11	-.455E+10	.215E+10
.484E+11	.215E+10	.368E+11

T0= .0450 M0= .643E+11 MT= .643E+11
DBCP.= 100.0%

D.C.:	∮A= 84.20	δA= 71.27	∮B= 215.70	δB= 27.10
	P-axis: trend= 158.92		plunge= 23.73	
	T-axis: trend= 22.06		plunge= 58.93	
	B-axis: trend= 257.55		plunge= 18.85	
	Quality index = 12.3		reverse fault	

L2 tensor for : #74

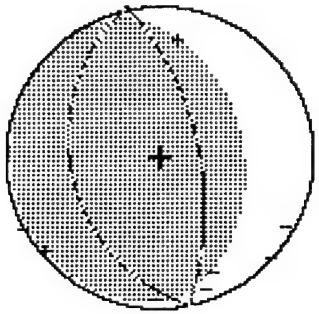

Full solution :

-.727E+11	-.357E+11	-.561E+12
-.357E+11	-.179E+12	-.284E+13
-.561E+12	-.284E+13	.979E+13

T0= .0617 M0= .750E+13 MT= .105E+14
Expl.= 18.6% CLVD.= 19.0% DBCP.= 62.3%

Full:	ϕA= 348.19	δA= 60.05	ϕB= 167.68	δB= 29.95
	P-axis: trend= 78.00		plunge= 15.05	
	T-axis: trend= 258.88		plunge= 74.94	
	B-axis: trend= 168.06		plunge= .22	
	Quality index = 22.0		reverse fault	

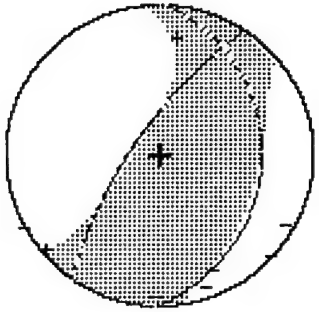

Trace null solution :

.544E+11	.172E+12	-.231E+12
.172E+12	-.315E+12	.326E+12
-.231E+12	.326E+12	.260E+12

T0= .0617 M0= .465E+12 MT= .524E+12
CLVD.= -22.1% DBCP.= 77.9%

Tr.0:	ϕA= 214.70	δA= 71.38	ϕB= .97	δB= 22.05
	P-axis: trend= 295.30		plunge= 25.44	
	T-axis: trend= 142.86		plunge= 61.78	
	B-axis: trend= 30.80		plunge= 11.39	
	Quality index = 17.7		reverse fault	

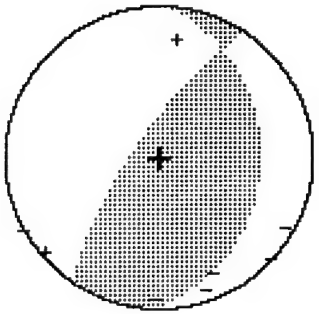

Double couple solution :

-.317E+10	.964E+11	-.231E+12
.964E+11	-.272E+12	.280E+12
-.231E+12	.280E+12	.275E+12

T0= .0617 M0= .465E+12 MT= .465E+12
DBCP.= 100.0%

D.C.:	ϕA= 214.67	δA= 71.36	ϕB= .96	δB= 22.07
	P-axis: trend= 295.27		plunge= 25.43	
	T-axis: trend= 142.84		plunge= 61.80	
	B-axis: trend= 30.77		plunge= 11.39	
	Quality index = 9.2		reverse fault	

L2 tensor for : #75

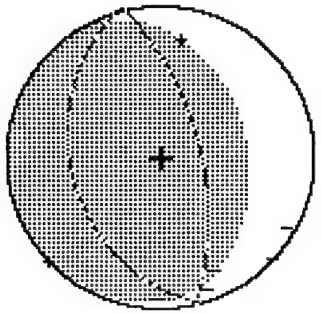

Full solution :

-.444E+11	-.110E+11	-.346E+12
-.110E+11	-.145E+11	-.163E+13
-.346E+12	-.163E+13	.577E+13

T0= .0583 M0= .441E+13 MT= .617E+13
Expl.= 18.8% CLVD.= 19.2% DBCP.= 61.9%
Full: ∮A= 346.38 δA= 59.99 ∮B= 165.06 δB= 30.01
P-axis: trend= 75.90 plunge= 14.99
T-axis: trend= 258.19 plunge= 75.00
B-axis: trend= 166.05 plunge= .57
Quality index = 22.1 reverse fault

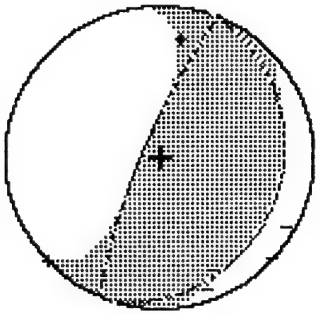

Trace null solution :

.180E+11	.769E+11	-.139E+12
.769E+11	-.154E+12	.329E+12
-.139E+12	.329E+12	.136E+12

T0= .0583 M0= .367E+12 MT= .393E+12
CLVD.= -12.8% DBCP.= 87.2%
Tr.0: ∮A= 202.88 δA= 77.99 ∮B= 17.48 δB= 12.06
P-axis: trend= 291.93 plunge= 32.98
T-axis: trend= 114.34 plunge= 57.00
B-axis: trend= 22.64 plunge= 1.10
Quality index = 19.7 reverse fault

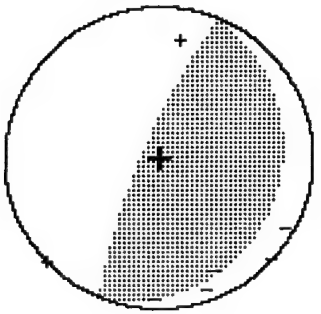

Double couple solution :

-.175E+11	.486E+11	-.132E+12
.486E+11	-.132E+12	.308E+12
-.132E+12	.308E+12	.150E+12

T0= .0583 M0= .367E+12 MT= .367E+12
DBCP.= 100.0%
D.C.: ∮A= 202.86 δA= 77.97 ∮B= 17.41 δB= 12.08
P-axis: trend= 291.90 plunge= 32.96
T-axis: trend= 114.34 plunge= 57.02
B-axis: trend= 22.62 plunge= 1.11
Quality index = 10.0 reverse fault

L2 tensor for : #76

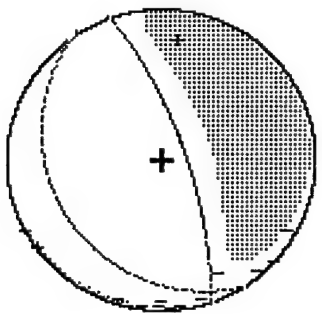

Full solution :

.527E+10	.453E+11	.161E+12
.453E+11	-.264E+11	.600E+12
.161E+12	.600E+12	-.923E+12

T0= .0833 M0= .902E+12 MT= .121E+13
Expl.= -33.3% CLVD.= -30.7% DBCP.= 36.0%

Full:	ϕA= 340.36	δA= 71.52	ϕB= 146.96	δB= 18.96
	P-axis: trend= 257.15		plunge= 63.24	
	T-axis: trend= 66.95		plunge= 26.39	
	B-axis: trend= 158.99		plunge= 4.10	
	Quality index = 56.0		normal fault	

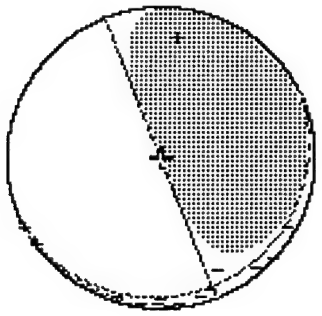

Trace null solution :

-.374E+10	.309E+11	.115E+12
.309E+11	-.126E+11	.280E+12
.115E+12	.280E+12	.164E+11

T0= .0833 M0= .291E+12 MT= .305E+12
CLVD.= 7.1% DBCP.= 92.9%

Tr.0:	ϕA= 158.27	δA= 89.68	ϕB= 64.43	δB= 4.82
	P-axis: trend= 253.03		plunge= 44.48	
	T-axis: trend= 63.45		plunge= 45.12	
	B-axis: trend= 158.30		plunge= 4.81	
	Quality index = 55.6		reverse fault	

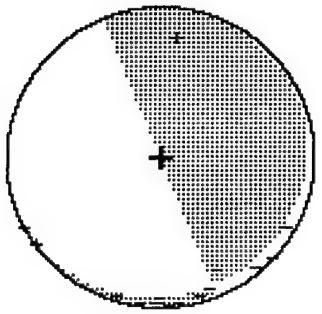

Double couple solution :

.166E+11	.162E+11	.110E+12
.162E+11	-.200E+11	.268E+12
.110E+12	.268E+12	.334E+10

T0= .0833 M0= .291E+12 MT= .291E+12
DBCP.= 100.0%

D.C.:	ϕA= 157.69	δA= 89.67	ϕB= 63.77	δB= 4.82
	P-axis: trend= 252.45		plunge= 44.47	
	T-axis: trend= 62.87		plunge= 45.13	
	B-axis: trend= 157.72		plunge= 4.81	
	Quality index = 54.8		reverse fault	

L2 tensor for : #78

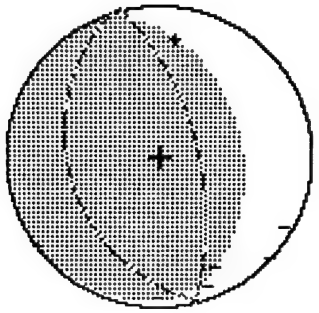

Full solution :

-.205E+12	-.107E+12	-.155E+13
-.107E+12	-.313E+11	-.764E+13
-.155E+13	-.764E+13	.254E+14

T0= .0600 M0= .196E+14 MT= .274E+14
Expl.= 18.8% CLVD.= 19.1% DBCP.= 62.1%

Full:	ϕA= 345.80	δA= 60.71	ϕB= 163.47	δB= 29.31
	P-axis: trend= 74.96		plunge= 15.70	
	T-axis: trend= 258.79		plunge= 74.27	
	B-axis: trend= 165.24		plunge= 1.00	
	Quality index = 12.4		reverse fault	

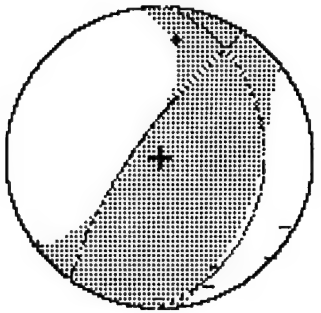

Trace null solution :

.113E+12	.323E+12	-.438E+12
.323E+12	-.541E+12	.630E+12
-.438E+12	.630E+12	.429E+12

T0= .0600 M0= .844E+12 MT= .969E+12
CLVD.= -25.2% DBCP.= 74.8%

Tr.0:	ϕA= 215.07	δA= 72.90	ϕB= .62	δB= 20.46
	P-axis: trend= 296.04		plunge= 27.04	
	T-axis: trend= 141.57		plunge= 60.50	
	B-axis: trend= 31.68		plunge= 10.89	
	Quality index = 8.8		reverse fault	

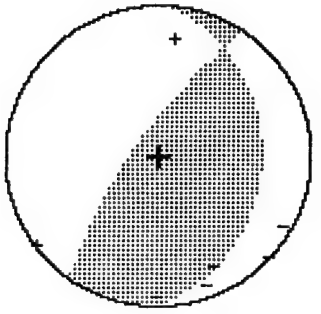

Double couple solution :

-.348E+10	.165E+12	-.433E+12
.165E+12	-.462E+12	.532E+12
-.433E+12	.532E+12	.466E+12

T0= .0600 M0= .844E+12 MT= .844E+12
DBCP.= 100.0%

D.C.:	ϕA= 215.04	δA= 72.88	ϕB= .62	δB= 20.47
	P-axis: trend= 296.01		plunge= 27.02	
	T-axis: trend= 141.55		plunge= 60.52	
	B-axis: trend= 31.64		plunge= 10.89	
	Quality index = 4.8		reverse fault	

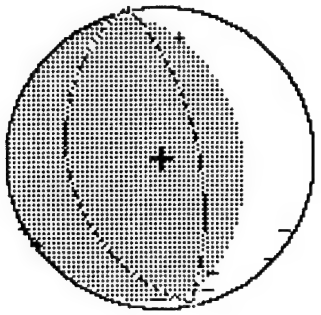

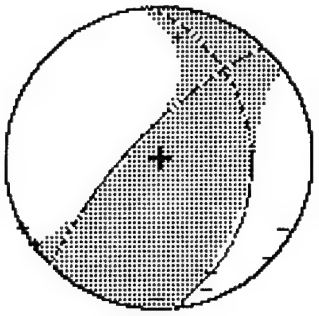

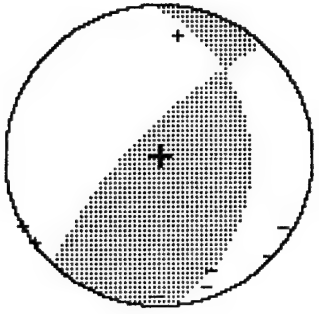

L2 tensor for : #79

Full solution :

-.354E+11	-.266E+11	-.241E+12
-.266E+11	-.107E+11	-.157E+13
-.241E+12	-.157E+13	.495E+13

T0= .0483 M0= .384E+13 MT= .539E+13
Expl.= 18.7% CLVD.= 19.0% DBCP.= 62.3%

Full:	∮A= 348.52	δA= 61.28	∮B= 166.00	δB= 28.75
	P-axis: trend= 77.63		plunge= 16.27	
	T-axis: trend= 261.57		plunge= 73.70	
	B-axis: trend= 167.94		plunge= 1.06	
	Quality index = 22.1		reverse fault	

Trace null solution :

.216E+11	.677E+11	-.853E+11
.677E+11	-.105E+12	.854E+11
-.853E+11	.854E+11	.831E+11

T0= .0483 M0= .148E+12 MT= .168E+12
CLVD.= -23.7% DBCP.= 76.3%

Tr.0:	∮A= 223.83	δA= 71.13	∮B= 354.74	δB= 27.56
	P-axis: trend= 298.20		plunge= 23.46	
	T-axis: trend= 162.36		plunge= 58.82	
	B-axis: trend= 36.95		plunge= 19.32	
	Quality index = 17.1		reverse fault	

Double couple solution :

.820E+10	.404E+11	-.879E+11
.404E+11	-.931E+11	.675E+11
-.879E+11	.675E+11	.849E+11

T0= .0483 M0= .148E+12 MT= .148E+12
DBCP.= 100.0%

D.C.:	∮A= 223.79	δA= 71.11	∮B= 354.75	δB= 27.57
	P-axis: trend= 298.17		plunge= 23.44	
	T-axis: trend= 162.33		plunge= 58.85	
	B-axis: trend= 36.90		plunge= 19.31	
	Quality index = 9.0		reverse fault	

L2 tensor for : #80

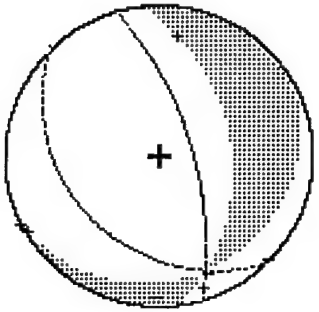

Full solution :

.399E+12	.133E+13	-.636E+12
.133E+13	-.134E+13	.872E+13
-.636E+12	.872E+13	-.195E+14

T0= .0550 M0= .164E+14 MT= .231E+14
Expl.= -41.9% CLVD.= -41.9% DBCP.= 16.2%

Full:	∮A= 343.20	δA= 64.76	∮B= 135.78	δB= 27.97
	P-axis: trend= 277.06		plunge= 67.82	
	T-axis: trend= 63.91		plunge= 18.84	
	B-axis: trend= 157.81		plunge= 11.26	
	Quality index = 21.7		normal fault	

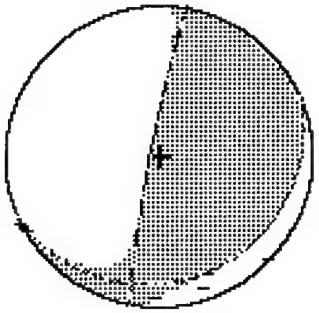

Trace null solution :

-.162E+12	.127E+13	-.122E+13
.127E+13	-.106E+13	.656E+13
-.122E+13	.656E+13	.122E+13

T0= .0550 M0= .674E+13 MT= .689E+13
CLVD.= -4.2% DBCP.= 95.8%

Tr.0:	∮A= 190.85	δA= 84.26	∮B= 66.95	δB= 10.22
	P-axis: trend= 288.52		plunge= 38.69	
	T-axis: trend= 91.52		plunge= 50.05	
	B-axis: trend= 191.70		plunge= 8.43	
	Quality index = 20.9		reverse fault	

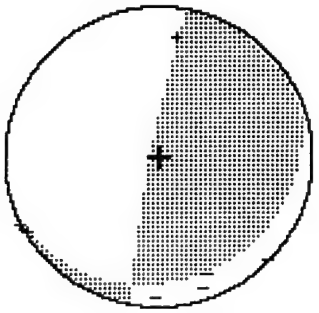

Double couple solution :

-.411E+12	.116E+13	-.113E+13
.116E+13	-.921E+12	.643E+13
-.113E+13	.643E+13	.133E+13

T0= .0550 M0= .674E+13 MT= .674E+13
DBCP.= 100.0%

D.C.:	∮A= 190.85	δA= 84.23	∮B= 66.78	δB= 10.22
	P-axis: trend= 288.49		plunge= 38.67	
	T-axis: trend= 91.53		plunge= 50.08	
	B-axis: trend= 191.70		plunge= 8.41	
	Quality index = 10.4		reverse fault	

L2 tensor for : #81

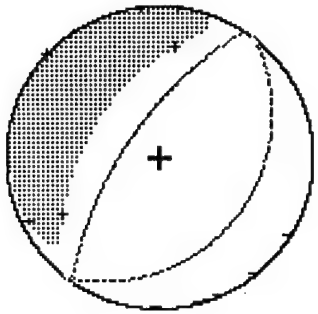

Full solution :

.639E+09	-.166E+11	.487E+12
-.166E+11	-.325E+11	-.777E+12
.487E+12	-.777E+12	-.208E+13

T0= .0633 M0= .173E+13 MT= .240E+13
Expl.= -40.3% CLVD.= -38.8% DBCP.= 20.9%
Full: ∡A= 214.45 δA= 65.73 ∡B= 37.99 δB= 24.31
P-axis: trend= 121.54 plunge= 69.23
T-axis: trend= 305.55 plunge= 20.72
B-axis: trend= 215.05 plunge= 1.33
Quality index = 56.2 normal fault

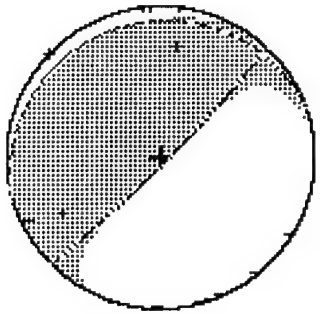

Trace null solution :

-.923E+10	.971E+10	.426E+11
.971E+10	-.251E+10	-.431E+11
.426E+11	-.431E+11	.117E+11

T0= .0633 M0= .603E+11 MT= .623E+11
CLVD.= -6.4% DBCP.= 93.6%
Tr.0: ∡A= 44.74 δA= 83.66 ∡B= 251.34 δB= 7.08
P-axis: trend= 137.61 plunge= 38.58
T-axis: trend= 311.17 plunge= 51.24
B-axis: trend= 45.09 plunge= 3.15
Quality index = 51.5 reverse fault

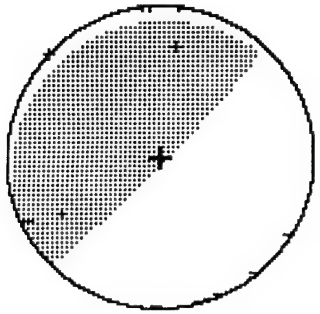

Double couple solution :

-.971E+10	.670E+10	.407E+11
.670E+10	-.351E+10	-.424E+11
.407E+11	-.424E+11	.132E+11

T0= .0633 M0= .603E+11 MT= .603E+11
DBCP.= 100.0%
D.C.: ∡A= 44.17 δA= 83.66 ∡B= 250.67 δB= 7.08
P-axis: trend= 137.02 plunge= 38.58
T-axis: trend= 310.61 plunge= 51.24
B-axis: trend= 44.52 plunge= 3.13
Quality index = 51.5 reverse fault

L2 tensor for : #82

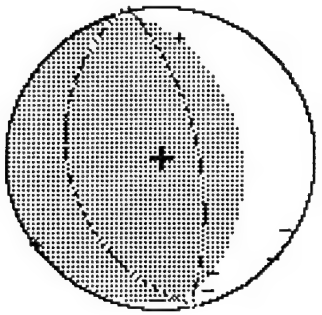

Full solution :

-.890E+11	-.738E+11	-.688E+12
-.738E+11	-.365E+11	-.433E+13
-.688E+12	-.433E+13	.132E+14

T0= .0700 M0= .103E+14 MT= .145E+14
Expl.= 18.7% CLVD.= 18.9% DBCP.= 62.4%

Full:	ϕA= 348.42	δA= 61.67	ϕB= 165.97	δB= 28.35
	P-axis: trend= 77.56		plunge= 16.66	
	T-axis: trend= 261.28		plunge= 73.30	
	B-axis: trend= 167.87		plunge= 1.02	
	Quality index = 12.4		reverse fault	

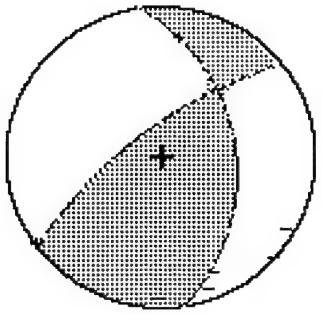

Trace null solution :

.623E+11	.174E+12	-.265E+12
.174E+12	-.295E+12	.103E+12
-.265E+12	.103E+12	.232E+12

T0= .0700 M0= .426E+12 MT= .428E+12
CLVD.= -.8% DBCP.= 99.2%

Tr.0:	ϕA= 232.94	δA= 69.84	ϕB= 350.99	δB= 37.98
	P-axis: trend= 299.09		plunge= 18.28	
	T-axis: trend= 182.85		plunge= 53.23	
	B-axis: trend= 40.38		plunge= 30.65	
	Quality index = 8.5		reverse fault	

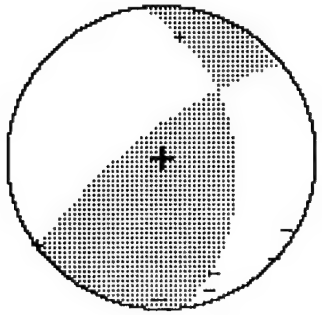

Double couple solution :

.614E+11	.171E+12	-.266E+12
.171E+12	-.293E+12	.101E+12
-.266E+12	.101E+12	.232E+12

T0= .0700 M0= .426E+12 MT= .426E+12
DBCP.= 100.0%

D.C.:	ϕA= 232.90	δA= 69.81	ϕB= 351.00	δB= 37.98
	P-axis: trend= 299.06		plunge= 18.26	
	T-axis: trend= 182.82		plunge= 53.27	
	B-axis: trend= 40.32		plunge= 30.63	
	Quality index = 6.0		reverse fault	

L2 tensor for : #83

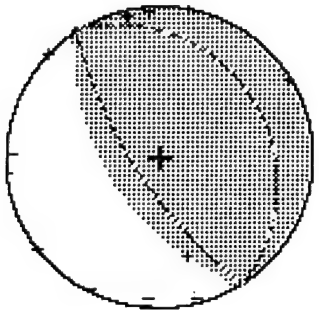

Full solution :

-.157E+10	-.282E+10	.284E+12
-.282E+10	.100E+10	.444E+12
.284E+12	.444E+12	.808E+12

T0= .1100 M0= .777E+12 MT= .107E+13
Expl.= 16.8% CLVD.= 16.7% DBCP.= 66.5%
Full: ∮A= 147.08 δA= 71.22 ∮B= 326.25 δB= 18.79
P-axis: trend= 236.87 plunge= 26.22
T-axis: trend= 57.50 plunge= 63.78
B-axis: trend= 326.99 plunge= .25
Quality index = 49.8 reverse fault

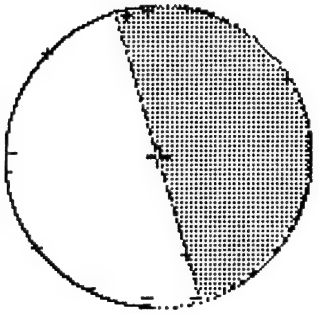

Trace null solution :

-.467E+10	-.269E+10	.176E+12
-.269E+10	.552E+10	.596E+12
.176E+12	.596E+12	-.846E+09

T0= .1100 M0= .620E+12 MT= .622E+12
CLVD.= .4% DBCP.= 99.6%
Tr.0: ∮A= 343.53 δA= 89.91 ∮B= .00 δB= .47
P-axis: trend= 253.07 plunge= 45.09
T-axis: trend= 74.00 plunge= 44.90
B-axis: trend= 343.53 plunge= .46
Quality index = 49.7 normal fault

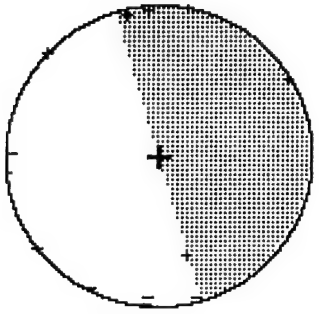

Double couple solution :

-.256E+10	-.365E+10	.176E+12
-.365E+10	.459E+10	.595E+12
.176E+12	.595E+12	-.203E+10

T0= .1100 M0= .620E+12 MT= .620E+12
DBCP.= 100.0%
D.C.: ∮A= 343.53 δA= 89.91 ∮B= .00 δB= .47
P-axis: trend= 253.07 plunge= 45.09
T-axis: trend= 74.00 plunge= 44.90
B-axis: trend= 343.53 plunge= .46
Quality index = 35.1 normal fault

L2 tensor for : #84

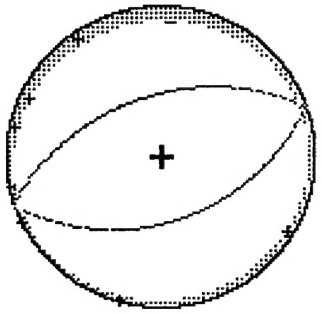

Full solution :

.225E+10	-.580E+09	.124E+11
-.580E+09	.897E+09	-.291E+10
.124E+11	-.291E+10	-.350E+12

T0= .0383 M0= .248E+12 MT= .350E+12
Expl.= -49.4% CLVD.= -49.7% DBCP.= 1.0%

Full:	ϕA= 251.32	δA= 47.05	ϕB= 70.92	δB= 42.95
	P-axis: trend= 166.79		plunge= 87.94	
	T-axis: trend= 341.13		plunge= 2.05	
	B-axis: trend= 71.13		plunge= .20	
	Quality index = 12.4		normal fault	

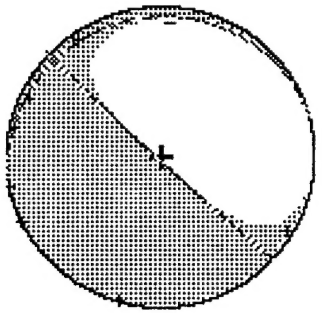

Trace null solution :

.196E+10	-.341E+09	-.997E+10
-.341E+09	-.587E+08	-.949E+10
-.997E+10	-.949E+10	-.190E+10

T0= .0383 M0= .133E+11 MT= .139E+11
CLVD.= -9.2% DBCP.= 90.8%

Tr.0:	ϕA= 132.83	δA= 87.31	ϕB= 254.85	δB= 5.06
	P-axis: trend= 47.33		plunge= 47.52	
	T-axis: trend= 218.74		plunge= 42.16	
	B-axis: trend= 312.63		plunge= 4.29	
	Quality index = 10.9		normal fault	

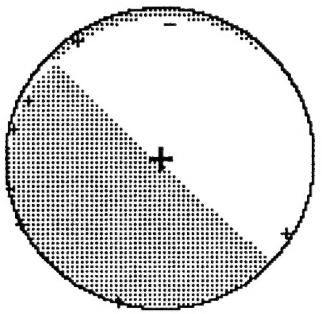

Double couple solution :

.165E+10	.543E+09	-.962E+10
.543E+09	-.414E+09	-.898E+10
-.962E+10	-.898E+10	-.124E+10

T0= .0383 M0= .133E+11 MT= .133E+11
DBCP.= 100.0%

D.C.:	ϕA= 132.83	δA= 87.31	ϕB= 254.89	δB= 5.06
	P-axis: trend= 47.32		plunge= 47.52	
	T-axis: trend= 218.75		plunge= 42.16	
	B-axis: trend= 312.63		plunge= 4.28	
	Quality index = 7.6		normal fault	

L2 tensor for : #85

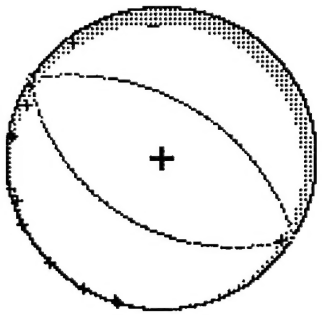

Full solution :

.113E+10	-.271E+09	.317E+11
-.271E+09	.244E+10	.108E+11
.317E+11	.108E+11	-.525E+12

T0= .0400 M0= .373E+12 MT= .525E+12
Expl.= -49.5% CLVD.= -50.2% DBCP.= .2%

Full:	∮A= 300.99	δA= 48.54	∮B= 122.63	δB= 41.48
	P-axis: trend= 198.75		plunge= 86.38	
	T-axis: trend= 31.76		plunge= 3.53	
	B-axis: trend= 301.71		plunge= .81	
	Quality index = 46.1		normal fault	

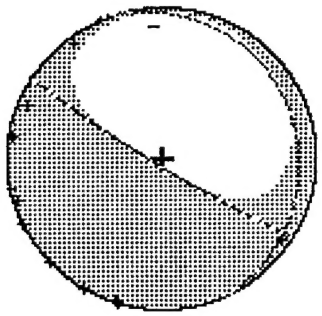

Trace null solution :

.326E+09	.930E+08	-.372E+10
.930E+08	.871E+09	-.222E+10
-.372E+10	-.222E+10	-.120E+10

T0= .0400 M0= .411E+10 MT= .447E+10
CLVD.= -15.5% DBCP.= 84.5%

Tr.0:	∮A= 122.05	δA= 84.25	∮B= 335.60	δB= 6.89
	P-axis: trend= 27.81		plunge= 50.61	
	T-axis: trend= 215.51		plunge= 39.13	
	B-axis: trend= 122.43		plunge= 3.78	
	Quality index = 37.8		normal fault	

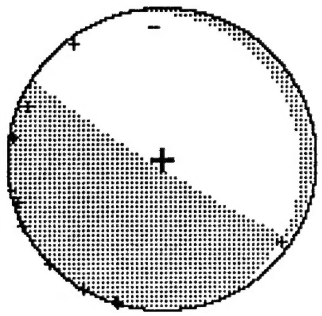

Double couple solution :

.349E+09	.487E+09	-.342E+10
.487E+09	.472E+09	-.211E+10
-.342E+10	-.211E+10	-.822E+09

T0= .0400 M0= .411E+10 MT= .411E+10
DBCP.= 100.0%

D.C.:	∮A= 122.01	δA= 84.23	∮B= 335.19	δB= 6.89
	P-axis: trend= 27.81		plunge= 50.64	
	T-axis: trend= 215.44		plunge= 39.11	
	B-axis: trend= 122.39		plunge= 3.74	
	Quality index = 26.6		normal fault	

L2 tensor for : #86

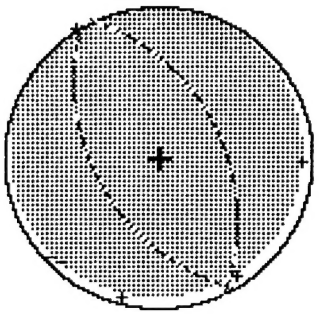

Full solution :

-.491E+11	-.289E+11	.220E+13
-.289E+11	-.133E+12	-.590E+12
.220E+13	-.590E+12	.603E+14

T0= .0450 M0= .427E+14 MT= .603E+14
Expl.= 19.9% CLVD.= 20.0% DBCP.= 60.1%

Full:	ϕA= 149.89	δA= 45.52	ϕB= 334.09	δB= 44.55
	P-axis: trend= 241.97		plunge= .49	
	T-axis: trend= 344.98		plunge= 87.84	
	B-axis: trend= 151.96		plunge= 2.10	
	Quality index = 12.5		reverse fault	

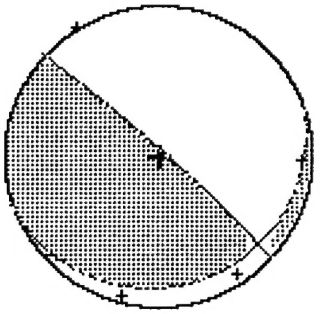

Trace null solution :

-.382E+12	-.939E+11	-.137E+13
-.939E+11	.112E+12	-.126E+13
-.137E+13	-.126E+13	.271E+12

T0= .0450 M0= .189E+13 MT= .189E+13
CLVD.= .9% DBCP.= 99.1%

Tr.0:	ϕA= 312.00	δA= 85.98	ϕB= 71.10	δB= 8.22
	P-axis: trend= 35.33		plunge= 40.57	
	T-axis: trend= 229.67		plunge= 48.54	
	B-axis: trend= 131.50		plunge= 7.16	
	Quality index = 11.8		reverse fault	

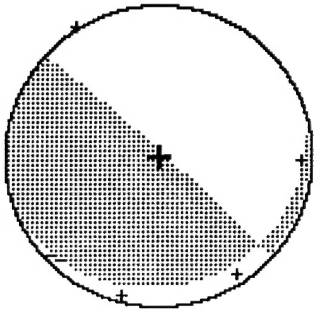

Double couple solution :

-.378E+12	-.105E+12	-.137E+13
-.105E+12	.116E+12	-.125E+13
-.137E+13	-.125E+13	.261E+12

T0= .0450 M0= .189E+13 MT= .189E+13
DBCP.= 100.0%

D.C.:	ϕA= 312.00	δA= 85.99	ϕB= 71.13	δB= 8.20
	P-axis: trend= 35.34		plunge= 40.57	
	T-axis: trend= 229.65		plunge= 48.53	
	B-axis: trend= 131.50		plunge= 7.14	
	Quality index = 5.9		reverse fault	

L2 tensor for : #87

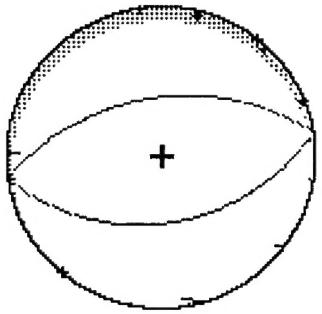

Full solution :

.868E+09	.336E+07	.234E+11
.336E+07	.516E+09	-.469E+10
.234E+11	-.469E+10	-.434E+12

T0= .0383 M0= .308E+12 MT= .435E+12
Expl.= -49.6% CLVD.= -49.8% DBCP.= .6%

Full:	∮A= 261.03	δA= 48.13	∮B= 81.31	δB= 41.87
	P-axis: trend= 168.67		plunge= 86.86	
	T-axis: trend= 351.16		plunge= 3.13	
	B-axis: trend= 261.16		plunge= .14	
	Quality index = 50.0		normal fault	

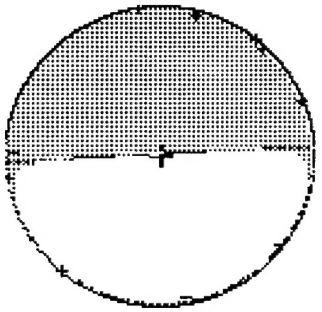

Trace null solution :

.558E+09	.358E+08	.207E+11
.358E+08	.271E+09	-.108E+10
.207E+11	-.108E+10	-.829E+09

T0= .0383 M0= .206E+11 MT= .207E+11
CLVD.= -1.3% DBCP.= 98.7%

Tr.0:	∮A= 267.00	δA= 89.04	∮B= 95.33	δB= .97
	P-axis: trend= 176.86		plunge= 45.96	
	T-axis: trend= 357.14		plunge= 44.04	
	B-axis: trend= 267.01		plunge= .14	
	Quality index = 49.5		normal fault	

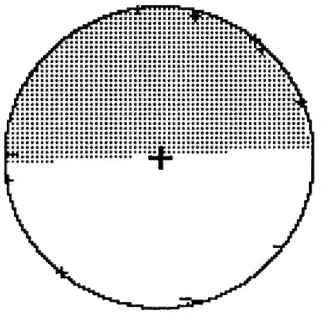

Double couple solution :

.710E+09	.141E+08	.205E+11
.141E+08	-.342E+07	-.108E+10
.205E+11	-.108E+10	-.706E+09

T0= .0383 M0= .206E+11 MT= .206E+11
DBCP.= 100.0%

D.C.:	∮A= 267.01	δA= 89.02	∮B= 95.26	δB= .99
	P-axis: trend= 176.86		plunge= 45.98	
	T-axis: trend= 357.15		plunge= 44.02	
	B-axis: trend= 267.01		plunge= .14	
	Quality index = 24.7		normal fault	